OCTOBER–DECEMBER 2024 VOL. 16 № 4 (63)

ISSN 2075-8251

ActaNaturae

Platforms for the Search for New Antimicrobial Agents Using *In Vivo C. elegans* Models

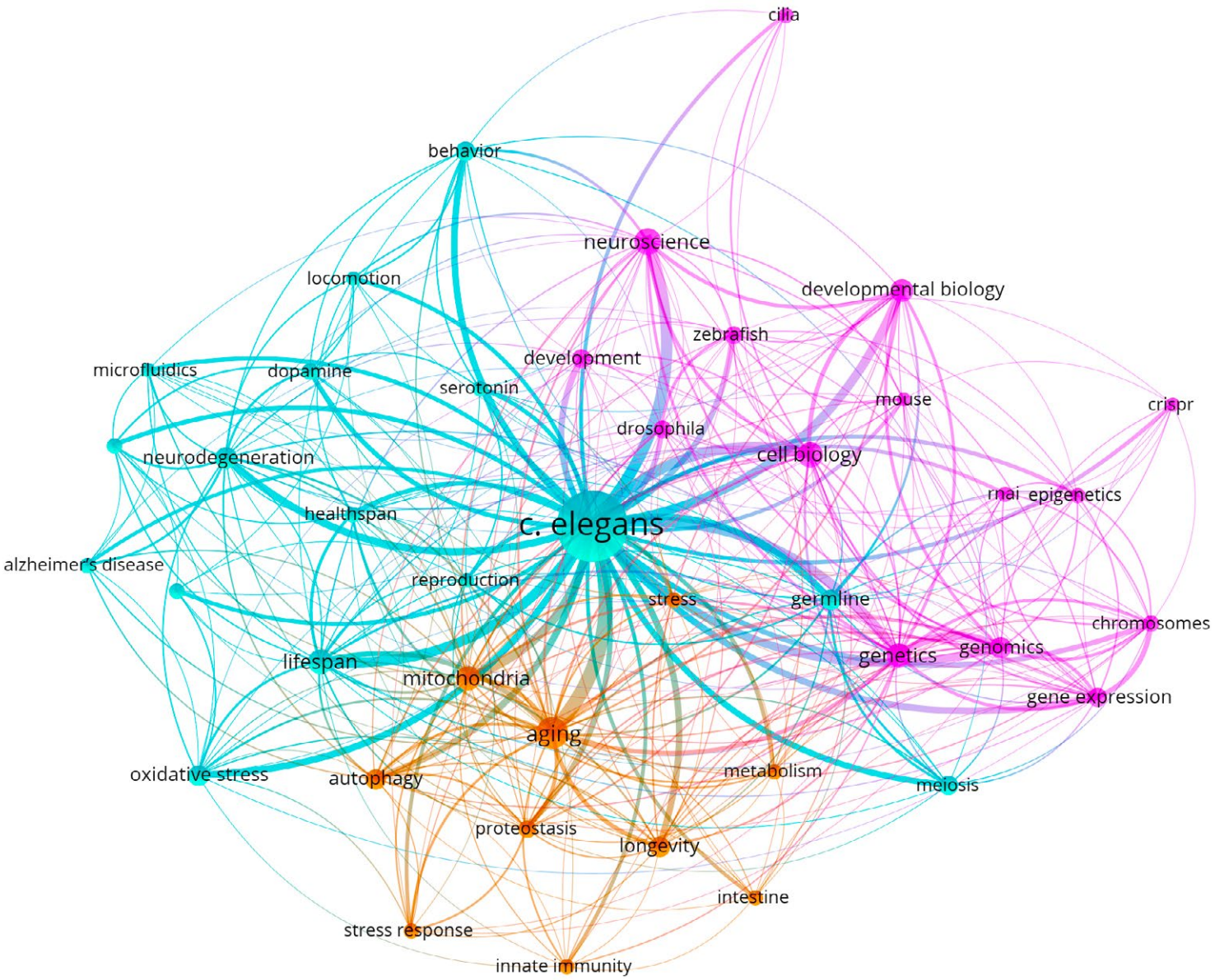

Peptide Mimicking Loop II of the Human Epithelial Protein SLURP-2 Enhances the Viability and Migration of Skin Keratinocytes

O. V. Shlepova, T. Ya. Gornostaeva, I. D. Kukushkin, V. N. Azev, M. L. Bychkov, Z. O. Shenkarev, M. P. Kirpichnikov, E. N. Lyukmanova

The secreted human protein SLURP-2 is a regulator of epithelial homeostasis, which enhances the viability and migration of keratinocytes. This work is devoted to the search for the SLURP-2 functional regions responsible for enhancing keratinocyte viability and migration. Authors produced synthetic peptides corresponding to the SLURP-2 loop regions and studied their effect on the viability and migration of HaCaT skin keratinocytes using the WST-8 test and scratch-test, respectively.

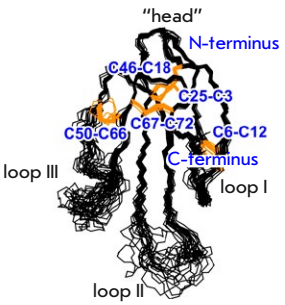

Spatial structure of SLURP-2

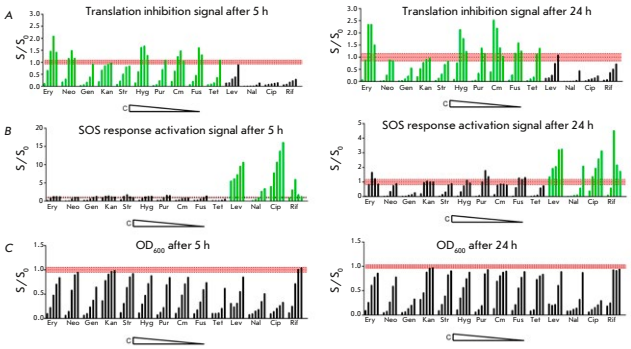

Testing the double fluorescent protein reporter assay on known antibiotics

The Antibacterial Activity of Yeasts from Unique Biocenoses

O. V. Shulenina, E. A. Sukhanova, B. F. Yarovoy, E. A. Tolstyko, A. L. Konevega, A. Paleskava

The results of this study of a unique collection containing more than 3,000 samples of yeasts found on the Kamchatka Peninsula, the Kuril Islands, and Sakhalin Island, Russia. It was uncovered that the Sakhalin strains for the most part stimulate bacterial growth, while most of the strains found on the Kamchatka Peninsula possess inhibitory properties.

Bacteriocin from the Raccoon Dog Oral Microbiota Inhibits the Growth of Pathogenic Methicillin-Resistant *Staphylococcus aureus*

M. N. Baranova, E. A. Soboleva, M. A. Kornienko, M. V. Malakhova, Yu. A. Mokrushina, A. G. Gabibov, S. S. Terekhov, I. V. Smirnov

The microbiome of wild animals can be considered a natural reservoir of biodiversity for antibiotic discovery. In this study, the *Staphylococcus pseudintermedius* E18 strain was isolated from the oral microbiome of a raccoon dog (*Nyctereutes procyonoides*) using a microfluidic ultrahigh-throughput screening platform. *S. pseudintermedius* E18 efficiently inhibited the growth of pathogenic methicillin-resistant *Staphylococcus aureus* (MRSA). It was established that the main active substance of the *S. pseudintermedius* E18 strain was a bacteriocin.

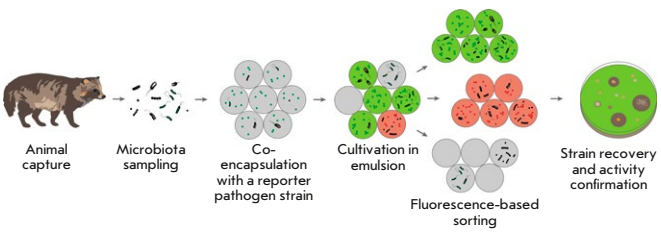

Schematic diagram of an ultra-high-throughput screening platform for selecting microorganisms that inhibit the growth of a target bacterium

ActaNaturae

OCTOBER–DECEMBER 2024 VOL. 16 № 4 (63)
since april 2009, 4 times a year

Founders
Acta Naturae, Ltd,
National Research University
Higher School of Economics

Adress: 101000, Moscow, Myasnitskaya Ulitsa, 13, str. 4
Phone/Fax: +7 (495) 727 38 60
E-mail: actanaturae@gmail.com

Номер подписан в печать 30 декабря 2024 г.
Тираж 15 экз. Цена свободная.
Отпечатано в типографии: НИУ ВШЭ,
г. Москва, Измайловское шоссе, 44, стр. 2

Founder and Chairman
of the Editorial Board (from 2009 to 2023)
of the journal Acta Naturae
Academician Grigoriev Anatoly Ivanovich

Indexed in PubMed, Web of Science, Scopus, and RISC

Impact Factor: 2.0 (WOS); 3.5 (Scopus)

CONTENTS

REVIEWS

RESEARCH ARTICLES

SHORT REPORTS

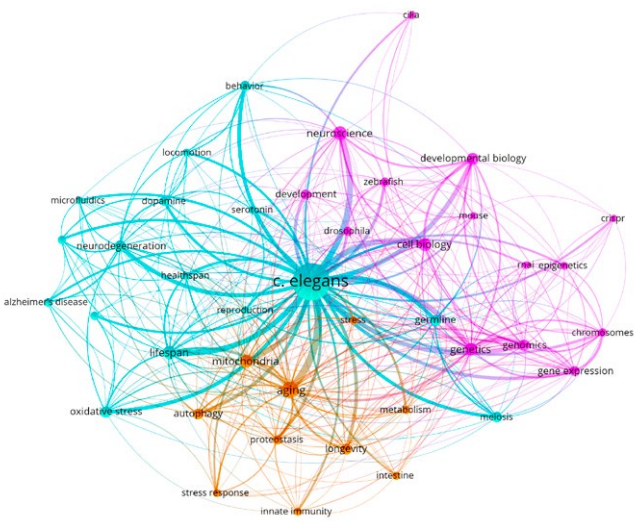

IMAGE ON THE COVER PAGE
(see the article by Kalganova et al.)

Recombinant VSVs: A Promising Tool for Virotherapy

K. A. Vorona, V. D. Moroz*, N. B. Gasanov, A. V. Karabelsky
Sirius University of Science and Technology, Krasnodar Region, Sirius Federal Territory, 354340 Russian Federation
*E-mail: moroz.vd@talantiuspeh.ru
Received August 23, 2024; in final form, October 18, 2024
DOI: 10.32607/actanaturae.27501

ABSTRACT **Cancer is one of the leading causes of death worldwide. Traditional cancer treatments include surgery, radiotherapy, and chemotherapy, as well as combinations of these treatments. Despite significant advances in these fields, the search for innovative ways to treat malignant tumors, including the application of oncolytic viruses, remains relevant. One such virus is the vesicular stomatitis virus (VSV), which possess a number of useful oncolytic properties. However, VSV-based drugs are still in their infancy and are yet to be approved for clinical use. This review discusses the mechanisms of oncogenesis, the antiviral response of tumor and normal cells, and markers of tumor cell resistance to VSV virotherapy. In addition, it examines methods for producing and arming recombinant VSV and provides examples of clinical trials. The data presented will allow better assessment of the prospects of using VSV as an oncolytic.**
KEYWORDS **oncolytic viruses, vesicular stomatitis virus, cancer immunotherapy, interferon-stimulated gene, biomarker of resistance.**
ABBREVIATIONS **VSV – vesicular stomatitis virus; rVSV – recombinant vesicular stomatitis virus; ISG – interferon-stimulated gene; IFNs – interferons; PAMP – pathogen-associated molecular pattern; MHC – major histocompatibility complex; IFNAR – type I IFN receptor; PKR – protein kinase R.**

INTRODUCTION

Cancer is one of the leading causes of death in developed countries. Over the past years, the application of immunotherapy strategies in clinical practice has improved treatment effectiveness for many cancers. Unfortunately, positive outcomes have been achieved in only a limited type of malignant tumors which account for approximately one-third of all cases. Furthermore, not all patients appear to respond to therapy [1, 2].

It is anticipated that obstacles to the treatment of malignant tumors can be bypassed using oncolytic viruses (oncolytics). These viruses are capable of specifically replicating in cancer cells while remaining safe for the organism [3]. The viruses can replicate in cancer cells due to the impaired antiviral response associated with dysfunctional interferon (IFN) production. Interferons inhibit viral replication as well as the formation and spread of virus particles by activating signaling pathways that slow down metabolism in infected and neighboring cells. Oncolytic viruses are highly specific to cancer cells with a restricted IFN response; they induce an inflammatory response in the tumor and fine-tune the immune system to target the inflammation site, whereas in healthy cells, viruses are destroyed due to IFN-mediated immune responses.

The vesicular stomatitis virus (VSV), a negative-sense RNA virus belonging to the family *Rhabdoviridae*, is one of the promising oncolytic viruses [4]. VSV has a number of advantages: it is not integrated into the host genome and has a broad tropism; its genome can be relatively easily modified, and a very small percentage of people are seropositive for VSV [5].

Recombinant VSV (rVSV)-based drugs are being investigated *in vitro* and *in vivo* [6–10]; clinical trials to assess their effectiveness in the treatment of colorectal cancer, melanoma, lung cancer, breast cancer, malignant lymphoma, and other cancers are ongoing (NCT02923466, NCT04046445, NCT04291105, NCT03017820, NCT03865212, NCT04291105, NCT03120624, NCT03456908, NCT05846516, NCT05644509, and NCT01042379).

Research into the oncolysis mechanisms, markers, and signaling pathways responsible for the resistance of cancer and healthy cells to the virus can explain the variability in the response of different tumors to virotherapy and allow one to find ways to optimize recombinant therapeutic VSVs [11].

THE PROBLEM OF CANCER AND ONCOGENESIS

Approximately one in five people develops cancer throughout their lifetime; cancer-related deaths have been documented in almost one in nine men and one in twelve women. The most common types of cancer (> 60% of all cancer cases) include lung cancer, breast cancer, colorectal cancer, prostate cancer, stomach cancer, liver cancer, thyroid cancer, cervical cancer, bladder cancer, and non-Hodgkin lymphoma [12, 13].

D. Hanahan [14] described the key characteristics of malignant tumors. They include eight hallmarks: the ability to evade the impact of oncosuppressors; resistance to apoptosis; the ability to sustain proliferative signaling and induce angiogenesis; invasion and metastasis; replicative immortality; and immune evasion and alteration of cellular metabolism. The emergence of tumor cells is associated with genomic instability and the accumulation of mutations altering the cell morphology and function, as well as with epigenetic reprogramming of cell identity and chronic inflammation.

At the molecular level, carcinogenesis is caused by mutations in oncogenes and tumor suppressor genes. Mutations in proto-oncogenes may promote their transformation into oncogenes, in turn inducing the synthesis of oncoproteins, which enhance cell proliferation and promote the evasion of apoptosis [15, 16]. On the other hand, suppressor genes encode functional proteins that inhibit the oncogenic transformation of cells, including factors controlling cell division, cell death, and DNA repair. Mutations in tumor suppressor genes lead to inactivation of their products and, therefore, tumor development [15–17]. In addition, there is a growing body of evidence indicating other potential reasons for cancer development. Thus, epigenetic changes may contribute to the development of the main characteristics of tumor. Changes in the epigenetic DNA profile in tumor cells are associated with hypoxia caused by insufficient vascularization of tissues and cells, which leads to reduced activity of TET demethylases, resulting in significant changes in the methylome, and DNA hypermethylation in particular [14, 18]. Chronic inflammation can be another reason behind tumor growth induction [19]. Chronic inflammation processes can be induced, and the risk of cancer development or progression can be increased by *Helicobacter pylori* in patients with stomach cancer and MALT lymphoma, by the papillomavirus and hepatitis virus in patients with cervical and liver cancer, respectively, by autoimmune diseases (e.g., inflammatory bowel disease in patients with colorectal cancer), and by an inflammation of unknown origin (e.g., prostatitis in patients with prostate cancer) [20].

CANCER VIROTHERAPY

Surgical intervention, radiation therapy and chemotherapy, as well as their combinations, are still the key strategies used in cancer treatment. However, poor treatment effectiveness at late stages and the high risk of recurrence necessitate a search for innovative methods. Thus, cytokines activating immune cells [21, 22], adoptive cell therapy (CAR-T therapy) [23–25], immunotherapy based on antibodies (immune checkpoint inhibitors or antibody drug conjugates) [26, 27], antitumor vaccines, etc. [28–30] are used in cancer immunotherapy. In recent years, immunotherapy methods increasing the treatment effectiveness in some cancers are moving ever closer to clinical practice, but not all patients respond to therapy [1].

The main reasons for the lack of response to immunotherapy include the insufficient immunogenicity of cancer cells as well as challenges related to the delivery of immunocompetent cells and immunotherapeutic agents to their targets [2]. These hurdles can be overcome by using oncolytic viruses, a new class of antitumor agents promoting tumor regression through the preferential replication of viruses in cancer cells, induction of immunogenic apoptosis, and stimulation of antitumor immunity [3]. Oncolytic viruses display enhanced tropism for tumors where the dysfunction of antiviral response factors allows viruses to preferentially replicate in cancer cells [31].

Several drugs based on oncolytic viruses have been approved for cancer treatment worldwide. In 2004, the State Agency of Medicines of the Republic of Latvia approved Rigvir for the virotherapy of melanoma. Rigvir is derived from the native strain of echovirus serotype 7 (ECHO-7), a nonpathogenic intestinal cytopathic RNA enterovirus belonging to the family *Picornaviridae*. However, Rigvir production was suspended in 2019 because of violations of the manufacturing process and quality control standards [3, 32]. In 2006, the use of oncolytic virus H101, a genetically modified adenovirus, in combination with cytotoxic chemotherapy, was approved for the treatment of head and neck cancer in China [3, 33]. In 2015, the U.S. Food and Drug Administration (FDA) approved Talimogene Laherparepvec (T-VEC), an attenuated herpes simplex virus type 1 (HPV-1) encoding the granulocyte-macrophage colony-stimulating factor (GM-CSF), for topical treatment of inoperable dermal, subcutaneous, and nodular lesions in patients with recurrent melanoma after primary surgery [3, 32, 34]. The effectiveness and safety of T-VEC were studied in a multicenter randomized clinical trial; afterwards, the drug was approved in Europe, Australia, and Israel. Recent clinical trials have demonstrated that a combination of oncolytic viruses and immune

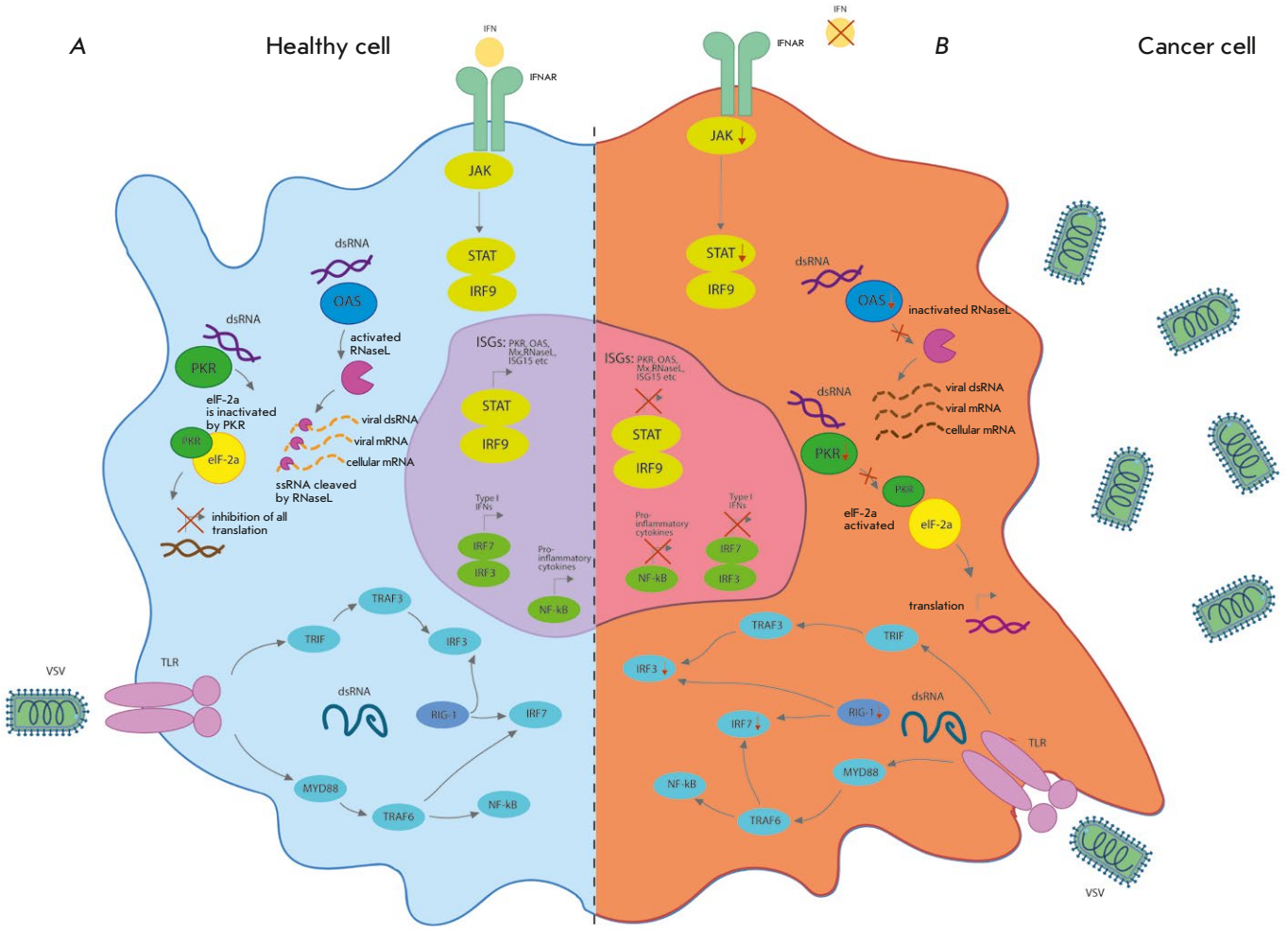

Fig. 1. Oncolytic viruses in tumor cells with defective antiviral responses. (*A*) During viral infection, most normal cells activate an antiviral mechanism that can be triggered by PAMPs associated with the viral pathogen or by detection of viral nucleic acids. TLRs transmit signals through MYD88, inducing the production of pro-inflammatory cytokines and interferons that activate the JAK-STAT signaling pathway; (*B*) the cancer cell response to a viral infection is altered. In cancer cells, the activity of critical components of the innate signaling pathway, including RIG-I, IRF7, and IRF3, can be suppressed, thus limiting the detection of virus particles and making cancer cells more susceptible to viral replication. Additionally, critical components of the IFN signaling pathway can be inhibited in cancer cells [39]

checkpoint blockade improves the therapeutic response [35, 36].

Antiviral response in normal and cancer cells

Innate immunity is the body's defense system against foreign and potentially harmful pathogens that exists before the initial entry of pathogens into the body [37, 38]. In healthy cells, various signaling pathways are activated in response to a viral infection (*Fig. 1*), which can be stimulated by a local release of type I interferon (IFN-I) or the activation of intracellular Toll-like receptors (TLRs). TLRs recognize evolutionarily conserved pathogen-associated molecular patterns (PAMPs), which may include elements of viral origin (capsids, DNA, RNA, and proteins). TLR signaling activates host cell's antiviral responses and systemic innate immunity. Several host cell factors such as TRAF3 (TNF receptor-associated factor 3), IRF3 (IFN regulatory factor 3), IRF7 (IFN regulatory factor 7), and RIG-I (retinoic acid-inducible gene I) were found to play an important role in halting viral replication and reducing viral infectivity. These factors activate the JAK-STAT pathway coordinating the antiviral response in infected cells [39].

In response to virus entry, interferon production is also activated in cells. There are three types of in-

terferons: type I interferons (IFN-I): IFN-α, IFN-β, and IFN-ω; type II interferons (IFN-II): IFN-γ; and type III interferons (IFN-III): IFN-λ1, IFN-λ2, IFN-λ3 (also known as IL29, IL28A, and IL28B, respectively), and IFN-λ4 [40, 41]. Interferons inhibit viral replication, the formation of virus particles, and virion spread both in the infected cell and in neighboring cells by activating signaling cascades that slow down metabolism. Interferons enhance the synthesis of the major histocompatibility complex classes I and II (MHC-I, MHC-II) molecules and stimulate the activity of immunoproteasomes. The elevated MHC-I level promotes efficient presentation of viral peptides by cytotoxic T lymphocytes and killer cells. The immunoproteasome performs the proteolysis of viral peptides, which are then transported to the endoplasmic reticulum and are presented as part of MHC class I. The high MHC-II level ensures that viral antigens are presented by T-helper cells, which in response secrete cytokines regulating the rest of the immune system. Meanwhile, interferons reduce cell proliferation and activate p53 proapoptotic protein [42].

IFN-I activates the IFNAR (type I IFN receptor) complex, which involves the IFNAR1 and IFNAR2 subunits. IFN-I is essential for eliciting a robust antiviral response. Mice lacking IFNAR were shown to be characterized by higher susceptibility to many viruses but were resistant to pathogens such as *Listeria monocytogenes* [43, 44]. Furthermore, genetic defects in interferon signaling pathway components cause severe forms of immunodeficiency [45–48]. IFN-I binding to IFNAR initiates a signaling pathway leading to the induction of a group of interferon-stimulated genes (ISGs) [42, 49]. However, only few ISGs are directly involved in the development of the antiviral state. Many of them encode pattern recognition receptors (PRRs), which detect viral molecules and modulate signaling pathways or transcription factors increasing IFN production.

Some ISGs encode proteins exhibiting potential antiviral activity, including the proteins involved in cytoskeletal remodeling, apoptosis induction, and the regulation of posttranscriptional events (splicing, mRNA editing, RNA degradation, and different steps of protein synthesis), as well as the proteins involved in posttranslational modification [42]: for example, protein kinase R (PKR, also known as EIF2αK2), 2'-5'-oligoadenylate synthetase (2'-5'-OAS) and Mx GTPases (dynamin-like GTPases belonging to the Mx family), ribonuclease L (RNase L), ISG15 (15-kDa IFN-induced protein) have well-described antiviral functions. Mice carrying mutations or abnormalities in the key stages of signaling pathways activated by these proteins are characterized by increased susceptibility to viral infections [42].

PKR is an intracellular protein kinase that recognizes viral dsRNA, phosphorylates eIF2a (translation initiation factor 2A), and inhibits translation [39, 42, 50, 51]. PKR activation leads to the inhibition of protein synthesis in virus-infected cells, contributing to the rapid death of these cells and preventing the spread of infection.

2'-5'-OAS and ribonuclease L are components of the antiviral immune response of a cell. 2'-5'-OAS forms short oligoadenylates from ATP, which activate ribonuclease L, leading to viral RNA degradation. This process impedes virus replication and promotes destruction of the infected cells [42, 52].

ISG15 is a protein that modifies many cellular and viral targets via a process known as ISGylation. ISG15-induced ISGylation prevents the degradation of IRF3, an important transcription factor involved in the antiviral immune response [53]. Moreover, ISG15 indirectly stops virion release. ISG15 inhibits the ubiquitination of HIV Gag (group-specific antigen) and Tsg101 (tumor susceptibility gene 101 protein), which prevents viral release from the host cell. The interaction between the N-terminal domain of Tsg101 and the viral Gag protein is critical for the formation of new virus particles [52–54].

The Mx GTPase family plays an important role in the antiviral immune response. Human MxA interacts with the virus nucleocapsid and prevents viral transport, thus blocking replication. Furthermore, MxA inhibits viral transcription: thus, MxA was shown to bind to the PB2 subunit of influenza virus RNA polymerase and prevent viral genome transcription. This impedes viral replication and promotes the destruction of infected cells [52, 55, 56].

Antiviral functions were also reported for other ISGs: the adenosine deaminase (ADAR1) and APOBEC proteins; ISG20 exonuclease; TRIM (tripartite motif-containing) proteins such as TRIM19 (also known as PML), TRIM5a [57], Viperin (Cig5) [58]; and IFN-inducible translation regulators (IFIT1, IFIT2, and IFIT3) [42, 59, 60]. However, the functions of most of these ISGs remain poorly characterized to this day and their antiviral response mechanisms remain unknown.

Downregulating IFN expression or signaling of this cytokine by decreasing receptor expression or altering subsequent signaling may lead to the suppression of antiviral signaling pathways in different types of tumors. Furthermore, the antiviral response in cancer cells can be reduced by ISG deactivation: for example, downregulated PKR expression in tumor cells increases viral replication. In other cases, such as in

low malignant tumors, PKR can remain active, which may have an impact on the effectiveness of oncolytic virotherapy [39]. Oncolytic viruses have a heightened specificity for cancer cells with a limited response to IFN, since in healthy cells viruses are eliminated through IFN-mediated responses [39].

Vesicular stomatitis virus as an oncolytic

VSV is a virus with a nonsegmented negative-sense RNA genome, belonging to the family *Rhabdoviridae*. The family *Rhabdoviridae* comprises more than 100 viruses, which infect both vertebrates and invertebrates, as well as plants [4]. There are eight major serotypes of VSVs: Indiana (VSVInd), New Jersey (VSVNJ), Cocal virus (COCV), Alagoas VSV (VSVala), Isfahan (ISFV), Chandipura (CHAV), Maraba, and Piry virus (PIRYV) [61–64]. A VSV mostly affects livestock and is transmitted by direct contact through aerosols and fomites. In humans, VSV infections are usually asymptomatic. However, fever, chills, muscle pain, and nausea are observed in some cases [65]. Recombinant VSV (rVSV) is a promising vaccine vector, because its simple genome can accommodate multiple foreign genes; it neither undergoes recombination nor does it integrate the host cell DNA but achieves high titers ($>10^9$ plaque-forming units, PBU/mL [66]) in various cell types, which facilitates the production of virus-based drug. Moreover, VSV-based vaccines induce a potent cell-mediated and humoral immune response to abundantly expressed foreign antigens [67]. Furthermore, a very small percentage of people are seropositive for VSV [66].

There are several protocols for the assembly of recombinant VSVs [68–71]; most of them involve transfection of mammalian cells with plasmids expressing the N, P, G, and L proteins of VSV VSV-based drugs still in their infancy, followed by coinfection of cells with viruses expressing the DNA-dependent T7 RNA polymerase (T7 RNA polymerase). In addition, protocols where an accessory plasmid also encoding T7 RNA polymerase is used during cell transfection [72], or VSV assembly occurs in genetically modified cell lines, have been published [71].

Most of the protocols describe methods for producing the VSV using the wild-type or modified vaccinia virus (VACV or VV) [70] to ensure more efficient translation of the VSV genes [68]. However, the assembly scheme involving cell transfection with five plasmids (the plasmid expressing the virus genome and four accessory plasmids expressing the N, P, G, and L proteins of VSV) and additional transduction of VV imposes a significant cellular burden and reduces the efficiency of virus assembly. Furthermore, one needs to take into account that the virus-based drugs used *in vivo* must not contain residues of VV or other viruses; so, there needs to be an additional step involving the purification of the resulting virus-based drug [71]. Therefore, other assembly techniques are recommended for producing drugs of high-purity grade and free of viral contamination.

Application of the accessory fifth plasmid expressing T7 RNA polymerase helps avoid drug contamination but can significantly reduce cell transfection efficiency. Successful virus assembly involves the simultaneous expression of six plasmids (the plasmid expressing the viral genome, the plasmid expressing T7 RNA polymerase, and four accessory plasmids expressing the N, P, G, and L proteins of VSV). However, not all of these plasmids can penetrate into cells in the amounts needed for virus assembly; furthermore, they impose a metabolic burden on cells.

Genetic modification of cell lines for the assembly of recombinant VSV seems to be the most practical way of virus assembly that requires no additional purification steps. Thus, Moroz et al. demonstrated that VSV could be efficiently assembled in the HEK293TN-T7 cell line expressing the T7 RNA polymerase gene and transfected with the plasmid expressing the viral genome and four accessory plasmids expressing the N, P, G, and L proteins of VSV.

Although there exist operational protocols for VSV assembly, it is necessary to continue searching for the most efficient assembly schemes that could be simpler and help one produce high-quality virus-based drugs.

The chance of using rVSV in many types of cancers, including prostate [6], skin [7], colon [8], pancreatic [9], and other types of cancer [10], is being considered. The VSV is a potent inducer of apoptosis in many types of cancer cells; it is very susceptible to the antiviral effects of IFN and, therefore, selectively replicates in cancer cells with defects in the IFN pathway [73]. Attenuated VSV strains were constructed to ensure heterologous gene expression, improved selectivity with respect to cancer cells, better cancer cell destruction rate, or enhanced antitumor immunity. In preclinical trials, recombinant VSV strains were found to be highly effective against a wide range of tumors [74–76]. Thirteen clinical trials to assess the effectiveness of VSV in different cancers are currently underway (https://www.clinicaltrials.gov/). Thus, rVSV expressing the human interferon beta (IFN-β) gene and rVSV expressing two supplementary genes (the *IFN-β* gene and the *TYRP1* gene that encodes tyrosinase-related protein 1 and is expressed in melanocytes), are currently in phase I clinical trials aiming to assess treatment of hepatocellular carcinoma (NCT01628640) and stage III/IV melanoma (NCT03865212), respectively.

Methods for arming (editing) VSVs to enhance the effectiveness of VSV-based drugs

The development of novel safe VSV strains is extremely important, since this virus has a broad tropism. Different genomic modifications are introduced into VSV in order to improve safety and clinical efficacy. There are several strategies for VSV attenuation: (1) limiting replication (e.g., using pseudotyped viruses with *G*-gene deletion [77]); (2) reducing the viral gene expression (e.g., moving the *N* gene from position 1 to position 4 in the genome [78, 79]); (3) inhibiting virus maturation (e.g., by truncating the C-terminus of the G protein [80]); and (4) ensuring a faster antiviral response of the host to attenuate viral replication, production and transmission by incorporating a mutation in the M protein (e.g., by amino acid deletion or substitution at position 51 [81, 82]).

Additional insertions into the virus genome are made to increase the effectiveness of VSV-based drugs [83]. Many genes are inserted into the genome to stimulate the immune response to the tumor (e.g., the genes encoding IL-12, GM-CSF, tyrosine kinase, CD40L, IL-15, etc. are inserted into the rVSV genome) [5, 84–86]. Thus, Shin et al. experimentally demonstrated that VSV-IL12 expressing the proinflammatory cytokine IL-12 has a direct cytotoxic effect in mice with squamous cell carcinoma (SCC) of the head and neck: they observed a reduced tumor volume and increased chances of animal survival [30, 86, 87]. MicroRNAs, short non-coding RNAs regulating gene expression by inhibiting the translation of target transcripts, were also used to modify VSVs in order to enhance selectivity and effectiveness. The microRNA expression profiles vary in different tissues and change along with progression of the disease, including cancer [88].

Recombinant VSVs in clinical research

The vesicular stomatitis virus has proved to be a highly effective oncolytic for treating a broad range of malignant tumors in a large number of preclinical studies [30, 83, 89]. Most of the clinical trials currently underway seek to evaluate the effectiveness and safety of VSV-hIFNβ-NIS carrying the human interferon-beta (IFNβ) gene for enhancing the selectivity of the oncolytic and the sodium iodide symporter (NIS) to control biodistribution of the virus. Clinical trials are underway for the VSV-GP154 and VSV-GP128 viruses, in which the *G* gene is replaced with the *GP* gene of the lymphocytic choriomeningitis virus (LCMV) in order to reduce the potential neurotoxicity of VSV. The VSV-hIFNβ-TYRP1 variant has been used in clinical trials as an agent against stage III/IV melanoma. Along with the gene encoding human IFNβ, the TYRP1 gene expressed in melanocytes was also inserted into its genome in order to increase the oncolytic selectivity of VSV-hIFNβ-TYRP1. Most clinical trials of VSV-based drugs are conducted in combination with various immunotherapeutic approaches.

The VSV is used for patients with a broad range of malignancies; patients with recurrent and metastatic solid tumors (colorectal cancer (NCT02923466, NCT04046445, and NCT04291105), melanoma (NCT03017820, NCT03865212, and NCT04291105), endometrial cancer (NCT03120624 and NCT03456908), head and neck cancer (NCT04291105), pancreatic cancer (NCT05846516), and other tumors (NCT05644509 and NCT01042379) are chosen the most often. Clinical trials involving patients with malignant lymphoma (NCT06508463 and NCT04046445) are also being conducted. Unfortunately, the results of these clinical trials are yet to be published.

Obstacles to the application of virotherapy

Despite the significant therapeutic potential of oncolytic viruses, there also exist many limitations that impede their use, such as the risk of a profound systemic immune response of the body; physical barriers in the tumor and barriers in the immunosuppressive tumor microenvironment (TME) and the challenges related to the delivery of virus particles and their replication in cancer cells; the choice of the optimal combination of oncolytic viruses and other drugs, the administration scheme and route; as well as challenges related to the production of virus-based drugs and maintaining a high titer of virus particles.

A viral platform should be carefully selected in order to minimize the risk of a systemic immune response of the body. The oncolytic properties of the viruses safest for humans, which include those belonging to the families *Adenoviridae*, *Herpesviridae*, *Poxviridae*, *Picornaviridae*, *Paramyxoviridae*, *Rhabdoviridae*, *Parvoviridae*, and *Reoviridae* [30], are being studied for this purpose. Capsid modification is used to solve the problems related to the delivery of oncolytic viruses to cancer cells and the insufficient specificity of delivery: it strengthens the binding of virus particles to the receptors responsible for penetration into target cells [90] and the deletion of viral genes needed for virus replication in normal cells. Thus, ONYX-015, an oncolytic adenovirus with deleted gene coding for the E1B protein, shows an increased ability for selective replication in tumors, since the modified virus cannot inactivate protein p53 in normal cells [91, 92]. Polyethylene glycol (PEG), poly-N-(2-hydroxypropyl)methacrylamide, thiol groups for attaching transferrin to capsid proteins, etc. are also used to modify oncolytic viruses [91–95].

Table 1. Changes in the expression of the *EGFR* and *HER2* genes in cell lines characterized by different susceptibilities to VSV

Cell line	Level of *EGFR* and *HER2* expression	Susceptibility to virotherapy with recombinant VSV	VSV serotype
HOS (osteosarcoma)	Upregulated [96]	High [96]	VSV strain Indiana
DBTRG-05MG (glioblastoma)	Downregulated [96]	Low [96]	VSV strain Indiana
U251MG (glioblastoma)	Upregulated [96]	High [96]	VSV strain Indiana
A172 (glioblastoma)	Upregulated [96]	High [96]	VSV strain Indiana
U87MG (glioblastoma)	Upregulated [101]	High [102]	rVSV-ΔM51
A375 (melanoma)	Downregulated [99]	High [103]	Wild-type VSV
A549	Upregulated [104]	Low [105]	VSV strain Indiana
HepG2	Upregulated [106]	High [107]	rVSV-GFP
SW982 (synovial sarcoma)	Upregulated [108]	Low [109]	rVSV-G/GFP
BxPC-3	Moderate [110]_	High [111]	rVSV-ΔM51-GFP
AsPC-1	Downregulated [112]	Low [9, 111]	rVSV-ΔM51-GFP
Capan-1	Downregulated [113]	Low [9, 111]	rVSV-ΔM51-GFP
Panc-1	Downregulated [112]	Low [9, 111]	rVSV-ΔM51-GFP
MIA PaCa2	Moderate [112]	Low [9, 111]	rVSV-ΔM51-GFP
Capan-2	High [113]	Low [9, 111]	rVSV-ΔM51-GFP
T3M4	Moderate [114]	Low [9, 111]	rVSV-ΔM51-GFP
CFPAC	Upregulated [110]_	High [9, 111]	rVSV-ΔM51-GFP
HPAC	Upregulated [110]_	High [9, 111]	rVSV-ΔM51-GFP
HPDE	High [115]	High [9, 111]	rVSV-ΔM51-GFP
Hs766T	High [113]	High [9, 111]	rVSV-ΔM51-GFP

Furthermore, a search for markers of susceptibility of cancer cells to this virus is underway [96] in order to improve the effectiveness of VSV for the treatment of malignant tumors, which will be discussed more thoroughly in the following sections.

Biomarkers of cancer cell resistance to rVSV virotherapy

Defects in interferon pathways that are typical of cancer cells [97] make oncolytic viruses promising therapeutic agents, but tumors differ greatly in terms of their susceptibility to viruses. For example, *in vitro* experiments demonstrated that some cancer cell lines incubated with IFN-1 acquired resistance to VSV, while others remained susceptible to its cytopathic activity [11]. J. Noser et al. showed that the activated RAS/Raf1/MEK/ERK pathway plays a crucial role in the emergence of abnormalities in the antiviral response in cancer cells. In particular, they demonstrated that infection with VSV causes rapid death of the NIH 3T3 cell line stably expressing active RAS or Raf1 [98].

The search for biomarkers of the susceptibility of cancer cells to oncolytic viruses, and VSV in particular, revealed that the *EGFR* and *HER2* genes are typically overexpressed in VSV-susceptible cell lines, unlike in resistant ones [96, 99] (*Table 1*). These findings suggest that activation of the EGFR/HER2 pathway and *HER2* gene overexpression can be potential biomarkers of tumor vulnerability to VSV oncolytic therapy [100].

Disturbances in the antiviral response in cancer cells, such as changes in IFN production pathways and deactivation of the JAK-STAT pathway, as well as reduced ISG production (Mx GTPase, OAS, TRIM, IFIT, Irf7, STING, APOBEC, viperin, etc.) [116, 117], may affect susceptibility to oncolytic viruses. The

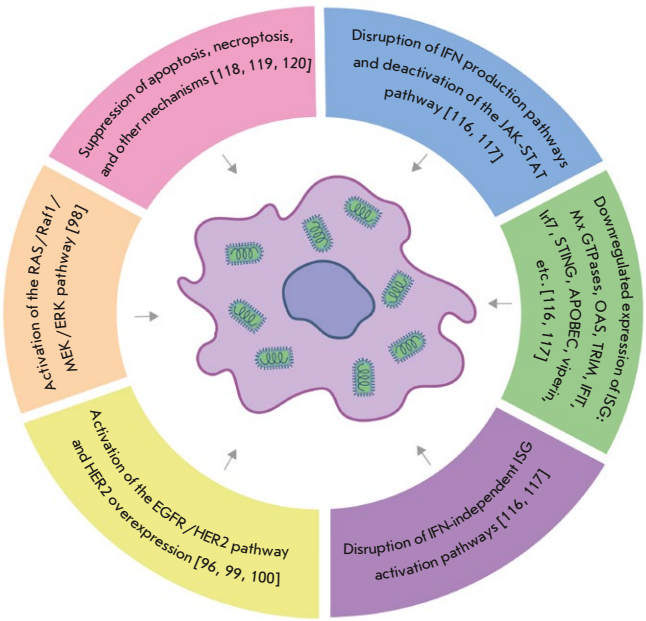

Fig. 2. A cell susceptible to VSV therapy. Knowing the molecular mechanisms underlying the differences in the susceptibility of cancer cells to viruses is essential for elaborating approaches to cancer treatment, identifying biomarkers of susceptibility to specific oncolytic viruses, predicting the effectiveness of virotherapy in each individual patient [96], and improving the effectiveness of cancer treatment

molecules involved in other mechanisms can also act as potential susceptibility markers. Thus, the hepatitis C virus (HCV) activates mitochondrial fission in the host cell, resulting in apoptosis inhibition and virus replication [118]. Inhibition of mitochondrial fission and mitophagy via the suppression of Drp1 (dynamin-related protein 1) led to reduced HCV replication and increased cellular resistance to viral infection [119]. Inhibition of necroptosis in cells was shown to enhance replication of the Zika virus (ZIKV) [120]. Meanwhile, downregulated RIPK3 expression can increase the susceptibility of cells to viral infection [121] (*Fig. 2*).

CONCLUSIONS

VSV-based drugs are promising antitumor agents, but it still remains essential to search for novel molecules that, as they are integrated into the VSV, would enhance its lytic and immunostimulatory properties, thus increasing the effectiveness and safety of such drugs.

Designing an effective VSV-based drug is complicated by the fact that some cancer cells are insusceptible to the virus, which may lead to poor therapy effectiveness in these types of malignant tumors. The effectiveness and safety of VSV-based drugs can be improved by incorporating mutations that increase the susceptibility of the virus to the cancer cells in the virus genome [81, 82], as well as by combining them with other oncolytic viruses, immunomodulators, CAR-T cell therapy agents, and conventional methods such as chemotherapy, surgery, and radiation therapy [5, 122, 123]. No universal markers for susceptibility to VSV virotherapy that would allow one to evaluate the effectiveness of the oncolytic in a specific tumor type and assess whether VSV virotherapy is suitable for a given patient have been identified thus far [96]. Therefore, more thorough research into the molecular mechanisms underlying the differences in the susceptibility of cancer cells to viruses, as well as the features of antiviral defense in cells in response to a VSV infection, is needed. ●

This work was supported by the grant of the State Program of the Sirius Federal Territory "Scientific and Technological Development of the Sirius Federal Territory" (Agreement No. 18-03 dated September 10, 2024).

REFERENCES

1. Khoshandam M., Soltaninejad H., Hamidieh A.A., Hosseinkhani S. // Genes Dis. 2024. V. 11. № 4. P. 101121.
2. Kroemer G., Chan T.A., Eggermont A.M.M., Galluzzi L. // CA Cancer J. Clin. 2024. V. 74. № 2. P. 187–202.
3. Macedo N., Miller D.M., Haq R., Kaufman H.L. // J. Immunother. Cancer. 2020. V. 8. № 2. P. e001486.
4. Dietzgen R.G., Kondo H., Goodin M.M., Kurath G., Vasilakis N. // Virus Res. 2017. V. 227. P. 158–170.
5. Gao Y. // DNA Cell. Biol. 2024. V. 43. № 2. P. 57–60.
6. Ahmed M., Cramer S.D., Lyles D.S. // Virology. 2004. V. 330. № 1. P. 34–49.
7. Wollmann G., Davis J.N., Bosenberg M.W., van den Pol A.N. // J. Virol. 2013. V. 87. № 12. P. 6644–6659.
8. Huang T.-G., Ebert O., Shinozaki K., García-Sastre A., Woo S.L.C. // Mol. Ther. 2003. V. 8. № 3. P. 434–440.
9. Murphy A.M., Besmer D.M., Moerdyk-Schauwecker M., Moestl N., Ornelles D.A., Mukherjee P., Grdzelishvili V.Z. // J. Virol. 2012. V. 86. № 6. P. 3073–3087.
10. Cary Z.D., Willingham M.C., Lyles D.S. // J. Virol. 2011. V. 85. № 12. P. 5708–5717.
11. Tarasova I.A., Tereshkova A.V., Lobas A.A., Solovyeva E.M., Sidorenko A.S., Gorshkov V., Kjeldsen F., Bubis J.A., Ivanov M.V., Ilina I.Y., et al. // Oncotarget. 2018. V. 9. № 2. P. 1785–1802.
12. Bray F., Laversanne M., Sung H., Ferlay J., Siegel R.L., Soerjomataram I., Jemal A. // CA Cancer J. Clin. 2024. V. 74. № 3. P. 229–263.

13. Santucci C., Mignozzi S., Malvezzi M., Boffetta P., Collatuzzo G., Levi F., La Vecchia C., Negri E. // Ann. Oncol. 2024. V. 35. № 3. P. 308–316.
14. Hanahan D. // Cancer Discov. 2022. V. 12. № 1. P. 31–46.
15. Lee E.Y.H.P., Muller W.J. // Cold Spring Harb. Perspect. Biol. 2010. V. 2. № 10. P. a003236.
16. Bertram J.S. // Mol. Aspects Med. 2000. V. 21. № 6. P. 167–223.
17. Bastos I.M., Rebelo S., Silva V.L.M. // Biochem. Pharmacol. 2024. V. 221. P. 116045.
18. Thienpont B., van Dyck L., Lambrechts D. // Mol. Cell. Oncol. 2016. V. 3. № 6. P. e1240549.
19. Zhao H., Wu L., Yan G., Chen Y., Zhou M., Wu Y., Li Y. // Signal Transduct. Target Ther. 2021. V. 6. № 1. P. 263.
20. Colotta F., Allavena P., Sica A., Garlanda C., Mantovani A. // Carcinogenesis. 2009. V. 30. № 7. P. 1073–1081.
21. Singh M., Overwijk W.W. // Cancer Immunol. Immunother. 2015. V. 64. № 7. P. 911–921.
22. Boisgerault N., Tangy F., Gregoire M. // Immunotherapy. 2010. V. 2. № 2. P. 185–199.
23. Ahmad A., Uddin S., Steinhoff M. // Int. J. Mol. Sci. 2020. V. 21. № 11. P. 3906.
24. Gershovich P.M., Karabelskii A.V., Ulitin A.B., Ivanov R.A. // Biochemistry (Moscow). 2019. V. 84. № 7. P. 695–710.
25. Petukhov A.V., Markova V.A., Motorin D.V., Titov A.K., Belozerova N.S., Gershovich P.M., Karabelsky A., Ivanov R.A., Zaikova E., Smirnov E.Y., et al. // Klinicheskaya Onkogematologiya/Clinical Oncohematology. 2018. V. 11. № 1. P. 1–9.
26. Hoos A. // Nat. Rev. Drug Discov. 2016. V. 15. № 4. P. 235–247.
27. Karabelskii A.V., Nemankin T.A., Ulitin A.B., Vaganov A.S., Mosina E.A., Ivanov R.A. // Biotekhnologiya. 2017. № 1. P. 10–29.
28. de Gruijl T.D., Janssen A.B., van Beusechem V.W. // Expert Opin. Biol. Ther. 2015. V. 15. № 7. P. 959–971.
29. Puduvalli V.K. // Oncology (Williston Park). 2016. V. 30. № 3. P. 222–223.
30. Malogolovkin A., Gasanov N., Egorov A., Weener M., Ivanov R., Karabelsky A. // Viruses. 2021. V. 13. № 7. P. 1271.
31. Kiaheyrati N., Babaei A., Ranji R., Bahadoran E., Taheri S., Farokhpour Z. // Life Sci. 2024. V. 349. P. 122734.
32. Babiker H.M., Riaz I.B., Husnain M., Borad M.J. // Oncolytic Virother. 2017. V. 6. P. 11–18.
33. Liang M. // Curr. Cancer Drug Targets. 2018. V. 18. № 2. P. 171–176.
34. Andtbacka R.H.I., Kaufman H.L., Collichio F., Amatruda T., Senzer N., Chesney J., Delman K.A., Spitler L.E., Puzanov I., Agarwala S.S., et al. // J. Clin. Oncol. 2015. V. 33. № 25. P. 2780–2788.
35. Puzanov I., Milhem M.M., Minor D., Hamid O., Li A., Chen L., Chastain M., Gorski K.S., Anderson A., Chou J., et al. // J. Clin. Oncol. 2016. V. 34. № 22. P. 2619–2626.
36. Ribas A., Dummer R., Puzanov I., VanderWalde A., Andtbacka R.H.I., Michielin O., Olszanski A.J., Malvehy J., Cebon J., Fernandez E., et al. // Cell. 2017. V. 170. № 6. P. 1109-1119.e10.
37. Kumar H., Kawai T., Akira S. // Int. Rev. Immunol. 2011. V. 30. № 1. P. 16–34.
38. Olive C. // Expert Rev. Vaccines. 2012. V. 11. № 2. P. 237–256.
39. Kaufman H.L., Kohlhapp F.J., Zloza A. // Nat. Rev. Drug Discov. 2015. V. 14. № 9. P. 642–662.
40. Wack A., Terczyńska-Dyla E., Hartmann R. // Nat. Immunol. 2015. V. 16. № 8. P. 802–809.
41. Vilcek J. // Nat. Immunol. 2003. V. 4. № 1. P. 8–9.
42. Sadler A.J., Williams B.R.G. // Nat. Rev. Immunol. 2008. V. 8. № 7. P. 559–568.
43. O'Connell R.M., Saha S.K., Vaidya S.A., Bruhn K.W., Miranda G.A., Zarnegar B., Perry A.K., Nguyen B.O., Lane T.F., Taniguchi T., et al. // J. Exp. Med. 2004. V. 200. № 4. P. 437–445.
44. Müller U., Steinhoff U., Reis L.F., Hemmi S., Pavlovic J., Zinkernagel R.M., Aguet M. // Science. 1994. V. 264. № 5167. P. 1918–1921.
45. Casrouge A., Zhang S.-Y., Eidenschenk C., Jouanguy E., Puel A., Yang K., Alcais A., Picard C., Mahfoufi N., Nicolas N., et al. // Science. 2006. V. 314. № 5797. P. 308–312.
46. Dupuis S., Jouanguy E., Al-Hajjar S., Fieschi C., Al-Mohsen I.Z., Al-Jumaah S., Yang K., Chapgier A., Eidenschenk C., Eid P., et al. // Nat. Genet. 2003. V. 33. № 3. P. 388–391.
47. Jouanguy E., Zhang S.-Y., Chapgier A., Sancho-Shimizu V., Puel A., Picard C., Boisson-Dupuis S., Abel L., Casanova J.-L. // Biochimie. 2007. V. 89. № 6–7. P. 878–883.
48. Minegishi Y., Saito M., Morio T., Watanabe K., Agematsu K., Tsuchiya S., Takada H., Hara T., Kawamura N., Ariga T., et al. // Immunity. 2006. V. 25. № 5. P. 745–755.
49. Der S.D., Zhou A., Williams B.R., Silverman R.H. // Proc. Natl. Acad. Sci. USA. 1998. V. 95. № 26. P. 15623–15628.
50. Meurs E., Chong K., Galabru J., Thomas N.S., Kerr I.M., Williams B.R., Hovanessian A.G. // Cell. 1990. V. 62. № 2. P. 379–390.
51. Elde N.C., Child S.J., Geballe A.P., Malik H.S. // Nature. 2009. V. 457. № 7228. P. 485–489.
52. Liu S.-Y., Sanchez D.J., Cheng G. // Curr. Opin. Immunol. 2011. V. 23. № 1. P. 57–64.
53. Shi H.-X., Yang K., Liu X., Liu X.-Y., Wei B., Shan Y.-F., Zhu L.-H., Wang C. // Mol. Cell. Biol. 2010. V. 30. № 10. P. 2424–2436.
54. Okumura A., Lu G., Pitha-Rowe I., Pitha P.M. // Proc. Natl. Acad. Sci. USA. 2006. V. 103. № 5. P. 1440–1445.
55. Haller O., Staeheli P., Kochs G. // Biochimie. 2007. V. 89. № 6–7. P. 812–818.
56. Haller O., Stertz S., Kochs G. // Microbes Infect. 2007. V. 9. № 14–15. P. 1636–1643.
57. Berthoux L., Sebastian S., Sokolskaja E., Luban J. // J. Virol. 2004. V. 78. № 21. P. 11739–11750.
58. Wang X., Hinson E.R., Cresswell P. // Cell Host Microbe. 2007. V. 2. № 2. P. 96–105.
59. Brass A.L., Huang I.-C., Benita Y., John S.P., Krishnan M.N., Feeley E.M., Ryan B.J., Weyer J.L., van der Weyden L., Fikrig E., et al. // Cell. 2009. V. 139. № 7. P. 1243–1254.
60. Pindel A., Sadler A. // J. Interferon Cytokine Res. 2011. V. 31. № 1. P. 59–70.
61. Kim G.N., Kang C.Y. // Virology. 2007. V. 357. № 1. P. 41–53.
62. Nunamaker R.A., Lockwood J.A., Stith C.E., Campbell C.L., Schell S.P., Drolet B.S., Wilson W.C., White D.M., Letchworth G.J. // J. Med. Entomol. 2003. V. 40. № 6. P. 957–963.
63. Rodríguez L.L. // Virus Res. 2002. V. 85. № 2. P. 211–219.
64. Letchworth G.J., Rodriguez L.L., Del Cbarrera J. // Vet. J. 1999. V. 157. № 3. P. 239–260.
65. Roberts A., Kretzschmar E., Perkins A.S., Forman J., Price R., Buonocore L., Kawaoka Y., Rose J.K. // J. Virol.

1998. V. 72. № 6. P. 4704–4711.
66. Geisbert T.W., Feldmann H. // J. Infect. Dis. 2011. V. 204 Suppl 3. P. S1075–1081.
67. Johnson J.E., Nasar F., Coleman J.W., Price R.E., Javadian A., Draper K., Lee M., Reilly P.A., Clarke D.K., Hendry R.M., et al. // Virology. 2007. V. 360. № 1. P. 36–49.
68. Whelan S.P., Ball L.A., Barr J.N., Wertz G.T. // Proc. Natl. Acad. Sci. USA. 1995. V. 92. № 18. P. 8388–8392.
69. Slough M.M., Chandran K., Jangra R.K. // mBio. 2019. V. 10. № 1. P. e02372-18.
70. Whitt M.A. // J. Virol. Meth.. 2010. V. 169. № 2. P. 365–374.
71. Moroz V.D., Gasanov N.B., Egorov A.D., Malogolovkin A.S., Nagornykh M.O., Subcheva E.N., Kolosova E.S., Fizikova A.Y., Ivanov R.A., Karabelsky A.V. // Acta Naturae. 2024. V. 16. № 1. P. 59–66.
72. Li H., Zhao C., Zhang Y., Yuan F., Zhang Q., Shi X., Zhang L., Qin C., Zheng A. // Emerg Microbes Infect. 2020. V. 9. № 1. P. 2269–2277.
73. Stewart J.H., Ahmed M., Northrup S.A., Willingham M., Lyles D.S. // Cancer Gene Ther. 2011. V. 18. № 12. P. 837–849.
74. Kurisetty V.V.S., Heiber J., Myers R., Pereira G.S., Goodwin J.W., Federspiel M.J., Russell S.J., Peng K.W., Barber G., Merchan J.R. // Head Neck. 2014. V. 36. № 11. P. 1619–1627.
75. Obuchi M., Fernandez M., Barber G.N. // J. Virol. 2003. V. 77. № 16. P. 8843–8856.
76. Porosnicu M., Mian A., Barber G.N. // Cancer Res. 2003. V. 63. № 23. P. 8366–8376.
77. Publicover J., Ramsburg E., Rose J.K. // J. Virol. 2005. V. 79. № 21. P. 13231–13238.
78. Ball L.A., Pringle C.R., Flanagan B., Perepelitsa V.P., Wertz G.W. // J. Virol. 1999. V. 73. № 6. P. 4705–4712.
79. Wertz G.W., Perepelitsa V.P., Ball L.A. // Proc. Natl. Acad. Sci. USA. 1998. V. 95. № 7. P. 3501–3506.
80. Publicover J., Ramsburg E., Rose J.K. // J. Virol. 2004. V. 78. № 17. P. 9317–9324.
81. Stojdl D.F., Lichty B.D., tenOever B.R., Paterson J.M., Power A.T., Knowles S., Marius R., Reynard J., Poliquin L., Atkins H., et al. // Cancer Cell. 2003. V. 4. № 4. P. 263–275.
82. Zemp F., Rajwani J., Mahoney D.J. // Biotechnol. Genet. Eng. Rev. 2018. V. 34. № 1. P. 122–138.
83. Bishnoi S., Tiwari R., Gupta S., Byrareddy S.N., Nayak D. // Viruses. 2018. V. 10. № 2. P. 90.
84. Fernandez M., Porosnicu M., Markovic D., Barber G.N. // J. Virol. 2002. V. 76. № 2. P. 895–904.
85. Gao Y., Whitaker-Dowling P., Watkins S.C., Griffin J.A., Bergman I. // J. Virol. 2006. V. 80. № 17. P. 8603–8612.
86. Shin E.J., Wanna G.B., Choi B., Aguila D., Ebert O., Genden E.M., Woo S.L. // Laryngoscope. 2007. V. 117. № 2. P. 210–214.
87. Ryapolova A., Minskaia E., Gasanov N., Moroz V., Krapivin B., Egorov A.D., Laktyushkin V., Zhuravleva S., Nagornych M., Subcheva E., et al. // Int. J. Mol. Sci. 2023. V. 25. № 1. P. 211.
88. Toropko M., Chuvpilo S., Karabelsky A. // Pharmaceutics. 2024. V. 16. № 8. P. 986.
89. Felt S.A., Grdzelishvili V.Z. // J. Gen. Virol. 2017. V. 98. № 12. P. 2895–2911.
90. Hagedorn C., Kreppel F. // Hum. Gene Ther. 2017. V. 28. № 10. P. 820–832.
91. Zheng M., Huang J., Tong A., Yang H. // Mol. Ther. Oncolytics. 2019. V. 15. P. 234–247.
92. Hamid O., Hoffner B., Gasal E., Hong J., Carvajal R.D. // Cancer Immunol. Immunother. 2017. V. 66. № 10. P. 1249–1264.
93. Kreppel F., Gackowski J., Schmidt E., Kochanek S. // Mol. Ther. 2005. V. 12. № 1. P. 107–117.
94. Fisher K.D., Stallwood Y., Green N.K., Ulbrich K., Mautner V., Seymour L.W. // Gene Ther. 2001. V. 8. № 5. P. 341–348.
95. Choi J.-W., Lee Y.S., Yun C.-O., Kim S.W. // J. Control Release. 2015. V. 219. P. 181–191.
96. Nikitina A.S., Lipatova A.V., Goncharov A.O., Kliuchnikova A.A., Pyatnitskiy M.A., Kuznetsova K.G., Hamad A., Vorobyev P.O., Alekseeva O.N., Mahmoud M., et al. // Int. J. Mol. Sci. 2022. V. 23. № 9. P. 5244.
97. Stojdl D.F., Lichty B., Knowles S., Marius R., Atkins H., Sonenberg N., Bell J.C. // Nat. Med. 2000. V. 6. № 7. P. 821–825.
98. Noser J.A., Mael A.A., Sakuma R., Ohmine S., Marcato P., Lee P.W., Ikeda Y. // Mol. Ther. 2007. V. 15. № 8. P. 1531–1536.
99. Yang F., Yang Y., Zeng W. // Natural Prod. Comm. 2020. V. 15. P. 1934578X2091286.
100. Wu S., Zhang Q., Zhang F., Meng F., Liu S., Zhou R., Wu Q., Li X., Shen L., Huang J., et al. // Nat. Cell. Biol. 2019. V. 21. № 8. P. 1027–1040.
101. Zhu H.-J., Ogawa M., Magata Y., Hirata M., Ohmomo Y., Namba H., Sakahara H. // Asia Ocean J. Nucl. Med. Biol. 2013. V. 1. № 2. P. 47–52.
102. Lun X., Senger D.L., Alain T., Oprea A., Parato K., Stojdl D., Lichty B., Power A., Johnston R.N., Hamilton M., et al. // J. Natl. Cancer Inst. 2006. V. 98. № 21. P. 1546–1557.
103. Kimpel J., Urbiola C., Koske I., Tober R., Banki Z., Wollmann G., von Laer D. // Viruses. 2018. V. 10. № 3. P. 108.
104. Bunn P.A., Helfrich B., Soriano A.F., Franklin W.A., Varella-Garcia M., Hirsch F.R., Baron A., Zeng C., Chan D.C. // Clin. Cancer Res. 2001. V. 7. № 10. P. 3239–3250.
105. Malilas W., Koh S.S., Lee S., Srisuttee R., Cho I.-R., Moon J., Kaowinn S., Johnston R.N., Chung Y.-H. // Int. J. Oncol. 2014. V. 44. № 4. P. 1177–1184.
106. Shi J.-H., Guo W.-Z., Jin Y., Zhang H.-P., Pang C., Li J., Line P.-D., Zhang S.-J. // Cancer Med. 2019. V. 8. № 3. P. 1269–1278.
107. Li X., Sun X., Wang B., Li Y., Tong J. // Asian J. Pharm. Sci. 2023. V. 18. № 1. P. 100771.
108. Nuciforo P.G., Pellegrini C., Fasani R., Maggioni M., Coggi G., Parafioriti A., Bosari S. // Hum. Pathol. 2003. V. 34. № 7. P. 639–645.
109. Paglino J.C., van den Pol A.N. // J. Virol. 2011. V. 85. № 18. P. 9346–9358.
110. Thomas G., Chardès T., Gaborit N., Mollevi C., Leconet W., Robert B., Radosevic-Robin N., Penault-Llorca F., Gongora C., Colombo P.-E., et al. // Oncotarget. 2014. V. 5. № 16. P. 7138–7148.
111. Moerdyk-Schauwecker M., Shah N.R., Murphy A.M., Hastie E., Mukherjee P., Grdzelishvili V.Z. // Virology. 2013. V. 436. № 1. P. 221–234.
112. Walsh N., Kennedy S., Larkin A., Corkery B., O'Driscoll L., Clynes M., Crown J., O'Donovan N. // Invest. New Drugs. 2013. V. 31. № 3. P. 558–566.
113. Shibata W., Kinoshita H., Hikiba Y., Sato T., Ishii Y., Sue S., Sugimori M., Suzuki N., Sakitani K., Ijichi H., et al. // Sci. Rep. 2018. V. 8. № 1. P. 6150.
114. Kimple R.J., Vaseva A.V., Cox A.D., Baerman K.M.,

Calvo B.F., Tepper J.E., Shields J.M., Sartor C.I. // Clin. Cancer Res. 2010. V. 16. № 3. P. 912–923.
115. Chang Z., Li Z., Wang X., Kang Y., Yuan Y., Niu J., Wang H., Chatterjee D., Fleming J.B., Li M., et al. // Clin. Cancer Res. 2013. V. 19. № 3. P. 549–559.
116. Goad D.W., Bressy C., Holbrook M.C., Grdzelishvili V.Z. // Mol. Ther. Oncolytics. 2022. V. 24. P. 59–76.
117. Larrieux A., Sanjuán R. // iScience. 2023. V. 26. № 1. P. 105749.
118. Lee J., Ou J.-H.J. // Curr. Opin. Virol. 2022. V. 52. P. 244–249.
119. Kim S.-J., Syed G.H., Khan M., Chiu W.-W., Sohail M.A., Gish R.G., Siddiqui A. // Proc. Natl. Acad. Sci. USA. 2014. V. 111. № 17. P. 6413–6418.
120. Wen C., Yu Y., Gao C., Qi X., Cardona C.J., Xing Z. // Front Cell Infect. Microbiol. 2021. V. 11. P. 637710.
121. Pan Y., Cai W., Cheng A., Wang M., Yin Z., Jia R. // Front. Immunol. 2022. V. 13. P. 829433.
122. Evgin L., Kottke T., Tonne J., Thompson J., Huff A.L., van Vloten J., Moore M., Michael J., Driscoll C., Pulido J., et al. // Sci. Transl. Med. 2022. V. 14. № 640. P. eabn2231.
123. Martin N.T., Bell J.C. // Mol. Ther. 2018. V. 26. № 6. P. 1414–1422.

Platforms for the Search for New Antimicrobial Agents Using *In Vivo C. elegans* Models

A. I. Kalganova[1], I. E. Eliseev[1], I. V. Smirnov[1,2,3*], S. S. Terekhov[1]
[1]Shemyakin–Ovchinnikov Institute of Bioorganic Chemistry, Moscow, 117997 Russian Federation
[2]Department of Chemistry, Lomonosov Moscow State University, Moscow, 119991 Russian Federation
[3]Endocrinology Research Center, Moscow, 117292 Russian Federation
*E-mail: ivansmr@inbox.ru
Received December 11, 2023; in final form, November 19, 2024
DOI: 10.32607/actanaturae.27348

ABSTRACT **Despite the achievements brought about by high-throughput screening technologies, there is still a lack of effective platforms to be used to search for new antimicrobial drugs. The antimicrobial activity of compounds continues, for the most part, to be assessed mainly using *in vitro* pathogen cultures, a situation which does not make easy a detailed investigation of the molecular mechanisms underlying host–pathogen interactions. *In vivo* testing of promising compounds using chordate models is labor-intensive and expensive and, therefore, is used in preclinical studies of selected drug candidates but not in primary screening. This approach does not facilitate the selection of compounds with low organ toxicity and is not suitable for the identification of therapeutic compounds that affect virulence factors. The use of microscopic nematode *C. elegans* to model human infections is a promising approach that enables one to investigate the host–pathogen interaction and identify anti-infective compounds with new mechanisms of action.**
KEYWORDS ***C. elegans*, microfluidics, infection model, pathogens, drug discovery, antimicrobials.**
ABBREVIATIONS **AMP – antimicrobial peptide; MIC – minimum inhibitory concentration; QS – quorum sensing.**

INTRODUCTION

The antibiotic resistance crisis goes hand in hand with the problem of searching for and developing new antibiotics. The first antibiotics were discovered using the principle of screening small compound libraries *in vivo* on animals, such as infected mice and rabbits [1]. This approach was soon abandoned in favor of a more productive, ethical, and convenient one: the testing of antibiotics on pathogen cultures *in vitro* [2]. Almost a century after the discovery of the first classes of antibiotics, the spread of resistance and an acute shortage of new antibiotics forced researchers to look for new high-throughput platforms and return to *in vivo* screening [3].

Currently, there are a number of effective platforms for screening antibacterial drugs active against multidrug-resistant pathogens, biofilms, and intracellular pathogens [3]. However, microbial resistance seems to remain a step ahead of efforts towards modern approaches to the search for and testing of new therapeutic molecules. Antimicrobial activity is for the most part assessed in pathogen cultures *in vitro*, but that hampers any detailed investigation of the molecular mechanisms mediating the host–pathogen interaction.

A new strategy may be searching for molecules possessing alternative mechanisms of action; e.g., compounds that block virulence, stimulate the immune response, or are prodrugs. Such compounds, which are called anti-infectives, as opposed to antibacterials, cannot be identified in conventional experiments on pathogen cultures *in vitro*. To search for them, in-

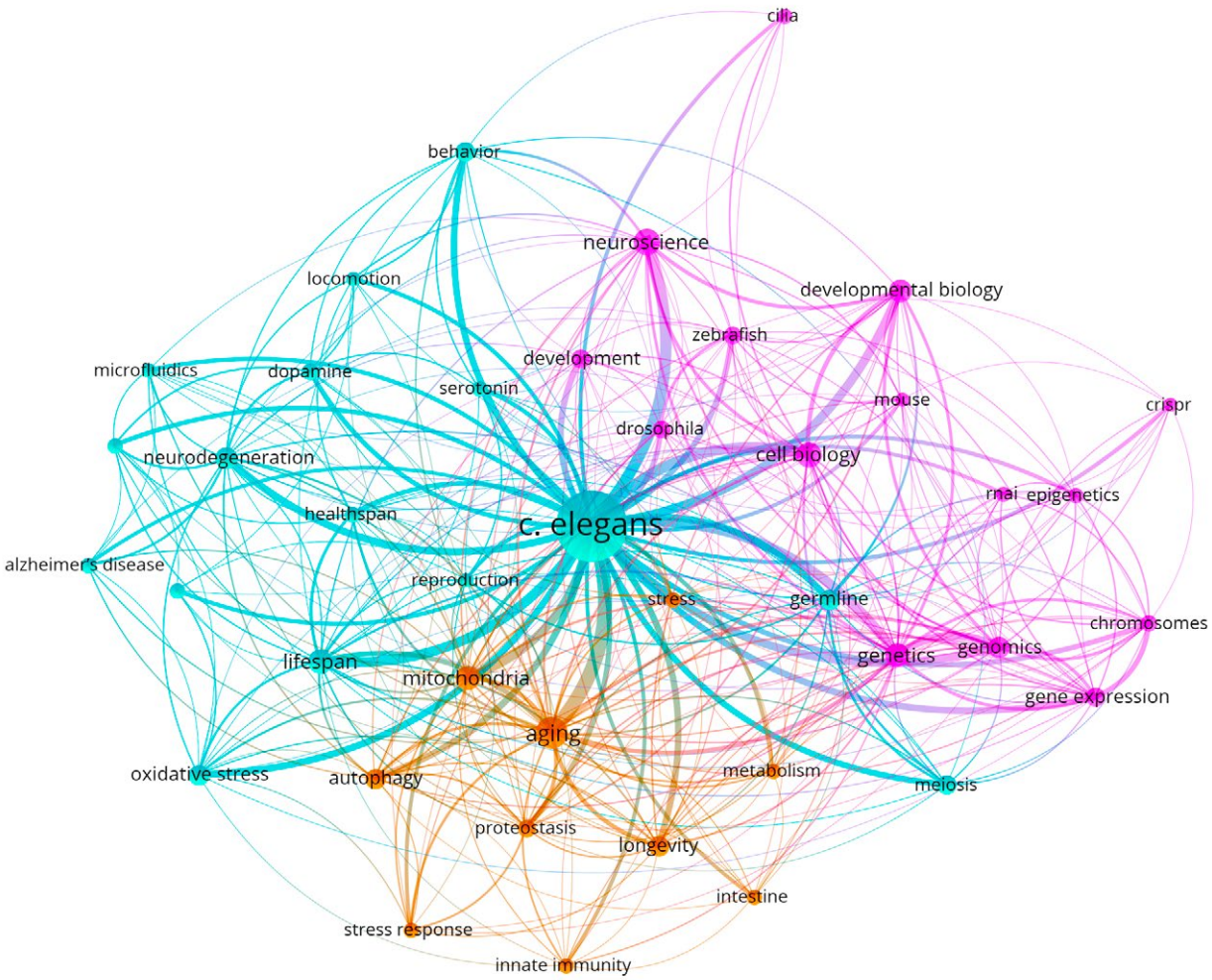

Fig. 1. Most popular areas of research with *C. elegans*. The map was generated using the VosViewer software; the search was performed using data from the PubMed database, from 2018 to 2023

fections are currently modeled on whole organisms: the nematode *Caenorhabditis elegans*, the fruit fly *Drosophila melanogaster*, and the fish *Danio rerio* [4]. The objective is to identify, by screening large compound libraries, both compounds that inhibit the activity of regulators of virulence factor production in certain pathogens and compounds that activate innate immunity [5].

Screening at the organism level has a number of advantages, the main one being the simultaneous acquisition of data on activity and toxicity, which makes the transition to other models more linear. Off-target effects, complete absorption, physiological distribution, general metabolism, and assessment of early toxicity *in vivo* also help to prioritize the selection of potential candidates [6]. The solution is to use small animals that have a simple biological system for the implementation of natural infection mechanisms in laboratory conditions. The model organism nematode *C. elegans* is suitable for high-throughput screening thanks to its small body size, short life cycle, and easy culture maintenance.

C. elegans is a popular model used in genetic and physiological studies (*Fig. 1*). Recently, this organ-

Table 1. Main nematode infection protocols

Protocol	Main characteristics
Slow killing	The destruction mechanism based on an infection-like process includes identification and proliferation of the pathogen in the intestine, with biofilm formation, and investigation of the suppression of bacterial pathogenesis
Fast killing	The main role is played by phenazine-1-carboxylic acid, which is extremely toxic to cells in an acidic environment
Liquid killing	Released endotoxins provide hypoxic conditions

ism has found increasing importance as a model for studying the mechanisms of host–pathogen interactions at the systemic level [3, 4].

The microscopic nematode *C. elegans* was first used to screen antibiotics in an infection model in 2006 [7]. The very first study discovered several compounds that suppressed development of the infection but did not kill the pathogenic bacteria. This points to the ability of such an *in vivo* model to identify molecules with alternative mechanisms of action. Soon, *C. elegans* was being shown to be well suited for modeling many human infections, both bacterial and fungal ones [8], and for studying intracellular infections [9] and biofilms [10].

The results of screening and identification of antimicrobial compounds using *C. elegans* have been published [11, 12]. Several research groups that have developed *in vivo* infection models and technologies for screening chemical libraries in *C. elegans* have identified a number of promising antimicrobial molecules using this system. In particular, a low-molecular-weight compound was discovered that protects the nematode from a *Pseudomonas aeruginosa* infection via the activation of innate immunity [13]. In a resistant *Staphylococcus aureus* infection model, a new class of retinoid antibiotics (CD437 and analogs) effective against bacterial persister cells was discovered [14].

The nematode *C. elegans* is a simple host model for studying the interactions between the innate immune system of animals and various pathogens [15]. Extensive genetic and molecular tools are available for *C. elegans*, which facilitate the in-depth analysis of host defense system components shared with mammals, and pathogen virulence factors.

Those investigations of the *C. elegans* response to bacterial infections revealed that the immune system of this organism uses evolutionarily conserved signaling pathways and synthesizes a number of effector molecules, some of which are also conserved (e.g., p38 MAPK signaling pathway) [16]. Despite having demonstrated immune responses to infection, the precise pattern recognition receptors in *C. elegans* remain to be identified.

C. elegans is the first multicellular organism with a fully sequenced genome. A high degree of similarity (60–80%) between many nematode genes and human ones has been established using bioinformatic approaches [17], which makes *C. elegans* a valuable model test object for toxicity studies [6]. As a result, the nematode *C. elegans* has become an instrumental model through which to understand the mechanisms of molecular pathogenesis of many human diseases. The innate immunity of *C. elegans* has become a subject matter in the study of immune defense and the role of cellular stress in the organism's response to infection, in particular in modeling gene activation in response to infection [18].

C. elegans BACTERIAL INFECTION MODELS

C. elegans can be infected with a selected pathogen by substituting its usual laboratory food source; e.g.,

with the *Escherichia coli* strain OP50, which is relatively non-pathogenic for this nematode. The bacterial environment is natural for nematodes [19]. The use of heat-killed *E. coli* bacteria is no more advantageous than the use of live bacteria, because thermal destruction makes such food unattractive for nematodes and, also, because they no longer contain all the nutrients essential for nematodes' normal development. In the control group of the *C. elegans* experiment, the use of bacteria killed by UV radiation is believed to be optimal [20]. Nematodes display behavioral reactions that develop in response to a bacterial pathogen [21]. Bacterial evasion and innate immune response are two ways in which *C. elegans* respond to pathogens [22].

There are various possible ways how the active substance can act in the model under consideration: direct killing, alteration of the nematode behavior, reduced pumping of the neuromuscular pump that joins the mouth to the intestine, activation of innate immunity, and influence on the quorum sense in bacteria; i.e., suppression of biofilm formation and transition to a chronic infection.

To date, there are standard protocols for infection and analysis of the bacterial effects on the vital activity of nematodes: e.g., a quantitative assessment of the bacterial load in *C. elegans* ISO 10872 [23–27]. Slow-killing models an infection-like process. The protocol uses agar, which is difficult to automate. In this case, it should be taken into account that the optimal temperature for nematodes to be maintained is 25°C; i.e., bacteria, when eaten by worms, continue to grow nonetheless. After the use of nematodes as a model organism for the investigation of bacterial infections had been demonstrated as fitting, liquid killing and fast killing protocols were also developed (*Table 1*). To date, these are the main protocols used [28].

The fast-killing mechanism is mainly focused on the action of the toxins in the medium. The liquid protocol does not provide for stable intestinal colonization or a normal life cycle for the nematode (difficult defecation, long egg retention, and, as a result, the formation of a 'bag of worms' phenotype). For example, infection with *P. aeruginosa* is accompanied by the secretion of pyoverdin, which is necessary for the replenishing of the intracellular iron pool in the bacterium. This siderophore, along with other substances, is absorbed by *C. elegans* from the liquid medium [29, 30]. After entering the host, pyoverdin gains access to ferric iron and removes it [31, 32], which leads to rapid cellular death of the nematode. Most protocols focus on the total toxic load, whereas the level of bacterial load in the nematode's digestive tract is often not analyzed.

C. elegans survival analysis

Many traits and characteristics of the nematode are used to assess the effect of a pathogen or a test compound: lifespan, body curvature and length, pharyngeal pump activity, number of bacteria inside the body, fat storage, vulva integrity changes, and progeny number. Also, stress assays are performed: the effects of thermal, acoustic, and oxidative stress are analyzed; changes in host gene expression and fluorescence initiated by the triggering of a certain signaling pathway are assessed; and accumulation of certain proteins is measured [33, 34]. The estimate of mean survival time of worms exposed to a certain bacterial isolate corresponds to the measure of bacterial virulence [35]. In such experiments, the 50% lethal time (LT50) is determined [34].

The lifespan can be determined in both solid and liquid media. A typical protocol involves counting live and dead worms from an initial synchronized population over a particular period of time [6]. Live and dead worms are counted in response to poking with a platinum wire, shaking, or exposure to light or based on the fluorescence signal of a vital dye (in liquid media). Upon nutrient deficiency, bacteria can secrete toxic metabolites and endotoxins into the medium. In this case, the survival analysis is multifactorial.

The first study on the use of *C. elegans* to model infections demonstrated that nematodes seeded into the wells of a plate with the culture medium remained viable for at least 14 days [7]. What allows nematodes to retain viability? Apparently, this is achieved thanks to simultaneous transfer of nematodes with bacteria, which are a feed source for the worms, as well as a sufficient amount of the nutrient medium to maintain the bacterial population.

Work with *C. elegans* began with detailed genetic typing, which later, together with the relative simplicity and convenience of experiments with this nematode, made this species a model [35]. Investigation of the microorganism–host interaction in the *C. elegans* model may ultimately provide information on how microbes affect the nervous system function in more complex animals [36], because a very close similarity between data obtained in mice and nematodes has been repeatedly demonstrated [37, 38].

The results obtained to date indicate the importance of accumulating a large body of homogeneous data. There exists a methodology for massive, si-

multaneous observation of nematodes, which may help in conducting complex genetic and behavioral studies, increasing the number of phenotypes that can currently be detected using larger numbers of simultaneously observed organisms [39]. However, this approach, although increasing the significance of the results, does not intensify the testing process.

Social behavior

Nematodes feeding on bacteria on agar often engage in communal feeding, which also influences the amount and rate of bacterial feeding [21]. Wild-type *C. elegans* isolates aggregate and feed in groups when grown in laboratory conditions, while the N2 laboratory strain consists of solitary feeders. The most potent hypothesis for why wild-type isolates aggregate is that aggregation allows the avoidance of high-oxygen environments. Pathogenic bacteria can infect *C. elegans* by attaching themselves to the cuticle, and collective feeding may mitigate the risk of infection by reducing surface exposure to bacteria [40]. Additionally, the developing phenotype is influenced by the presence and concentration of ascarosides, which are important small-molecule signals in nematodes. Different combinations of ascarosides mediate different phenotypes, and even small differences in their chemical structure are often associated with highly altered activity profiles in nematodes [41].

Probiotics

C. elegans has turned into a useful model for studying innate immunity in terms of microbiota–host interactions [42]. The molecular pathways initially triggered by pathogens are highly conserved in a large variety of organisms, from insects and nematodes, to mammals [43].

Animal probiotics can include diverse members of the microbiome, in particular *Bacillus subtilis*, *Lactobacillus spp.*, *Pseudoalteromonas spp.*, etc. [44–46]. The mechanisms of disease control by probiotics include enhanced immune response, competitive adhesion, pathogen antagonism, and disruption of the QS system. An important way in which probiotics can protect the host from pathogenic bacteria is to reduce bacterial colonization of the host gut and inhibit subsequent bacterial growth, which maintains the overall balance of the host gut microbiome composition [47]. Although many studies have shown that probiotics exhibit antibacterial and antifungal activity, their main mechanism of action is to reduce zoonotic pathogen infection-induced toxicity, either by displacing pathogens or by neutralizing toxic molecules [48].

The *C. elegans* model can be used not only in tests of antimicrobial drugs, but also in the search for new probiotics [49–51]. The relevance of *C. elegans* as a model organism in probiotic studies and elucidation of various molecular mechanisms is associated with highly conserved signaling pathways similar to those in higher mammals [51, 52].

The bacteria used to infect *C. elegans*

The effects of gram-negative *P. aeruginosa* and gram-positive *Staphylococcus aureus* have been well studied in nematodes [53, 54]. But recently, investigation of pathogenesis and biofilm formation has enabled the application of existing approaches to pathogen species (*Table 2*).

C. elegans is capable of mounting a specific response to bacterial pathogens at the transcriptome level. However, various bacterial pathogens, including *Enterococcus faecalis*, *Enterococcus faecium*, *Staphylococcus aureus*, *Serratia marcescens*, and *Photorhabdus luminescens*, also activate the expression of the same innate immune genes [55]. All of these bacterial pathogens cause colonization and bloating of the *C. elegans* intestinal lumen. Colonization with *P. aeruginosa* results in the activation of immune response genes and pathogen avoidance responses in *C. elegans*. Intestinal bloating caused by microbial colonization activates immune response genes and neuroendocrine pathways, inducing an avoidance response [56]. The ability to reveal specifically the regulated genes and pathways in the host or pathogen may help identify the novel metabolites produced by bacteria that affect host physiology [57].

Colonization by multiple bacterial species

The gastrointestinal microbiota is a complex microbial ecosystem. The influence of particular microorganisms on host signaling pathways can vary. There is growing evidence that genetic host variability determines the abundance of specific taxa living in the body [58]. For example, the possibility of co-culture of several pathogens in the nematode intestine was shown in [59]: two [60] or three [58] bacterial species and even transfer of the human intestinal microbiome [61]. Such experiments are performed to elucidate the role of interspecies interactions in the formation of host-associated microbial communities. Experimental bottom-up microbial ecology is a tool for studying the dynamics of bacterial gut communities in a model organism *C. elegans*, allowing us to elucidate the role of interspecies interactions in the combined microbiome–host system and bacterial competition within an *in vivo* environment [62].

Table 2. Examples of last-decade studies with testing of different bacterial pathogens in the *C. elegans* infection model

Bacterial pathogen	Test antibacterial compound	Protocol type	Reference
E. coli	–	Liquid killing	[104]
	Bacteriophages		[87]
A. baumannii	Curcumin, flavonoids	Liquid killing	[105]
	–	Slow killing	[106]
	AMP library	Liquid killing	[86]
M. nematophilum	–	Dar phenotype formation	[107], [108]
S. typhimurium	–	Liquid killing	[109]
S. aureus	Amoxicillin	Liquid killing	[110]
	P. guajava leaves extract	Liquid killing	[111]
	Resveratrol, econazole, paraquat	Slow killing	[74]
	AMP library	Liquid killing	[86]
	Panchgavya	Liquid killing	[50]
	Lactobacillus curvatus BGMK2-41	Slow killing	[43]
S. gordonii	–	Slow killing	[112]
L. monocytogenes	–	Slow killing	[113], [114]
P. aeruginosa	*P. guajava* leaves extract	Liquid killing	[111]
	Combination of linezolid and polymyxin B	Liquid killing	[73]
	Peonol	Liquid killing	[115]
	AMP library	Liquid killing	[86]
	Bacteriophages	Liquid killing	[87]
	B. megaterium and *P. mendocina*	Slow killing	[52]
	Gentamicin	Slow killing	[116]
	Holothuria atra	Liquid killing	[117]
	Lactobacillus curvatus BGMK2-41	Slow killing	[43]
S. marcescens	*P. guajava* leaves extract	Liquid killing	[111]
S. pyogenes	*P. guajava* leaves extract	Liquid killing	[73]
C. violaceum	*P. guajava* leaves extract	Liquid killing	[73]
B. thuringiensis	–	Liquid killing	[118]
	Lipopeptide thumolycin		[119]
B. anthracis	–	Slow killing	[120]
E. faecalis	AMP library	Liquid killing	[86]
	–	Slow killing	[55]
E. faecium	–	Slow killing	[55]
B. cepacia	–	Slow killing	[121]
E. cloacae	–	Slow killing	[122]
	Bacteriophages	Liquid killing	[87]
B. cereus	Carvacrol	Slow killing	[123]
H. pylori	Fucoidan extract	Slow killing	[124]
S. pyogenes	Biflavonoid fukugiside	Liquid killing	[125]
C. diphtheriae	–	Dar phenotype formation	[126]
C. violaceum	Peonol	Liquid killing	[115]
K. pneumoniae	Bacteriophages	Liquid killing	[87]
	Range of antibiotics		[127]

DRUG DELIVERY

Toxicological tests

One of the first areas of testing compounds using *C. elegans* as a model was toxicity testing in a liquid culture. Such tests were initially performed using the live/dead assay, plotting dose–response survival curves [63], then using behavioral tests [63, 64], and assessing specific phenotypes [65–67]. Later studies have demonstrated that the nematode is an organism suitable for studying toxicity and assessing the efficacy of some medicinal compounds.

Rapid toxicity tests are still used to this day [68–70]. Often, this model is used to test the toxic activity of bactericidal drugs with the efficacy proven *in vitro* [71]. In this case, not only solutions of synthetic compounds [72], but also natural extracts [73], nanoparticles [73, 74], and natural isolates [75, 76] are tested. This model was exploited to figure out a way to reduce the toxicity of a cryoprotectant applied in transplantation [77].

Screening of compounds using *C. elegans* enables a preliminary assessment of drug toxicity, which allows one to exclude compounds toxic to the host at an early stage, whereas *in vitro* testing identifies only bactericidal or bacteriostatic compounds [78]. Nematodes have been used in high-throughput drug screening to assess both toxicity and efficacy, and this screening approach has been commercialized by several companies (Nagi Bioscience, *InVivo* Biosystems, Magnitude Biosciences) [79].

Drug screening

In the nematode infection model, there is a limited choice of approaches for the delivery of test compounds: delivery by mixing a solution of the active agent with nematodes in a liquid nutrient medium [80] or adding to the solid medium [81]; delivery by mixing a solution of the active agent with a bacterial nutrient source (including labeling of bacteria) [82, 83].

If we consider such a method of delivery of the active agent as its packaging into micro- or nanoparticles, then the delivery will be one of the simplest ones, but an effective strategy that mimics the natural feeding of nematodes by the swallowing of bacteria-like microparticles. When the food content in the environment is low, nematodes can reduce the level of pharyngeal pumping to avoid ingesting non-nutritional particles; however, at high particle levels, many foreign particles still get inside worms [84]. This method provides targeted delivery of the active agent to the pathogen, avoiding toxic effects on tissues. Similar methods are also useful for assessing the pharmacokinetics of natural compounds [32]. Although nematodes are a promising model system for screening antimicrobial compounds, they are still far from fully reproducing mammalian biology. For example, nematodes have an effective detoxification system that can limit potential identification of compounds that act through the modification of host defense systems [85].

Many different classes of compounds have been tested for toxicity and efficacy using the *C. elegans* model [23–27]. The widest range of diversity comes with antimicrobial compounds, because the possibility to induce an infectious process in *C. elegans* using a variety of microorganisms provides for a large number of test pathogen–antimicrobial agent combinations, even without the simultaneous use of several drugs.

C. elegans lacks professional immune cells. Due to the lack of an adaptive immune system, this nematode relies solely on its innate immune defense to cope with a pathogen attack. In response to external stimuli, a cascade of reactions is triggered, which leads to the release of antimicrobial peptides (AMPs). AMPs are biologically active molecules produced by a variety of organisms and are an important component of nematode's innate immune response. For example, the effect of a small AMP library was tested and data on the efficacy of cecropin derivatives were collected. They were consistent with generally approved data [86].

This approach was first applied in a *C. elegans* model for a relatively low-throughput screening of 7,136 synthetic compounds and natural product extracts for activity against the opportunistic human pathogen *Enterococcus faecalis* [7]. Of these, 12 compounds were shown to provide host protection *in vivo* at concentrations significantly lower than the minimum inhibitory concentrations *in vitro*.

C. elegans infection models allow high-throughput screening of new anti-infective molecules. Such molecules may be used as probes to identify new mechanisms of bacterial pathogenesis [12]. These models may also be used to test the antimicrobial activity of bacteriophages before large-scale preclinical studies in mice [87]. The production of nematode biosensors that respond to changes in the intestinal microbiome composition seems promising. A biosensor for analyzing the host–microbiome interaction in the digestive tract was created in [62].

There are studies devoted to the search for new compounds using bioinformatic methods in the *C. elegans* model. For example, the effect of some compounds on the nematode lifespan was predicted using the DrugAge database [88]. This approach

may be translated into a prediction of the effect of compounds and pathogens on the nematode by creating a database of their mechanisms of action. Another method to analyze the response of nematodes is optogenetics. The use of optical methods enables quantitative monitoring of the metabolism of intestinal bacteria to assess the local and systemic effects of test compounds on nematode health [89].

Microfluidic technologies as a transition to personalized medicine

The possibility to manipulate single live *C. elegans* nematodes using microfluidics [76] is widely used in behavioral studies and microscopy. Studies in this area are focused on the search for antibiotics using medium-sized chemical libraries; for this purpose, 384-well plates are suitable. The development and behavior of *C. elegans* are studied using a variety of microfluidic technologies [78].

The use of any microfluidic chip ensures low consumption of synthesized bioactive molecules, such as AMPs, as well as targeted delivery of potential drugs in a small volume of liquid. The use of microfluidic trap technologies excludes the mutual influence of nematodes. Therefore, the natural development of elaborated approaches would be the use of high-throughput microfluidic screening technologies, which enable an analysis of large libraries of active compounds.

The existing platforms are divided mainly into four types: (i) platforms for monitoring lifespan and aging [90], (ii) platforms for screening toxicity and pathogenesis, (iii) platforms for studying neurobiological phenomena and behavioral tests [91], and (iv) platforms for drug discovery. Most of the developed microfluidic chips are aimed at solving the problems of sorting and studying the larval stages of nematodes.

The significant advantages of microfluidics have led to the development of devices for survival curve measurements. Microfluidic encapsulation of nematodes in single compartments was shown not to affect their lifespan [92]. Similar developments in the field of microfluidic technologies enable a transition from labor-intensive experiments on Petri dishes to automated and productive platforms for candidate selection. Metabolic by-products accumulate in worms and bacteria, and the biological state of bacteria changes in response to stress factors, which can have a secondary effect on worms. Although this effect can be minimized by repeated transfer of animals to new dishes, physical manipulations can lead to additional stress and partial loss of the population. The possibility to accurately and quickly control the environment is one of the many advantages of microfluidic devices [93]. There are also a number of responses to starvation as a stress factor. One such response is the cessation of egg-laying in adulthood. Cessation of egg-laying leads to matricidal internal hatching of progeny that is subsequently used by the mother as a food source. Such data are usually censored during statistical processing [94].

The use of microfluidic technologies solves such automation problems as (i) programmable control of fluid flows, handling small volumes of active compounds; (ii) uniform dosing of nematodes by volume; (iii) compartmentalization, in particular by sorting, and phenotypic profiling of individuals; (iv) long-term culturing under relatively constant environmental conditions; and (v) real-time monitoring, tracking multiple checkpoints.

A microfluidic chip with progeny filtration can be used to investigate aged populations without chemical sterilization (FUDR) or frequent plate-to-plate transfers, thereby avoiding the use of sterile strains [95]. Immobilization of single nematodes in a channel can be an excellent way to score high-resolution, real-time images [96].

The main drawback of many devices is that *C. elegans* swims in specially designed chambers, like liquid cultures in multi-well plates. Physiologically, swimming in a liquid culture is more energy consuming than crawling and extends the sleep period, which complicates the phenotyping procedure [97]. While *C. elegans* larvae exhibit quiescence during lethargus, adult worms occur in quiescence only in a few situations; e.g., after several hours of swimming or after exposure to extreme environmental conditions. In a broader context, sleep induced by flow events is defined as a behavior in which experimentally controlled external stimuli strongly influence the animal's transition speed between behavioral states.

Swimming and crawling worms exhibit significantly different gene expression profiles and lifespans [98]. Therefore, it is assumed that the results obtained using devices in which worms crawl rather than swim are best comparable to those obtained in a solid medium. The problem of immobility in many individuals can be overcome by using light to stimulate arousal and movement [99].

The introduction of microfluidic approaches to advanced visualization of bacterial colony dynamics and digestion kinetics *in vivo* opens the way to increased information content, throughput, and versatility of the methods aimed at assessing the interactions between microbiota and the *C. elegans* gut.

Microfluidic platforms for parallel on-chip studies are based on feeding worms with different bacterial strains and/or applying antimicrobial compounds [100]. The immune response was measured by expression of the immune response gene *irg-1* and was used to monitor expression changes upon exposure to the pathogenic bacterial strain *P. aeruginosa* [101]. The most common feature of such platforms is real-time phenotypic analysis of individuals and generation of survival curves from the data obtained [102].

Microfluidic technology that enables the study of bacterial pathogenesis was demonstrated in the Celab system [102]. The technology combines the capabilities of other devices to perform high-throughput monitoring, long-term microfluidic incubation of worms, individual tracking, and semi-automated measurements with progeny washing and food replenishment.

Therefore, microfluidics enables personalized phenotyping because microfluidic chips are able to collect individual responses throughout the worm's life [103]. Modern microfluidic systems exclude the need for repeated manual transfer of adults during survival tests, progeny sorting, or avoidance of swimming-induced stress throughout the life of fluid-grown animals. Therefore, the overall number of censored worms is reduced [93].

CONCLUSION

The *C. elegans* infection model can be empirically used as a host–pathogen system to assess the virulence of a new pathogen in studies of the innate immune response. Most of the studies of intestinal infection in *C. elegans* have been performed using a monobacterial culture. However, under natural conditions, the microbiome is represented by a complex consortium of microorganisms. Thus, further research on co-culture of several species is needed.

A logical continuation of the development of the technologies discussed in this review will be creating a microfluidic device that provides the nematode infection stage, followed by testing libraries of potential anti-infective compounds in infected individuals. The creation of such a device is based on the possibility to trigger a stable invasive infection in the nematode gut, as well as in a targeted way deliver test compounds and monitor their effects. Since microfluidics is scalable and adaptable, a microfluidic device may be used not only for basic research of pathogenesis, but also for high-throughput screening of candidate molecules.

A promising area is the combined use of the proposed platform for infection and screening on *C. elegans* and the technology of synthetic libraries of antimicrobial peptide biodiversity. The field of antimicrobial peptide development suffers from a lack of a high-tech tool for high-throughput synthesis and testing of candidate peptides. Formation of synthetic microbiota of antimicrobial peptide producers in *C. elegans* would fill this gap. ●

This study was supported by the Russian Science Foundation (grant No. 19-14-00331).

REFERENCES

1. Gensini G.F., Conti A.A., Lippi D. // Journal of Infection. 2007. V. 54(3). P. 221–224.
2. https://www.mdpi.com/2075-1729/13/5/1073. (Accessed August 14, 2024).
3. Lewis K. // Biochemistry (Mosc.). 2020. V. 85. № 12. P. 1469–1483.
4. Clatworthy A.E., Romano K.P., Hung D.T. // Nat. Chem. Biol. 2018. V. 14. № 4. P. 331–341.
5. Pujol N., Cypowyj S., Ziegler K., Millet A., Astrain A., Goncharov A., Jin Y., Chisholm A.D., Ewbank J.J. // Curr. Biol. 2008. V. 18. № 7. P. 481–489.
6. Nass R., Hamza I. //Current Protocols in Toxicology. 2007. V. 31. № 1. P. 1.9.1–1.9.18.
7. Moy T.I., Ball A.R., Anklesaria Z., Casadei G., Lewis K., Ausubel F.M. // Proc. Natl. Acad. Sci. USA. 2006. V. 103. № 27. P. 10414–10419.
8. Powell J.R., Ausubel F.M. // Methods Mol. Biol. 2008. V. 415. P. 403–427.
9. Balla K.M., Troemel E.R. // Cell Microbiol. 2013. V. 15. № 8. P. 1313–1322.
10. Desai S.K., Padmanabhan A., Harshe S., Zaidel-Bar R., Kenney L.J. // Proc. Natl. Acad. Sci. USA. 2019. V. 116. № 25. P. 12462–12467.
11. Kim W., Hendricks G.L., Lee K., Mylonakis E. // Expert Opin. Drug Discov. 2017. V. 12. № 6. P. 625–633.
12. Peterson N.D., Pukkila-Worley R. // Curr Opin Immunol. 2018. V. 54. P. 59–65.
13. Pukkila-Worley R., Feinbaum R., Kirienko N.V., Larkins-Ford J., Conery A.L., Ausubel F.M. // PLoS Genet. 2012. V. 8. № 6. P. e1002733.
14. Kim W., Zhu W., Hendricks G.L., van Tyne D., Steele A.D., Keohane C.E., Fricke N., Conery A.L., Shen S., Pan W., et al. // Nature. 2018. V. 556. № 7699. P. 103–107.

15. Siddhardha B., Dyavaiah M., Syed A. Model organisms for microbial pathogenesis, biofilm formation and antimicrobial drug discovery. Springer Nature, 2020. P. 684.
16. Ausubel F.M. // Nat. Immunol. 2005. V. 6. № 10. P. 973–979.
17. Helmcke K.J., Avila D.S., Aschner M. // Neurotoxicol. Teratol. 2010. V. 32. № 1. P. 62–67.
18. Kim D.H., Ausubel F.M. // Curr. Opin. Immunol. 2005. V. 17. № 1. P. 4–10.
19. Khan F., Jain S., Oloketuyi S.F. // Microbiol. Res. 2018. V. 215. P. 102–113.
20. Stuhr N.L., Curran S.P. // MicroPubl. Biol. V. 2023. doi: 10.17912/micropub.biology.000902.
21. Shtonda B.B., Avery L. // J. Exp. Biol. 2006. V. 209. № 1. P. 89–102.
22. Lee Y.-T., Wang M.C. // Dev. Cell. 2019. V. 49. № 1. P. 7–9.
23. Walker A.C., Bhargava R., Vaziriyan-Sani A.S., Brust A.S., Czyz D.M. // Bio Protoc. 2022. V. 12. № 2. P. e4291.
24. Höss S., Römbke J. // Environ. Sci. Pollut. Res. Int. 2019. V. 26. № 25. P. 26304–26312.
25. Wang L., Graziano B., Bianchi L. // STAR Protoc. 2023. V. 4. № 2. P. 102241.
26. Wibisono P., Sun J. // STAR Protoc. 2022. V. 3. № 3. P. 101558.
27. Moore R.S., Kaletsky R., Murphy C.T. // STAR Protoc. 2021. V. 2. № 1. P. 100384.
28. Manan A., Bazai Z.A., Fan J., Yu H., Li L. // Int. J. Mol. Sci. 2018. V. 19. № 12. P. 3915.
29. Kang D., Kirienko D.R., Webster P., Fisher A.L., Kirienko N.V. // Virulence. 2018. V. 9. № 1. P. 804–817.
30. Qi B., Han M. // Cell. 2018. V. 175. № 2. P. 571–582.e11.
31. Yang Z.-Z., Yu Y.-T., Lin H.-R., Liao D.-C., Cui X.-H., Wang H.-B. // Free Radic. Biol. Med. 2018. V. 129. P. 310–322.
32. Ha N.M., Tran S.H., Shim Y.-H., Kang K. // Appl. Biol. Chem. 2022. V. 65. № 1. P. 18.
33. Fayolle M., Morsli M., Gelis A., Chateauraynaud M., Yahiaoui-Martinez A., Sotto A., Lavigne J.-P., Dunyach-Remy C. // Genes (Basel). 2021. V. 12. № 12. P. 1883.
34. Caldwell G.A. // Dis. Model. Mech. 2023. V. 16. № 6. P. dmm050333.
35. Vasquez-Rifo A., Veksler-Lublinsky I., Cheng Z., Ausubel F.M., Ambros V. // Genome Biol. 2019. V. 20. № 1. P. 270.
36. Kim D.H., Flavell S.W. // J. Neurogenet. 2020. V. 34. № 3–4. P. 500–509.
37. Feigman M.S., Kim S., Pidgeon S.E., Yu Y., Ongwae G.M., Patel D.S., Regen S., Im W., Pires M.M. // Cell Chem. Biol. 2018. V. 25. № 10. P. 1185–1194.e5.
38. Kaito C., Murakami K., Imai L., Furuta K. // Microbiol. Immunol. 2020. V. 64. № 9. P. 585–592.
39. Perni M., Casford S., Aprile F.A., Nollen E.A., Knowles T.P.J., Vendruscolo M., Dobson C.M. // J. Vis. Exp. 2018. № 141. P. 1352–1362
40. Ding S.S., Romenskyy M., Sarkisyan K.S., Brown A.E.X. // Genetics. 2020. V. 214. № 3. P. 577–587.
41. https://www.ncbi.nlm.nih.gov/books/NBK153595/. (Accessed December 6, 2024).
42. Kumar A., Baruah A., Tomioka M., Iino Y., Kalita M.C., Khan M. // Cell Mol. Life Sci. 2020. V. 77. № 7. P. 1229–1249.
43. Dinić M., Jakovljević S., Đokić J., Popović N., Radojević D., Strahinić I., Golić N. // Sci. Rep. 2021. V. 11. № 1. P. 21258.
44. Roselli M., Schifano E., Guantario B., Zinno P., Uccelletti D., Devirgiliis C. // Int. J. Mol. Sci. 2019. V. 20. № 20. P. 5020.
45. Sugawara T., Sakamoto K. // Br. J. Nutr. 2018. V. 120. № 8. P. 872–880.
46. https://www.mdpi.com/1422-0067/25/1/537. (Accessed August 14, 2024).
47. Li Y.-X., Wang N.-N., Zhou Y.-X., Lin C.-G., Wu J.-S., Chen X.-Q., Chen G.-J., Du Z.-J. // Mar. Drugs. 2021. V. 19. № 3. P. 150.
48. Wang B., Zhou Y., Wang Q., Xu S., Wang F., Yue M., Zeng Z., Li W. // Cells. 2023. V. 12. № 10. P. 1438.
49. Wu-Chuang A., Bates K.A., Obregon D., Estrada-Peña A., King K.C., Cabezas-Cruz A. // Sci. Rep. 2022. V. 12. № 1. P. 14045.
50. Patel P., Joshi C., Funde S., Palep H., Kothari V. // F1000Res. 2018. V. 7. P. 1612.
51. Sharma K., Pooranachithra M., Balamurugan K., Goel G. // Microb. Pathog. 2019. V. 127. P. 39–47.
52. Mahesh R., Ilangovan P., Nongbri D., Suchiang K. // Indian J. Microbiol. 2021. V. 61. № 4. P. 404–416.
53. Matsunami K. // Front Nutr. 2018. V. 5. P. 111.
54. Schifano E., Marazzato M., Ammendolia M.G., Zanni E., Ricci M., Comanducci A., Goldoni P., Conte M.P., Uccelletti D., Longhi C. // Microbiologyopen. 2019. V. 8. № 6. P. e00756.
55. Yuen G.J., Ausubel F.M. // Virulence. 2018. V. 9. № 1. P. 683–699.
56. Singh J., Aballay A. // Dev. Cell. 2019. V. 49. № 1. P. 89–99.e4.
57. Chan J.P., Wright J.R., Wong H.T., Ardasheva A., Brumbaugh J., McLimans C., Lamendella R. // Sci. Rep. 2019. V. 9. № 1. P. 5545.
58. Ortiz A., Vega N.M., Ratzke C., Gore J. // ISME J. 2021. V. 15. № 7. P. 2131–2145.
59. Herman M.A., Irazoqui J.E., Samuel B.S., Vega N. // Front. Cell. Infect. Microbiol. 2022. V. 12. P. 1035545.
60. Pike V.L., Stevens E.J., Griffin A.S., King K.C. // Parasitology. 2023. V. 150. № 9. P. 805–812.
61. Walker A.C., Bhargava R., Vaziriyan-Sani A.S., Pourciau C., Donahue E.T., Dove A.S., Gebhardt M.J., Ellward G.L., Romeo T., Czyż D.M. // PLoS Pathog. 2021. V. 17. № 5. P. e1009510.
62. Rutter J.W., Ozdemir T., Galimov E.R., Quintaneiro L.M., Rosa L., Thomas G.M., Cabreiro F., Barnes C.P. // ACS Synth. Biol. 2019. V. 8. № 12. P. 2620–2628.
63. Peres T.V., Arantes L.P., Miah M.R., Bornhorst J., Schwerdtle T., Bowman A.B., Leal R.B., Aschner M. // Neurotox. Res. 2018. V. 34. № 3. P. 584–596.
64. Kudelska M.M., Lewis A., Ng C.T., Doyle D.A., Holden-Dye L., O'Connor V.M., Walker R.J. // Invert. Neurosci. 2018. V. 18. № 4. P. 14.
65. Yan J., Zhao N., Yang Z., Li Y., Bai H., Zou W., Zhang K., Huang X. // J. Biol. Chem. 2020. V. 295. № 50. P. 17323–17336.
66. Lenz K.A., Miller T.R., Ma H. // Chemosphere. 2019. V. 214. P. 60–69.
67. Kim S., Lee J.-H., Kim Y.-G., Tan Y., Lee J. // Int. J. Mol. Sci. 2022. V. 23. № 18. P. 10683.
68. Yu Z., Yin D., Hou M., Zhang J. // Chemosphere. 2018. V. 211. P. 278–285.
69. Schultz C.L., Lahive E., Lawlor A., Crossley A., Puntes V., Unrine J.M., Svendsen C., Spurgeon D.J. // Environ. Toxicol. Chem. 2018. V. 37. № 10. P. 2609–2618.
70. Moyson S., Town R.M., Joosen S., Husson S.J., Blust R.

// J. Appl. Toxicol. 2019. V. 39. № 2. P. 282–293.
71. Pormohammad A., Firrincieli A., Salazar-Alemán D.A., Mohammadi M., Hansen D., Cappelletti M., Zannoni D., Zarei M., Turner R.J. // Microbiol. Spectr. 2023. V. 11. № 4. P. e00628-23.
72. Zhou D. // Environ. Toxicol. Chem. 2018. V. 37. № 10. P. 2560–2565.
73. Huang T., Zeng M., Fu H., Zhao K., Song T., Guo Y., Zhou J., Zhai L., Liu C., Prithiviraj B., et al. // Ann. Clin. Microbiol. Antimicrob. 2022. V. 21. № 1. P. 38.
74. Mizdal C.R., Stefanello S.T., da Costa Flores V., Agertt V.A., Bonez P.C., Rossi G.G., da Silva T.C., Antunes Soares F.A., de Lourenço Marques L., de Campos M.M.A. // Microb. Pathog. 2018. V. 123. P. 440–448.
75. Moon J., Kwak J.I., An Y.-J. // Chemosphere. 2019. V. 215. P. 50–56.
76. Lee S., Kim Y., Choi J. // Ecotoxicol. Environ. Saf. 2020. V. 187. P. 109777.
77. Tedesco P.M., Schumacher G.J., Johnson T.E. // Cryobiology. 2019. V. 86. P. 71–76.
78. Mir D.A., Balamurugan K. // Biofouling. 2019. V. 35. № 8. P. 900–921.
79. Kukhtar D., Fussenegger M. // Biotechnol. Bioeng. 2023. V. 120. № 8. P. 2056–2071.
80. Gemeinder J.L.P., Barros N.R. de, Pegorin G.S., Singulani J. L., Borges F.A., Arco M.C.G.D., Giannini M.J.S.M., Almeida A.M.F., Salvador S.L. S., Herculano R.D. // J. Biomater. Sci. Polym. Ed. 2021. V. 32. № 1. P. 93–111.
81. Li J., Chotiko A., Chouljenko A., Gao C., Zheng J., Sathivel S. // Int. J. Food Sci. Nutr. 2019. V. 70. № 2. P. 172–181.
82. Qu M., Xu K., Li Y., Wong G., Wang D. // Sci. Total Environ. 2018. V. 643. P. 119–126.
83. Yang Y., Xu G., Xu S., Chen S., Xu A., Wu L. // Ecotoxicol. Environ. Saf. 2018. V. 165. P. 291–298.
84. Fueser H., Rauchschwalbe M.-T., Höss S., Traunspurger W. // Aquat. Toxicol. 2021. V. 235. P. 105827.
85. Chen J., Yang Y., Yao H., Bu S., Li L., Wang F., Chen F., Yao H. // Front. Cell Infect. Microbiol. 2021. V. 11. P. 818308.
86. Jayamani E., Rajamuthiah R., Larkins-Ford J., Fuchs B.B., Conery A.L., Vilcinskas A., Ausubel F.M., Mylonakis E. // Antimicrob. Agents Chemother. 2015. V. 59. № 3. P. 1728–1737.
87. Manohar P., Loh B., Elangovan N., Loganathan A., Nachimuthu R., Leptihn S. // Microbiol. Spectr. 2022. V. 10. № 1. P. e0139321.
88. Ribeiro C., Farmer C.K., de Magalhães J.P., Freitas A.A. // Aging (Albany NY). 2023. V. 15. № 13. P. 6073–6099.
89. Hartsough L.A., Park M., Kotlajich M.V., Lazar J.T., Han B., Lin C.-C.J., Musteata E., Gambill L., Wang M.C., Tabor J.J. // Elife. 2020. V. 9. P. e56849.
90. Rezaeianaran F., Gijs M.A.M. // RSC Adv. 2023. V. 13. № 25. P. 17230–17243.
91. Katzen A., Chung H.-K., Harbaugh W.T., Della Iacono C., Jackson N., Glater E.E., Taylor C.J., Yu S.K., Flavell S.W., Glimcher P.W., et al. // Elife. 2023. V. 12. P. e69779.
92. Wu J., Gao Y., Xi J., You X., Zhang X., Zhang X., Cao Y., Liu P., Chen X., Luan Y. // Ecotoxicol. Environ. Saf. 2022. V. 245. P. 114089.
93. Lee K.S., Lee L.E., Levine E. // Sci. Rep. 2016. V. 6. № 1. P. 35862.
94. Banse S.A., Blue B.W., Robinson K.J., Jarrett C.M., Phillips P.C. // PLoS One. 2019. V. 14. № 5. P. e0216283.
95. Saberi-Bosari S., Huayta J., San-Miguel A. // Lab. Chip. 2018. V. 18. № 20. P. 3090–3100.
96. Levine E., Lee K.S. // Anim. Cells Syst (Seoul). 2020. V. 24. № 6. P. 311–320.
97. Rahman M., Edwards H., Birze N., Gabrilska R., Rumbaugh K.P., Blawzdziewicz J., Szewczyk N.J., Driscoll M., Vanapalli S.A. // Sci. Rep. 2020. V. 10. № 1. P. 16190.
98. Laranjeiro R., Harinath G., Hewitt J.E., Hartman J.H., Royal M.A., Meyer J.N., Vanapalli S.A., Driscoll M. // Proc. Natl. Acad. Sci. USA. 2019. V. 116. № 47. P. 23829–23839.
99. Gonzales D.L., Zhou J., Fan B., Robinson J.T. // Nat. Commun. 2019. V. 10. P. 5035.
100. Viri V., Arveiler M., Lehnert T., Gijs M.A.M. // Micromachines (Basel). 2021. V. 12. № 7. P. 832.
101. Midkiff D., San-Miguel A. // Molecules. 2019. V. 24. № 23. P. 4292.
102. Sohrabi S., Cota V., Murphy C.T. // Lab on a Chip. 2023. V. 12. P. 2738–2757.
103. Atakan H.B., Xiang R., Cornaglia M., Mouchiroud L., Katsyuba E., Auwerx J., Gijs M.A.M. // Sci. Rep. 2019. V. 9. № 1. P. 14340.
104. Zhou M., Liu X., Yu H., Yin X., Nie S.-P., Xie M.-Y., Chen W., Gong J. // Front. Immunol. 2018. V. 9. P. 1745.
105. Raorane C.J., Lee J.-H., Kim Y.-G., Rajasekharan S.K., García-Contreras R., Lee J. // Front. Microbiol. 2019. V. 10. P. 990.
106. Espinal P., Pantel A., Rolo D., Marti S., López-Rojas R., Smani Y., Pachón J., Vila J., Lavigne J.-P. // Microb. Drug Resist. 2019. V. 25. № 5. P. 752–760.
107. Gravato-Nobre M.J., Nicholas H.R., Nijland R., O'Rourke D., Whittington D.E., Yook K.J., Hodgkin J. // Genetics. 2005. V. 171. № 3. P. 1033.
108. Hodgkin J., Kuwabara P.E., Corneliussen B. // Curr. Biol. 2000. V. 10. № 24. P. 1615–1618.
109. Aballay A., Ausubel F.M. // Curr. Opin. Microbiol. 2002. V. 5. № 1. P. 97–101.
110. Kong C., Tan M.-W., Nathan S. // Biol. Open. 2014. V. 3. № 7. P. 644–655.
111. Patel P., Joshi C., Birdi T., Kothari V. // F1000Res. 2019. V. 8. P. 12.
112. Naji A., Houston IV J., Skalley Rog C., Al Hatem A., Rizvi S., van der Hoeven R. // PLoS One. 2018. V. 13. № 8. P. e0202233.
113. Ke T., Santamaría A., Tinkov A.A., Bornhorst J., Aschner M. // Curr. Protoc. Toxicol. 2020. V. 84. № 1. P. e94.
114. Yang K.H., Yun B., Choi H.J., Ryu S., Lee W.J., Oh M.-H., Song M.-H., Kim J.N., Oh S., Kim Y., et al. // Food Sci. Anim. Resour. 2019. V. 39. № 1. P. 84–92.
115. Yang D., Hao S., Zhao L., Shi F., Ye G., Zou Y., Song X., Li L., Yin Z., He X., et al. // Front. Microbiol. 2021. V. 12. P. 692474.
116. Chadha J., Ravi, Singh J., Chhibber S., Harjai K. // Front. Cell Infect. Microbiol. 2022. V. 12. P. 899566.
117. Wang H., Chu W., Ye C., Gaeta B., Tao H., Wang M., Qiu Z. // Appl. Microbiol Biotechnol. 2019. V. 103. № 2. P. 903–915.
118. Wan L., Lin J., Du H., Zhang Y., Bravo A., Soberón M., Sun M., Peng D. // Environ. Microbiol. 2019. V. 21. № 3. P. 1086–1098.
119. Zheng D., Zeng Z., Xue B., Deng Y., Sun M., Tang Y.-J., Ruan L. // Microbiol. Res. 2018. V. 215. P. 22–28.
120. Turner M.J., Cox J.K., Spellman A.C., Stahl C., Bavari S. // Dev. Comp. Immunol. 2020. V. 102. P. 103453.
121. Pande A., Veale T.C., Grove A. // Infect. Immun. 2018. V. 86. № 9. P. e00322-18.
122. Khan S., Paravastu P., Jha P.N., Marathe S.A. // Microb. Pathog. 2020. V. 148. P. 104449.

123. Rajabli N., Williamson L., Nimmer P.S., Kelly-Worden M., Bange J.S., Ho Y., McKillip J.L. // Int. J. Biochem. Mol. Biol. 2018. V. 9. № 2. P. 11–21.
124. Palacios-Gorba C., Pina R., Tortajada-Girbés M., Jiménez-Belenguer A., Siguemoto É., Ferrús M.A., Rodrigo D., Pina-Pérez M.C. // Food Funct. 2020. V. 11. № 5. P. 4525–4534.
125. Nandu T.G., Subramenium G.A., Shiburaj S., Viszwapriya D., Iyer P.M., Balamurugan K., Rameshkumar K.B., Karutha Pandian S. // J. Med. Microbiol. 2018. V. 67. № 9. P. 1391–1401.
126. Chen Y.-W., Ton-That H. // Curr. Protoc. Microbiol. 2020. V. 58. № 1. P. e109.
127. Yao H., Xu A., Liu J., Wang F., Yao H., Chen J. // Front. Pharmacol. 2022. V. 13. P. 973551.

The Characteristics of the Metabolomic Profile in Patients with Parkinson's Disease and Vascular Parkinsonism

E. V. Predtechenskaya, A. D. Rogachev*, P. M. Melnikova
Novosibirsk State University, Novosibirsk, 630090 Russian Federation
*E-mail: artrogachev@yandex.ru
Received September 04, 2024; in final form, November 21, 2024
DOI: 10.32607/actanaturae.27511

ABSTRACT **The gradually increasing age of the world population implies that the prevalence of neurodegenerative diseases also continues to rise. These diseases are characterized by a progressive loss of cognitive and motor functions. Parkinson's disease, which involves the gradual death of specialized neural tissue, is a striking example of a neurodegenerative process. The pathomorphological analysis shows that chronic cerebral ischemia is accompanied by extensive complex neurodegeneration; parkinsonism is its clinical manifestation in 20–30% of cases. Although Parkinson's disease and vascular parkinsonism are similar, these two pathologies have fundamentally different etiopathogeneses. But their set of differential diagnosis traits is confined to some features of the neurological status. There currently exist no diagnostic markers for individual neurodegenerative pathologies or the neurodegeneration phenomenon in general. Metabolomic profiling can be a promising means for finding a unique "fingerprint" of the disease. Identifying the biomarkers of various neurodegenerative diseases will help shorten the time to the diagnosis, forecast the course of the disease, and personalize the therapeutic approach. This review summarizes and compares the current concepts of metabolomics research into Parkinson's disease and vascular parkinsonism, as well as the respective animal models.**
KEYWORDS **metabolomics, mass spectrometry, biomarker, Parkinson's disease, vascular parkinsonism.**
ABBREVIATIONS **PD – Parkinson's disease; HPLC/MS – high-performance liquid chromatography–mass spectrometry; BBB – blood–brain barrier; LC/MS – liquid chromatography–mass spectrometry; MRI – magnetic resonance imaging; CSF – cerebrospinal fluid; VP – vascular parkinsonism; CNS – central nervous system; CVD – cerebrovascular disease.**

INTRODUCTION

Neurodegenerative diseases are among the most common causes of disability in developed countries. The growing wellbeing of the planet's population has come with increasing human life expectancy and higher demands on the quality of life. Neurodegeneration is also an integral part of aging, being as it is responsible for the erosion in human functional ability and loss of cognitive capacity. Parkinson's disease (PD) is a multisystem neurodegenerative disease with motor (hypokinesia, tremor, and rigidity) and non-motor symptoms (cognitive impairment). The pathogenesis profile of PD is mostly characterized by the destruction of dopaminergic neurons in the substantia nigra. But many different structures of the central nervous system are also caught up in it. Such widespread neurodegeneration leads to pronounced neurological deficit, which manifests itself as significant social and household disorientation of patients [1–3].

Vascular parkinsonism (VP) is clinically described as symmetric lower-body parkinsonism, which is characterized by postural instability, freezing of gait, and frequent falls [4]. However, there exists no specific clinical symptom that would be pathognomonic of VP. Various chronic cerebrovascular diseases (CVDs) are the pathophysiological foundation of VP, microangiopathy induced by chronic hypertension being the most common one [5]. During brain imaging, VP is shown to be associated with white matter hyperintensities or multiple infarcts in the basal ganglia and subcortical regions [6, 7]. CVDs are characterized by the involvement of the whole brain tissue (neuronal and non-neuronal) into degeneration, which implies that complex post-ischemic neurodegeneration follows [8].

Hence, although the impact of neurodegenerative processes on the life of our contemporaries is quite relevant, such diseases often remain difficult to diag-

nose. Currently, there are specific diagnostic laboratory markers for neither neurodegeneration in general nor neurodegenerative diseases in particular. Thus, PD and VP are differentially diagnosed in practice only according to the clinical findings, which is often insufficient.

This review focuses on the features of the changes in the metabolomic profile of patients with PD and VP. Metabolomic analysis is a promising research method that allows one to mine data on the biochemical changes taking place during a pathological process and identify potential biomarkers of the disease. Such data may both deepen the fundamental knowledge of the pathogenesis of parkinsonian disorders and propose potential diagnostic tools for practical application.

METABOLOMIC STUDIES IN BIOMARKER SEARCH

Metabolomics is the systematic identification and quantitation of all the metabolites present in a biological system, which consists of numerous molecules that exhibit different physical and chemical properties and exist over an extensive dynamic range. The overall analysis of metabolites can improve our knowledge about the physiological, pathological and biochemical statuses of a being, information which can be further combined with chemical and informatics methods [9].

Metabolites are not only endogenous substances present in the body; they can also include products of the metabolism of pharmaceuticals, environmental chemicals, and such substances as the products of the interaction between the host organism and its gut microbiota. Even minor changes in endogenous and exogenous factors can affect metabolite levels. Hence, metabolomics has a great potential to help us identify the relationship existing between genetic, environmental, and physiological elements and certain pathological conditions [10].

Metabolomic studies can improve our understanding of the mechanisms of diseases and therapeutic effects; they can also enable us to predict individual disease progression.

PATHOGENETIC PATHWAYS OF PARKINSON'S DISEASE

PD is based on progressive degeneration of the nigrostriatal dopaminergic pathway, with significant neuronal loss in the substantia nigra pars compacta and dopamine depletion. Along with disruption of the nigrostriatal dopaminergic system, in patients with PD neurodegeneration affects many groups of neurons residing in certain parts of the cerebral cortex, thalamus, brainstem, spinal cord, as well as in sympathetic and parasympathetic ganglia. This leads to the degeneration and death of both nigral neurons and the neurons located in extranigral areas [11]. According to Braak et al., neurodegeneration progression involves certain morphological stages: from the primary lesion of nuclei of the vagus nerve and the olfactory bulb to the gradual death of neurons in the substantia nigra pars compacta. This sequence is consistent with the development of clinical symptoms of PD ranging from autonomic disorders to motor and cognitive impairment [12]. It is noteworthy that early clinical signs of the disease occur only after 60–80% of substantia nigra neurons have been lost [13], which becomes responsible for the severity of the pathological process down the road.

The etiology and pathogenesis of PD still need thorough study; however, they are known to involve many predisposing factors (primarily genetic ones) and pathogenic pathways. The latter include:

(1) the formation of pathological specific α-synuclein in the form of Lewy bodies or Lewy neurites;

(2) oxidative stress associated with mitochondrial dysfunction;

(3) proteolytic stress caused by dysfunction of the ubiquitin–proteasome system; and

(4) local inflammation [11, 14].

Probably, none of the aforelisted mechanisms acts on its own; on the contrary, they mutually potentiate each other's effect. Moreover, each of the aforementioned pathways can induce intracellular apoptosis, which is the final common mechanism of neuronal loss in PD.

The native α-synuclein molecule in the brain is mostly unfolded and has no well-defined tertiary structure. When interacting with negatively charged lipids such as phospholipids (components of cell membranes), α-synuclein (α-Syn) acquires a β-sheet-rich amyloid-like structure that is prone to aggregation [15]. In turn, formation of α-Syn inhibits potentiation in mitochondria, thus causing the dysfunction associated with complex I, a component of the electron transport chain [16]. For this and probably other reasons, patients with PD show multiple signs of oxidative stress in the substantia nigra. In particular, this is manifested as reduced levels of endogenous antioxidants (e.g., glutathione), while the levels of oxidation products of proteins, lipids, and DNA are significantly elevated. Hence, there appears to be a relationship between the theories of α-synuclein accumulation and mitochondrial stress [17].

Another important clue to the importance of mitochondria in disease pathogenesis is that many of the known genes causing familial PD are involved in mitochondrial homeostasis. These genes include the known *PINK1/Parkin* genes, which participate in the pathway regulating dysfunctional mitochondria: the process known as mitophagy [18].

Failures in protein clearance are also observed in patients with PD, along with mitochondrial dysfunction. Within cells, there are two central systems responsible for the removal of malfunctioning proteins: the ubiquitin–proteasome system and the autophagy lysosomal pathway. Monomeric α-Syn is normally cleared by both systems, and disruption of either of these mechanisms is implicated in the pathogenesis of PD, as it promotes the accumulation of defective proteins, including misfolded α-Syn [19].

METABOLOMIC STUDIES OF PARKINSON'S DISEASE

The metabolome of patients with PD is studied using both non-targeted and targeted analytical approaches. The former involve large-scale metabolite screening followed by biomarker search among unknown metabolites, while the latter are based on the analysis and evaluation of a range of metabolites of interest, such as catecholamines, amino acids, purines, and urates. Most metabolomic studies rely on the analysis of cerebrospinal fluid (CSF) and blood, although other biological specimens such as patient urine, feces, or brain tissue were examined in some studies.

Metabolomic studies of cerebrospinal fluid in Parkinson's disease

Irregularities in the CSF composition is directly related to pathological changes in the brain, making CSF one of the preferred specimens for neuropathologic research. Taking into account the marked depletion of nigrostriatal dopaminergic neurotransmission in patients with PD, by measuring the levels of dopamine and its metabolites, one could identify potential markers of the pathophysiological stage of the disease. However, such compounds can be reliably detected only in patients who are not on levodopa. Thus, a reduced level of dihydroxyphenylacetic acid (DOPAC) is one of the markers of changes in dopamine metabolism in PD [20]. Furthermore, it was demonstrated that DOPAC can be used as a marker of early stages of the disease [21]. Not only DOPAC, but also homovanillic acid (HVA, the major catabolite of dopamine) is regarded as a biomarker of PD; however, it currently is considered a less reliable marker of central dopamine metabolism compared to DOPAC [22]. Trupp et al. reported that the CSF level of 3-hydroxyisovaleric acid is reduced in patients with PD [23]. Interestingly, 3-hydroxyisovaleric acid is degraded by the same enzyme as tyrosine (levodopa precursor). The same study additionally reported that tryptophan and creatinine levels are decreased in PD patients.

Purines circulating in the CSF of patients with PD are also of interest. LeWitt et al. studied changes in the level of xanthine (a precursor of urates) in PD and demonstrated that the ratio of xanthine to homovanillic acid concentrations in CSF can be both a sign of the disease *per se* and a biomarker of the gravity of the patient's condition [24].

An analysis of the CSF metabolome in patients with PD showed changes in the metabolism of glycine, serine, and threonine amino acids [25]. Differences in the contents of metabolites such as sarcosine and alpha-N-phenylacetyl-*L*-glutamine were found in the blood plasma and CSF of patients with PD compared to healthy donors. These compounds are involved in oxidative stress response in the metabolic pathways of sphingolipids, glycerophospholipids, and amino acids and can help in the early diagnosis of PD. The association of the oxidative stress metabolic pathways with PD is also supported by changes in the tricarboxylic acid profile, which is indicative of the development of mitochondrial dysfunction in this disease [26]. The same study revealed changes in the lipid profile in PD patients: an elevated level of medium- and long-chain fatty acids, as well as changes in diacylglycerol, phosphatidylcholine, and phosphatidylethanolamine metabolism.

Metabolomic studies of blood plasma in Parkinson's disease

Metabolomic studies of blood plasma are becoming increasingly the preferred route thanks to the minimal invasiveness of sampling and the relative availability of blood specimens. Various amino acids, fatty acids, acylcarnitines, lipids, purines, organic acids, which are the components of the energy metabolic pathway, oxidative stress responses, and metabolic pathways specific only to PD, are considered as potential blood plasma biomarkers in PD (*Table 1*).

Chang et al. [27] described changes in the contents of kynurenine metabolites in PD: they considered these compounds a potential pool of disease biomarkers and discovered a novel therapeutic strategy, where kynurenic acid was additionally used or the quinolinic acid level was reduced using kynurenine-3-monooxygenase inhibitors [27]. Moreover, Havelund et al. showed that kynurenine metabolism is also associated with the development of levodopa-induced dyskinesia, and that the elevated blood plasma ratio of 3-hydroxykynurenine to kynurenic acid can predict the potential progression of dyskinesia [28].

There are studies where urates are regarded as a promising biomarker of risk, diagnosis, and prognosis of PD. It was reported that the CSF and blood levels of urates are significantly reduced in patients with PD compared to the controls; high urate levels can be indicative of lower risk and slower disease progression. Elevated levels of these metabolites, which are impor-

Table 1. Potential metabolomic markers of Parkinson's disease

Biological matrix	Clinical stage of the disease	Patients receiving specialized therapy	Found biomarkers	Reference
CSF	n/d	No	DOPAC, HVA	[20]
CSF	n/d	No	DOPAC	[21]
CSF	n/d	n/d	3-Hydroxyisovaleric acid, tryptophan	[23]
CSF, blood plasma	Early stages (1–2 according to the Hoehn and Yahr scale)	No	Xanthine/HVA ratio (CSF); caffeine metabolites and inosine (blood plasma)	[24]
CSF	Different stages (1–4 according to the Hoehn and Yahr scale)	Yes	Glycine, serine, threonine	[25]
CSF	n/d	Yes	Profile of tricarboxylic acids, medium- and long-chain fatty acids, diacylglycerol, phosphatidylcholine, phosphatidylethanolamine	[26]
Blood plasma	Different stages (1–4 according to the Hoehn and Yahr scale)	Yes	Kynurenic acid, kynurenic acid/kynurenine ratio, quinolinic acid (late stages)	[27]
Blood plasma	n/d	Yes	3-Hydroxykynurenine/kynurenic acid ratio, 5-hydroxytryptophan	[28]
Blood plasma	n/d	Yes	Uric acid (PD, LRKK), hypoxanthine (PD)	[30]

Note: n/d – no data in the original article.

tant biogenic antioxidants, may help combat oxidative stress in the pathogenesis of PD. Various mechanisms have been proposed to explain the paradoxical effects of uric acid, but its significance as a causative, compensatory, or arbitrary risk factor remains unclear. High uric acid levels were shown to play an important role in preventing the involvement of dopaminergic cells in the pathophysiology of PD through its function as an endogenous antioxidant [29]. LeWitt et al. revealed changes in the profile of caffeine metabolites during the progression of PD, as well as a decline in the plasma level of inosine in patients with PD [24]. Differences in uric acid levels and purine profiles were also found in PD patients carrying a mutation in the *LRRK2* gene and in healthy donors [30].

Changes in the bile acid profile can be a potential metabolomic marker of PD. For example, Shao et al. found increased levels of a number of bile acids (including microbiota-associated ones) in patients with PD [31]. Changes in the bile acid profile were shown both for patients carrying a mutation in the *LRRK2* gene and in patients with idiopathic PD along with changes in the purine base profile [32].

As mentioned previously, PD is a multifactorial disease; compelling epidemiologic data suggest a possible association between traumatic brain injury (TBI) and the onset of parkinsonian syndrome. Changes in the plasma levels of glutamate were observed by HPLC/MS in patients with TBI and those with PD, thus an indication of a possible "excitotoxic" role of glutamate in their pathogenesis [33].

The metabolomic approach can also identify biomolecular and metabolic changes affecting the onset and progression of the disease. Thus, changes in the spermidine metabolism and the N1,N8-acetylspermidine level can be a prognostic marker of PD progression, which may lead to a new strategy for delaying or slowing down the progression [34]. A strong correlation between the levels of alanine, methionine, serine, purine, a number of fatty acids, polyamines, and tryptophan metabolites and progression of PD was demonstrated [23, 35, 36].

Acylcarnitines can be potential markers of oxidative stress and mitochondrial dysfunction in patients with PD. Thus, changes in the acylcarnitine profile may be indicative of early stages of PD [37]. In addition, differences in the acylcarnitine profile were found in patients with PD and those with essential tremor [38].

Metabolomic studies of Parkinson's disease in experimental models

Different types of animal models have been developed to study PD, but only a number of them have been used in metabolomic studies. For example, such models include α-Syn knockout, transgenic α-Syn, α-Syn overexpression, Park2 knockout, and toxicological models. The metabolic profile of the experimental-

ly induced disease has been studied mainly in animal brain tissue, which better reflects pathophysiological changes but has obvious limitations in extrapolating similar processes to humans with PD.

Farmer et al. reported significant changes in the levels of lipids (belonging to the phosphatidylcholine and lysophosphatidylcholine classes) in brain tissue in the toxin (6-hydroxydopamine)-induced model of PD. These findings can be attributed to increased oxidative damage to lipids and also indicate that these molecules play an important structural and neurofunctional role [39].

Another study focusing on the metabolome of brain tissue, conducted in a model of PD induced by unilateral injection of preformed fibrils of α-synuclein into the olfactory bulb, showed dysregulation of taurine and the hypotaurine metabolism, bile acid synthesis, metabolism of glycine, serine, and threonine, as well as the tricarboxylic acid cycle, which correlated with the emergence and progression of pathologic α-Syn [40]. Theoretically, the emergence of these α-Syn aggregates is accompanied by the suppression of the metabolic pathways of glycine, serine, and threonine (in normal nervous tissue, these substances can be converted to creatine, which is a donor of phosphate groups for ATP).

Kim et al. showed a reduction in the levels of *L*-3,4-dihydroxyphenylalanine (levodopa) and dihydroxyphenylacetic acid in mice at the preclinical prodromal stage of PD induced by 1-methyl-4-phenyl-1,2,3,6-tetrahydropyridine (MPTP) [41]. Theoretically, these changes can be regarded as biomarkers of the "presymptomatic" stage of PD. Other potential markers of PD can include 5'-methylthioadenosine, tetradecanoylcarnitine, phytosphingosine-1-P, ceramide d18:0/18:0, lysophosphatidylcholine 20:4(5Z,8Z,11Z,14Z), *L*-palmitoylcarnitine, tetracosanoylglycine, morphiceptin, and stearoylcarnitine; their levels were found to have changed when studying the midbrain in the MPTP-induced mouse model of PD [42].

Lu et al. identified the metabolites involved in oxidative stress, energy deficiency, and neuronal damage in goldfish with MPTP-induced PD using NMR [43]. The model was characterized by elevated levels of leucine, isoleucine, valine, and alanine amino acids, as well as alanylalanine, creatinine, myo-inositol, 18:2 fatty acid and total fatty acids, as well as simultaneous reduction in the levels of N-acetylaspartate, phosphocreatine, phosphocholine, betaine, glutamine, 3-hexenedioate, acetamide, malonate, isocitrate, scyllo-inositol, phosphatidylcholines, cholesterols, omega-3 fatty acids, and polyunsaturated fatty acids in the brain of goldfish. It was demonstrated by NMR that activity of the glutamate–glutamine cycle in the striatum of MPTP-treated mice was excessively high [44]. In the same mouse model, Pedro Amorim Neto et al. showed changes in the metabolic profile both in brain tissues and in peripheral structures such as the intestine using NMR [45]. Metabolite expression in blood, brain, colon, and feces specimens was deemed mostly indicative of inflammatory aspects, cytotoxicity, and mitochondrial dysfunction (oxidative stress and energy metabolism). A study conducted in mice showing symptoms of MPTP-induced PD and gut dysbiosis showed that biomarkers characteristic of such damage include 67 molecules associated with lipid and amino acid metabolism [46].

It is worth mentioning that the pharmacological effect of different anti-PD drugs in animal models can be controlled using metabolomics methods. Thus, the ability of various therapeutic agents to regulate the metabolism of amino acids, unsaturated fatty acids [47], purines, glycerophospholipids [48], as well as the neuroprotective effect of drugs through modulation of the gut microbiota–metabolite axis, has been demonstrated in MPTP-induced models of PD [49–52].

PATHOGENETIC PATHWAYS OF VASCULAR PARKINSONISM

Pathogenetic disorders leading to VP are primarily associated with cardiocerebrovascular risk factors, which include hypertension, hypercholesterolemia, cardiovascular diseases, type 2 diabetes mellitus, and advanced age [7]. These factors cause cerebrovascular disorders and affect the functioning of cerebral vessels (small vessel disease). Thus, arterial occlusion caused by the aforementioned factors would lead to various lesions in the basal ganglia and the pons, lacunar infarcts in the white matter, cerebral microangiopathy, disruption of endothelial tight junctions, and destruction of the BBB. Such disorders will be crucial in the pathogenesis of vascular ischemia [53]. In addition, small vessel changes such as gliosis, perivascular pallor, hyaline arteriolosclerosis, and especially enlarged perivascular spaces were observed in autopsy specimens from patients with VP [54].

There is mounting evidence that vascular risk factors contribute to the development of neurodegeneration. They affect the structure and function of cerebral vessels and associated cells; the so-called neurovascular unit. The neurovascular unit involves neurons, glia, as well as perivascular and vascular cells that work in close cooperation to maintain the homeostasis of the brain microenvironment. This structure regulates blood flow, controls exchange through the BBB, facilitates immune surveillance in the brain, and provides trophic support. Hemodynamic changes affect the structure of the

neurovascular apparatus, leading to its dysfunction [53]. Pathomorphologically, this phenomenon will be characterized by a thickening of the vascular wall matrix, undesirable collagen accumulation, smooth muscle collapse, and vascular stenosis [55]. Damage to the neurovascular system alters the regulation of the cerebral blood flow, depletes the blood supply reserve, disrupts the BBB, and reduces the regenerative potential of the brain. These effects secondarily increase ischemia and the attending neurodegeneration, thus closing the pathological vicious circle [56]. Therefore, neurodegeneration in patients with VP will be secondary in nature because of the effect of hypoxia on all the nervous tissue: not only on neurons, but on glial cells as well.

The effect of chronic ischemia on nervous tissue is primarily characterized by the occurrence of oxidative stress and inflammation. Disturbance in the redox state of cells resulting from ischemia can cause toxic effects through the formation of peroxides and free radicals that damage almost all cell components, including proteins, lipids, and DNA [8]. Chronic ischemia also leads to mitochondrial dysfunction and inhibition of protein synthesis, which can disrupt the balance between antioxidants and reactive oxygen species. Such oxidative damage to vascular endothelial cells, glia, and neurons may further impair the vascular function and intercellular interactions between neurons, astrocytes, and microvessels, followed by a drop in cerebral perfusion [57].

Permanent bilateral carotid artery stenosis is an experimental model of chronic ischemia in laboratory animals. In particular, the rat model was used to show the emergence of synaptic dysfunction in the hippocampus associated with cognitive impairment [58]. Reduced pyruvate dehydrogenase level and increased oxidative stress were also observed, indicating that mitochondrial energy deficiency affects memory [59].

Extensive damage to the white matter of the brain is also observed in chronic arterial occlusion. The degree of ischemic damage positively correlates with white matter involvement in the pathological process, the greatest structural damage being observed within the corpus callosum [60]. White matter dysfunction is associated with activation of glial cells: on the one hand, glial cells are activated immediately in response to damage to white matter by oxidative stress, while on the other hand, damage to the BBB facilitates penetration of immune cells and release of an enormous number of proinflammatory cytokines, as well as serine proteases, matrix metalloproteinase 2, elastase, and collagenase [55]. These released components damage the extracellular matrix and cause a remodeling of vascular walls, which eventually leads to damage and further destruction of the BBB and white matter. Axonal injury (of the white matter) caused by destruction of afferent neuronal connections, or their retrograde injury, will be followed by apoptosis of neurons *per se*. Furthermore, pro-inflammatory cytokines infiltrating the white matter disrupt growth factor signaling, inducing the state of "neurotrophin resistance". Loss of trophic support can impede proliferation, migration, and differentiation of oligodendrocyte progenitor cells as well as impair white matter repair. Glial scars will develop at the damage site [61]. Hence, chronic ischemia is characterized by atrophy of cortical neurons and a reduced volume of the entire cerebral cortex, as well as edema and damage to the white matter in the form of demyelination, apoptosis of oligodendrocytes and atrophy, as well as glial proliferation in the form of astrocytogliosis [62].

In other studies, endothelial dysfunction worsening the ability of vessels to respond to changes in cerebral hemodynamics is reported to play the leading role in the pathophysiology of chronic ischemia. The resulting impairment of neurovascular coupling leads to transient or chronic cerebral hypoperfusion [63]. Endothelial cells are capable of recognizing immune signals and expressing adhesion molecules (P- and E-selectin, intercellular adhesion molecules, vascular cell adhesion, etc.), which recognize certain molecules on circulating immune cells, leading to transmigration of these cells into the brain [64]. Cytokines produced by perivascular macrophages, endothelium, and glia regulate the expression of adhesion molecules, other cytokines and chemokines, as well as promote leukocyte trafficking across the BBB [65]. This process is important for both immune surveillance in the normal brain and the brain's immune response to injury. Moreover, oxidative stress-induced endothelial dysfunction may cause the release of the vascular endothelial growth factor (VEGF) and prostanoids, which promote endothelial leakage of active substances and inflammation [66]. Extravasation of plasma proteins also causes vascular inflammation, oxidative stress, perivascular edema, and axonal demyelination. However, it is most likely that the described processes (arterial occlusion, impaired cerebral microcirculation, BBB damage, and endothelial dysfunction) run simultaneously and mutually exacerbate each other's effects.

Potential markers of vascular parkinsonism in metabolomic studies of various cerebrovascular diseases

There are very few metabolomic studies of vascular parkinsonism; so, this review discusses data on the metabolomic profile in cerebrovascular diseas-

Table 2. Metabolomic markers of various cerebrovascular diseases related to the development of vascular parkinsonism

Biological matrix	Cerebrovascular disease/condition	Found biomarkers	Reference
Blood plasma	White matter hyperintensity in MRI scans	Sphingomyelin 38:1 (SM 38:1), ceramide 34:1 (Cer 34:1)	[67]
Blood serum	Small vessel disease	Creatine, fatty acid 18:2(OH), sphingomyelin (d18:2/24:1), N1-acetylspermidine, N-acetylputrescine, isoleucine, creatinine, creatine, cytosine, 5'-methylthioadenosine	[68]
Blood plasma	Large artery atherosclerosis (LA), small vessel disease (SVD)	Cer (d36:3), Cer (d34:2), Cer (d38:6) (for LA); SM (d34:1), Cer (d34:2), Cer (d36:4) (for SVD)	[69]
Blood serum	Vascular dementia	7α-hydroxycholesterol, primary bile acids	[70]
Blood serum	Vascular dementia, mixed dementia	*L*-arginine, *L*-arginine/asymmetric dimethylarginine ratio, *L*-arginine/nitric acid pathway	[71]
Blood serum	Vascular dementia	Dihydroxybutanoic, docosapentaenoic and uric acid	[72]
Blood plasma	Chronic cerebral ischemia	Proteins SERPINF2, HRG, KNG1, APCS, C1R, C5, AGT, PROS1, ITIH1, etc.	[73]
Cerebral cortex	Vascular dementia	Proteins SOD1, NCAM, and ATP5A	[74]

es as a basis for the development of VP. Numerous metabolites are regarded as biomarkers of cerebrovascular parkinsonism in experiments: ranging from low-molecular-weight (amino acids, nucleotides and other products of impaired metabolic pathways) to groups of proteins responsible for a number of body functions (*Table 2*).

Many metabolomic studies aim to establish a connection between the known structural changes in patients with CVDs and the metabolic pathways that lead to them. For example, white matter hyperintensity is a frequent sign of CVD in MRI images. One study of plasma metabolites from patients whose MRI scans had shown white matter hyperintensity but who had not been diagnosed with ischemic stroke or transient ischemic attacks revealed an association between sphingolipids and the severity of the changes in MRI scans [67]. Two such metabolites, sphingomyelin 38:1 (SM 38:1) and ceramide 34:1 (Cer 34:1), were identified using HPLC/MS. Both ceramides and sphingomyelins are components of lipid envelopes, which play a crucial role in maintaining the myelin structure. It was hypothesized that these molecules can be specific biomarkers of white matter damage and can also be indicative of CVD progression based on the degree of white matter involvement in the pathological process.

Data from another study employing a combination of HPLC/MS and NMR showed higher levels of creatine, unsaturated acid 18:2(OH), and sphingomyelin (d18:2/24:1), which were associated with a larger number of lacunae, white matter damage in MRI scans, and worsened cognitive performance [68]. Elevated levels of seven amino acids and nucleotides (N1-acetylspermidine, N-acetylputrescine, isoleucine, creatinine, creatine, cytosine, and 5'-methylthioadenosine) were found to be associated with the emergence of similar lesions. Low serum levels of several sphingomyelins and glycerophospholipids turned out to be markers of more severe white matter damage, brain atrophy, and cognitive impairment.

You et al. detected 276 sphingolipids, including 39 ceramides (Cer), three ceramide phosphates, 72 glycosphingolipids, and 162 sphingomyelins (SM), in patients' plasma; their levels differed from those in the control group [69]: the levels of Cer (d36:3), Cer (d34:2), Cer (d38:6), etc. were elevated in patients with large artery atherosclerosis; the levels of SM (d34:1), Cer (d34:2), Cer (d36:4), etc. were increased in patients with age-related small vessel disease. The levels of Cer (d36:4) and SM (d34:1) in patients with age-related small vessel disease were elevated compared to those in patients with large artery atherosclerosis.

Changes in the lipid profile may play a role in the pathogenesis of CVDs. Hence, a reduced serum cholesterol level was reported to be associated with the emergence of neuroimaging markers of vascular dementia, while statin-induced pharmacological reduction in cholesterol levels can be associated with an increased risk of vascular dementia in males [70]. The

low serum levels of 7α-hydroxycholesterol and primary bile acids are associated with a higher degree of cerebral amyloid deposition, significant white matter damage, and more rapid brain atrophy. The study used a combination of such methods as targeted plasma metabolomic profiling, positron emission tomography, brain MRI, and pharmacoepidemiologic analysis.

The *L*-arginine/nitric oxide pathway was shown to be altered in people with dementia [71]. Thus, plasma specimens from patients with vascular dementia, Alzheimer's disease, and mixed dementia were studied using targeted metabolomic screening by HPLC-MS. All the types of dementia were found to be associated with reduced levels of L-arginine, asymmetric dimethylarginine and L-citrulline, as well as with reduced L-arginine/asymmetric dimethylarginine ratio. Meanwhile, the level of *L*-arginine and the *L*-arginine/asymmetric dimethylarginine ratio differentiated vascular dementia and Alzheimer's disease. Changes in the levels of these metabolites were indicative of structural brain alterations and correlated with the severity of the cognitive impairment.

Metabolomic profiling can also predict the development of vascular dementia. Thus, the role of dihydroxybutanoic, docosapentaenoic, and uric acids in a 5-year progression of the disease was demonstrated [72]. Plasma specimens from patients with vascular dementia and Alzheimer's disease, as well as subjects without diagnosed dementia but with a potential to develop age-related dementia, was analyzed by HPLC-MS in a prospective study. The levels of the aforementioned substances were elevated in the group of patients with both types of dementia and in incident cases within five years before the onset of dementia.

Along with analyzing the low-molecular-weight metabolites, metabolomic studies of the plasma protein profile of patients with CVDs were also conducted. Thus, a group comprising 44 proteins involved in the blood coagulation pathway (SERPINF2, HRG, KNG1, etc., a total of ten proteins), in activation of innate immunity (APCS, C1R, C5, etc., a total of 13 proteins), and in regulation of the activities of hydrolases AGT, PROS1, ITIH1, etc. was revealed [73]. The observed shift in the weights of functional protein clusters is supposedly attributable to the activation of compensatory mechanisms aiming to maintain a homeostasis.

Another study showed upregulated expression of the SOD1 and NCAM proteins and downregulated expression of the ATP5A protein in patients with vascular dementia, an indication of nervous tissue hypometabolism and vascular insufficiency, along with inflammation [74]. The increased SOD1 level, as well as a trend toward increasing levels of iron uptake proteins (FTL and FTH1) can be indicative of an oxidative imbalance that is accompanied by iron metabolism disorders.

Metabolomic studies of cerebrovascular diseases in experimental models

Metabolomic studies of CVDs are also conducted on experimental models. Desorption electrospray ionization mass spectrometry was employed to illustrate lipid distribution in the rat brain in a similar model. In the experimental specimens, reduced levels of dihomo-γ-linolenic, stearic, arachidonic, docosahexaenoic, and hydroxyeicosatetraenoic acids, as well as ethanolamine glycerophosphate, were observed in the entire brain, and especially in the hippocampus. The reduced levels of these substances in patients with CVDs can be attributed to the anti-inflammatory properties of some of them (e.g., dihomo-γ-linolenic acid), as well as to the loss of nervous tissue *per se*. In the corpus callosum, the signal intensities of three glycerophospholipids (LMGP06010075, LMGP00000053, and LMGP0601010168) and sulfatide, which are myelin components, were reduced [75].

In this section, we would also like to summarize some results of a proteomic analysis, or high-throughput protein analysis. In proteomics, Tukacs et al. revealed changes in the protein profile in rats with stepwise bilateral occlusion of the common carotid artery. They identified a large number of proteins whose regulation in the occipital lobe of the cortex differs from that in the frontal cortex and hippocampus [76]. The altered proteins possess the functions associated with cytoskeletal organization and energy metabolism. Thus, the expression of proteins involved in the citric acid cycle and electron transport chain (fructose-bisphosphate aldolase C, ATP synthase alpha, isocitrate dehydrogenase, NADH dehydrogenase, etc.) was found to be downregulated.

CONCLUSIONS

It is obvious that the commonality of the neurodegeneration concept not only makes clinical sense, but it also implies common metabolic pathways and metabolomic targets. Searching for markers of individual neurodegenerative processes, such as PD and ischemic neurodegeneration, is of particularly specific interest, as it encompasses such clinical concepts as early manifestations, prediction of the disease course, diagnostic criteria, and personalization of the therapeutic approach. For PD, such markers are metabolites of amino acids, acylcarnitines, fatty acids, bile acids; for CVDs, these markers are the proteins involved in the

coagulation pathway or the regulation of the immune response.

The capabilities of a metabolomic analysis open up prospects for the clinical diagnostics of neurodegenerative diseases, shortening the time between admission and diagnosis, which currently takes ten years.

A review of the literature focusing on the search for metabolomic markers of Parkinson's disease (PD) and vascular parkinsonism (VP) yields conflicting results. All the available evidence indicates that studying metabolomic abnormalities in a single humoral environment alone is of little practical value. In order to identify both general signs of primary neurodegeneration (characteristic of PD) and the ischemic nature (as in the case of VP), as well as their differential markers, one needs to simultaneously examine blood plasma and cerebrospinal fluid. Differences in the neurotransmitter activity of the subcortical structures associated with PD and VP infer that there are significant differences in metabolites characteristic of each of these conditions. In patients with PD, the neurons of the substantia nigra, which produce dopamine, are primarily affected. Meanwhile, VP is characterized by damage to the globus pallidus and putamen, which function at the expense of other mediators such as GABA, glutamate, choline, etc. Further research should avail itself of the benefits of widespread use of available diagnostic tests such as whole blood or dried serum spot analysis.

Furthermore, the study of the range of low-molecular-weight markers is supposed to help one decipher the cascade of metabolic disorders, the stage of their involvement, and their effect on the clinical picture of motor as well as cognitive mental disorders, with allowance for patient sex. This approach will allow one to assess the significance of metabolic failures in the pathogenesis of two different types of neurodegenerative disorders. ●

REFERENCES

1. Tolosa E., Garrido A., Scholz S.W., Poewe W. // Lancet Neurol. 2021. V. 20. № 5. P. 385–397. doi: 10.1016/S1474-4422(21)00030-2.
2. Massano J., Bhatia K.P. // Cold Spring Harb. Perspect. Med. 2012. V. 2. № 6. P. a008870. doi: 10.1101/cshperspect.a008870.
3. DeMaagd G., Philip A. // P&T. 2015. V. 40. № 8. P. 504.
4. Kalra S., Grosset D.G., Benamer H.T. // Mov. Disord. 2010. V. 25. № 2. P. 149–156. doi: 10.1002/mds.22937.
5. Thanvi B., Lo N., Robinson T. // Age Ageing. 2005. V. 34. № 2. P. 114–119. doi: 10.1093/ageing/afi025.
6. Korczyn A.D. // Nat. Rev. Neurol. 2015. V. 11. № 6. P. 319–326. doi: 10.1038/nrneurol.2015.61.
7. Che Mohd Nassir C.M.N., Damodaran T., Yusof S.R., Norazit A., Chilla G., Huen I., Bhanu Prakash K.N., Mohamed Ibrahim N., Mustapha M. // Pharmaceutics. 2021. V. 13. № 8. P. 1207. doi: 10.3390/pharmaceutics13081207.
8. Iadecola C. // Acta Neuropathol. 2010. V. 120. P. 287–296. doi: 10.1007/s00401-010-0718-6.
9. Ren J.L., Zhang A.H., Kong L., Wang X.J. // RSC Adv. 2018. V. 8. № 40. P. 22335–22350. doi: 10.1039/c8ra01574k.
10. Luan H., Wang X., Cai Z. // Mass Spectrom. Rev. 2019. V. 38. № 1. P. 22–33. doi: 10.1002/mas.21553.
11. Alexander G.E. // Dialogues Clin. Neurosci. 2004. T. 6. № 3. P. 259–280. doi: 10.31887/DCNS.2004.6.3/galexander.
12. Braak H., Del Tredici K., Rüb U., De Vos R.A., Steur E.N.J., Braak E. // Neurobiol. Aging. 2003. V. 24. № 2. P. 197–211. doi: 10.1016/s0197-4580(02)00065-9.
13. Baziyan B.K. // Bull. Exp. Biol. Med. 2012. V. 154. № 2. P. 186–188. doi: 10.1007/s10517-012-1907-1.
14. Shao Y., Le W. // Mol. Neurodegener. 2019. V. 14. № 1. P. 1–12. doi: 10.1186/s13024-018-0304-2.
15. Kouli A., Torsney K.M., Kuan W.L. // Exon Publ. 2018. P. 3–26. doi: 10.15586/codonpublications.parkinsonsdisease.2018.ch1.
16. Grassi D., Diaz-Perez N., Volpicelli-Daley L.A., Lasmézas C.I. // Neurobiol. Dis. 2019. V. 124. P. 248–262. doi: 10.1016/j.nbd.2018.11.015.
17. Murgia F., Atzori L., Carboni E., Santoru M.L., Hendren A., Pisanu A., Caboni P., Boi L., Fusco G., Carta A.R. // Int. J. Mol. Sci. 2020. V. 21. № 18. P. 6745. doi: 10.3390/ijms21186745.
18. Quinn P.M.J., Moreira P.I., Ambrósio A.F., Alves C.H. // Acta Neuropathol. Commun. 2020. V. 8. № 1. P. 1–20. doi: 10.1186/s40478-020-01062-w.
19. Minakaki G., Krainc D., Burbulla L.F. // Front. Cell. Dev. Biol. 2020. V. 8. P. 580634. doi: 10.3389/fcell.2020.580634.
20. Andersen A.D., Blaabjerg M., Binzer M., Kamal A., Thagesen H., Kjaer T.W., Stenager E., Gramsbergen J.B.P. // J. Neurochem. 2017. V. 141. № 4. P. 614–625. doi: 10.1111/jnc.13997.
21. Goldstein D.S., Holmes C., Sharabi Y. // Brain. 2012. V. 135. № 6. P. 1900–1913. doi: 10.1093/brain/aws055.
22. Havelund J.F., Heegaard N.H.H., Færgeman N.J.K., Gramsbergen J.B. // Metabolites. 2017. V. 7. № 3. P. 42. doi: 10.3390/metabo7030042.
23. Trupp M., Jonsson P., Ohrfelt A., Zetterberg H., Obudulu O., Malm L., Wuolikainen A., Linder J., Moritz T., Blennow K. // J. Parkinsons Dis. 2014. V. 4. № 3. P. 549–560. doi: 10.3233/JPD-140389.
24. LeWitt P., Schultz L., Auinger P., Lu M., Parkinson Study Group DATATOP Investigators. // Brain Res. 2011. V. 1408. P. 88–97. doi: 10.1016/j.brainres.2011.06.057.
25. Stoessel D., Schulte C., Teixeira Dos Santos M.C., Scheller D., Rebollo-Mesa I., Deuschle C., Walther D., Schauer N., Berg D., Nogueira da Costa A. // Front. Aging Neurosci. 2018. V. 10. P. 51. doi: 10.3389/fnagi.2018.00051.
26. Willkommen D., Lucio M., Moritz F., Forcisi S., Kanawati B., Smirnov K.S., Schroeter M., Sigaroudi A., Schmitt-Kopplin P., Michalke B. // PLoS One. 2018. V. 13. № 12. P. e0208752. doi: 10.1371/journal.pone.0208752.

27. Chang K.H., Cheng M.L., Tang H.Y., Huang C.Y., Wu Y.R., Chen C.M. // Mol. Neurobiol. 2018. V. 55. № 8. P. 6319–6328. doi: 10.1007/s12035-017-0845-3.
28. Havelund J.F., Andersen A.D., Binzer M., Blaabjerg M., Heegaard N.H.H., Stenager E., Faergeman N.J., Gramsbergen J.B. // J. Neurochem. 2017. V. 142. № 5. P. 756–766. doi: 10.1111/jnc.14104.
29. Çelık R.G.G., Köksal A., Şahın B., Şen A., Sakalli N.K., Nalbantoğlu M. // Noro. Psikiyatr. Ars. 2020. V. 57. № 1. P. 33. doi: 10.29399/npa.24761.
30. Johansen K.K., Wang L., Aasly J.O., White L.R., Matson W.R., Henchcliffe C., Beal M.F., Bogdanov M. // PLoS One. 2009. V. 4. № 10. P. e7551. doi: 10.1371/journal.pone.0007551.
31. Shao Y., Li T., Liu Z., Wang X., Xu X., Li S., Xu G., Le W. // Mol. Neurodegener. 2021. V. 16. P. 1–15. doi: 10.1186/s13024-021-00425-8.
32. Yakhine-Diop S.M.S., Morales-García J.A., Niso-Santano M., González-Polo R.A., Uribe-Carretero E., Martinez-Chacon G., Durand S., Maiuri M.C., Aiastui A., Zulaica M. // Aging (Albany NY). 2020. V. 12. № 17. P. 16690. doi: 10.18632/aging.103992.
33. Fiandaca M.S., Gross T.J., Johnson T.M., Hu M.T., Evetts S., Wade-Martins R., Merchant-Borna K., Bazarian J., Cheema A.K., Mapstone M. // Metabolites. 2018. V. 8. № 3. P. 50. doi: 10.3390/metabo8030050.
34. Saiki S., Sasazawa Y., Fujimaki M., Kamagata K., Kaga N., Taka H., Li Y., Souma S., Hatano T., Imamichi Y. // Ann. Neurol. 2019. V. 86. № 2. P. 251–263. doi: 10.1002/ana.25516.
35. Roede J.R., Uppal K., Park Y., Lee K., Tran V., Walker D., Strobel F.H., Rhodes S.L., Ritz B., Jones D.P. // PLoS One. 2013. V. 8. № 10. P. e77629. doi: 10.1371/journal.pone.0077629.
36. Hatano T., Saiki S., Okuzumi A., Mohney R.P., Hattori N. // J. Neurol. Neurosurg. Psychiatry. 2016. V. 87. № 3. P. 295–301. doi: 10.1136/jnnp-2014-309676.
37. Saiki S., Hatano T., Fujimaki M., Ishikawa K.I., Mori A., Oji Y., Okuzumi A., Fukuhara T., Koinuma T., Imamichi Y. // Sci. Rep. 2017. V. 7. № 1. P. 1–15. doi: 10.1038/s41598-017-06767-y.
38. Albillos S.M., Montero O., Calvo S., Solano-Vila B., Trejo J.M., Cubo E. // Parkinsonism Relat. Disord. 2021. V. 91. P. 167–172. doi: 10.1016/j.parkreldis.2021.09.014.
39. Farmer K., Smith C.A., Hayley S., Smith J. // Int. J. Mol. Sci. 2015. V. 16. № 8. P. 18865–18877. doi: 10.3390/ijms160818865.
40. Graham S.F., Rey N.L., Yilmaz A., Kumar P., Madaj Z., Maddens M., Bahado-Singh R.O., Becker K., Schulz E., Meyerdirk L.K. // J. Proteome Res. 2018. V. 17. № 7. P. 2460–2469. doi: 10.1021/acs.jproteome.8b00224.
41. Kim A., Nigmatullina R., Zalyalova Z., Soshnikova N., Krasnov A., Vorobyeva N., Georgieva S., Kudrin V., Narkevich V., Ugrumov M. // Mol. Neurobiol. 2019. V. 56. P. 3437–3450. doi: 10.1007/s12035-018-1315-2.
42. Li X.Z., Zhang S.N., Lu F., Wang Y., Bai Y., Wang N., Liu S.M. // Phytomedicine. 2013. V. 20. № 13. P. 1219–1229. doi: 10.1016/j.phymed.2013.06.002.
43. Lu Z., Wang J., Li M., Liu Q., Wei D., Yang M., Kong L. // Chem. Biol. Interact. 2014. V. 223. P. 18–26. doi: 10.1016/j.cbi.2014.09.006.
44. Lu Y., Zhang X., Zhao L., Yang C., Pan L., Li C., Liu K., Bai G., Gao H., Yan Z. // Front. Neurosci. 2018. V. 12. P. 90. doi: 10.3389/fnins.2018.00090.
45. Neto D.P.A., Vitor Pereira de Godoy J., Tostes K., Pelegrini Bosque B., Vieira Rodrigues P., Aparecida Rocco S., Luis Sforça M., de Castro Fonseca M. // Neuroscience. 2023. V. 526. P. 21–34. doi: 10.1016/j.neuroscience.2023.06.010.
46. Wang W., Zhu G., Wang Y., Li W., Yi S., Wang K., Fan L., Tang J., Chen R. // Front. Aging Neurosci. 2022. V. 14. P. 877078. doi: 10.3389/fnagi.2022.877078.
47. Wang X., Zhu X., Li X., Li Z., Mao Y., Zhang S., Liu X., Liu X., Liu Y., Cao F., et al. // Food Funct. 2023. V. 14. № 1. P. 277–291. doi: 10.1039/d2fo02595g.
48. Zhang C., Xue Z., Zhu L., Zhou J., Zhuo L., Zhang J., Zhang X., Liu W., Han L., Liao W. // Food Funct. 2023. V. 14. № 7. P. 3208–3219. doi: 10.1039/d2fo02939a.
49. Mi N., Ma L., Li X., Fu J., Bu X., Liu F., Yang F., Zhang Y., Yao L. // Open Med. (Wars). 2023. V. 18. № 1. P. 20230849. doi: 10.1515/med-2023-0849.
50. Zhang W., Chen S., Huang X., Tong H., Niu H., Lu L. // Cell Death Discov. 2023. V. 9. № 1. P. 251. doi: 10.1038/s41420-023-01549-0.
51. Jiang Z., Wang X., Zhang H., Yin J., Zhao P., Yin Q., Wang Z. // MedComm. 2023. V. 4. № 3. P. e268. doi: 10.1002/mco2.268.
52. Cui C., Han Y., Li H., Yu H., Zhang B., Li G. // Front. Cell Infect. Microbiol. 2022. V. 12. P. 887407. doi: 10.3389/fcimb.2022.887407.
53. Wardlaw J.M., Smith C., Dichgans M. // Lancet Neurol. 2013. V. 12. № 5. P. 483–497. doi: 10.1016/S1474-4422(13)70060-7.
54. Hughes A.J., Daniel S.E., Kilford L., Lees A.J. // J. Neurol. Neurosurg. Psychiatry. 1992. V. 55. № 3. P. 181–184. doi: 10.1136/jnnp.55.3.181.
55. Wang F., Cao Y., Ma L., Pei H., Rausch W.D., Li H. // Front. Aging Neurosci. 2018. V. 10. P. 376. doi: 10.3389/fnagi.2018.00376.
56. Enciu A.M., Popescu B.O. // Biomed. Res. Int. 2013. V. 2013. P. 316495. doi: 10.1155/2013/316495.
57. Zhao Y., Gong C.X. // Cell. Mol. Neurobiol. 2015. V. 35. № 1. P. 101–110. doi: 10.1007/s10571-014-0127-9.
58. Hai J., Yu F., Lin Q., Su S.H. // Brain Res. 2012. V. 1429. P. 9–17. doi: 10.1016/j.brainres.2011.10.023.
59. Du J., Ma M., Zhao Q., Fang L., Chang J., Wang Y., Fei R., Song X. // Neuroscience. 2013. V. 231. P. 345–352. doi: 10.1016/j.neuroscience.2012.11.062.
60. Yoshizaki K., Adachi K., Kataoka S., Watanabe A., Tabira T., Takahashi K., Wakita H. // Exp. Neurol. 2008. V. 210. № 2. P. 585–591. doi: 10.1016/j.expneurol.2007.12.005.
61. Viswanathan A., Gray F., Bousser M.G., Baudrimont M., Chabriat H. // Stroke. 2006. V. 37. № 11. P. 2690–2695. doi: 10.1161/01.STR.0000245091.28429.6a.
62. Alber J., Alladi S., Bae H.J., Barton D.A., Beckett L.A., Bell J.M., Berman S.E., Biessels G.J., Black S.E., Bos I. // Alzheimers Dement. 2019. V. 5. P. 107–117. doi: 10.1016/j.trci.2019.02.001.
63. Duncombe J., Kitamura A., Hase Y., Ihara M., Kalaria R.N., Horsburgh K. // Clin. Sci. 2017. V. 131. № 19. P. 2451–2468. doi: 10.1042/CS20160727.
64. Weber C., Fraemohs L., Dejana E. // Nat. Rev. Immunol. 2007. V. 7. №. 6. P. 467–477. doi: 10.1038/nri2096.
65. Konsman J.P., Drukarch B., Van Dam A.M. // Clin. Sci. 2007. V. 112. № 1. P. 1–25. doi: 10.1042/CS20060043.
66. Cotman C.W., Berchtold N.C., Christie L.A. // Trends Neurosci. 2007. V. 30. № 9. P. 464–472. doi: 10.1016/j.tins.2007.06.011.
67. Azizkhanian I., Sheth S.A., Iavarone A.T., Lee S., Kakarla V., Hinman J.D. // Front. Neurol. 2019. V. 10. P. 474611. doi: 10.3389/fneur.2019.00950.

68. Harshfield E.L., Sands C.J., Tuladhar A.M., de Leeuw F.E., Lewis M.R., Markus H.S. // Brain. 2022. V. 145. № 7. P. 2461–2471. doi: 10.1093/brain/awac041.
69. You Q., Peng Q., Yu Z., Jin H., Zhang J., Sun W., Huang Y. // Biosci. Rep. 2020. V. 40. № 9. P. BSR20201519. doi: 10.1042/BSR20201519.
70. Varma V.R., Wang Y., An Y., Varma S., Bilgel M., Doshi J., Legido-Quigley C., Delgado J.C., Oommen A.M. // PLoS Med. 2021. V. 18. № 5. P. e1003615. doi: 10.1371/journal.pmed.1003615.
71. Fleszar M.G., Wiśniewski J., Zboch M., Diakowska D., Gamian A., Krzystek-Korpacka M. // Sci. Rep. 2019. V. 9. № 1. P. 13764. doi: 10.1038/s41598-019-50205-0.
72. Mousavi M., Jonsson P., Antti H., Adolfsson R., Nordin A., Bergdahl J., Eriksson K., Moritz T., Nilsson L.G., Nyberg L. // Dement. Geriatr. Cogn. Dis. Extra. 2014. V. 4. № 2. P. 252–262. doi: 10.1159/000364816.
73. Kaysheva A.L., Kopylov A.T., Ponomarenko E.A., Kiseleva O.I., Teryaeva N.B., Potapov A.A., Izotov A.A., Morozov S.G., Kudryavtseva V.Y., Archakov A.I. // J. Mol. Neurosci. 2018. V. 64. P. 440–448. doi: 10.1007/s12031-018-1040-3.
74. Datta A., Qian J., Chong R., Kalaria R.N., Francis P., Lai M.K., Chen C.P., Sze S.K. // J. Proteomics. 2014. V. 99. P. 54–67. doi: 10.1016/j.jprot.2014.01.011.
75. Severiano D.L.R., Oliveira-Lima O.C., Vasconcelos G.A., Lemes Marques B., Almeida de Carvalho G., Freitas E.M.M., Xavier C.H., Gomez M.V., Pinheiro A.C.O., Gomez R.S. // Neuroscience. 2020. V. 426. P. 1–12. doi: 10.1016/j.neuroscience.2019.11.014.
76. Tukacs V., Mittli D., Györffy B.A., Hunyady-Gulyás É., Hlatky D., Tóth V., Ravasz L., Medzihradszky F.K., Nyitrai G., Czurkó A. // Sci. Rep. 2020. V. 10. № 1. P. 15999. doi: 10.1038/s41598-020-72868-w.

Visualization of Nucleic Acids in Micro- and Nanometer-Scale Biological Objects Using Analytical Electron Microscopy

O. S. Sokolova[1*], T. S. Trifonova[1], N. I. Derkacheva[2], A. V. Moiseenko[1]
[1]Lomonosov Moscow State University, Faculty of Biology, Moscow, 119234 Russian Federation
[2]Russian University of Medicine, Department of Biochemistry, Moscow, 127473 Russian Federation
*E-mail: sokolova@mail.bio.msu.ru
Received August 06, 2024; in final form, October 21, 2024
DOI: 10.32607/actanaturae.27483

ABSTRACT **Analytical electron microscopy techniques, including energy-dispersive X-ray spectroscopy (EDX) and electron energy-loss spectroscopy (EELS), are employed in materials science and biology to visualize and chemically map diverse elements. This review presents cases of successful identification of nucleic acids in cells and in DNA- and RNA-containing viruses that use the chemical element phosphorus as a marker.**
KEYWORDS **energy dispersive X-ray spectroscopy, electron energy loss spectroscopy, elemental mapping of phosphorus, bacteriophage, *P. aeruginosa*, SARS-CoV-2, tick-borne encephalitis virus.**
ABBREVIATIONS **EDX – energy dispersive X-ray spectroscopy; EELS – electron energy loss spectroscopy; TEM – transmission electron microscopy; EFTEM – energy-filtering transmission electron microscopy; STEM – scanning transmission electron microscopy; HAADF – high-angle annular dark-field; TBEV – tick-borne encephalitis virus; cryoEM – cryo-electron microscopy; GFP – green fluorescent protein.**

INTRODUCTION

The precise identification and ultrastructural localization of molecules, organelles, cells, and other biological structures are fundamental in determining their functions. The localization of macromolecules is achieved through immunolabeling techniques on tissue sections, facilitating the detection of specific targets [1]. Cryotomography enables the visualization of the tissue structures [2] and cryo-EM structures of protein macromolecules with atomic resolution [3, 4].

Nobel Prizes awarded for advancements in microscopy highlight the significance of high-resolution molecular imaging, which encompasses the use of green fluorescent protein (GFP) in living cells [5], the circumvention of the diffraction limit through super-resolution light fluorescence microscopy [6], and cryo-electron microscopy (cryoEM) [7].

Transmission electron microscopy (TEM) is a common technique used to study the structure of tissues, cells, organelles and protein molecules, which in turn helps to understand the mechanisms underlying the cellular function under normal and pathological conditions. Advancements in electron microscopy and computational power have established TEM as the premier structural biology technique over the past decade. The application of CryoEM allows for the visualization of the three-dimensional architecture and dynamic behavior of a wide array of biological nano-objects at resolutions ranging from 2 to 5 nm to atomic levels [3, 4]. Unlike other structural methods, cryoEM presents several advantages: it is not limited by particle size, the presence of crystals is not necessary, and a small amount of material is used. In addition, cryo-modification of the TEM method permits the visualization of molecules in their native, aqueous environment under near-physiological conditions, which is particularly important for the study of their functional features.

The underlying principle of transmission electron microscopy is the scattering of an electron beam by a thin section of the material being studied (*Fig. 1A*). Electron-atom collisions within a material give rise to several observable effects such as high-angle elastic scattering, inelastic scattering with concomitant energy loss, the generation of secondary electrons and ionization of target atoms, and characteristic X-ray emission (*Fig. 1B*). The nature of the observed phenomena is determined by factors such as the specific structure of the object under the electron beam, the distribution of the scattering potential, the average atomic number, the thickness of the object, and other parameters. Transmission electron microscopy facili-

tates the detection of signals that can account for the structure of the object in question.

ANALYTICAL ELECTRON MICROSCOPY

Biological and materials science research requires not only qualitative but also quantitative analysis, including mapping the elemental composition of microscopic sample areas. For this purpose, scanning and transmission analytical electron microscopes are employed. Analytical TEM detects inelastically scattered electrons. These electrons lost kinetic energy while traversing the sample within the microscope column (*Fig. 1B*).

The analytical electron microscope incorporates specialized detectors facilitating the chemical state analysis of samples via EDX (energy-dispersive X-ray spectrometry) or EELS (electron energy-loss spectrometry). Analytical TEM techniques offer a unique opportunity for acquiring nanometer-resolution elemental compositional data of the investigated specimens [8, 9]. Common analytical TEM methods employed for elemental analysis within biological samples include EDX [10], EELS, and EELS-based elemental mapping by energy-filtering TEM (EFTEM).

THE ENERGY DISPERSIVE X-RAY SPECTROSCOPY (EDX) METHOD

The EDX method is based on detecting X-ray photons emitted by samples during electron irradiation (*Fig. 2C*) and measuring their energies. Given the unique, quantized energy values of each atom, X-ray spectra are linear and identifiable to specific elements. The location of peaks on the abscissa axis of a typical EDX spectrum corresponds to the energy values of the X-ray photons absorbed by the detector: the higher the energy, the more to the right the peak is shifted (*Fig. 2E*). The amplitude of each peak is a function of the number of pulses detected on each respective channel.

Elemental analysis using the EDX method applies energy dispersive spectrometers (for example, X-Max, Oxford Instruments, UK). Elemental distribution mapping is achieved through electron energy loss spectrometers, which are typically integrated into transmission electron microscope columns.

Energy-dispersive X-ray spectra from specific areas of the sample are typically recorded using scanning transmission electron microscopy (STEM). In contrast to TEM, the electron beam in STEM is fo-

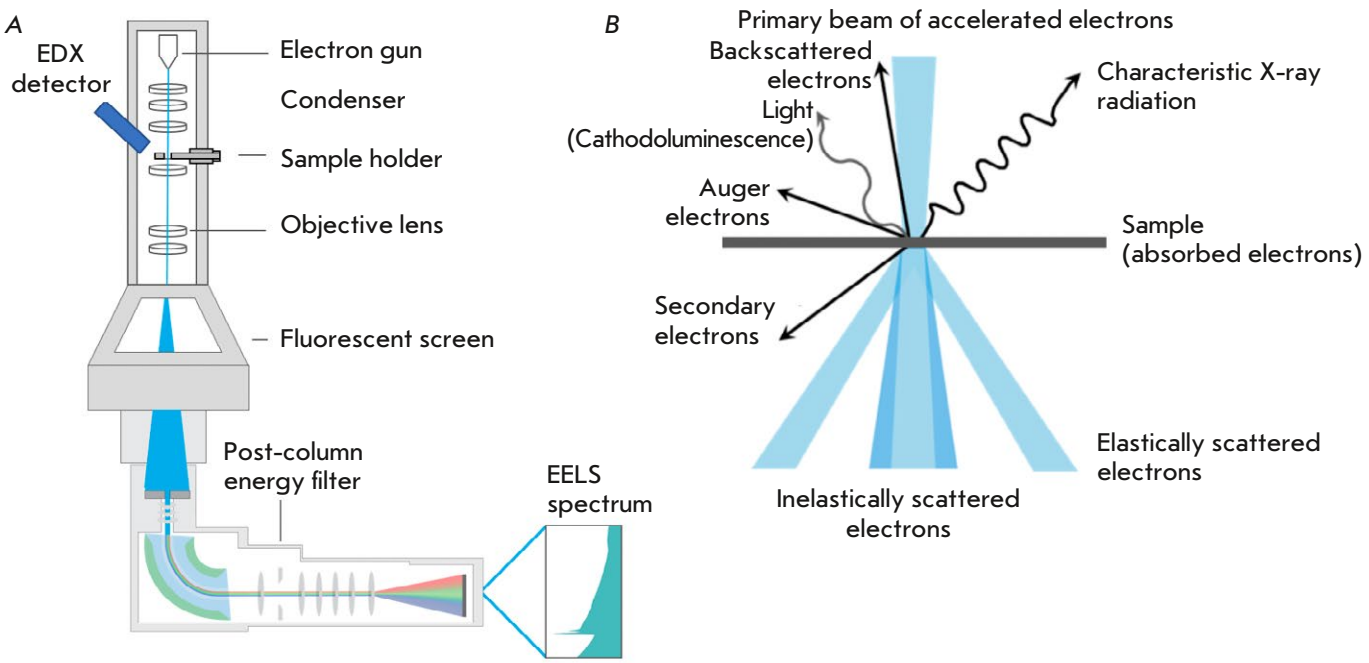

Fig. 1. (*A*) The architecture of an electron transmission analytical microscope. (*B*) Visualization of the energy distribution within a thin material following the passage of an accelerated electron beam and the subsequent secondary emissions (generated using BioRender.com)

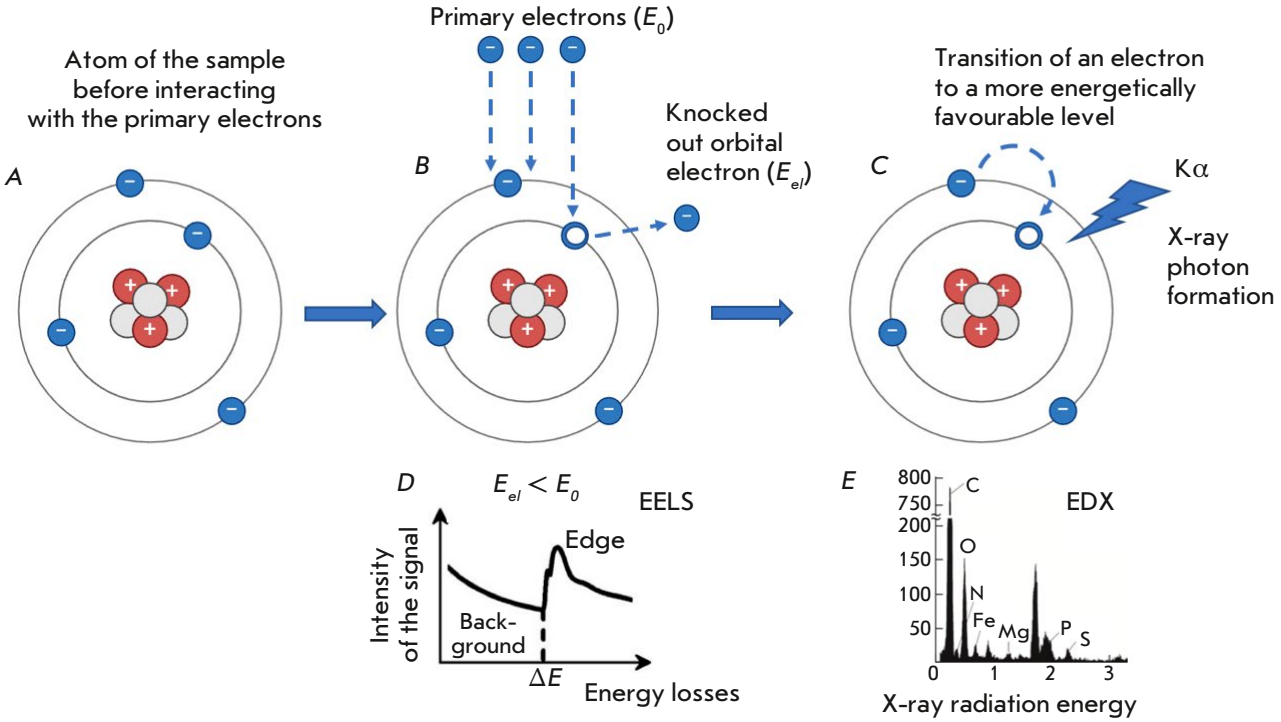

Fig. 2. Excitation of the inner shells of a sample atom in a transmission electron microscope column and the resulting EELS and EDX spectra. (*A*) The sample atom before interaction with the primary electron. (*B*) Energy loss detected by EELS. E_0 – energy of the primary electron before interaction with the sample; E_{el} is the energy of the primary electron after interaction with the sample. (*C*) The generation of the X-ray radiation quantum detected by the EDX method. *Kα* is the X-ray photon generated by the transition of the sample atom from the excited one. (*D*) The electron energy loss spectrum (EELS). (*E*) The energy dispersive spectrum (EDX) (generated using BioRender.com)

cused using electron optics to form a small probe that scans a thin sample. Biologically significant elements (P, N, O, K, Ca, Mg, Na, Cl, and S) exhibit their most intense X-ray emissions within the 0.15–4 keV energy range (*Fig. 2E*). The EDX method is generally considered a qualitative method, with its primary goal being the identification of a specific Kα peak. Specialized tables and databases facilitate the determination of characteristic X-ray peaks. Automated peak identification software is a standard feature in most X-ray analysis programs.

X-ray quantitative analysis achieves analytical accuracy at the ~1% level, making it possible to compare the content of the element in question in different cells and tissues when normalized to the carbon peak and superimposing the resulting graphs onto each other (see below). It is important to note that discrepancies in quantification may arise from the similar binding energies of specific chemical elements. For example, the Kα peak (2.013 keV) of phosphorus (P) is very close to the M-line (1.914 keV) of osmium (Os), which is commonly used to fix cell membranes. Consequently, differentiating between osmium membrane labeling and phospholipid membrane composition presents a challenge. The use of alternative heavy-metal compounds, for example manganese (distinguished by its unique peak position), is proposed to avoid spectral peak overlapping.

DETECTION OF PHOSPHORUS ON CELL AND TISSUE SECTIONS USING EDX

Phosphorus, a crucial macronutrient for living organisms, is a constituent of vital compounds, including nucleic acids, ATP (adenosine triphosphate), and phospholipids. It plays a critical role in cellular energy processes [11]. Many species of microalgae and cyanobacteria are characterized by phosphorus storage in the form of intracellular polyphosphate inclusions [12].

Of particular interest is DNA mapping, because it records phosphorus distribution – one atom bound to each nucleic acid base [13]. In recent years, a surge of interest has also been witnessed in the visualization of DNA within nanoparticles and origami structures [14].

Electron transmission microscopy first allowed researchers to visualize isolated DNA over 75 years ago [15]. A novel circular sputtering technique using heavy metals was developed for the purpose. Uranyl acetate negative staining has been extensively employed for the electron microscopic visualization of DNA and chromatin structures since the 1960s. Nonetheless, analytical TEM is still more frequently employed to identify phosphorus within cellular structures. The qualitative measurement of endogenous elements – like phosphorus in membranes and DNA, nitrogen in polypeptides, and sulfur in methionine- and cysteine-rich proteins ¾ can be conducted pointwise or areawise through the use of EDX and then superimposed on a map. This methodology allowed reasearchers to determine the location of nitrogen- and phosphorus-containing granules in eukaryotic cells (*Fig. 3A*) [16]. Using the same technique the complex elemental composition of vacuolar inclusions of green microalgae were determined [17]. The pphosphorus and other elements were identified in slices of *Drosophila* larval [18], the myelin sheath of human peripheral nerve [19], and in DNA origami (*Fig. 3B–E*).

Mapping on sections over the entire visual area, including total maps with subsequent color-coding of each chemical element of interest (*Fig. 3A*), provides valuable information on the elemental composition and concentration of components in different regions of the sample and allows one to ascertain the subcellular distribution and reveal membranes and cytoplasmic granules.

Recent studies that have employed the EDX method have elucidated the interaction between DNA and Dps proteins within bacterial cells [20]. Dps, a DNA-binding protein, plays a substantial role in shaping the architecture of the bacterial nucleoid [21]. Dps, a ferritin-like protein, is a dodecamer composed of twelve monomers. Each monomer possesses four alpha-helical subdomains arranged to create a dodecahedron exhibiting tetrahedral symmetry (*Fig. 4A*). Elevated Dps synthesis constitutes a common bacterial response to stress [22]. The cytoplasm of starved cells exhibits two- and three-dimensional crystal lattices, structures formed by Dps molecules interspersed with DNA helices (*Fig. 4B*). The crystallization process safeguards DNA from detrimental environmental factors.

A novel method utilizing analytical electron microscopy was developed to confirm the formation of a DNA-Dps complex. The authors of the method hypothesized that the Kα (2.307 keV) peak of sulfur indicates the existence of the DNA binding protein Dps (each Dps protein contains 48 methionine residues) and that the Kα (2.013 keV) peak corresponds to the phosphorus in DNA. Furthermore, the co-occurrence of both peaks in the EDX spectra was supposed to indicate the formation of a DNA-Dps complex (*Fig. 4D*). The results obtained indicated that in the nanocrystal the bulk of the Dps protein is tightly bound to nucleoid DNA, forming a compact structure, which is consistent with previous studies [23, 24]. No sulfur or phosphorus was detected in the control areas (*Fig. 4D*). The significant copper (Cu) signal detected in all the samples originated from the underlying copper substrate meshes.

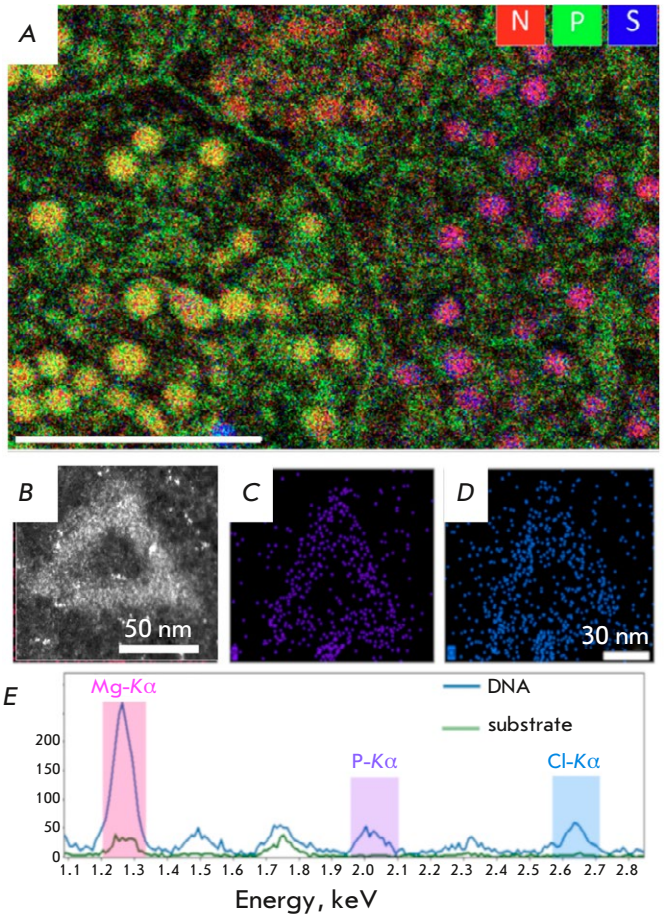

Fig. 3. Elemental mapping performed on cellular sections via EDX. (*A*) Rat Langerhans cells islet (reproduced from [16], open source). Overlapping the nitrogen (red), phosphorus (green), and sulfur (blue) compositional maps facilitates the discrimination of membranes and pellets according to their elemental content. The length of the scale bar is 2 μm. The HAADF image of the DNA-origami triangle (*B*). EDX mapping of phosphorus (C) and chlorine (D) distribution. (*E*) Two summed EDX spectra: the solid blue line is summed over the DNA structure while the green line is summed over the background support. Both spectra represent raw data without background subtraction (reproduced from [14], by permission of the authors)

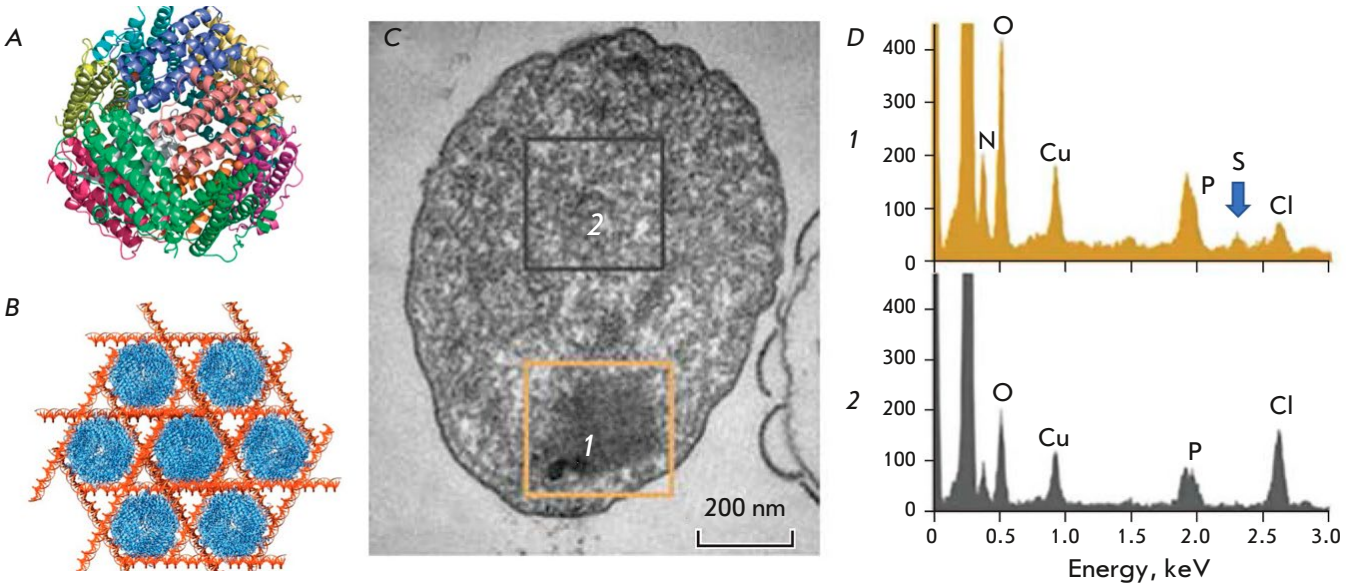

Fig. 4. (*A*) The structure of the Dps protein. (*B*) The model of nanocrystalline array during the formation of the DNA-Dps complex based on cryotomography (reproduced from [23], open source); (*C*) The TEM image of a nanocrystalline condensed structure of DNA-Dps in a resting *E. coli* cell starved for 7 months (reproduced from [20], open source): (*1*) nanocrystalline condensation type, (*2*) nucleoid control region. (*D*) The EDX spectra from selected regions *1* (condensed nucleoid) and 2 (control) in the previous image. The blue arrow indicates the position of the sulfur peak in the spectrum of region 1

An analogous approach was utilized to analyze the stress response following a bacteriophage infection in *Pseudomonas aeruginosa* [25]. The spectral overlap between the phosphorus Ka peak (2.013 keV) and the osmium (Os) M-line (1.914 keV), a consequence of osmium fixation, was circumvented by contrasting samples with 2% ammonium molybdate. All the EDX spectra were normalized against the carbon peak and then superimposed (*Fig. 5A*).

Post-infection, the phosphorus peak, indicative of the DNA content, demonstrated an increase, seemingly suggesting the contemporaneous presence of both phage and host DNA within the cell. A PCR study demonstrated the persistence of substantial quantities of bacterial DNA 40 min following phage infection [25]. Fifteen minutes after a bacteriophage infection, a small sulfur peak was detected by the authors in the EDX spectral analysis (*Fig. 5A*). This peak increased 30 min after infection, which may be a sign that the bacterial cell responds to stress by increasing the synthesis of the anti-stress protein Dps.

THE ELECTRON ENERGY LOSS SPECTROSCOPY (EELS) METHOD

The EELS method is based on the detection of the primary signal; namely, the measurement of the energy that is lost by a portion of the electrons that have passed through the sample as a result of the excitation of the sample atoms [8]. Inelastic electron scattering measurements following sample transmission are performed to determine energy loss during spectral acquisition (*Fig. 2B*). Therefore, the EELS approach accounts for all inelastic electron scattering events, such as collective valence electron excitations (plasmons), inner-shell atomic excitations, and the production of bremsstrahlung X-radiation. [26].

When passing through the sample, the primary electron in the transmission electron microscope column interacts with the inner K-shell electron of the sample atom and transfers part of its energy to it (*Fig. 2B*). Consequently, the electron, possessing elevated energy, achieves an excited state. Given that electrons in the ground state occupy all energy levels below the Fermi level, an electron in the excited state can transition only to unoccupied energy levels above the Fermi level. Therefore, when the incident electron undergoes an energy loss surpassing ΔE during its passage through the sample, the probability of transitioning from the K-shell to an energy level above the Fermi level significantly increases. Therefore, the electron energy loss spectrum (the relationship between signal intensity and energy loss) exhibits a sharp peak commencing at ΔE (*Fig. 2D*). Concurrently, this peak exhibits a “tail” within the higher energy

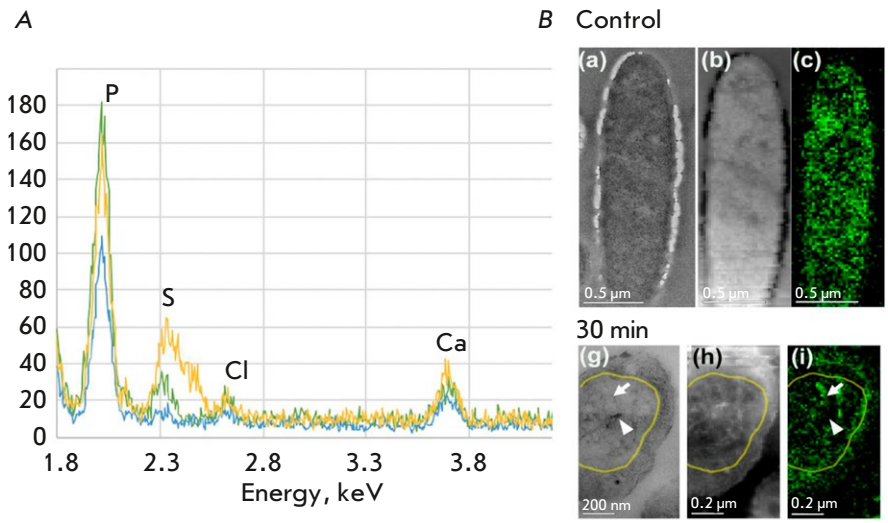

Fig. 5. Analysis of the elemental structure of bacteriophage PhiKZ-infected *P. aeruginosa* cells was conducted using analytical microscopy techniques. (*A*) EDX spectra of control cells (blue), and 15 (green) and 30 min (yellow) after infection with PhiKZ phage. The superimposed EDX spectra were normalized to the carbon peak (not shown in graph). The peaks are designated as follows: P for phosphorus, S for sulfur, Cl for chlorine, and Ca for calcium. (*B*) Distribution of phage and bacterial DNA in the control cells and those infected with *P. aeruginosa*. TEM images (a, g), HAADF images (b, h), EELS of phosphorus in the pseudonucleus (c, i). The phosphorus signal (P) is shown after background subtraction and multiple scattering correction, using Fourier deconvolution of the spectra. The arrows indicate DNA, the arrowheads indicate P-free regions, and the yellow line indicates the pseudonuclear boundary (reproduced from [25], open source)

range. This shape accounts for the designation of the energy loss spectrum peak as an absorption edge. As the threshold edge energy is unique to each chemical element, the ΔE value in the loss spectrum serves to distinguish the elements in the sample [8], enabling elemental analysis and the monitoring of the chemical bonding state and atomic distances by assessing the intensity of characteristic electron energy losses (*Fig. 2D*). The EELS method is typically employed to analyze the fine structure spectra of elements, thereby elucidating the nature of chemical bonds and the electronic structure of materials.

Elemental analysis via EELS typically employs a post-column energy filter (*Fig. 1A*) (for example, GIF Quantum ER, Gatan, USA). In this case, one can refer to energy-filtered transmission electron microscopy (EFTEM). Given the thickness constraints of this analytical method [26], ultrathin sample preparation is standard practice in EELS elemental analysis. EELS spectra are recorded from selected sample sections in the energy range from 100 to 600 eV in the dark-field scanning mode using a HAADF detector. The aforementioned energy range encompasses the most prominent spectral peaks corresponding to the biologically relevant elements phosphorus, nitrogen, oxygen, and calcium, as observed in electron energy loss spectroscopy.

A recent study utilized EELS mapping to depict the localization of phage DNA in the pseudo nucleus of bacteria following infection by the giant phiKZ bacteriophage [25]. Analysis of the bacterial DNA distribution within the cytoplasm was performed by overlaying a phosphorus signal with a HAADF image of the cell (*Fig. 5B*). Phosphorus signals were detected in all the cells examined, though their spatial distribution demonstrated temporal dependence on the infection. Within uninfected cells, the cytoplasmic phosphorus signal distribution was uniform, consistent with the diffuse nucleoid location (*Fig. 5B* (c)). Fifteen minutes post-infection, a uniform cytoplasmic distribution of phosphorus (nucleoid position) was observed. Thirty minutes post-infection, the pseudonuclei exhibited a near-spherical morphology and demonstrated centripetal migration, consistent with the results of prior research [27, 28]. A marked alteration in the phosphorus distribution revealed a complex phage DNA network structure within the pseudonucleus (*Fig. 5B* (i)).

IDENTIFICATION AND MAPPING OF NUCLEIC ACIDS IN VIRUSES

At present, the possibility of mapping nucleic acids on the example of much smaller objects – viruses and bacteriophages – is of particular interest. Prior

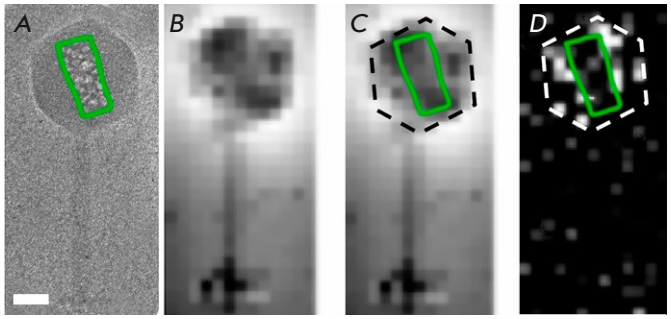

Fig. 6. Localization of the inner body in the phiEL bacteriophage, as demonstrated by phosphorus mapping. (*A*) A cryo-electron microscopy image of the phiEL bacteriophage subjected to high-dose electron irradiation. The inner body region is highlighted by a green line. The scale bar measures 50 nanometers. (*B*, *C*) The HAADF image of the phiEL bacteriophage. A dashed black line denotes the capsid boundary, with the inner body region indicated by a green line (*B*). (*D*) Phosphorus distribution map. The pixel intensities reflect the signal strength of the element in the characteristic electron energy loss spectra. A white dotted line indicates the limits of the capsid, with the inner body region denoted by a green line (reproduced from [31], by permission of the authors)

research has already documented elemental analysis of individual virions [19, 29, 30]. A pioneering study in this area was undertaken in 1980 [19]. Phosphorus was mapped on murine leukemia virus (MuLV) particles embedded in an epoxy resin. The authors successfully documented the phosphorus signal, a constituent of the viral membrane lipids. In 1998, a study on cell cultures infected with transmissible gastroenteritis coronavirus was published [29]. The authors reported recording phosphorus signals from individual viral particles within the cells. Nevertheless, the quality of the provided imagery was insufficient, resulting in ambiguous conclusions. In a later study [30], elemental mapping of whole virions of bacteriophage lambda within films was described. All these experiments were performed using the EFTEM method.

In more recent studies, scanning transmission electron microscopy, combined with energy-filtered electron microscopy (STEM-EELS), has been proposed for elemental mapping [31]. This original technique allows imaging at a lower electron dose than traditional EFTEM. The sensitivity of the method is significantly enhanced by implementing a comprehensive STEM-EELS analysis and using a cryogenic sample holder to mitigate radiation-induced damage. The cooling sample holder for TEM can maintain the observed sample at liquid nitrogen temperature, which reduces electron beam damage to the sample and allows the structure to be studied at low temperatures. This aspect is especially critical in the handling of biological samples [32].

STEM-EELS analysis was conducted on a range of viruses containing DNA and RNA. Contrasting the sample with 2% ammonium molybdate instead of uranium acetate proved better in determining with more accuracy the position of the phosphorus absorption peak (absorption limit near 132 eV), since the uranium absorption peak (absorption limit 96 eV) is located near the phosphorus absorption peak and interferes with background subtraction. The molybdenum absorption peak is characterized by an absorption limit near 400 eV.

In testing the STEM-EELS method, the nucleic acid content inside the capsid of the giant phiEL phage was examined. The bacteriophage capsid has a diameter of 145 nm [33], and its genome comprises of 211 base pairs [34]; in other words, it contains 422 thousand phosphorus atoms as part of double-stranded DNA. This study successfully mapped the genomic DNA location within the bacteriophage capsid and confirmed the existence of an internal protein structure around which the DNA is organized (*Fig. 6C,D*) [31].

The STEM-EELS method was also used to study the phosphorus content in purified inactivated SARS-CoV-2 particles included in the CoviVac vaccine (produced by the Federal Scientific Center for Research and Development of Immunobiological Preparations named after M.P. Chumakov of the Russian Academy of Sciences) [35]. The SARS-CoV-2 virus has a diameter of around 200 nm and contains a single-stranded RNA genome of approximately 30 base pairs. Thus, the phosphorus concentration within the SARS-CoV-2 capsid is five times lower than that of giant bacteriophages, a difference that remains significant even when accounting for the viral lipid envelope. STEM-EELS analysis confirmed the presence of nucleic acid within the virions. *Figure 7A* shows the SEM image of the virion and the corresponding map of the local phosphorus distribution. The phosphorus signal was recorded only from the interior of the virion, and not from the substrate outside it (*Fig. 7B*). Based on prior findings [36] demonstrating an uneven phosphorus signal distribution within the virion, it is posited that RNA is a more plausible source than the viral lipid envelope.

Finally, the application of STEM-EELS revealed a distribution of significantly less RNA within the purified inactivated tick-borne encephalitis virus (TBEV) virions [37]. TBEV nucleocapsids possess a diameter

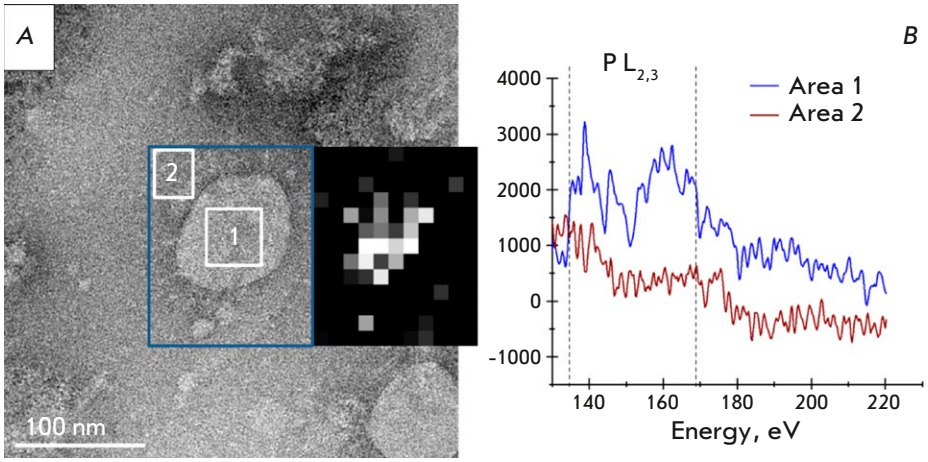

Fig. 7. Visualization and elemental analysis of the inactivated SARS-CoV-2 virion. (*A*) Phosphorus distribution map combined with TEM image. (*B*) Plots of EELS spectra obtained inside the virion (region 1 of *Fig. 7A*) and outside of the virion (region 2 of *Fig. 7A*) (reproduced from [35], by permission of the authors)

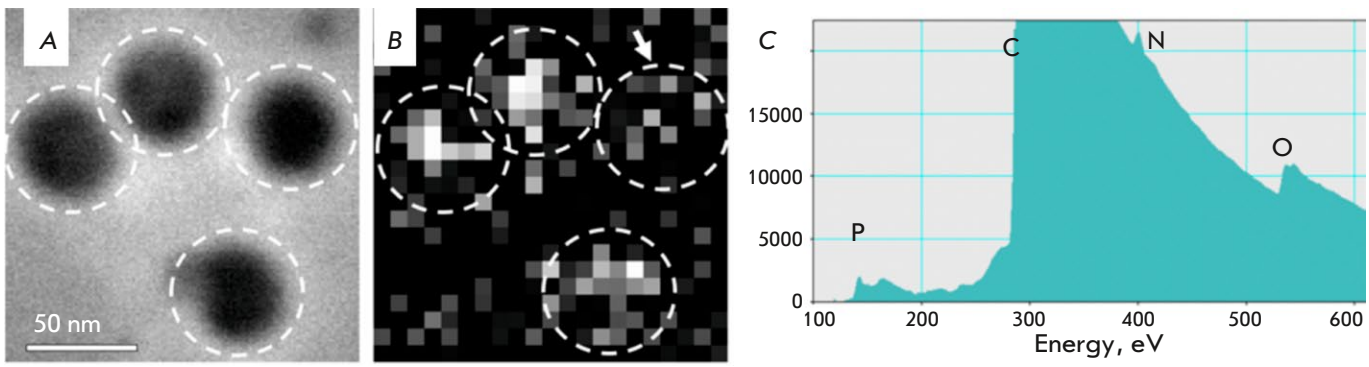

Fig. 8. STEM-EELS analysis of TBEV. (*A*) STEM image of TBEV virions. (*B*) Map of the distribution of phosphorus EELS signals within the same sample. The virion boundaries are indicated by white dashed lines, with the arrow pointing to the virion emitting a reduced phosphorus signal. (*C*) EELS spectrum from a single representative virion. Letters P, C, N, and O represent the spectral edge positions for phosphorus, carbon, nitrogen, and oxygen respectively (reproduced from [37], open source)

of 50 nm, while genomic single-stranded RNA comprises approximately 11 base pairs (*Fig. 8A*). Each virion utilized in this experiment demonstrated a phosphorus signal (*Fig. 8B*), with maximal intensity observed in the central region and minimal intensity at the periphery. This indirectly suggests that the signal originated from the phosphorus within RNA. Analogous heterogeneous phosphorus distributions were observed within SARS-CoV-2 virions (*Fig. 7A*) and phiEL bacteriophage capsids (*Fig. 6*). The TBEV virions under investigation exhibited differential signal intensities (*Fig. 8B*). Formaldehyde inactivation [38] likely accounts for the diminished phosphorus signal (*Fig. 8B*) observed in virions, indicating either RNA loss or disruption of the RNA structure.

CONCLUSIONS

TEM provides high-resolution (nanometer-scale) visualization of the cellular architecture. However, the functional interpretation of macromolecules remains problematic due to the challenges posed by unidentified molecular constituents within the imagery. Combining TEM with EDX permits a high-resolution analysis of endogenous vesicles, diverse tags (including gold or cadmium nanoparticles), and nucleic acids through elemental composition analysis. The application of a cooled sample holder to reduce radiation damage, in conjunction with a comprehensive STEM-EELS analysis, allows for the mapping of phosphorus, enabling the determination of nucleic acid location within nanostructures (50–200 nm), which includes

inactivated viruses. This methodology has proven effective in visualizing intermolecular interactions and identifying alterations in cellular DNA during a viral infection. Elemental mapping of phosphorus within nano-scale virions using EELS is performed at the detection limit, leading to the aqusition of data with a low signal-to-noise ratio. Nevertheless, the EELS method corroborates the presence of RNA in the majority of the analyzed particles, aligning well with prior research [38].

The application of elemental mapping yields objective biomedical information, as evidenced by the lack of phosphorus signal detection in virus-like vaccine components. Elemental mapping is expected to improve advanced experimental analysis of viruses and virus-like particles, thus establishing analytical electron microscopy as a valuable tool for biomedical product testing. ●

The authors express their gratitude to their colleagues, whose contributions were essential to the publication of several works referred to in this review: A.M. Egorov, T.V. Grebennikova, Y.F. Krupyanskii, D.I. Osolodkin, M.V. Burkaltseva, V.N. Krylov, and M.V. Yakunina.

Analytical electron microscopy was performed at the Shared Research Facility "Electron microscopy in life sciences" at Moscow State University (unique equipment "Three-dimensional electron microscopy and spectroscopy").

This work was supported by the Russian Science Foundation (grant No.19-74-30003).

REFERENCES

1. Philimonenko V.V., Philimonenko A.A., Šloufová I., Hrubý M., Novotný F., Halbhuber Z., Krivjanská M., Nebesářová J., Šlouf M., Hozák P. // Histochem. Cell. Biol. 2014. V. 141. № 3. P. 229–239. doi: 10.1007/s00418-013-1178-6.
2. Turk M., Baumeister W. // FEBS Lett. 2020 V. 594. № 20. P. 3243–3261. doi: 10.1002/1873-3468.13948.
3. Nakane T., Kotecha A., Sente A., McMullan G., Masiulis S., Brown P.M.G.E., Grigoras I.T., Malinauskaite L., Malinauskas T., Miehling J., et al. // Nature. 2020. V. 587. № 7832. P. 152–156. doi: 10.1038/s41586-020-2829-0.
4. Yip K.M., Fischer N., Paknia E., Chari A., Stark H. // Nature. 2020. V. 587. № 7832. P. 157–161. doi: 10.1038/s41586-020-2833-4.
5. Martin J.S., Renshaw S.A. // Biochem. Soc. Trans. 2009. V. 37. Pt 4. P. 830–837. doi: 10.1042/BST0370830.
6. Hell S.W. // Angew. Chem. Int. Ed Engl. 2015. V. 54. № 28. P. 8054–8066. doi: 10.1002/anie.201504181.
7. Frank J. // Angew. Chem. Int. Ed. Engl. 2018. V. 57. № 34. P. 10826–10841. doi: 10.1002/anie.201802770.
8. Egerton R.F. // Rep. Progr. Phys. 2009. V. 72. № 1. P. 016502.
9. Brydson R., Brown A., Benning L.G., Livi K. // Rev. Mineral Geochem. 2014. V. 78. P. 219–269.
10. Warley A. // J. Microscopy. 2016. V. 261. № 2. P. 177–184.
11. Bird R.P., Eskin N.A.M. // Adv. Food. Nutr. Res. 2021. V. 96. P. 27–88. doi: 10.1016/bs.afnr.2021.02.001.
12. Vasilieva S. G., Zaitsev P. A., Baulina O. I., Lobakova E. S., Solovchenko A. E., Gorelova O. A. // Russian Nanotechnologies. 2023. V. 18. № 1. P. 53–62 doi: 10.56304/S1992722323010168.
13. Bazett-Jones D.P., Hendzel M.J. // Methods. 1999. V. 17. № 2. P. 188–200. doi: 10.1006/meth.1998.0729.
14. Brintlinger T.H., Buckhout-White S., Bassim N.D., Mathur D., Samanta A., Robinson J.T., Idrobo J.C., Stroud R.M., Goldman E.R., Ancona M.G. // ACS Appl. Nano Materials. 2020. V. 3. № 2. P. 1123–1130.
15. Scott J.F. // Biochim. Biophys. Acta. 1948. V. 2. P. 1–6.
16. Scotuzzi M., Kuipers J., Wensveen D.I., de Boer P., Hagen K.C., Hoogenboom J.P., Giepmans B.N. // Sci. Rep. 2017. V. 7. P. 45970. doi: 10.1038/srep45970.
17. Shebanova A., Ismagulova T., Solovchenko A., Baulina O., Lobakova E., Ivanova A., Moiseenko A., Shaitan K., Polshakov V., et al. // Protoplasma. 2017. V. 254. № 3. P. 1323–1340. doi: 10.1007/s00709-016-1024-5.
18. Aronova M.A., Kim Y.C., Harmon R., Sousa A.A., Zhang G., Leapman R.D. // J. Struct. Biol. 2007. V. 160. № 1. P. 35–48. doi: 10.1016/j.jsb.2007.06.008.
19. Ottensmeyer F.P., Andrew J.W. // J. Ultrastruct. Res. 1980. V. 72. № 3. P. 336–348. doi: 10.1016/s0022-5320(80)90069-6.
20. Loiko N., Danilova Y., Moiseenko A., Kovalenko V., Tereshkina K., Tutukina M., Galina El-Registan G., Sokolova O., Krupyanskii Y. // PLoS One. 2020. V. 15. № 10. P. e0231562. doi: 10.1371/journal.pone.0231562.
21. Antipov S.S., Tutukina M.N., Preobrazhenskaya E.V., Kondrashov F.A., Patrushev M.V., Toshchakov S.V., Dominova I., Shvyreva U.S., Vrublevskaya V.V., Morenkov O.S., et al. // PLoS One. 2017. V. 12. № 8. P. e0182800.
22. Minsky A., Shimoni E., Frenkiel-Krispin D. // Nat. Rev. Mol. Cell Biol. 2002. V. 3. № 1. P. 50–60.
23. Kamyshinsky R., Chesnokov Yu., Dadinova L., Mozhaev A., Orlov I., Petoukhov M., Orekhov A., Shtykova E., Vasiliev A. // Biomolecules. 2019. V. 10. № 1. P. 39.
24. Frenkiel-Krispin D., Minsky A. // J. Struct. Biol. 2006. V. 156. № 2. P. 311–319.
25. Danilova Y.A., Belousova V.V., Moiseenko A.V., Vishnyakov I.E., Yakunina M.V., Sokolova O.S. // Viruses. 2020. V. 12. № 10. P. 1197. doi: 10.3390/v12101197.
26. Oikawa T., Shindo D. Analytical transmission electron microscopy. M.: Technosphere, 2006, 256 p.
27. Mendoza S.D., Nieweglowska E.S., Govindarajan S., Leon L.M., Berry J.D., Tiwari A., Chaikeeratisak V., Pogliano J., Agard D.A., Bondy-Denomy J. // Nature. 2020. V. 577. P. 244–248.
28. Chaikeeratisak V., Nguyen K., Khanna K., Brilot A.F., Erb M.L., Coker J.K.C., Vavilina A., Newton G.L., Buschauer R., Pogliano K., et al. // Science. 2017. V. 355. P. 194–197.
29. Quintana C., Marco S., Bonnet N., Risco C., Gutiérrez

M.L., Guerrero A., Carrascosa J.L. // Micron. 1998. V. 29. № 4. P. 297–307. doi: 10.1016/s0968-4328(98)00011-0.
30. Nevsten P., Evilevitch A., Wallenberg R. // J. Biol. Phys. 2012. V. 38. № 2. P. 229–240. doi: 10.1007/s10867-011-9234-8.
31. Trifonova T.S., Moiseenko A.V., Burkaltseva M.V., Shaburova O.V., Shaitan A.K., Krylov V.N., Sokolova O.S. // Voprosy virosologii. 2021. V. 66. № 6. P. 434–441. doi: 10.36233/0507-4088-80.
32. Mishyna M., Volokh O., Danilova Ya., Gerasimova N., Pechnikova E., Sokolova O.S. // Micron. 2017. V. 96. P. 57–64.
33. Sokolova O.S., Shaburova O.V., Pechnikova E.V., Shaytan A.K., Krylov S.V., Kiselev N.A., Krylov V.N. // Virology. 2014. V. 468–470. P. 472–478. doi: 10.1016/j.virol.2014.09.002.
34. Cornelissen A., Hardies S.C., Shaburova O.V., Krylov V.N., Mattheus W., Kropinski A.M., Lavigne R. // J. Virol. 2012. V. 86. № 3. P. 1844–1852. doi: 10.1128/JVI.06330-11.
35. Bagrov D.V., Glukhov G.S., Moiseenko A.V., Karlova M.G., Litvinov D.S., Zaitsev P.A., Kozlovskaya L.I., Shishova A.A., Kovpak A.A., Ivin Y.Y., et al. // Microscopy Res. Technique. 2022. V. 85. № 2. P. 562–569.
36. Klein S., Cortese M., Winter S.L., Wachsmuth-Melm M., Neufeldt C.J., Cerikan B., Stanifer M.L., Boulant S., Bartenschlager R., Chlanda P. // Nat. Commun. 2020. V. 11. P. 5885. doi: 10.1038/s41467-020-19619-7.
37. Moiseenko A.V., Bagrov D.V., Vorovitch M.F., Uvarova V.I., Veselov M.M., Kashchenko A.V., Ivanova A.L., Osolodkin D.I., Egorov A.M., Ishmukhametov A.A., et al. // Biomedicines. 2022. V. 10. P. 2478. doi: 10.3390/biomedicines10102478.
38. Moiseenko A., Zhang Y., Vorovitch M.F., Ivanova A.L., Liu Z., Osolodkin D.I., Egorov A.M., Ishmukhametov A.A., Sokolova O.S. // Emerging Microbes & Infections. 2024. V. 13. № 1. P. 2290833.

Reactive Byproducts of Plant Redox Metabolism and Protein Functions

E. I. Sharova*, S. S. Medvedev
St Petersburg University, St. Petersburg, 199034 Russian Federation
*E-mail: e.sharova@spbu.ru
Received August 02, 2024; in final form, October 18, 2024
DOI: 10.32607/actanaturae.27477

ABSTRACT **Living organisms exhibit an impressive ability to expand the basic information encoded in their genome, specifically regarding the structure and function of protein. Two basic strategies are employed to increase protein diversity and functionality: alternative mRNA splicing and post-translational protein modifications (PTMs). Enzymatic regulation is responsible for the majority of the chemical reactions occurring within living cells. However, plants redox metabolism perpetually generates reactive byproducts that spontaneously interact with and modify biomolecules, including proteins. Reactive carbonyls resulted from the oxidative metabolism of carbohydrates and lipids carbonylate proteins, leading to the latter inactivation and deposition in the form of glycation and lipoxidation end products. The protein nitrosylation caused by reactive nitrogen species plays a crucial role in plant morphogenesis and stress reactions. The redox state of protein thiol groups modified by reactive oxygen species is regulated through the interplay of thioredoxins and glutaredoxins, thereby influencing processes such as protein folding, enzyme activity, and calcium and hormone signaling. This review provides a summary of the PTMs caused by chemically active metabolites and explores their functional consequences in plant proteins.**
KEYWORDS **post-translational modifications (PTMs) of proteins; proteoforms; carbonylation; nitrosylation; glutathionylation; sulfenylation.**
ABBREVIATIONS **ABA – abscisic acid; AGEs – advanced glycation end products; ALEs – advanced lipoxidation end products; GAPDH – glyceraldehyde-3-phosphate dehydrogenase; GPX – glutathione peroxidase; Grx – glutaredoxin; GSH – glutathione; GSNO – nitrosoglutathione; GSSG – glutathione disulfide; GSNOR – nitrosoglutathione reductase; HNE – 4-hydroxy-2-nonenal; MG – methylglyoxal; MDA – malondialdehyde; MSR – methionine sulfoxide reductase; PDI – protein disulfide isomerase; PRX – peroxiredoxins; PTMs – post-translational modifications of proteins; ROS – reactive oxygen species; SA – salicylic acid; Trx – thioredoxin.**

INTRODUCTION

Living systems demonstrate a remarkable ability to substantially increase the basic information encoded within their genome as regards potential protein functionalities. The principal mechanisms involved here include, but are not limited to, alternative mRNA splicing [1–3] and post-translational modifications (PTMs) of proteins [4–7]. PTMs of proteins, which encompass enzymatic or spontaneous alterations to amino acid residues, can dramatically modulate protein functions or lead to their loss. PTMs significantly increase the diversity and functionality of proteins, serving as a foundation for numerous cellular signaling processes.

Recent studies [4, 8–11] have demonstrated an increasing preference for the term “proteoforms” to encompass the diverse modifications of a protein derived from a single gene. The term denotes protein isoforms originating from a single gene, exhibiting differences in splicing and PTMs [8, 9, 11]. Proteoforms encompass various mechanisms of biological variability (modification) a protein molecule undergoes, determining its functional specificity. Proteoform-level protein characterization is essential for a comprehensive understanding of the biological processes controlled by protein molecules. Protein functions are considerably altered by various PTMs, such as phosphorylation, N- and O-linked glycosylation, methylation, acylation, S-glutathionylation, ubiquitination, and sumoylation [7, 8, 11]. Furthermore, each protein usually posesses several PTM sites. As a result, the number of proteoforms can exceed the number of genes encoding these proteins by several orders of magnitude [8, 12]. Consequently, var-

ied PTM patterns within the same protein substantially increase proteoform heterogeneity [4, 8, 9, 11]. The production of diverse proteoforms from a single gene sequence constitutes an efficient strategy to expand the functional repertoire of the proteins that mediate plants response to changing environmental conditions [11]. A complete understanding of cellular physiological and biochemical processes at the protein level requires knowledge of the identity and functional specificity of these proteoforms.

Most chemical reactions occurring in the body are enzymatically controlled. However, it is possible for many metabolites to spontaneously react with each other and with the biomolecules that are crucial for homeostasis. Highly chemically reactive metabolites are of paramount importance, as they inflict rapid and frequently irreversible damage upon nucleic acids, lipids, carbohydrates, and proteins. Their impact on proteins is defined by the highest degree of complexity and variety [13]. For a long time, spontaneous reactions were thought to impede the well-regulated metabolism. It is now widely accepted that these reactions are fundamentally integrated within the mechanisms governing homeostasis under variable environmental pressures. Numerous PTMs serve as compelling examples illustrating the correlation between spontaneous and enzymatic processes [13, 14]. The strong electrophilic and oxidizing properties of reactive oxygen, nitrogen, and sulfur species and carbonyl-containing compounds are evident in their electron abstraction from carbon, sulfur, and nitrogen atoms and their addition to the nucleophilic groups within proteins [15]. Furthermore, a given active agent, for example the hydroxyl radical, may function as both an oxidant and an electrophile.

This field of study is characterized by rapid advancement necessitating frequent generalization. Our grasp of many phenomena remains incomplete, leading to conjectural interpretations. This review focuses on key findings that illuminate the modern concept of proteoforms produced by the reactive byproducts of plant redox metabolism.

REACTIVE CARBONYL COMPOUNDS

Carbonyl compounds are organic molecules containing a carbonyl group (oxo group), C=O. While typically limited to aldehydes and ketones, carbonyl groups are also present in esters, amides, and other carboxylic acid derivatives. First and foremost, they are intermediates of the glycolysis, the pentose phosphate pathway, and the Calvin cycle [16, 17]. At high concentrations, these compounds can cause spontaneous protein glycation and damage, which they do in humans with diabetes [17]. At the same time, there are carbonyl compounds in cells that exhibit such activity even in micromolar concentrations.

Approximately 20 carbonyl compounds have been identified in plants. The most prevalent among these are the dialdehydes: glyoxal, methylglyoxal (MG), malondialdehyde (MDA), and α,β-unsaturated aldehydes, with 4-hydroxy-2-nonenal (HNE) being the most frequently encountered [16, 17]. The carbonyl groups of these compounds exhibit a high degree of polarization ($C^+=O^-$), facilitating the electrophilic attack on nucleophilic protein residues. Reactive oxygen species (ROS) induce lipid peroxidation, ultimately yielding glyoxal, MDA, and HNE as end products [18]. MG is the result of the spontaneous dephosphorylation of triose phosphates, namely dihydroxyacetone phosphate and glyceraldehyde-3-phosphate [19]. Plant cells usually exhibit MG concentrations under 10 μM [20], but stressful conditions, including phosphate starvation [20] and heavy metal contamination [21], induce substantial elevations in the MG content.

The toxicity of active carbonyl compounds to proteins is a result of their ability to attach to the amino groups of lysine and arginine, and the thiol group of cysteine. The outcome of this addition is the carbonylation of proteins, manifested as an augmented presence of carbonyl groups in their structure. When carbonylation results from the binding of sugars and their derivatives to proteins, the process is termed protein glycation [20, 22], a non-enzymatic PTM resulting from the interaction of proteins with sugars and the carbonyl products of their degradation [17].

The mechanism of glycation, first studied over 100 years ago as a phenomenon of protein fructosylation during food preparation, is now known as the Maillard reaction. At elevated temperatures, spontaneous glucose and fructose degradation products bind to the ε-amino groups of protein lysine residues, forming Schiff bases that subsequently undergo Amadori rearrangement [23].

Similar processes are observed within living cells. Glucose and its oxidation products can launch an electrophilic attack on the ε-amino group of lysine (*Fig. 1A*). As a result, an unstable primary glycation product, a hemiaminal, is formed, with the glycation process being reversible at this stage. However, dehydration of the hemiaminal leads to a Schiff base formation, which then rapidly undergoes Amadori rearrangement, resulting in deoxyfructosyllysine. Further spontaneous reactions lead to the intracellular accumulation of advanced glycation end products (AGEs). AGEs classification is commonly predicated on their carbonyl precursors and/or intermediates [24]. AGEs exhibit significant structural heterogeneity, encompassing diverse aliphatic, aromatic, and heterocyclic

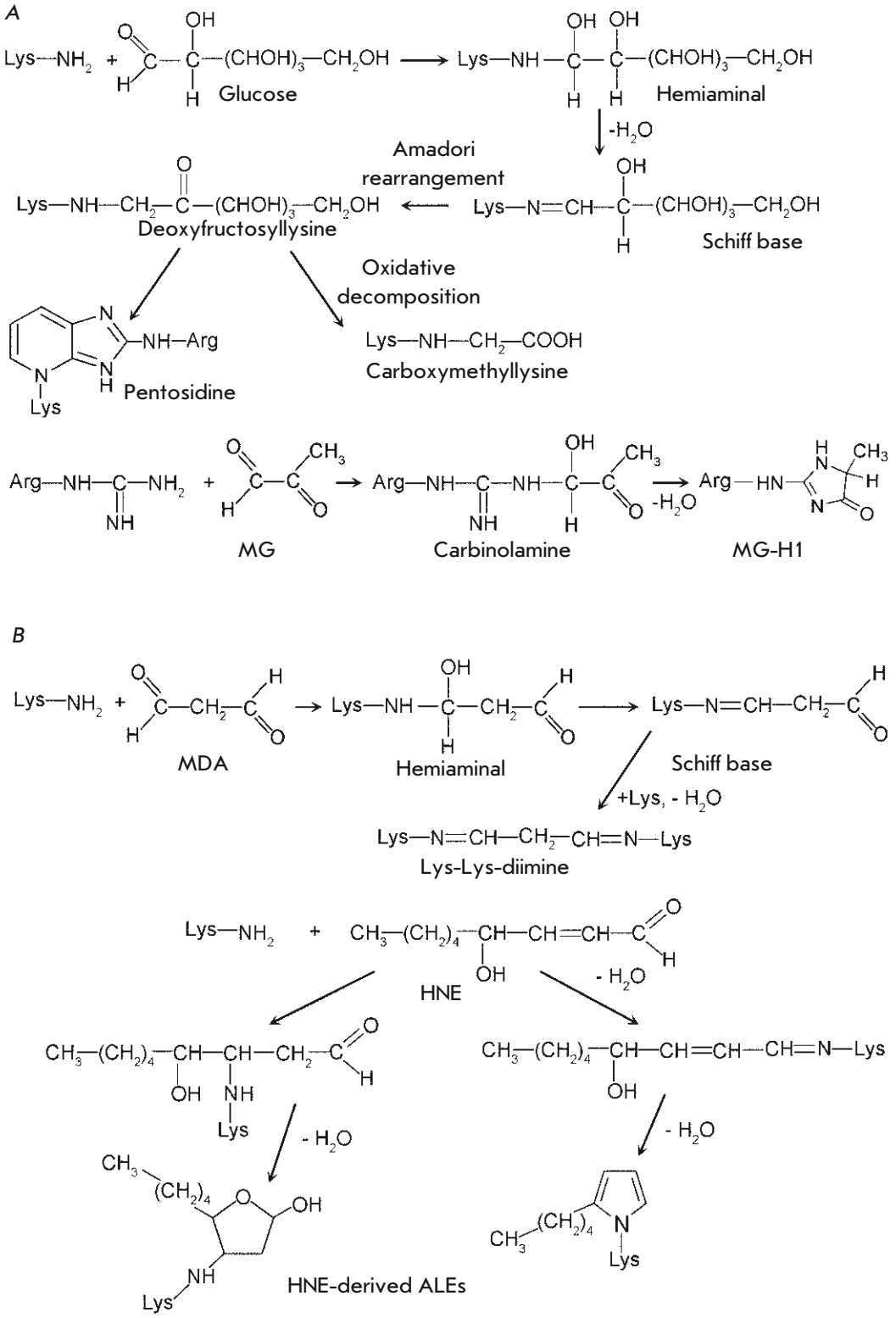

Fig. 1. Protein carbonylation. (*A*) Glycation by glucose and methylglyoxal (MG), (*B*) Lipoxidation by malondialdehyde (MDA) and 4-hydroxy-2-nonenal (HNE)

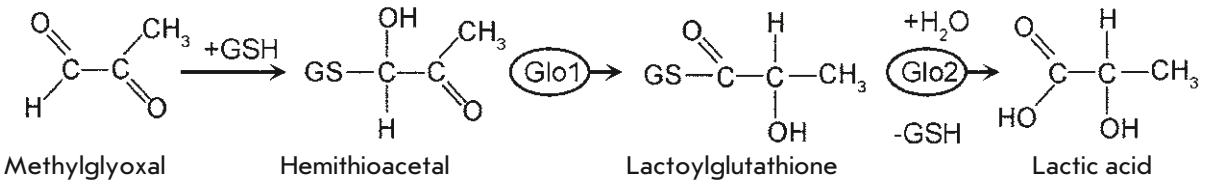

Fig. 2. Detoxification of methylglyoxal (MG) by Glo1 and Glo2 glyoxalases

moieties [17]. Carboxymethyllysine constitutes the most prevalent product of the Maillard reaction. The pentosidine cross-linking between modified lysine and arginine residues also serves as an indicator of protein glycation [25].

Glyoxal and MG exhibit activity a thousand times higher than that of glucose [20]. Their main target is the guanidine group of arginine, with which they form a carbinolamine (*Fig. 1A*) that is spontaneously converted into a series of hydroimidazolone derivatives: G-H (glyoxal-derived hydroimidazolone) and MG-H (methylglyoxal-derived hydroimidazolone) [26, 27]. In plants, MG-H1 is the most abundant AGE [20].

When the products of free-radical oxidation of lipids serve as carbonylation agents, then protein lipoxidation occurs [28]. While this modification is not inherently oxidative, it frequently exacerbates the damage to the protein under oxidative stress conditions. The accumulation of advanced lipoxidation end products (ALEs) results from the spontaneous transformations of unstable primary adducts, which exhibit a range of characteristic chemical structures within proteins [29]. The proteins involved in basic metabolic pathways, signal transduction, cytoskeletal structure, and transcriptional control are all targets of lipoxidation.

The end products of the free-radical oxidation of lipids actively attack lysine residues [27]. The interaction between MDA and lysine results in the formation of a hemiaminal, which is promptly converted to a Schiff base (*Fig. 1B*). The interaction of the second aldehyde group of MDA with a lysine residue of the same or another protein results in cross-linking in the form of lysine-lysine diimine, a common ALE [30]. The attachment of HNE and other α,β-unsaturated aldehydes to lysine residues in proteins occurs via the Michael addition (*Fig. 1B*) [27, 29]. Among the most significant hallmarks of protein damage resulting from lipid peroxidation are HNE-derived heterocyclic protein adducts.

Plant protein glycation and lipoxidation significantly augment under stressful conditions [17, 20, 31]. Given the irreversible nature of these alterations, the principal survival strategy of organisms involves antioxidant-mediated prevention of lipid peroxidation and enzymatic detoxification of MG and glyoxal by glyoxalases.

Glyoxalases convert MG into lactic acid *(Fig. 2)* and glyoxal into glycolic acid [24]. The reactions proceed with glutathione (GSH) functioning as a cofactor. The spontaneous reaction between MG and the sulfhydryl group of GSH produces a hemithioacetal. Glyoxalase I (Glo1) catalyzes the isomerization of this adduct to lactoylglutathione, which is then hydrolyzed by glyoxalase II (Glo2). The presence of glyoxalases has been documented across a wide range of prokaryotic and eukaryotic organisms. In Arabidopsis, 22 genes encoding Glo1 and 9 genes encoding Glo2 have been identified. These enzymes are the most active within chloroplasts. However, their presence has also been observed in mitochondria, nuclei, cytosol, cell walls, and peroxisomes [32].

Irreversible protein carbonylation occurs throughout the plant life cycle and is widely considered an unavoidable process of protein damage, aggravated by stress. It is evident that our understanding of the functional aspects of protein carbonylation lags considerably behind the progress made in its chemical study. Published data suggest that protein carbonylation is subjected to fine regulation and is involved in hormonal signaling, seed germination, flowering, and other processes, rather than being solely dependent on the reactive carbonyl compounds level [33].

REACTIVE NITROGEN SPECIES

Reactive nitrogen species are formed as a result of spontaneous redox transformations of nitric oxide ·NO and a number of other nitrogen-containing substances. The involvement of reactive nitrogen species in plant growth, stress response, and hormone signaling has gained significant attention in recent years [34–37].

The biosynthesis of ·NO in mammals involves the conversion of arginine by nitric oxide synthases. These enzymes are NADPH-dependent oxygenases with flavin, iron-porphyrin, and tetrahydrobiopterin

as essential cofactors. The function of NO synthases extends beyond ·NO synthesis to include the targeted nitrosylation of proteins, achieved through protein-protein interactions [38].

Plant genomes lack enzymes that are homologous to mammalian NO synthases. Yet, there is evidence that ·NO generation via arginine and polyamine oxidation is possible [39]. The primary mechanism of ·NO production in plants is the single-electron reduction of nitrite (NO_2^-), facilitated by cytoplasmic nitrate reductases. These molybdenum cofactor-containing NADPH-dependent oxidoreductases demonstrate a very limited (1%) nitrite reductase activity. Similar to many other higher plants, Arabidopsis possesses two nitrate reductases. NR1 demonstrates a high capacity to produce ·NO, while NR2 is responsible for 90% of the enzymatic activity converting nitrate to nitrite [39]. Under hypoxic conditions, the mitochondrial electron transport chain reduction of NO_2^- substantially contributes to cellular ·NO accumulation [39].

Peroxynitrite $ONOO^-$, nitrosonium cation NO^+, nitrogen dioxide $\cdot NO_2$, etc., interact readily with proteins (*Fig. 3A*). NO-dependent protein PTMs of biological significance involve the nitrosylation of transition metals, S-nitrosylation of cysteine residues, and tyrosine nitration [40]. S-nitrosylation serves a crucial regulatory function. Therefore, disruption of its activity in the human body is associated with severe neurodegenerative diseases, immune system impairment, and cardiovascular dysfunction [38]. In plants, S-nitrosylation affects enzymatic activity, subcellular localization, proteolytic degradation rates, and protein-protein/protein-DNA interactions [34, 41, 42].

Protein nitration is primarily inflicted by $ONOO^-$, while S-nitrosylation is predominantly mediated by nitrosoglutathione (GSNO), which is generated through the reaction of GSH with reactive nitrogen species (N_2O_3, NO^+) (*Fig. 3B*). GSNO serves as a storage and transport form of ·NO within plant cells [43]. Spontaneous transnitrosylation reactions transfer ·NO from GSNO to the thiol groups of proteins *(Fig. 3C)*.

GSNO denitrosylation is a function of the activity of nitrosoglutathione reductases (GSNORs), which are conserved proteins found in the cytoplasm and nucleoplasm [44]. The denitrosylation of SH-groups of proteins (R-SNO → R-SH) is achieved through the action of thioredoxins (Trx) or via GSH transnitrosylation (*Fig. 3C*). Along with GSNOR and Trx, reactive nitrogen species detoxification is facilitated by peroxiredoxins (PRX), which catalyze the conversion of peroxynitrite to nitrite (*Fig. 3D*) [34, 45]. This process yields a reduced thiol protein (R-SH) and oxidized Trx, with the latter undergoing reduction by NADPH-dependent Trx reductase. Transnitrosylation is catalyzed by a transnitrosylase possessing an SNO moiety, which facilitates the transfer of the ·NO to the target protein [34].

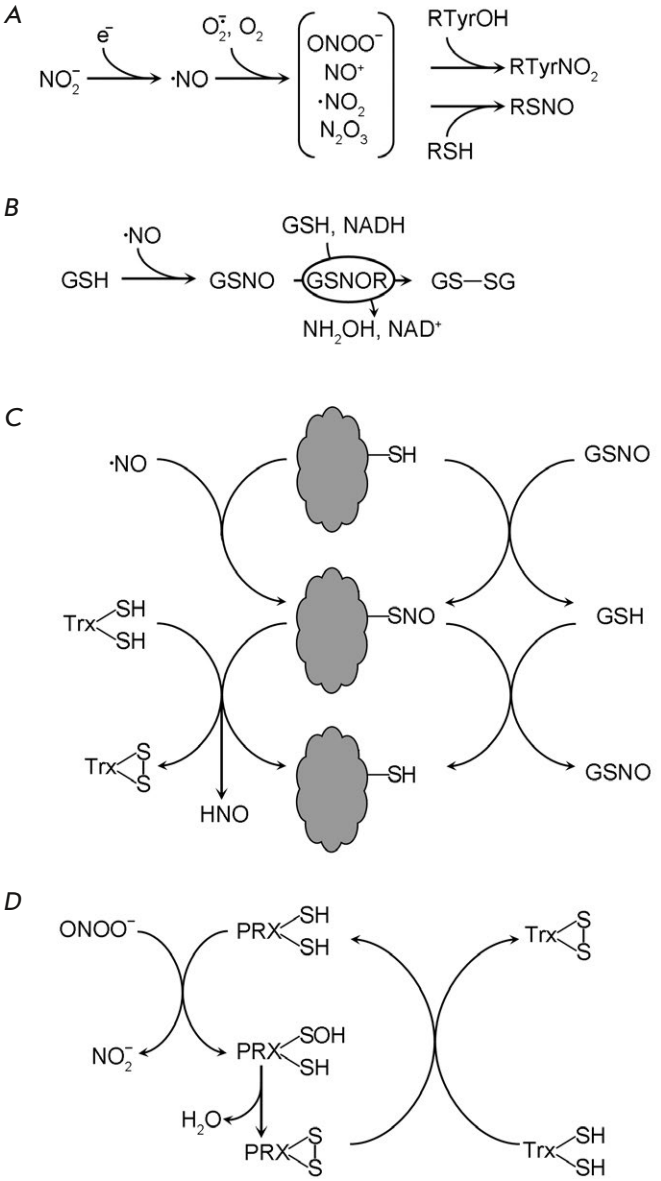

Fig. 3. The effect of reactive nitrogen species on proteins. (*A*) The general scheme of nitric oxide (·NO) formation, its conversion into chemically active species and incorporation into proteins, (*B*) Glutathione (GSH) nitrosylation and nitrosoglutathione (GSNO) denitrosylation with nitrosoglutathione reductase (GSNOR), (*C*) Nitrosylation, transnitrosylation and denitrosylation of proteins, (*D*) Utilization of peroxynitrite ($ONOO^-$) with peroxyredoxins (PRX). Trx – thioredoxins

In both plants and animals, nitration typically leads to the proteins damage and subsequent degradation. Particularly susceptible to nitration are catalase and the enzymes of the ascorbate-glutathione cycle, the main participant in ROS removal in plants [46].

Due to its lipophilic nature and ability to readily cross membranes, the free radical ·NO serves as an effective signaling molecule in autocrine and paracrine cellular communication. The signaling role of ·NO has been extensively investigated in studies of mammals and humans [38]. Guanylate cyclase, a key ·NO receptor, is known to undergo nitrosylation of its heme iron (Fe^{2+}), forming FeNO. The enzyme activated through this modification produces cyclic GMP, which functions as a secondary messenger [47].

The sensitivity to nitric oxide is an evolutionarily conserved characteristic of hemoproteins with H-NOX (Heme-nitric oxide/oxygen binding) domains. Domains with the ability to serve as ·NO sensors have been detected in bacteria, fungi, and animals, including humans [48, 49]. It used to be believed that these proteins were absent in plants; however, recent research has demonstrated the existence of several ·NO-sensitive hemoproteins in plants. Hemoproteins in plant organisms sensitive to ·NO were discovered as possessing conserved H-NOX domains that can bind both ·NO and O_2. Several signaling pathways utilizing these proteins as sensors for ·NO or O_2 have been characterized. Specifically, plant hemoproteins with H-NOX domains have been demonstrated to mediate crucial ·NO-dependent processes, including pollen tube growth and stomatal closure [51].

The understanding of ·NO-signaling pathways in plants is yet to be fully expanded. A dearth of reliable data exists regarding the functions of cyclic GMP and nitrosylation of the protein heme and non-heme iron. At the same time, the impact of S-nitrosylation on the enzymatic activity, subcellular localization, proteolysis rate, and protein-protein interactions affecting the proteins of the basic metabolism has been established [52]. The activating (+) and inhibitory (–) effects of S-nitrosylation were confirmed for enzymes that regulate the balance of ROS in plant cells: superoxide dismutase (–), catalase (–), ascorbate peroxidase (+), mono- and didehydroascorbate reductases (–).

The process of S-nitrosylation influences the proteins that participate in hormone signaling [47, 53]. In Arabidopsis seeds, the accumulation of ·NO during imbibition leads to the S-nitrosylation and proteasomal degradation of ABI5, a transcription factor crucial for abscisic acid (ABA)-dependent gene expression [42]. Consequently, ABA signaling is suppressed, thereby stimulating seed germination. In ABA-dependent stomatal closure, ·NO appears to mediate the termination of this process by suppressing ABA signaling; this is achieved via nitration/S-nitrosylation of the PYR1 hormone receptor [54] and the SnRK2.6 protein kinase, both crucial components of ABA signaling [55].

The effect of ·NO on gibberellin and auxin signaling in Arabidopsis has been reported. The conserved cysteine residue within the DELLA protein RGA has been demonstrated to undergo S-nitrosylation, thus inhibiting the proteasomal degradation of this negative regulator of gibberellin signaling [56]. S-nitrosylation-mediated prevention of Aux/IAA17 proteolysis leads to the suppression of auxin signaling [57].

So, the information on the effects of reactive nitrogen species on plant proteins largely describes the mechanisms and roles of S-nitrosylation. The existing literature on transition metal nitrosylation within proteins is scarce, notwithstanding the discovery of plant proteins containing NO-sensitive H-NOX domains [50].

REACTIVE OXYGEN SPECIES

Redox transitions $O_2 \leftrightarrow H_2O$ in living organisms invariably produce various ROS, including $O_2^{\cdot -}$, H_2O_2, ·OH, $^1O_2$, capable of direct interaction with proteins.

Molecular oxygen typically exists in a relatively unreactive triplet state ($^3O_2$). The formation of ROS occurs through enzymatic and non-enzymatic processes, specifically within the mitochondrial and chloroplast electron transport chains, peroxisomes during photorespiration, cell walls during hypersensitive responses, and in the cytoplasmic and nucleoplasmic compartments. $^3O_2$ is activated via two primary mechanisms: 1) increase in the energy of one of the electrons and appearance of the active singlet form of oxygen $^1O_2$ under the influence of photosensitizers (mainly excited triplet chlorophyll ^{3}P680*) and UV radiation; and 2) reduction of one of the $^3O_2$ atoms and its transformation into a superoxide anion radical ($O_2^{\cdot -}$) by metals with variable valency or organic electron donors [58]. In acidic environments (vacuoles, cell walls), $O_2^{\cdot -}$ is protonated and converted to the hydroperoxyl radical ($HO_2^{\cdot}$). Hydrogen peroxide (H_2O_2) is a product of the activity of superoxide dismutases, plant class III peroxidases, amine oxidases, and oxalate oxidases, as well as spontaneous transformations of $HO_2^{\cdot}$ and $O_2^{\cdot -}$. The formation of the hydroxyl radical ·OH occurs by the Fenton reaction from H_2O_2 with the participation of transition metals: $H_2O_2 + Fe^{2+}(Cu^{+}) \rightarrow {\cdot}OH + Fe^{3+}(Cu^{2+}) + OH^{-}$.

The high reactivity of ROS results in reactions with proteins, lipids, carbohydrates, and nucleic acids. Highly reactive oxygen species, such as ($HO_2^{\cdot}$ and

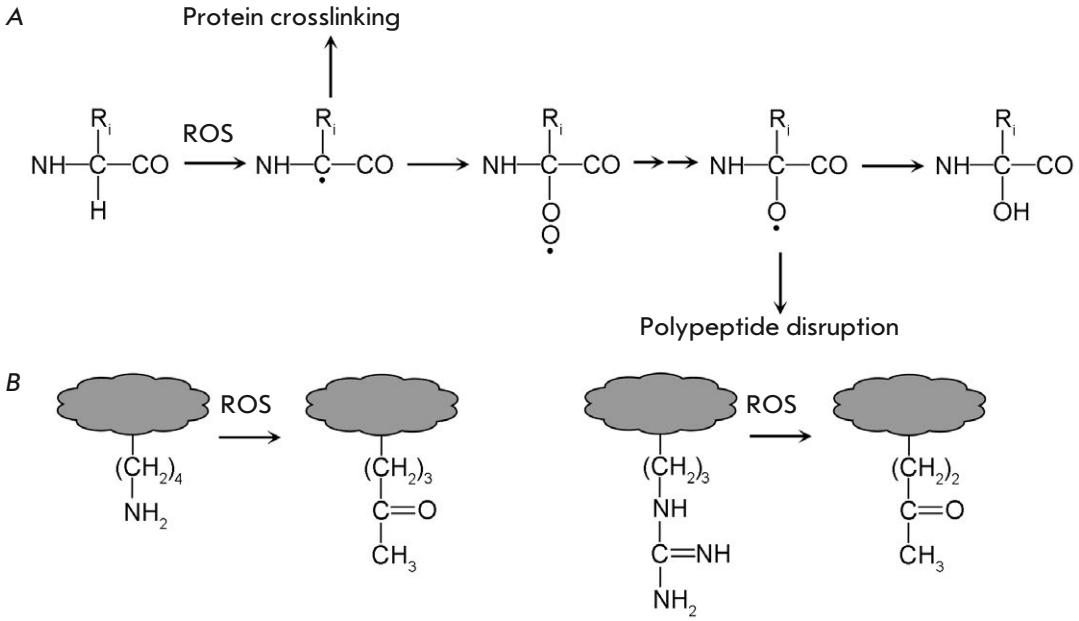

Fig. 4. Irreversible oxidation of the polypeptide chain (*A*) and amino acid side chains (*B*) under the action of ROS

·OH), initiate chain reactions resulting in the generation of numerous free radicals, thereby inducing biomolecular degradation [59].

ROS selectivity is inversely correlated with their activity. Thus, both the main protein chain and side chains of amino acid residues are vulnerable to ·OH (*Fig. 4*). Hydroxyl radical initiation of free radical processes causes irreversible damage to protein, including cross-linking, polypeptide chain disruption, and oxidative deamination of lysine and arginine, along with proline and glutamic acid degradation [60, 61]. The aforementioned modifications result in a higher relative carbonyl content within the proteins. Such carbonylation is referred to as direct or primary carbonylation, because the carbonyl groups are formed as a result of oxidation of the polypeptide itself. The involvement of $O_2^{\cdot -}$ in this process stems from the typical Haber-Weiss reaction-mediated genesis of ·OH ($O_2^{\cdot -} + H_2O_2 \rightarrow O_2 + {}^{\cdot}OH + OH^-$), a reaction catalyzed by iron and copper ions (Fenton reaction).

The inherent instability of singlet oxygen results in its immediate interaction with carbon-carbon double bonds within lipids, proteins, and carotenoids. In proteins, tryptophan residues constitute its principal target.

Given the substantial reactivity and lack of selectivity exhibited by $O_2^{\cdot -}$, ·OH, and $^1O_2$ with biomolecules, the primary defense mechanism involves preventing the formation of and eliminating these ROS.

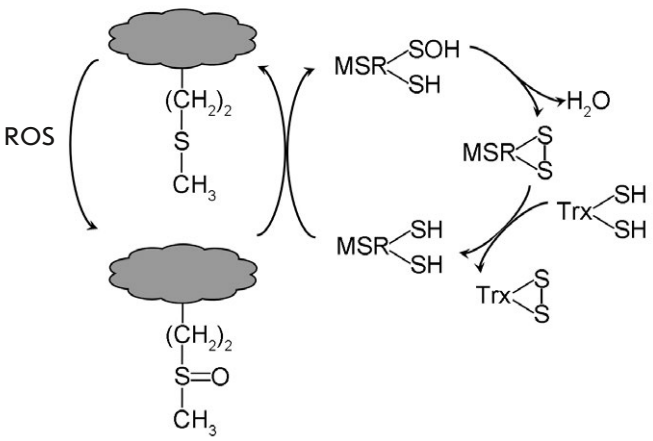

Fig. 5. Reduction of oxidized methionine with methionine sulfoxide reductase (MSR)

Thus, superoxide dismutases, present in all cell compartments, catalyze the conversion of $O_2^{\cdot -}$ to H_2O_2 whereas carotenoids physically quench $^1O_2$.

Hydrogen peroxide has proven to be a useful reagent for the highly selective and reversible redox modification of proteins [65–67]. Notably, it selectively oxidizes methionine and cysteine residues within living cells [13]. The single-step oxidation of methionine (*Fig. 5*) yields methionine sulfoxide, thereby in-

hibiting the proteins biological activity. The reduction of methionine sulfoxide is catalyzed by methionine sulfoxide reductases (MSRs). Plant MSRs are characterized by a catalytic site containing two cysteine residues [68]. One cysteine (catalytic) is in the form of the thiolate anion (S^-) and is converted into sulfenic acid (SOH), reducing methionine sulfoxide. The other (resolving cysteine) interacts with SOH, which leads to the formation of a disulfide bond. The regeneration of enzymes utilizes Trx, while the Trx regeneration is facilitated by NADPH-dependent or ferredoxin-dependent thioredoxin reductases, as described below. In plant cells, MSRs are located in the cytoplasm, mitochondria, plastids, and endoplasmic reticulum [68]. The methionine sulfoxide/MSR system is often regarded as an "emergency discharge" that channels the ROS attack in the repairable direction [69].

Protein oxidation mediated by ROS, unlike carbonylation with carbohydrate and lipid metabolism byproducts, frequently exhibits reversibility and regulatory functions. These modifications involve a close interplay between spontaneous and enzymatic processes. These reactions collectively comprise a complex network vital to living cells and comparable in significance to reversible protein phosphorylation. This justifies considering ROS as key signaling molecules in various signaling pathways, including those involved in the stress response [70–73].

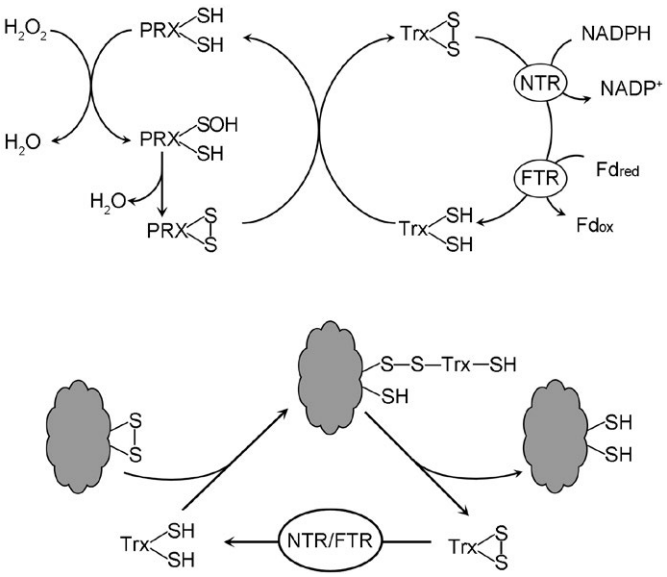

Fig. 6. Catalytic cycles of peroxiredoxins (PRX) and thioredoxins (Trx). NTR and FTR are NADPH–dependent and ferredoxin-dependent thioredoxin reductases, respectively. Fd_{red} – reduced ferredoxin, Fd_{ox} – oxidized ferredoxin

OXIDATION OF CYSTEINE RESIDUES IN PROTEINS

The thiol group of cysteine SH can undergo a range of significant modifications, including oxidation to sulfenic, sulfinic, and sulfonic acids (SOH, SO_2H, and SO_3H, respectively), disulfide bond formation (intra- or intermolecular), glutathionylation [74], and persulfidation (interaction with hydrogen sulfide) [75].

Under stress conditions, any SH group in proteins can be oxidized to sulfenic acid by various ROS, including H_2O_2 at elevated concentrations [13]. Under favorable conditions, ROS are primarily targeted at dissociated SH-groups, namely, thiolate S^- anions. Under physiological conditions, the SH group of cysteine is not dissociated: it has a pKa equal to 8.3. However, a number of proteins contain SH groups that have a pKa below 7 in their microenvironment and dissociate at physiological pH values. These are primarily PRX, glutathione peroxidases (GPX), glutaredoxins (Grx), Trx, and MSR.

H_2O_2 utilization involves thiol peroxidases, PRX and GPX, which thiolate anion is directly oxidized to sulfenic acid. Plants, in contrast to animals, exhibit diminished GPX activity yet display a diverse array of active PRXs [76, 77]. The interaction between the sulfenic acid and the resolving thiol group in a standard 2Cys-PRX leads to the formation of an intramolecular disulfide bond (*Fig. 6*).

2Cys-PRX reduction by Trx proceeds via mixed disulfide bond formation. Trx-mediated reduction of disulfide bonds occurs not only in PRX, but also in numerous other proteins residing within diverse cellular compartments, including the cytoplasm, nucleus, plastids, mitochondria, endoplasmic reticulum, and cell wall [78, 79]. The reduction of oxidized Trx is catalyzed by Trx reductases. In plants, these enzymes are represented by NADPH-dependent flavin NTRs and ferredoxin-dependent FTRs with iron-sulfur clusters [4Fe-4S] in their active site, as well as redox-active S-S bonds. Additionally, there is NADPH-dependent NTRC, which assumes the roles of Trx and NTR.

All the reviewed proteins possess redox-sensitive cysteine residues which mediate their involvement in the diverse processes governing the redox metabolism of all living organisms, including plants.

GLUTATHIONYLATION OF PROTEINS

Glutathionylation predominantly targets Grx, which catalytic cycle involves such modification of the thiolate anion (*Fig. 7*). Nonetheless, under conditions of oxidative stress, other proteins are also glutathionylated. More than 2,000 glutathionylation sites have been identified within the human proteome [82]. The -S$^{\bullet}$,

-S^-, -SOH protein groups exhibit susceptibility to glutathionylation [74]. Glutathionylation is not solely mediated by GSH but also by GSSG, which accumulates under conditions of stress. The glutathionylation of SOH is regarded as a way to prevent the progression of irreversible thiol group oxidation.

Protein deglutathionylation is carried out by Grx, although under stress conditions, they may, in contrast, act as agents of glutathionylation. Glutathionylation, therefore, is a reversible modification that typically inhibits the function of protein. The primary enzymatic targets in plants are cytoplasmic glyceraldehyde-3-phosphate dehydrogenase (GAPDH), other glycolytic enzymes, chloroplast β-amylases, and mitochondrial glycine decarboxylase [74].

FUNCTIONS OF REDOX MODIFICATIONS OF PROTEIN SULFHYDRYL GROUPS

The principal regulatory mechanism of ROS involves the modification of the target protein thiol groups via S-sulfenylation, S-nitrosylation, and S-glutathionylation. The oxidation of the thiol groups to sulfinic and sulfonic acids typically results in irreversible damage to protein function [83, 84].

Oxidative protein folding

Most proteins in the cytoplasm, nucleoplasm, and organelles contain reduced SH groups of cysteine. The process of oxidative folding, which involves the formation of disulfide bridges between the cysteine residues of newly synthesized proteins, is localized in the endoplasmic reticulum, Golgi apparatus, mitochondrial intermembrane space, and thylakoid lumens [85]. The most thoroughly investigated process is oxidative folding in the endoplasmic reticulum lumen. This process affects proteins possessing an N-terminal signal sequence, enabling them to co-translationally enter the endoplasmic reticulum and follow the secretory pathway to the vacuole, cell wall, and plasma membrane [86, 87]. It has been suggested that the stabilization of the native protein conformation in such oxidative compartments is the principal role of disulfide bonds [88].

Protein disulfide isomerase (PDI) with two cysteine residues per each of its two active sites [89] is the central catalyst for oxidative folding. The presence of a multicomponent redox system within the endoplasmic reticulum lumen results in a dynamic equilibrium, where PDI exists in both the oxidized and reduced forms (*Fig. 8*). PDI oxidation is facilitated by flavin-containing thiol oxidase ERO1 (endoplasmic reticulum oxidoreductin), which utilizes molecular oxygen and produces H_2O_2. H_2O_2 removal may be achieved through either aquaporin-mediated cytoplasmic diffusion or via thiol peroxidases situated within the endoplasmic reticulum lumen [77]. Furthermore, similar to mammals, plants possess QSOX, a thiol oxidase that combines the functionalities of ERO1 and PDI through O_2-dependent oxidation of cysteine residues within nascent substrate proteins [90].

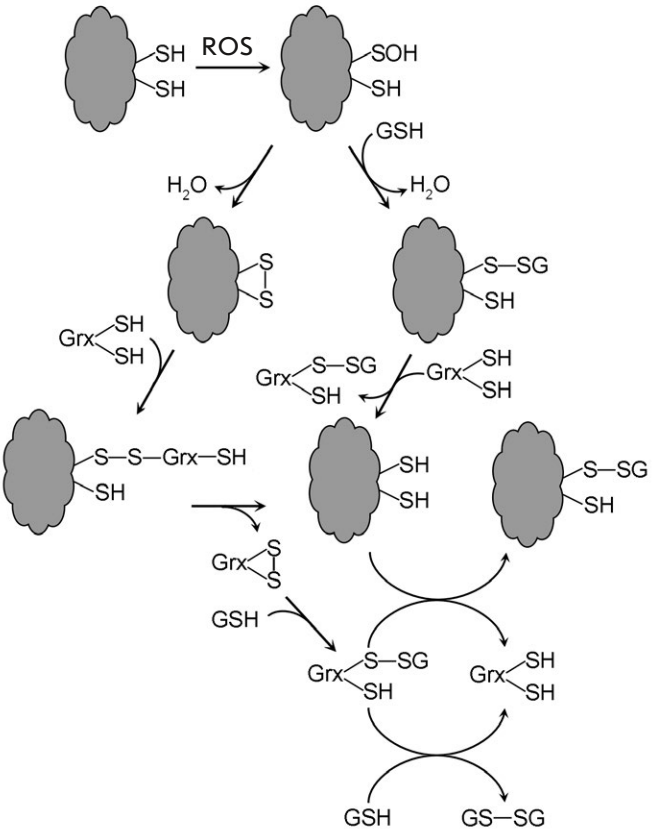

Fig. 7. Glutathionylation and deglutathionylation of proteins. Grx – glutaredoxins

Disulfide bond formation requires PDI in its oxidized state (*Fig. 8B*). During oxidative protein folding, PDI is reduced, contributing to the reduced/oxidized PDI balance. A critical component of this balance is the GSH/GSSG redox buffer within the endoplasmic reticulum. The reduction of PDI is possible at the expense of GSH. The reduced PDI facilitates isomerization and reduction of disulfide bonds (*Fig. 8C*).

Redox regulation of enzyme activity

Spontaneous and enzyme-controlled oxidative modifications of SH groups affect the conformation of proteins and thereby change their catalytic activity, localization, and ability to protein-protein interact. The cytoplasmic GAPDH in mammals appears

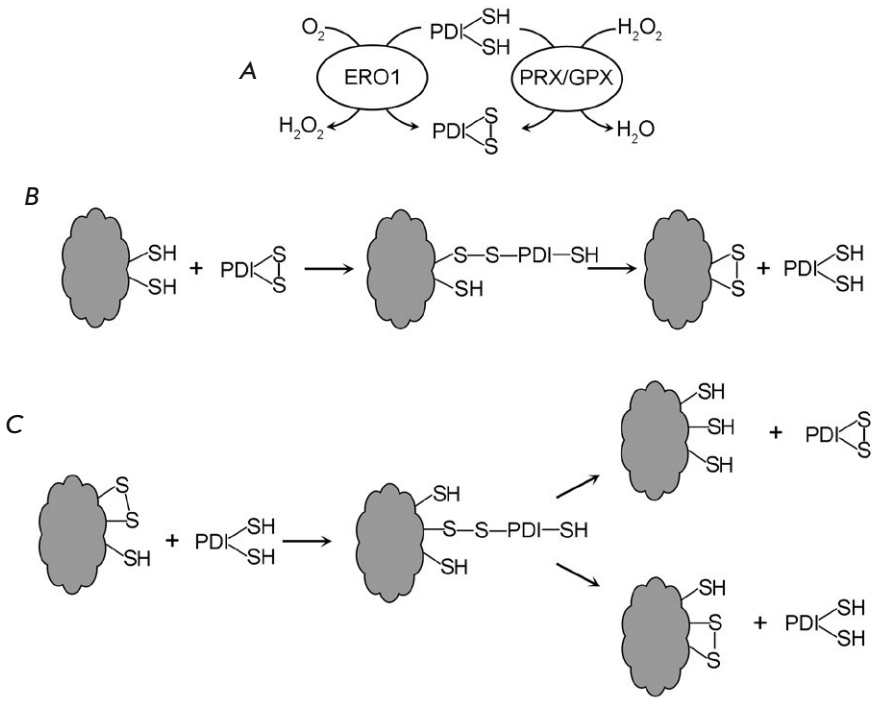

Fig. 8. Oxidative folding of proteins in the endoplasmic reticulum lumen. (*A*) Oxidation of protein disulfide isomerase (PDI) under the action of thiol oxidase (ERO1) and thiol peroxidases (PRX and GPX), (*B*) Formation of disulfide bonds by the oxidized form of PDI, (*C*) Isomerization and reduction of disulfide bonds by the reduced form of PDI

to be the most thoroughly researched enzyme in this regard [91]. The active center of this enzyme contains an SH-group with an acid dissociation constant pKa = 6, which is in the form of a thiolate anion ($-S^-$) and exhibits the properties of a strong nucleophile. Oxidation, glutathionylation, and S-nitrosylation of the thiolate anion inhibits GAPDH catalytic activity. Nuclear translocation of oxidized GAPDH initiates the apoptotic pathway. Plant cells possess both cytoplasmic NAD-dependent and plastid NADPH-dependent GAPDH enzymes, both highly sensitive to ROS [92].

Much research has explored the oxidative modifications of catalases in mammals. While oxidation inhibits the catalytic activity of these peroxisomal enzymes, it allows them to participate in protein-protein interactions, enter the nucleus, and influence gene expression. Plant studies have shown similar results [93].

Oxidative stress significantly impacts aconitase, a Krebs cycle enzyme, by oxidizing its iron-sulfur clusters ($[4Fe\text{-}4S]^{2+} \rightarrow [3Fe\text{-}4S]^{+}$) and sulfhydryl groups (SH → SOH) [94]. Glucose-6-phosphate dehydrogenase, an enzyme in the pentose phosphate pathway, is especially vulnerable to ROS [95].

Redox balance is critical for the processes within chloroplasts. Redox regulation plays a significant role in chlorophyll biosynthesis [96, 97]. This process is known to be controlled by NTRC, a C-type NADPH-dependent Trx reductase that combines the functions of Trx and Trx reductase, since unlike classical Trx reductases, the activity of this enzyme affects a wide range of proteins, not just Trx. NTRC maintains the reduced state of the SH-groups of the CHLI subunit of Mg-chelatase, one of the key enzymes of chlorophyll biosynthesis, as well as that of ADP-glucose pyrophosphorylase, an enzyme that determines the rate of starch biosynthesis. Inhibiting NTRC thus impairs chlorophyll and starch biosynthesis [98].

The presence of Trx and its reductases in chloroplasts is necessary in order to activate ribulose bisphosphate carboxylase and other enzymes in the Calvin cycle in response to light [98].

The examples above are all cases where the oxidation of SH groups inhibits enzyme activity. There is less information about the activation of enzymes by the oxidation of SH groups. For example, Arabidopsis ascorbate peroxidase is activated if the SH-group of Cys82 is glutathionylated or is involved in S-S-binding [99]. Dimerization of γ-glutamyl-cysteine synthetase due to the formation of S-S bonds leads to the activation of this key enzyme of GSH biosynthesis [74].

Signaling role of oxidative modifications of protein thiol groups

A significant number of components within plant signaling pathways are easily modified by oxidation. For example, the ABA receptor PYR1 and the negative

regulators of ABA signaling (ABI1 and ABI2) are inactivated upon oxidation of thiol groups [100]. Salicylic acid (SA) signaling is significantly influenced by redox regulation [101]. The signaling regulator NPR1 (a coactivator of SA-dependent gene transcription) is known to reside in the cytoplasm in an oligomeric form supported by S-S-bridges in the absence of SA. This oligomeric state is reinforced by S-nitrosylation [102]. Pathogen attack triggers SA synthesis, causing oxidative stress, which the plant compensates for by boosting antioxidant defenses, including Trx activation [103]. Thioredoxin-mediated reduction of disulfide bonds in NPR1 leads to oligomer dissociation and nuclear translocation of dimers. These dimers then interact with TGA transcription factors to activate the transcription of pathogenesis-related (PR) genes [104, 105].

The activation of the MAP kinase cascade by ROS is a well-understood phenomenon in animal models. Central to this process is the ASK1, a MAP3K which remains inactive upon binding to reduced Trx. Oxidative stress induces Trx oxidation, disrupting its ASK1 interaction, which subsequently promotes ASK1 dimerization, autophosphorylation, and activation [106]. This is how the MAP kinase cascade is triggered. Plant serine-threonine protein kinase OXI1 (oxidative stress-inducible) becomes activated in response to the oxidative stress induced by a pathogen attack or heavy metal poisoning, subsequently triggering MAPK3/6 activation [107]. However, it is not clear at what level this kinase activates the MAP-kinase cascade: whether it does so via activating MAP3K, MAP2K, or MAPK directly.

Over two decades ago, the first empirical data confirming the existence of ROS-activated cation channels in plants were reported [108, 109]. Currently, Demidchik et al. [110, 111] are developing the concept of the so-called ROS-Ca^{2+}-hub, a signaling center in the plasma membrane of the plant cell mediating not only stress reactions, but also the switching on the complex programs of plant development. The activation of Ca^{2+}-permeable cation channels, triggered by elevated $^{\cdot}OH$ production in the cell wall, facilitates the cellular uptake of Ca^{2+} and the release of K^{+}. Elevated cytosolic Ca^{2+} concentrations initiate signaling and regulatory cascades within the plant cell [111]. Furthermore, the activation of these channels may be modulated by phosphorylation catalyzed by the protein kinase HPCA (hydrogen peroxide calcium). Within the family of receptor kinases, HPCA is distinguished by its extracellular domain, which contains several redox-sensitive sulfhydryl groups [112]. Upon their oxidation by apoplastic ROS, the cytoplasmic domain of HPCA undergoes autophosphorylation, resulting in the activation of the enzyme, phosphorylation, and the opening of calcium channels in the plasma membrane [113].

It is known that organelles can send signals about their state of oxidative stress to the nucleus and affect the transcription of nuclear genes. In peroxisomes, this retrograde signaling is associated with catalase dysfunction [114]; in mitochondria, with dysfunction of alternative oxidase [115]. The phenomenon of chloroplast retrograde signaling under oxidative stress has been extensively investigated [101, 107, 116], with important observations in Arabidopsis chlorophyll biosynthesis mutants. These mutants accumulate intermediates possessing photosensitizing properties, resulting in singlet oxygen generation. The chloroplast-derived oxidative stress signal generated by light exposure is communicated to the nucleus through the intermediary action of EXE1 and EXE2 proteins, resulting in the activation of a cell death pathway [117]. Oxidation of Trp643 in Arabidopsis EXE1 by singlet oxygen results in EXE1 hydrolysis via the chloroplast metalloprotease FtsH. Retrograde signaling from chloroplasts to the nucleus, involving singlet oxygen and hydrogen peroxide, is modulated by the GUN1 protein [118]. The chloroplast accumulation of 3-phosphoadenosine-5-phosphate (PAP) has also been shown to mediate redox signaling. PAP accumulates under oxidative stress conditions due to the oxidation and inactivation of PAP kinase SAL, which catalyzes its conversion into AMP [116, 119].

The data presented show that the participation of redox modifications of proteins in plant signaling is often mediated by proteins reversible activation/inactivation, changes in their subcellular localization, and susceptibility to degradation in proteasomes.

CONCLUSION

The late 20th century witnessed the emergence of proteomics, a field of study focused on the exhaustive characterization of the life cycle of proteins within living organisms. This includes, but is not limited to, post-translational modifications, cellular transport, interactions with other molecules, and the processes of both partial and complete degradation. Post-translational modifications (PTMs), encompassing phosphorylation, glycosylation, methylation, acetylation, carbonylation, and other types of transformations, are typically analyzed in denatured proteins using a combination of chromatographic fractionation and mass spectrometric identification techniques. Advanced methodologies make it easier to both identify PTMs and better picture their dynamics, influence on the protein localization, degradation rates, and interactions with other biomolecules [120]. This pro-

gress has also affected the redox proteomics, particularly the proteomics of thiol groups [121]. This review details the chemistry of extensively studied plant protein redox modifications, offering insights into their potential biological functions. Elucidating the functional role of protein redox modifications represents a critical priority in plant proteomics. Recently, a new informational resource, the Plant PTM Viewer (https://www.psb.ugent.be/PlantPTMViewer), has been developed. The Plant PTM Resource database currently holds information on over 300,000 PTMs across more than 130,000 proteins, encompassing those mentioned in this article. ●

This study was supported by the Russian Science Foundation, grant No. 20-16-00086-P.

REFERENCES

1. Laloum T., Martín G., Duque P. // Trends Plant Sci. 2018. V. 23. № 2. P. 140–150.
2. Lam P.Y., Wang L., Lo C., Zhu F.-Y.// Int. J. Mol. Sci. 2022. V. 23. P. 7355.
3. Muhammad S., Xu X., Zhou W., Wu L. // WIREs RNA. 2023. V. 14. № 3. P. e1758.
4. Vu L.D., Gevaert K., De Smet I. // Trends Plant Sci. 2018. V. 23. № 12. P. 1068–1080.
5. Ramazi S., Zahiri J. // Database. 2021. V. 2021. ID baab012.
6. Willems P., Horne A., van ParysT., Goormachtig S., De Smet I., Botzki A., van Breusegem F., Gevaert K. // Plant J. 2019. V. 99. № 4. P. 752–762.
7. Willems P., Sterck L., Dard A., Huang J., De Smet I., Gevaert K., van Breusegem F. // J. Exp. Bot. 2024. V. 74. № 15. P. 4611–4624.
8. Smith L.M., Kelleher N.L. // Nat. Methods. 2013. V. 10. № 3. P. 186–187.
9. Smith L.M., Kelleher N.L. // Science. 2018. V. 359. № 6380. P. 1106–1107.
10. Aebersold R., Agar J.N., Amster I.J., Baker M.S., Bertozzi C.R., Boja E.S., Costello C.E., Cravatt B.F., Fenselau C., Garcia B.A., et al. // Nat. Chem. Biol. 2018. V. 14. № 3. P. 206–214.
11. Kosová K., Vítámvás P., Prášil I.T., Klíma M., Renaut J. // Front. Plant Sci. 2021. V. 12. P. 793113.
12. Heinemann B., Künzler P., Eubel H., Braun H.P., Hildebrandt T.M. // Plant Physiol. 2021. V. 185. № 2. P. 385–404.
13. Horn P.J. // Phytochem. Rev. 2021. V. 20. P. 367–407.
14. Ye T., Ma T., Chen Y., Liu C., Jiao Z., Wang X., Xue H. // Plant Physiol. Biochem. 2024. V. 213. P. 108810.
15. Mukherjee S., Corpas F.J. // Plant Cell Environ. 2023. V. 46. P. 688–717.
16. Mano J., Biswas M.S., Sugimoto K. // Plants. 2019. V. 8. P. 391.
17. Shumilina J., Kusnetsova A., Tsarev A., Janse van Rensburg H.C., Medvedev S., Demidchik V., van den Ende W., Frolov A. // Int. J. Mol. Sci. 2019. V. 20. P. 2366.
18. Valgimigli L. // Biomolecules. 2023. V. 13. № 9. P. 1291.
19. Chakraborty S., Karmakar K., Chakravortty D. // IUBMB Life. 2014. V. 66. № 10. P. 667–678.
20. Rabbani N., Al-Motawa M., Thornalley P.J. // Int. J. Mol. Sci. 2020. V. 21. P. 3942.
21. Zeng Q., Xin J., Zhao C., Tian R. // Plant Cell Rep. 2024. V. 43. № 4. P. 103.
22. Rabbani N., Thornalley P.J. // Amino Acids. 2012. V. 42. № 4. P. 1133–1142.
23. Kutzli I., Weiss J., Gibis M. // Foods. 2021. V. 10. № 2. P. 376.
24. Soboleva A., Vikhnina M., Grishina T., Frolov A. // Int. J. Mol. Sci. 2017. V. 18. P. 2557.
25. Twarda-Clapa A., Olczak A., Białkowska A.M., Koziołkiewicz M. // Cells. 2022. V. 11. № 8. P. 1312.
26. Antonova K., Vikhnina M., Soboleva A., Mehmood T., Heymich M.-L., Leonova T., Bankin M., Lukasheva E., Gensberger-Reigl S., Medvedev S., et al. // Int. J. Mol. Sci. 2019. V. 20. P. 3659.
27. Zheng Q., Maksimovic I., Upad A., David Y. // Protein Cell. 2020. V. 11. № 6. P. 401–416.
28. Viedma-Poyatos Á., González-Jiménez P., Langlois O., Company-Marín I., Spickett C.M., Pérez-Sala D. // Antioxidants (Basel). 2021. V. 10. № 2. P. 295.
29. Vistoli G., De Maddis D., Cipak A., Zarkovic N., Carini M., Aldini G. // Free Rad. Res. 2013. V. 47. Suppl. 1. P. 3–27.
30. Jové M., Mota-Martorell N., Pradas I., Martín-Gari M., Ayala V., Pamplona R. // Antioxidants (Basel). 2020. V. 9. № 11. P. 1132.
31. Alché J.D. // Redox Biol. 2019. V. 23. P. 101136.
32. Sankaranarayanan S., Jamshed M., Kumar A., Skori L., Scandola S., Wang T., Spiegel D., Samuel M.A. // Int. J. Mol. Sci. 2017. V. 18. № 4. P. 898.
33. Tola A.J., Jaballi A., Missihoun T.D. // Plants (Basel). 2021. V. 10. № 7. P. 1451.
34. Gupta K.J., Kaladhar V.C., Fitzpatrick T.B., Fernie A.R., Møller I.M., Loake G.J. // Mol. Plant. 2022. V. 15. P. 228–242.
35. Aranda-Cano L., Valderrama R., Chaki M., Begara-Morales J.C., Barroso J.B. // Prog. Bot. 2024. V. 84. P. 103–152.
36. Khator K., Parihar S., Jasik J., Shekhawat G.S. // Plant Signal. Behav. 2024. V. 19. № 1. P. 2298053.
37. Zhao H., Ma L., Shen J., Zhou H., Zheng Y. // Plant Cell. 2024. V. 36. № 2. P. 367–382.
38. Lundberg J.O., Weitzberg E. // Cell. 2022. V. 185. № 16. P. 2853–2878.
39. Allagulova C.R., Lubyanova A.R., Avalbaev A.M. // Int. J. Mol. Sci. 2023. V. 24. № 14. P. 11637.
40. Astier J., Lindermayr C. // Int. J. Mol. Sci. 2012. V. 13. P. 15193–15208.
41. Yu M., Lamattina L., Spoel S.H., Loake G.J. // New Phytol. 2014. V. 202. № 4. P. 1142–1156.
42. Albertos P., Romero-Puertas M.C., Tatematsu K., Mateos I., Sánchez-Vicente I., Nambara E., Lorenzo O. // Nat. Commun. 2015. V. 6. P. 8669.
43. Leterrier M., Chaki M., Airaki M., Valderrama R., Palma J.M., Barroso J.B., Corpas F.J. // Plant Signal. Behav. 2011. V. 6. № 6. P. 789–793.
44. Treffon P., Vierling E. // Antioxidants (Basel). 2022. V. 11. № 7. P. 1411.
45. Trujillo M., Ferrer-Sueta G., Thomson L., Flohé L., Radi R. // Subcell. Biochem. 2007. V. 44. P. 83–113.
46. León J. // Front. Plant Sci. 2022. V. 13. P. 859374.

47. Mamaeva A.S., Fomenkov A.A., Nosov A.V., Moshkov I.E., Novikova G.V., Mur L.A.J., Hall M.A. // Rus. J. Plant Physiol. 2015. V. 62. № 4. P. 427–440.
48. Pellicena P., Karow D.S., Boon E.M., Marletta M.A., Kuriyan J. // Proc. Natl. Acad. Sci. USA. 2004. V. 101. P. 12854–12859.
49. Yoo B.-K., Kruglik S.G., Lambry J.-C., Lamarre I., Raman C.S., Niochede P., Negrerie M. // Chem. Sci. 2023. V. 14. P. 8408–8420.
50. Wong A., Tian X., Yang Y., Gehring C. // Mol. Plant. 2021. V. 14. P. 195–197.
51. Wong A., Hu N., Tian X., Yang Y., Gehring C. // Trends Plant Sci. 2021. V. 26. № 9. P. 885–896.
52. Begara-Morales J.C., Sánchez-Calvo B., Chaki M., Valderrama R., Mata-Pérez C., Padilla M.N., Corpas F.J., Barroso J.B. // Front. Plant Sci. 2016. V. 7. P. 152.
53. Pande A., Mun B.G., Rahim W., Khan M., Lee D.S., Lee G.M., Al Azzawi T.N.I., Hussain A., Kim C.K., Yun B.W. // Front Plant Sci. 2022. V. 13. P. 865542.
54. Castillo M.C., Lozano-Juste J., González-Guzmán M., Rodriguez L., Rodriguez P.L., León J. // Sci. Signal. 2015. V. 8. № 392. P. ra89.
55. Wang P., Du Y., Hou Y.J., Zhao Y., Hsu C.C., Yuan F., Zhu X., Tao W.A., Song C.P., Zhu J.K. // Proc. Natl. Acad. Sci. USA. 2015. V. 112. № 2. P. 613–618.
56. Chen L., Sun S., Song C.-P., Zhou J.-M., Li J., Zuo J. // J. Genet. Genomics. 2022. V. 49. № 8. P. 756–765.
57. Shi H., Liu W., Wei Y., Ye T. // J. Exp. Bot. 2017. V. 68. № 5. P. 1239–1249.
58. Smirnoff N., Arnaud D. // New Phytol. 2019. V. 221. № 3. P. 1197–1214.
59. Noctor G., Lelarge-Trouverie C., Mhamdi A. // Phytochemistry. 2015. V. 112. P. 33–53.
60. Berlett B.S., Stadtman E.R. // J. Biol. Chem. 1997. V. 272. № 33. P. 20313–20316.
61. Davies M.J. // Biochem. J. 2016. V. 473. № 7. P. 805–825.
62. Goggin F.L., Fischer H.D. // Plant Cell Environ. 2024. V. 47. P. 1957–1970.
63. Dogra V., Rochaix J.D., Kim C. // Plant Cell Environ. 2018. V. 41. № 8. P. 1727–1738.
64. Dmitrieva V.A., Tyutereva E.V., Voitsekhovskaja O.V. // Int. J. Mol. Sci. 2020. V. 21. № 9. P. 3237.
65. Cerny M., Habanova H., Berka M., Luklova M., Brzobohaty B. // Int. J. Mol. Sci. 2018. V. 19. P. 2812.
66. Fu Z.-W., Feng Y-R., Gao X., Ding F., Li J.-H., Yuan T.-T., Lu Y.-T. // Plant Cell. 2023. V. 35. P. 1593–1616.
67. Ji E., Hu S., Lu Q., Zhang M., Jiang M. // Plant Physiol. Biochem. 2024. V. 213. P. 108844.
68. Rey P., Tarrago L. // Antioxidants (Basel). 2018. V. 7. № 9. P. 114.
69. Boschi-Muller S., Branlant G. // Bioorg. Chem. 2014. V. 57. P. 222–230.
70. Kreslavski V.D., Los D.A., Allakhverdiev S.I., Kuznetsov V.V. // Rus. J. Plant Physiol. 2012. V. 59. № 2. P. 141–154.
71. Waszczak C., Carmody M., Kangasjärvi J. // Annu. Rev. Plant Biol. 2018. V. 69. P. 209–236.
72. Martin R.E., Postiglione A.E., Muday G.K. // Curr. Opin. Plant Biol. 2022. V. 69. P. 102293.
73. Mittler R., Zandalinas S., Fichman Y., van Breusegem F. // Nat. Rev. Mol. Cell Biol. 2022. V. 23. № 10. P. 663–679.
74. Dorion S., Ouellet J.C., Rivoal J. // Metabolites. 2021. V. 11. P. 641.
75. Jurado-Flores A., Aroca A., Romero L.C., Gotor C. // J. Exp. Bot. 2023. V. 74. № 15. P. 4654–4669.
76. Liebthal M., Maynard D., Dietz K.J. // Antioxid. Redox Signal. 2018. V. 28. № 7. P. 609–624.
77. Bela K., Riyazuddin R., Csiszár J. // Antioxidants. 2022. V. 11. P. 1624.
78. Kang Z., Qin T., Zhao Z. // Gene. 2019. V. 706. P. 32–42.
79. Jedelská T., Luhová L., Petřivalský M. // Plants (Basel). 2020. V. 9. № 11. P. 1426.
80. Geigenberger P., Thormählen I., Daloso D.M., Fernie A.R. // Trends Plant Sci. 2017. V. 22. № 3. P. 249–262.
81. Nikkanen L., Rintamäki E. // Biochem. J. 2019. V. 476. № 7. P. 1159–1172.
82. Li X., Zhang T., Day N.J., Feng S., Gaffrey M.J., Qian W.J. // Antioxidants (Basel). 2022. V. 11. P. 2272.
83. Paulsen C.E., Carroll K.S // Chem. Rev. 2013. V. 113. P. 4633–4679.
84. Musaogullari A., Chai Y.-C. // Int. J. Mol. Sci. 2020. V. 21. P. 8113.
85. Urade R. // Biosci. Biotechnol. Biochem. 2019. V. 83. № 5. P. 781–793.
86. Sharova E.I. // Rus. J. Plant Physiol. 2002. V. 49. № 2. P. 255–268.
87. Hsieh H.H., Shan S.O. // Int. J. Mol. Sci. 2021. V. 23. № 1. P. 281.
88. Bechtel T.J., Weerapan E. // Proteomics. 2017. V. 6. P. 1600391.
89. Gansemer E.R., Rutkowski D.T. // Front. Mol. Biosci. 2022. V. 9. P. 858142.
90. Meyer A.J., Riemer J., Rouhier N. // New Phytol. 2019. V. 221. P. 1230–1246.
91. Tossounian M.A., Zhang B., Gout I. // Antioxidants (Basel). 2020. V. 9. № 12. P. 1288.
92. Hildebrandt T., Knuesting J., Berndt C., Morgan B., Scheibe R. // Biol. Chem. 2015. V. 396. № 5. P. 523–537.
93. Baker A., Lin C.-C., Lett C., Karpinska B., Wright M.H., Foyer C.H. // Free Rad. Biol. Med. 2023. V. 199. P. 56–66.
94. Lushchak O.V., Piroddi M., Galli F., Lushchak V.I. // Redox Rep. 2014. V. 19. № 1. P. 8–15.
95. Fuentes-Lemus E., Reyes J.S., Figueroa J.D., Davies M.J., López-Alarcón C. // Biochem. Soc. Trans. 2023. V. 51. № 6. P. 2173–2187.
96. Stenbaek A., Jensen P.E. // Phytochemistry. 2010. V. 71. P. 853–859.
97. Cejudo F.J., González M.C., Pérez-Ruiz J.M. // Plant Physiol. 2021. V. 186. № 1. P. 9–21.
98. Yoshida K., Hisabori T. // Plant Cell Physiol. 2023. V. 64. № 7. P. 704–715.
99. Liu H., Song S., Zhang H., Li Y., Niu L., Zhang J., Wang W. // Int. J. Mol. Sci. 2022. V. 23. № 23. P. 14824.
100. Li S. // Redox Biol. 2023. V. 64. P. 102789.
101. Bali S., Gautam A., Dhiman A., Michael R., Dogra V. // Physiol. Plant. 2023. V. 175. № 5. P. e14041.
102. Kohli S.K., Khanna K., Bhardwaj R., Corpas F.J., Ahmad P. // Plant Physiol. Biochem. 2022. V. 184. P. 56–64.
103. De Brasi-Velasco S., Sánchez-Guerrero A., Castillo M.-C., Vertommen D., León J., Sevilla F., Jiménez A. // Redox Biol. 2023. V. 63. P. 102750.
104. Backer R., Naidoo S., van den Berg N. // Front. Plant Sci. 2019. V. 10. P. 102.
105. Zavaliev R., Dong X.// Mol. Cell. 2024. V. 84. P. 131–141.
106. Averill-Bates D. // Biochim. Biophys. Acta - Molecular Cell Research. 2024. V. 1871. P. 119573.
107. Dietz K.-J., Turkan I., Krieger-Liszkay A. // Plant Physiol. 2016. V. 171. P. 1541–1550.
108. Demidchik V., Shabala S.N., Coutts K.B., Tester M.A., Davies J.M. // J. Cell Sci. 2003. V. 116. P. 81–88.
109. Foreman J., Demidchik V., Bothwell J.H.F., Mylona P.,

Miedema H., Torres M.A., Linstead P., Costa S., Brownlee C., Jones J.D., et al. // Nature. 2003. V. 422. P. 442–446.
110. Demidchik V., Shabala S. // Funct. Plant Biol. 2017. V. 45. P. 9–27.
111. Demidchik V. // Int. J. Mol. Sci. 2018. V. 19. № 4. P. 1263.
112. Wu F., Chi Y., Jiang Z., Xu Y., Xie L., Huang F., Wan D., Ni J., Yuan F., Wu X., et al. // Nature. 2020. V. 578. № 7796. P. 577–581.
113. Fichman Y., Zandalinas S.I., Peck S., Luan S., Mittler R. // Plant Cell. 2022. V. 34. № 11. P. 4453–4471.
114. Mhamdi A., Queval G., Chaouch S., Vanderauwera S., van Breusegem F., Noctor G. // J. Exp. Bot. 2010. V. 61. № 15. P. 4197–4220.
115. Vanlerberghe G.C. // Int. J. Mol. Sci. 2013. V. 14. № 4. P. 6805–6847.
116. Sevilla F., Martí M.C., De Brasi-Velasco S., Jiménez A. // J. Exp. Bot. 2023. V. 74. № 19. P. 5955–5969.
117. Laloi C., Havaux M. // Front. Plant Sci. 2015. V. 6. P. 39.
118. Fortunato S., Lasorella C., Tadini L., Jeran N., Vita F., Pesaresi P., de Pinto M.C. // Plant Sci. 2022. V. 320. P. 111265.
119. Foyer C.H., Hanke G. // Plant J. 2022. V. 111. № 3. P. 642–661.
120. Yan S., Bhawal R., Yin Z., Thannhauser T.W., Zhang S. // Mol. Hortic. 2022. V. 2. P. 17.
121. Degen G.E. // Plant Physiol. 2024. V. 195. № 2. P. 1111–1113.

Embryonic Stem Cell Differentiation to Definitive Endoderm As a Model of Heterogeneity Onset During Germ Layer Specification

M. N. Gordeev[1,2,3], A. S. Zinovyeva[1,2], E. E. Petrenko[1,2,4], E. V. Lomert[5], N. D. Aksenov[6], A. N. Tomilin[2*], E. I. Bakhmet[1,2**]

[1]Pluripotency Dynamics Group, Institute of Cytology, Russian Academy of Sciences, St. Petersburg, 194064 Russian Federation

[2]Laboratory of the Molecular Biology of Stem Cells, Institute of Cytology, Russian Academy of Sciences, St. Petersburg, 194064 Russian Federation

[3]Institute of Evolution, University of Haifa, Haifa, 3498838 Israel

[4]Faculty of Biology, Technion – Israel Institute of Technology, Haifa, 3200003 Israel

[5]Laboratory of Molecular Medicine, Institute of Cytology, Russian Academy of Sciences, St. Petersburg, 194064 Russian Federation

[6]Department of Intracellular Signaling and Transport, Institute of Cytology, Russian Academy of Sciences, St. Petersburg, 194064 Russian Federation

*E-mail: a.tomilin@incras.ru

**E-mail: e.bakhmet@incras.ru

Received August 29, 2024; in final form, October 23, 2024

DOI: https://doi.org/10.32607/actanaturae.27510

ABSTRACT **Embryonic stem cells (ESCs) hold great promise for regenerative medicine thanks to their ability to self-renew and differentiate into somatic cells and the germline. ESCs correspond to pluripotent epiblast — the tissue from which the following three germ layers originate during embryonic gastrulation: the ectoderm, mesoderm, and endoderm. Importantly, ESCs can be induced to differentiate toward various cell types by varying culture conditions, which can be exploited for *in vitro* modeling of developmental processes such as gastrulation. The classical model of gastrulation postulates that mesoderm and endoderm specification is made possible through the FGF-, BMP-, Wnt-, and Nodal-signaling gradients. Hence, it can be expected that one of these signals should direct ESC differentiation towards specific germ layers. However, ESC specification appears to be more complicated, and the same signal can be interpreted differently depending on the readout. In this research, using chemically defined culture conditions, homogeneous naïve ESCs as a starting cell population, and the *Foxa2* gene-driven EGFP reporter tool, we established a robust model of definitive endoderm (DE) specification. This *in vitro* model features formative pluripotency as an intermediate state acquired by the epiblast *in vivo* shortly after implantation. Despite the initially homogeneous state of the cells in the model and high Activin concentration during endodermal specification, there remains a cell subpopulation that does not reach the endodermal state. This simple model developed by us can be used to study the origins of cellular heterogeneity during germ layer specification.**

KEYWORDS **pluripotency, specification, differentiation, embryonic stem cells, ESCs, CRISPR/Cas9, gastrulation, endoderm, Foxa2.**

ABBREVIATIONS **ESCs – embryonic stem cells; FGF – fibroblast growth factor; BMP – bone morphogenic protein; EGFP – enhanced green fluorescent protein; DE – definitive endoderm; iPSCs – induced pluripotent stem cells; LIF – leukemia inhibitory factor; EpiLCs – epiblast-like stem cells; EpiSCs – epiblast stem cells; PGCs – primordial germ cells; DNA – deoxyribonucleic acid; RNA – ribonucleic acid; KSR – knockout serum replacement; TGFβ – transforming growth factor beta.**

INTRODUCTION

Embryonic stem cells (ESCs), which were first derived more than 40 years ago, are remarkable in their ability to self-renew and differentiate into all types of somatic cells [1, 2]. The discovery of induced pluripotent stem cells (iPSCs) in 2006 was a real breakthrough in the stem cell field. iPSCs are similar to ESCs in most aspects, but they originate from differentiated somatic cells by being converted to the early pluripotent state by the exogenous expression of Oct4, Sox2, Klf4, and c-Myc. [3, 4]. Both ESCs and iPSCs correspond to the pluripotent epiblast before implantation [5, 6]. During mouse development, the epiblast emerges, along with primitive endoderm and trophectoderm on embryonic day 4.5 (E4.5) [7, 8]. After implantation, due to the alterations in their expression profiles, epiblast cells become receptive to external signals that prod them to proceed with differentiation into ecto-, meso-, and endoderm [9]. At E6.5, the gastrulation process mediated by FGF, Wnt, BMP, and Activin/Nodal signaling leads to the formation of the primitive streak in the posterior epiblast [10–16]. This structure, which is formed by cells undergoing the epithelial-to-mesenchymal transition, subsequently produces the mesoderm and definitive endoderm (DE) [17, 18]. DE is established in the distal part of the primitive streak, where Activin/Nodal signaling, which is ensured by the visceral endoderm, shows the strongest effect and is more potent than the BMP signal produced by the extraembryonic ectoderm [17, 19]. Accordingly, applying high Activin doses should promote ESC differentiation into DE *in vitro* [20, 21]. The transcription factors Foxa2, Eomes, and Sox17 are responsible for DE formation [22–27]. Interestingly, several reports have indicated a possible role for the core markers of ESCs – Oct4, Sox2, and Nanog – not only in the maintenance of the pluripotent state, but also in lineage specification [28–32]. It has been suggested that Nanog, which is also a target for Activin/Nodal signaling, can facilitate DE specification [33–35].

The future of regenerative medicine depends on ESCs and iPSCs; however, safe, efficient, and reproducible protocols for the *in vitro* differentiation of these cells must be developed before the cells can be used in practice. Several such protocols which mimic early embryogenesis are already available. First, culturing of ESCs/iPSCs in the chemically defined N2B27 medium allows one to dispose of undefined serum components; then, addition of the leukemia inhibitory factor (LIF), MEK inhibitor PD0325901, and GSK3 inhibitor CHIR99021 to this 2i-LIF-N2B27 medium promotes the propagation of the so-called "naïve" ESCs, which are homogeneous and have a transcription profile that corresponds to that in the pre-implantation epiblast at E4.5 [5, 36]. These cultivation conditions are usually applied in a limited experimental time, since prolonged culturing leads to epigenetic and genomic changes in ESCs [37, 38]. Subsequent replacement of this medium with the N2B27 medium, supplemented with bFGF, Activin, and knockout serum replacement (KSR), for two days promotes the transition of "naïve" ESCs to the "formative" pluripotent state, designated as the epiblast-like cells (EpiLCs). EpiLCs correspond to the epiblast of an implanted embryo at E5.5 and are capable of forming both primordial germ cells (PGCs) and derivatives of primary germ layers [6, 39–42]. The chemically defined medium that facilitates the maintenance of a stable formative pluripotent state has been described in several recent publications [43–46].

Here, we applied the Naïve-to-EpiLC transition protocol with addition of high doses of Activin to trigger DE specification. This strategy allowed us to derive DE precursors efficiently and reproducibly. Importantly, a homogeneous cell culture and the use of the Naïve-to-EpiLC transition scheme make this differentiation highly similar to that occurring *in vivo*. Additionally, we have derived a reporter ESC line that allows one to monitor the DE specification process in living cells. It would seem that the addition of a given growth factor should lead to that particular growth factor's cellular specification. Thus, if we use a homogeneous 2D ESCs culture and add some of these signals, we can expect a homogeneous response and one-way specification. Yet, irrespective of the Activin concentration, we could not derive DE with 100% efficiency. The reaction–diffusion model in [47] might be able to help explain this.

EXPERIMENTAL

Plasmid construction

The left and right homology arms (941 bp and 810 bp, respectively) near the stop codon of the *Foxa2* gene were amplified from mouse genome DNA using Phusion DNA polymerase (ThermoFisher, USA). Next, the arms were ligated into the Oct4-TA2-EGFP vector (produced by A.A. Kuzmin, unpublished data) to replace the Oct4 locus-specific arms. The arms were ligated at the AvrII, NsiI, MluI, and SalI restriction sites. The guide-RNA sequences for the CRISPR-mediated DNA double-strand break were selected using the Benchling platform (benchling.com) in the region near the stop codon of the mouse *Foxa2* gene. The selected guide RNA had the lowest probability of nonspecific activity, accord-

ing to the method proposed by Hsu et al. [48]. The chosen guide was purchased from Evrogen (Russia), annealed, and ligated in the lentiCRISPRv2 vector (Addgene). All the final constructs were verified by Sanger sequencing. *Table 1* lists all the oligonucleotides used.

Cell culture

Unless specified otherwise, all cell culture products were purchased from ThermoFisher Scientific (Gibco, USA). Murine E14 Tg2a ESCs (Bay Genomics, USA) were grown at 37°C with 5% CO_2. Cells were passaged using 0.05% Trypsin–0.01% EDTA solution under standard feeder-free conditions on gelatinized tissue culture dishes or plates in the mES medium: knockout Dulbecco's modified Eagle's medium (Knockout DMEM) supplemented with a 15% embryonic stem (ES) cell-qualified fetal bovine serum (Biosera, USA), 100 U/mL penicillin, 100 μg/mL streptomycin, 2 mM L-glutamine, 1× nonessential amino acids, 50 μM β-mercaptoethanol (Merck, Germany), and 500 U/mL of in-house bacterially expressed hLIF.

For the derivation of naïve ESCs, ESCs cultured in a serum-containing medium were seeded on poly-L-ornithine-treated (0.01%) plastic in the 2i-LIF-N2B27 medium: N2B27 supplemented with 500 U/mL hLIF, 3 μM CHIR99021 (Axon, USA), and 1 μM PD0325901 (Axon) as described in ref. [39]. For the derivation of EpiLCs, naïve ESCs were seeded on fibronectin (Merck)-coated (15 μg/mL) plastic in a EpiLC medium: N2B27 supplemented with 12 ng/mL bFGF (Peprotech, USA), 20 ng/mL Activin A (Peprotech), and 1% of the knockout serum replacement. For the RNA analysis, the cells were seeded at a density of 25,000 cells/cm^2. For the differentiation experiments, the cells were initially seeded at a low density of 250 cells/cm^2 in a EpiLC medium. After 2 days, the EpiLC medium was replaced with N2B27 with the addition of specific factors: 10 μM SB505124 (Tocris, UK) for ectoderm specification, 50 ng/mL BMP4 (Peprotech) for mesoderm specification, and 100 ng/mL of Activin A (Peprotech) for DE specification.

Generation of the Foxa2::TA2-EGFP ESC line

The Foxa2::TA2-EGFP donor vector and lentiCRISPRv2 plasmid harboring gRNA (500 ng with a 1 : 1 molar ratio) were co-transfected in ESCs using a FuGENE transfection reagent (Promega, USA) in a OptiMEM medium. Next day, cells were transferred onto a 10 cm gelatinized dish. One day later, 2 μg/mL puromycin (Merck) was added to the culture medium for two additional days. The cells were cultured for an additional 10 days without the addition of selective antibiotics. Then, single clones were picked, expanded, and tested for transgene insertion by PCR using the gtM_FoxA2 primers and LR HS-PCR kit (Biolabmix, Russia). The EGFP level during the differentiation experiments was measured by flow cytometry on a CytoFLEX system (Beckman Coulter) and by time-lapse microscopy on a CQ1 confocal system (Yokogawa).

Preparation of metaphase spreads

The metaphase spread was prepared according to the previously described procedure [49]. Exponentially growing ESCs were treated with 0.1 μg/mL Colcemid (Sigma-Aldrich, USA) in a 5% CO_2 incubator for 2 h at 37°C. Cells were collected and incubated in a hypotonic 0.56% KCl solution for 20 min, fixed in a methanol/acetic acid solution (3 : 1, v/v), washed, and stored in a fixative solution at −20°C. The cell suspension was dropped onto microscope glass slides (Superfrost; Thermo Scientific, Germany), air-dried, and kept overnight at room temperature in air. The metaphase spreads were then stained with DAPI and visualized on an EVOS fl Auto microscope.

RNA isolation and RT-PCR

Total RNA was isolated from the cells using the ExtractRNA reagent (Evrogen, Russia). For cDNA synthesis, 1 μg of total RNA was used. cDNA was synthesized using M-MuLV Reverse Transcriptase (Evrogen) and the oligo(dT) primer (Thermo Scientific). Quantitative RT-PCR was performed using a 5× qPCRmix-HS SYBR buffer (Evrogen) on a LightCycler 96 instrument (Roche, Switzerland). Expression levels were normalized to the endogenous GAPDH RNA level; dCq values were taken for visualization. The primers for RT-PCR are listed in *Table 2*.

Immunocytochemistry

Cells were fixed in 4% paraformaldehyde (ThermoFisher) for 10 min, permeabilized with 0.1% Triton X-100 for 15 min, blocked in 3% BSA for 1 h at room temperature, and stained with the appropriate antibodies (*Table 3*) overnight at 4°C. Samples were then washed five–six times with PBS plus 0.1% Tween (PBST), stained with secondary fluorescent antibodies (Jackson ImmunoResearch, USA) for 2 h at room temperature, and also washed with PBST. Immunostained cells were examined under an EVOS fl Auto fluorescent microscope (Life Technologies, ThermoFisher) equipped with DAPI, GFP, RFP, and CY5 filter cubes.

Table 1. Oligonucleotides used for CRISPR/Cas9

Name	Sequence
cM_LA-Foxa2_F (AvrII)	TATcctaggGACATACCGACGCAGCTACA
cM_LA-Foxa2_R (NsiI)	TATatgcatGGATGAGTTCATAATAGGCCTGGA
cM_RA-Foxa2_F (MluI)	TATcgcgttAGAGAAGATGGCTTTCAGGCCC
cM_RA-Foxa2_R (SalI)	ATAgtcgacTATTGACCCCGTCTCCCACA
Foxa2_guide_F	caccgATGAACTCATCCTAAGAAGA
Foxa2_guide_R	aaacTCTTCTTAGGATGAGTTCATc
gtM_FoxA2-F3	CAGTCACGAACAAAGCGGGC
gtM-FoxA2-R2	TCAGCGCATCTCCCAGTAAC

Table 2. Oligonucleotides used for RT-PCR

Name	Sequence
Nanog_F	GCTCCATAACTTCGGGGAGG
Nanog_R	GTGCTAAAATGCGCATGGCT
Esrrb_F	GTCTGACACTTGGGGACCAG
Esrrb_R	CTACCAGGCGAGAGTGTTCC
Klf4_F	TACCCCTACACTGAGTCCCG
Klf4_R	GGAAAGGAGGGTAGTTGGGC
Fgf5_F	TCCTTCACCGTCACTGTTCC
Fgf5_R	TTCACTGGGCTGGGACTTCT
Otx2_F	ACTTGCCAGAATCCAGGGTG
Otx2_R	CTTCTTCTTGGCAGGCCTCA

Table 3. Specific antibodies used in this study

Target	Cat. No	Manufacturer
Oct4	sc-5279 (C-10)	Santa-Cruz
Sox2	MA1-014	ThermoFisher
Nanog	A300-397	Bethyl
Foxa2	sc-374375	Santa-Cruz
Brachyury	AF2085	R&D Systems
Sox1	ab109290	Abcam
Sox17	AF1924	R&D Systems

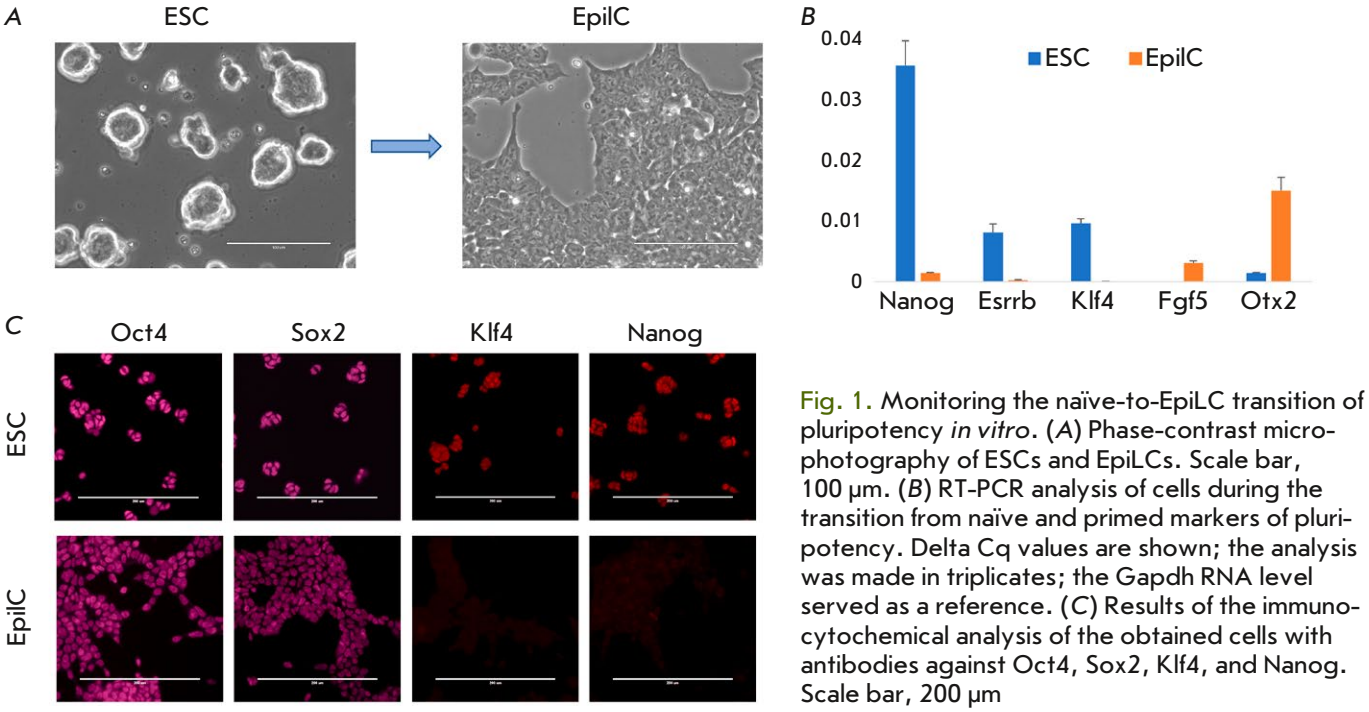

Fig. 1. Monitoring the naïve-to-EpiLC transition of pluripotency *in vitro*. (*A*) Phase-contrast microphotography of ESCs and EpiLCs. Scale bar, 100 μm. (*B*) RT-PCR analysis of cells during the transition from naïve and primed markers of pluripotency. Delta Cq values are shown; the analysis was made in triplicates; the Gapdh RNA level served as a reference. (*C*) Results of the immunocytochemical analysis of the obtained cells with antibodies against Oct4, Sox2, Klf4, and Nanog. Scale bar, 200 μm

RESULTS

Application of the Naïve-to-EpiLC transition of ESCs

During cultivation in the defined 2i-LIF-N2B27 medium [36] for five days, ESC colonies were able to form round-shaped colonies without any signs of differentiated cells (*Fig. 1A*, left image). For the Naïve-to-EpiLC transition, cells were seeded on the fibronectin-coated surface in the EpiLC medium for two days [39]. During this period, morphological changes were observed: cells became flattened and formed monolayer colonies (*Fig. 1A*, right image). The RNA and immunocytochemistry analysis confirmed the naïve and formative pluripotency states of these cells (*Fig. 1B,C*). As expected, the naïve pluripotency markers Nanog, Esrrb, and Klf4 were expressed in ESCs but downregulated upon their differentiation to EpiLCs. Instead, the latter cells displayed the expression of primed pluripotency markers Fgf5 and Otx2 (*Fig. 1B*).

Directing EpiLCs toward ectoderm, mesoderm, and endoderm

To direct EpiLCs toward distinct developmental trajectories, naïve ESCs were first seeded on the EpiLC medium at a low density. After two days, the medium was replaced with N2B27 supplemented with one of the following factors: the TGFβ-receptor inhibitor SB505124 (to promote ectoderm differentiation [34, 44, 50]), recombinant BMP4 (to promote mesoderm differentiation [51, 52]), or recombinant Activin A at a high concentration (100 ng/ml, to promote endoderm specification [20, 21, 43]). Immunostaining for lineage-specific markers revealed the successful onset of the desired differentiation trajectories: the mesendoderm marker Brachyury was detected in BMP4-treated cells; the neuroectoderm master-gene Sox1, in cells treated with SB inhibitor; and DE factor Foxa2, in Activin-treated cells (*Fig. 2A*). It appeared plausible that the Foxa2 could also mark cardiac progenitors, i.e. mesoderm lineage; hence, endoderm specification had to be additionally confirmed with Sox17 expression. The generated $Foxa2^+$ cells indeed turned out to be positive for Sox17 (*Fig. 2B*).

During early embryogenesis, Nanog is downregulated at the implantation stage but is further re-expressed in the primitive streak region [53–55]. It has also been suggested that Nanog is needed for an appropriate DE differentiation through Eomes regulation [35]. Nanog expression, indeed, had disappeared in EpiLCs (*Fig. 1C*), reminiscent of its downregulation in the epiblast during implantation. To properly mimic the DE specification process *in vivo*, an *in vitro* model must feature Nanog re-expression. In our differentiation system, we observed Nanog re-expression as early as on Day 1 (*Fig. 2C*). At the same time, this expression preceded Foxa2 expression, which was de-

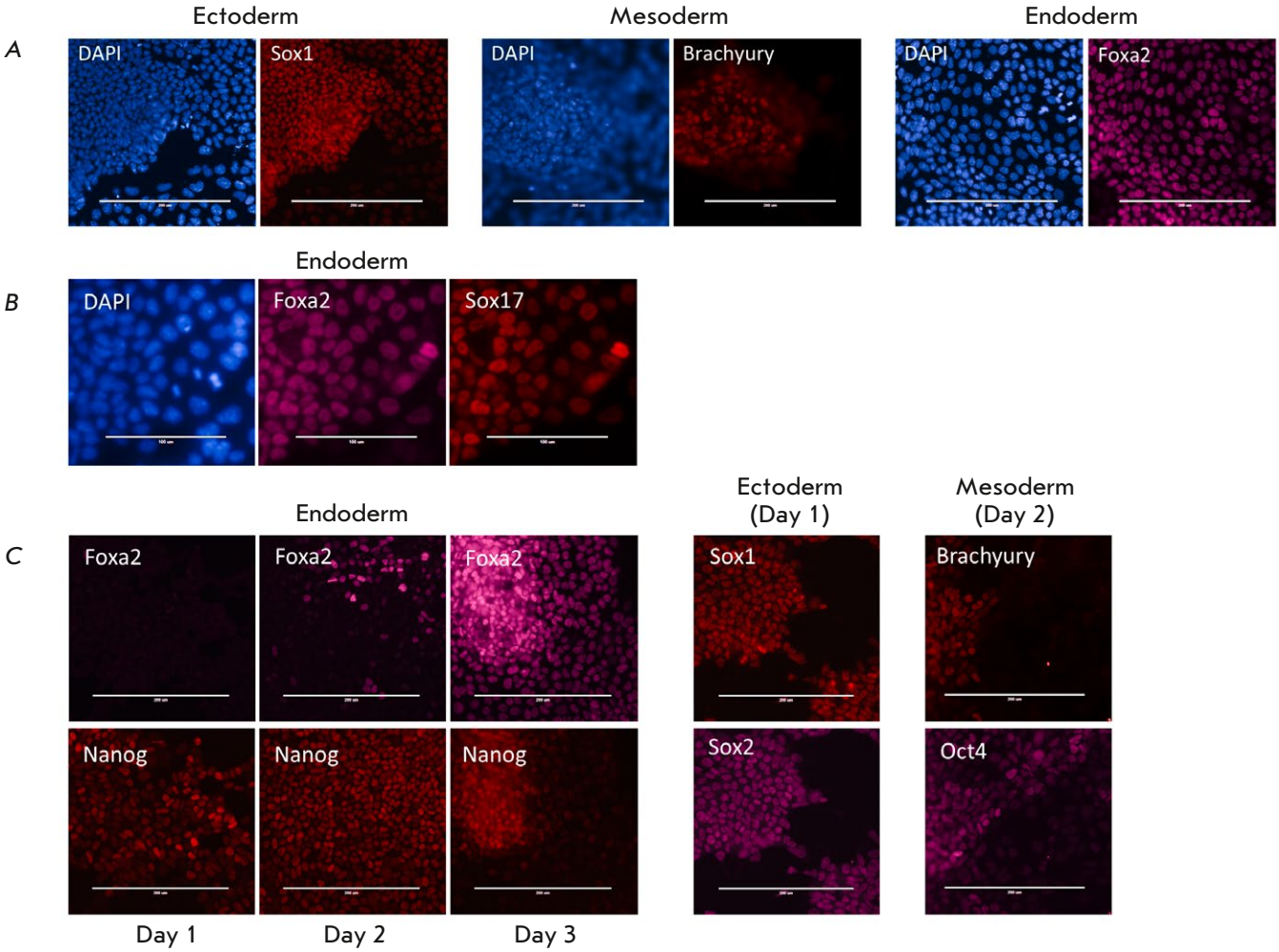

Fig. 2. EpiLCs are receptive to external signals and can be directed toward three lineages. (*A*) Immunostaining of differentiated cells for Sox1, Brachyury, and Foxa2. Scale bar, 200 μm. (*B*) Immunostaining of endoderm derivatives for Foxa2 and Sox17. Scale bar, 100 μm. (*C*) Nanog re-expression during endoderm specification. Oct4 co-localizes with Brachyury during mesoderm specification, while Sox2 is co-stained with Sox1 during neuroectoderm differentiation. Scale bar, 200 μm

tected on Day 2 and further increased by Day 3 of DE specification (*Fig. 2C*). While Oct4 and Sox2 function cooperatively in self-renewing ESCs, during the differentiation of these cells, the functions of the two factors diverge and are restricted to mesendoderm and neuroectoderm specification, respectively [30, 31]. Accordingly, we observed co-localization of Oct4 with the mesendoderm marker Brachyury and co-localization of Sox2 with the neuroectoderm marker Sox1 (*Fig. 2C*).

Establishment of the reporter ESC line Foxa2::T2A-EGFP

For the purpose of live monitoring of DE specification, we inserted the T2A-EGFP cassette just in front of the stop codon within the last exon of the *Foxa2* gene using the CRISPR/Cas9-driven homology-directed repair (HDR) approach (*Fig. 3A*). This modification strategy has an obvious advantage over conventional gene targeting, which is rather inefficient [56–58]. In our case, CRISPR/Cas9 allowed accurate cassette insertion, producing chimeric Foxa2::T2A-EGFP mRNA. The presence of the T2A self-cleaving protein allows production of two distinct proteins (Foxa2 and EGFP), thus precluding the effects of EGFP on the Foxa2 functions. Furthermore, the Foxa2 and EGFP levels correlate, facilitating a rough quantification of the Foxa2 level by visualization of EGFP in living cells.

Following transfection with targeting plasmids, several ESC clones were chosen and verified for cor-

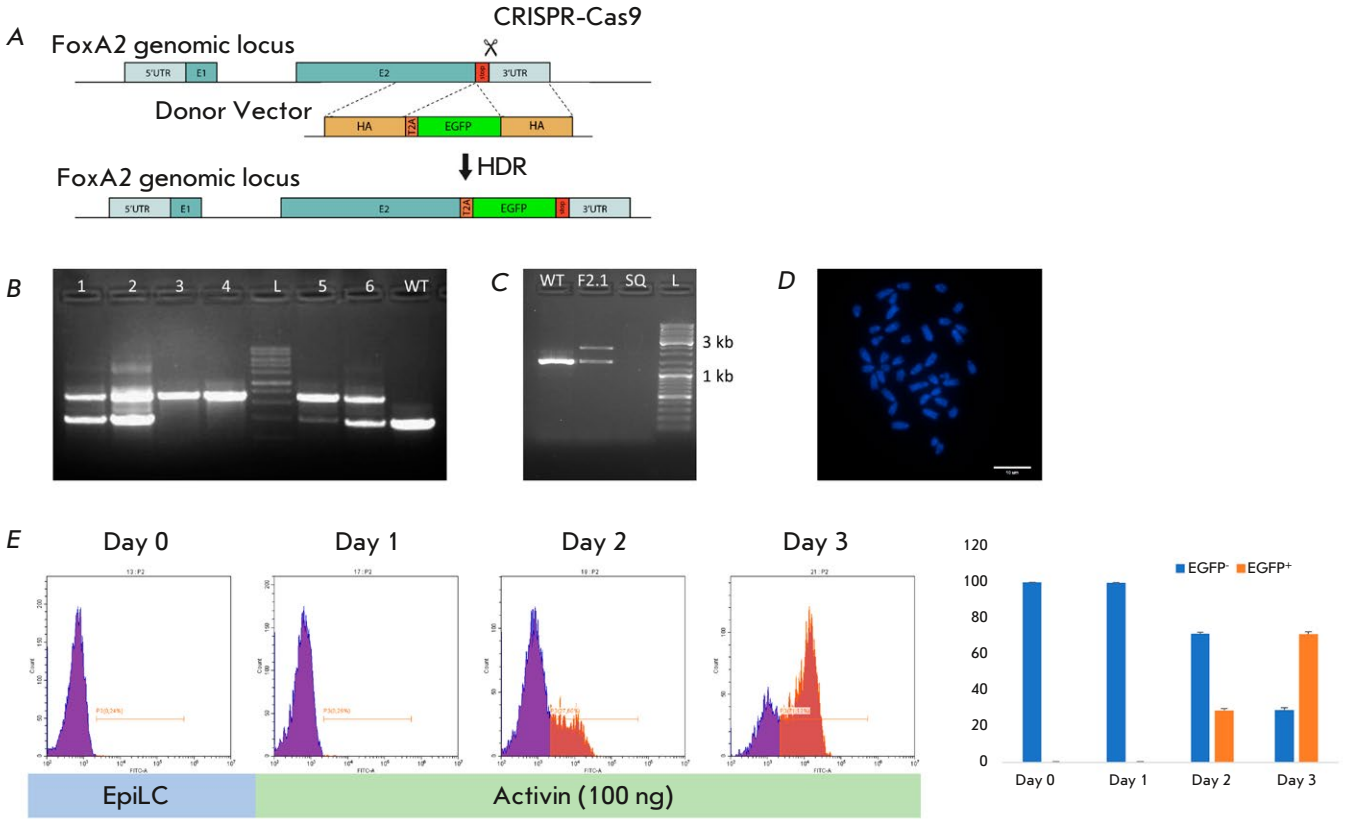

Fig. 3. Establishment of the Foxa2::T2A-EGFP reporter ESC line. (*A*) Schematic representation of the targeting strategy. E1, E2 – exons; HA – homology arm; UTR – untranslated region; stop – stop codon. (*B*) Insertion verification by PCR in picked ESC clones. Genomic DNA of the parental cell line (WT) was used as a control. (*C*) Repeated insertion verification in the subcloned cell line. (*D*) Normal karyotype (40 XY) of the established reporter ESC line F2.1. Scale bar, 10 μm. (*E*) Left panel – flow cytometry analysis of EGFP expression of the F2.1 ESCs during DE specification; right panel – percentage of $EGFP^-$ and $EGFP^+$ cells during DE differentiation; results are expressed as the mean of three replicates ± SD

rect cassette insertion into the *Foxa2* locus (*Fig. 3B*). One of these clones (F2), the targeted one allele, was subcloned (F2.1, *Fig. 3C*). This subclone, showing a normal karyotype (*Fig. 3D*), was used in the subsequent experiments. We next performed EGFP visualization of F2.1 ESC differentiation into DE at different time points using flow cytometry analysis (*Fig. 3E*). Activation of EGFP was first observed on Day 2 of differentiation (29% of the cells), while the number of $EGFP^+$ cells had increased to 71% by Day 3 of differentiation into DE (*Fig. 3E*, right panel). This result is consistent with the immunocytochemistry analysis of Foxa2 during DE specification (*Fig. 2C*).

Heterogeneity induction in response to the single-growth factor

Time-lapse microscopy was used to visualize DE specification in the living cells (*Fig. 4A*, Suppl. Video). In agreement with the results of the flow cytometry analysis, a EGFP signal was not observed within the first 24 h, implying some chromatin preparation for further specification. EGFP was detected for the first time 38 h after the addition of Activin to EpiLCs with the maximum amount of $EGFP^+$ cells observed after 72 h of the treatment. The most interesting feature repeatedly noted throughout the experiments was the heterogeneity of the EGFP distribution across the cell population (*Fig. 4A*, right panel). The number of $EGFP^+$ cells gradually increased during the specification and reached nearly 70%; however, it peaked at that level. Interestingly, the EGFP distribution did not show any bias towards the center or edge of colonies, as opposed to the previous studies where *in vitro* specifications as "micropatterns" was demonstrated [51, 59]. During immunocytochemical staining of the differentiated cell culture, we observed colocalization

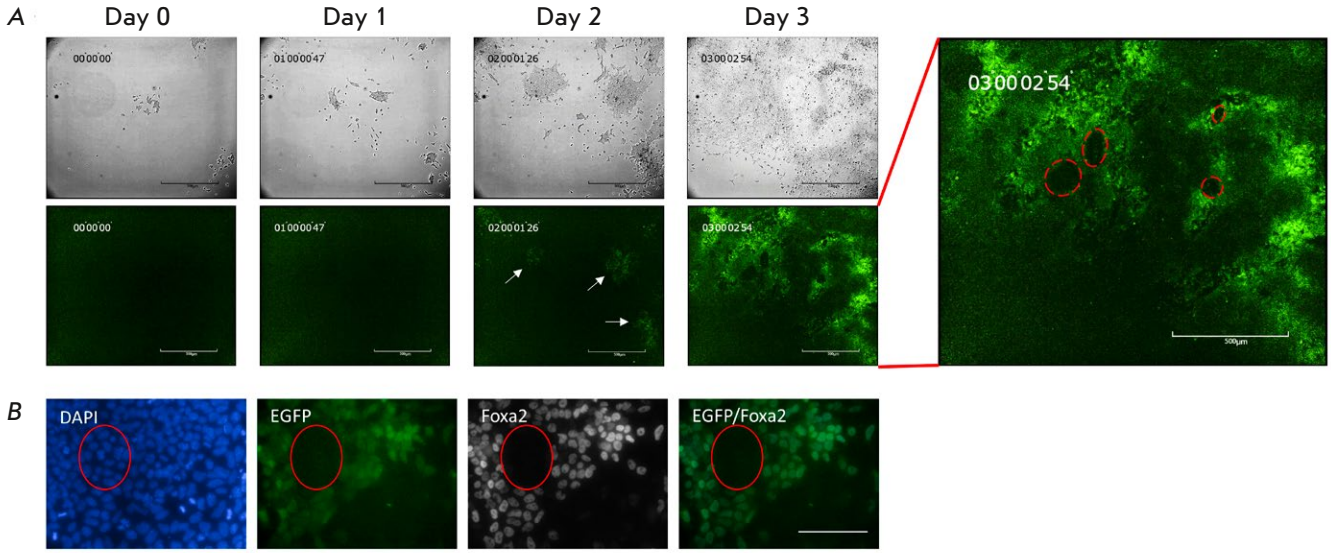

Fig. 4. Live imaging of DE specification *in vitro*. (*A*) Time-lapse microscopy of the F2.1 ESCs during DE specification. Arrows indicate EGFP$^+$ emerging cells. Scale bar, 500 μm. The time-lapse video can be found in the Supplementary material. (*B*) Co-localization of EGFP with Foxa2 following differentiation of the F2.1 ESCs into DE. Scale bar, 100 μm

of the signal from antibodies with EGFP, proving the adequacy of the functioning of the resulting reporter cell line (*Fig. 4B*).

DISCUSSION

Over the past decade, many valuable techniques of cultivating and differentiating pluripotent stem cells have been developed. These cells can now be maintained in various pluripotent states under chemically defined culture conditions and, importantly, precisely match the epiblast cells at different stages of embryonic development [5, 6, 44]. During recent years, several studies reporting *ex vivo* embryogenesis have appeared, including the establishment of blastoids, gastruloids, and even the whole embryos until embryonic day 8.5 (E8.5) [60–67]. At the same time, modeling the simple and homogeneous processes of directed differentiation of pluripotent cells for the purpose of grasping the molecular mechanisms that underlie these processes, remains a worthwhile approach. Data obtained via this approach can then be extrapolated with a high probability of accuracy to embryonic development.

Here, we used chemically defined culture conditions to establish a simple and robust method for mouse ESC specification to DE. All the experiments were performed in a chemically defined serum-free medium (N2B27) purposely supplemented with various additional factors. We also established Foxa2::T2A-EGFP ESCs and demonstrated their usability during DE specification. We anticipate that the combination of chemically defined media and reporter cell lines will facilitate more comprehensive studies of the mechanisms that control lineage choice by pluripotent cells during the differentiation process.

New data challenging the paradigm that the transcription factors Oct4, Sox2, and Nanog act solely as guardians of the pluripotent state has recently appeared [30–32, 35]. Manipulations with the expression level of these factors in murine ESCs, indeed, without fail triggered differentiation toward extraembryonic tissues [68–70]; however, in human ESCs, these manipulations promoted a differentiation into primary germ layers [35, 71]. One can speculate that these differences are mostly related to naïve and primed pluripotent states rather than to species peculiarities. In this study, we have provided compelling evidence that Oct4, Sox2, and Nanog do not immediately disappear but transiently co-localize with known germ layer markers. Moreover, Nanog expression is re-activated during the DE specification. It would be of research value to modulate the level of this transcription factor during DE specification in future research, with the established F2.1 ESCs being a highly valuable tool in these attempts.

Differentiation to ectoderm, mesoderm, and definitive endoderm has been studied mostly in human ESCs, which are in the primed pluripotency state and correspond to the post-implantation epiblast [50, 52, 72, 73]. Meanwhile, murine ESCs are more complicat-

ed in this regard, as they are in the naïve pluripotency state and must be differentiated into the primed one prior to any specification of the germ layers. The situation has changed since the establishment of murine epiblast stem cells (EpiSCs), which correspond to epiblast cells after implantation and are similar to primed human ESCs [74, 75]. Subsequently, the ability of murine ESCs to transform into EpiSCs has been shown [39]. On their way to become EpiSCs, ESCs progress through the formative pluripotent state (EpiLCs), which corresponds to the epiblast right after implantation (E5.5) [41]. The most distinctive feature of EpiLCs resides in their ability to produce primordial germ cells (PGCs) [39, 76]. EpiLCs are homogeneous, and their expression profile makes them more suitable for embryogenesis modeling than EpiSCs. Besides, the latter cell type corresponds to the epiblast at E7.5, which is more committed [77]. Formative pluripotent stem cells have indeed been used for *in vitro* modeling of murine embryogenesis [40, 43–45, 51, 78] and can be regarded, in our view, as the golden standard in germ layer specification. Their homogeneous state also facilitates the precise deciphering of the mechanisms that underlie cellular specification. It is now obvious that this process is not controlled solely by the gradients of FGF, BMP, Wnt, and Nodal. Our study clearly shows that in excess of Activin and absence of any additional signals, EpiLCs do not uniformly reach the DE state. Hence, certain cell-autonomous stochastic processes also have to contribute to the specification of this lineage.

It seems to us that the Nodal–Lefty antagonism is not limited to the left-right asymmetry in mouse embryogenesis [79], but also operates in DE specification. It is known that Activin/Nodal signaling activates Lefty, which in turn inhibits this pathway, thereby ensuring the negative feedback mechanism [80]. This mechanism is a good example of the reaction–diffusion model [47], which explains the origin of heterogeneity in initially homogeneous systems [81]. According to this model, it would appear that there is about a 70% probability that adding Activin to EpiLCs would activate Nodal and just a 30% probability that it would activate Lefty. Further development of DE would proceed in accordance with the presence of an activator (Nodal) or an inhibitor (Lefty). Overall, the developed model could serve as a good starting point for further research into the mechanisms of heterogeneity onset during germ layer specification.

CONCLUSIONS

The presented ESC – EpiLC – DE transition *in vitro* closely resembles DE maturation during embryogenesis. The transcription factor Nanog is downregulated in EpiLCs but is re-expressed in DE precursors. Despite the defined *in vitro* conditions of DE differentiation, only 70% of cells enter this developmental state. The molecular mechanisms underlying this phenomenon require clarification through future research.

Supplementary video. Time-lapse microscopy of DE specification *in vitro*. Registration was started at the timepoint when Activin A was added to EpiLC. Available at https://doi.org/10.32607/actanaturae.27510. ●

The authors proclaim no conflict of interest.
The study was supported by the Russian Science Foundation (RSF) grant No. 23-75-10096, https://rscf.ru/en/project/23-75-10096/.

REFERENCES

1. Martin G.R. // Proc. Natl. Acad. Sci. USA. 1981. V. 78. № 12. P. 7634–7638.
2. Evans M.J., Kaufman M.H. // Nature. 1981. V. 292. № 5819. P. 154–156.
3. Takahashi K., Yamanaka S. // Cell. 2006. V. 126. № 4. P. 663–676.
4. Takahashi K., Tanabe K., Ohnuki M., Narita M., Ichisaka T., Tomoda K., Yamanaka S. // Cell. 2007. V. 131. № 5. P. 861–872.
5. Boroviak T., Loos R., Bertone P., Smith A., Nichols J. // Nat. Cell. Biol. 2014. V. 16. № 6. P. 516–528.
6. Plusa B., Hadjantonakis A.K. // Nat. Cell. Biol. 2014. V. 16. № 6. P. 502–504.
7. Schrode N., Xenopoulos P., Piliszek A., Frankenberg S., Plusa B., Hadjantonakis A.K. // Genesis. 2013. V. 51. № 4. P. 219–233.
8. Tarkowski A.K. // Nature. 1959. V. 24. № 184. P. 1286–1287.
9. Tam P.P., Loebel D.A. // Nat. Rev. Genet. 2007. V. 8. № 5. P. 368–381.
10. Baker C.L., Pera M.F. // Cell. Stem Cell. 2018. V. 22. № 1. P. 25–34.
11. Arnold S.J., Robertson E.J. // Nat. Rev. Mol. Cell Biol. 2009. V. 10. № 2. P. 91–103.
12. Conlon F.L., Lyons K.M., Takaesu N., Barth K.S., Kispert A., Herrmann B., Robertson E.J. // Development. 1994. V. 120. № 7. P. 1919–1928.
13. Mishina Y., Suzuki A., Ueno N., Behringer R.R. // Genes Dev. 1995. V. 9. № 15. P. 3027–3037.
14. Liu P., Wakamiya M., Shea M.J., Albrecht U., Behringer R.R., Bradley A. // Nat. Genet. 1999. V. 22. № 4. P. 361–365.
15. Lu C.C., Robertson E.J. // Dev. Biol. 2004. V. 273. № 1. P. 149–159.

16. Gattiglio M., Protzek M., Schroter C. // Biol. Open. 2023. V. 12. № 8. bio059941.
17. Nowotschin S., Hadjantonakis A.K., Campbell K. // Development. 2019. V. 146. № 11. dev150920.
18. Shahbazi M.N., Zernicka-Goetz M. // Nat. Cell Biol. 2018. V. 20. № 8. P. 878–887.
19. Vincent S.D., Dunn N.R., Hayashi S., Norris D.P., Robertson E.J. // Genes Dev. 2003. V. 17. № 13. P. 1646–1662.
20. D'Amour K.A., Agulnick A.D., Eliazer S., Kelly O.G., Kroon E., Baetge E.E. // Nat. Biotechnol. 2005. V. 23. № 12. P. 1534–1541.
21. Si-Tayeb K., Noto F.K., Nagaoka M., Li J., Battle M.A., Duris C., North P.E., Dalton S., Duncan S.A. // Hepatology. 2010. V. 51. № 1. P. 297–305.
22. Kaestner K.H. // Curr. Opin. Genet. Dev. 2010. V. 20. № 5. P. 527–532.
23. Ang S.L., Rossant J. // Cell. 1994. V. 78. № 4. P. 561–574.
24. Fu S., Fei Q., Jiang H., Chuai S., Shi S., Xiong W., Jiang L., Lu C., Atadja P., Li E., et al. // PLoS One. 2011. V. 6. № 11. P. e27965.
25. Wang P., Rodriguez R.T., Wang J., Ghodasara A., Kim S.K. // Cell Stem Cell. 2011. V. 8. № 3. P. 335–346.
26. Arnold S.J., Hofmann U.K., Bikoff E.K., Robertson E.J. // Development. 2008. V. 135. № 3. P. 501–511.
27. Dufort D., Schwartz L., Harpal K., Rossant J. // Development. 1998. V. 125. № 16. P. 3015–3025.
28. Loh K.M., Lim B., Ang L.T. // Physiol. Rev. 2015. V. 95. № 1. P. 245–295.
29. Malleshaiah M., Padi M., Rue P., Quackenbush J., Martinez-Arias A., Gunawardena J. // Cell Rep. 2016. V. 14. № 5. P. 1181–1194.
30. Thomson M., Liu S.J., Zou L.N., Smith Z., Meissner A., Ramanathan S. // Cell. 2011. V. 145. № 6. P. 875–889.
31. Valcourt J.R., Huang R.E., Kundu S., Venkatasubramanian D., Kingston R.E., Ramanathan S. // Cell Repts. 2021. V. 37. № 6. P. 109990.
32. Koch F., Scholze M., Wittler L., Schifferl D., Sudheer S., Grote P., Timmermann B., Macura K., Herrmann B.G. // Dev Cell. 2017. V. 42. № 5. P. 514–526.
33. Xu R.H., Sampsell-Barron T.L., Gu F., Root S., Peck R.M., Pan G., Yu J., Antosiewicz-Bourget J., Tian S., Stewart R., et al. // Cell Stem Cell. 2008. V. 3. № 2. P. 196–206.
34. Vallier L., Mendjan S., Brown S., Chng Z., Teo A., Smithers L.E., Trotter M.W., Cho C.H., Martinez A., Rugg-Gunn P., et al. // Development. 2009. V. 136. № 8. P. 1339–1349.
35. Teo A.K., Arnold S.J., Trotter M.W., Brown S., Ang L.T., Chng Z., Robertson E.J., Dunn N.R., Vallier L. // Genes Dev. 2011. V. 25. № 3. P. 238–250.
36. Ying Q.-L., Wray J., Nichols J., Batlle-Morera L., Doble B., Woodgett J., Cohen P., Smith A. // Nature. 2008. V. 453. № 7194. P. 519–523.
37. Choi J., Huebner A.J., Clement K., Walsh R.M., Savol A., Lin K., Gu H., Di Stefano B., Brumbaugh J., Kim S.Y., et al. // Nature. 2017. V. 548. № 7666. P. 219–223.
38. Yagi M., Kishigami S., Tanaka A., Semi K., Mizutani E., Wakayama S., Wakayama T., Yamamoto T., Yamada Y. // Nature. 2017. V. 548. № 7666. P. 224–227.
39. Hayashi K., Ohta H., Kurimoto K., Aramaki S., Saitou M. // Cell. 2011. V. 146. № 4. P. 519–532.
40. Buecker C., Srinivasan R., Wu Z., Calo E., Acampora D., Faial T., Simeone A., Tan M., Swigut T., Wysocka J. // Cell Stem Cell. 2014. V. 14. № 6. P. 838–853.
41. Kinoshita M., Smith A. // Development, Growth & Differentiation. 2018. V. 60. № 1. P. 44–52.
42. Morgani S., Nichols J., Hadjantonakis A.K. // BMC Dev. Biol. 2017. V. 17. № 1. P. 7.
43. Kinoshita M., Barber M., Mansfield W., Cui Y., Spindlow D., Stirparo G.G., Dietmann S., Nichols J., Smith A. // Cell Stem Cell. 2020. V. 28. № 3. P. 453–471.
44. Yu L., Wei Y., Sun H.X., Mahdi A.K., Pinzon Arteaga C.A., Sakurai M., Schmitz D.A., Zheng C., Ballard E.D., Li J., et al. // Cell Stem Cell. 2020. V. 28. № 3. P. 550–567.
45. Wang X., Xiang Y., Yu Y., Wang R., Zhang Y., Xu Q., Sun H., Zhao Z.A., Jiang X., Wang X., et al. // Cell Res. 2021. V. 31. № 5. P. 526–541.
46. Pera M.F., Rossant J. // Cell Stem Cell. 2021. V. 28. № 11. P. 1896–1906.
47. Turing A.M. // Bull. Math. Biol. 1990. V. 52. № 1–2. P. 153–197; discussion 119–152.
48. Hsu P.D., Scott D.A., Weinstein J.A., Ran F.A., Konermann S., Agarwala V., Li Y., Fine E.J., Wu X., Shalem O., et al. // Nat. Biotechnol. 2013. V. 31. № 9. P. 827–832.
49. Ponomartsev S.V., Sinenko S.A., Skvortsova E.V., Liskovykh M.A., Voropaev I.N., Savina M.M., Kuzmin A.A., Kuzmina E.Y., Kondrashkina A.M., Larionov V., et al. // Cells. 2020. V. 9. № 4. P. 879.
50. Shi Y., Kirwan P., Livesey F.J. // Nat. Protoc. 2012. V. 7. № 10. P. 1836–1846.
51. Morgani S.M., Metzger J.J., Nichols J., Siggia E.D., Hadjantonakis A.K. // Elife. 2018. V. 7. e32839.
52. Warmflash A., Sorre B., Etoc F., Siggia E.D., Brivanlou A.H. // Nat. Methods. 2014. V. 11. № 8. P. 847–854.
53. Bardot E., Calderon D., Santoriello F., Han S., Cheung K., Jadhav B., Burtscher I., Artap S., Jain R., Epstein J., et al. // Nat. Commun. 2017. V. 8. P. 14428.
54. Chambers I., Colby D., Robertson M., Nichols J., Tweedie S., Smith A. // Cell. 2003. V. 113. № 5. P. 643–655.
55. Hart A.H., Hartley L., Ibrahim M., Robb L. // Dev. Dyn. 2004. V. 230. № 1. P. 187–198.
56. Hoffman J.A., Wu C.I., Merrill B.J. // Development. 2013. V. 140. № 8. P. 1665–1675.
57. Aubert J., Stavridis M.P., Tweedie S., O'Reilly M., Vierlinger K., Li M., Ghazal P., Pratt T., Mason J.O., Roy D., et al. // Proc. Natl. Acad. Sci. USA. 2003. V. 100. Suppl 1. P. 11836–11841.
58. Sladitschek H.L., Neveu P.A. // Mol. Syst. Biol. 2019. V. 15. № 12. P. e9043.
59. Fehling H.J., Lacaud G., Kubo A., Kenned y M., Robertson S., Keller G., Kouskoff V. // Development. 2003. V. 130. № 17. P. 4217–4227.
60. Tewary M., Ostblom J., Prochazka L., Zulueta-Coarasa T., Shakiba N., Fernandez-Gonzalez R., Zandstra P.W. // Development. 2017. V. 144. № 23. P. 4298–4312.
61. Aguilera-Castrejon A., Oldak B., Shani T., Ghanem N., Itzkovich C., Slomovich S., Tarazi S., Bayerl J., Chugaeva V., Ayyash M., et al. // Nature. 2021. V. 593. № 7857. P. 119–124.
62. Amadei G., Lau K.Y.C., De Jonghe J., Gantner C.W., Sozen B., Chan C., Zhu M., Kyprianou C., Hollfelder F., Zernicka-Goetz M. // Dev. Cell. 2021. V. 56. № 3. P. 366–382.e9.
63. Liu X., Tan J.P., Schroder J., Aberkane A., Ouyang J.F., Mohenska M., Lim S.M., Sun Y.B.Y., Chen J., Sun G., et al. // Nature. 2021. V. 591. № 7851. P. 627–632.
64. Rossant J., Tam P.P.L. // Stem Cell Reports. 2021. V. 16. № 5. P. 1031–1038.
65. Yu L., Wei Y., Duan J., Schmitz D.A., Sakurai M., Wang L., Wang K., Zhao S., Hon G.C., Wu J. // Nature. 2021.

V. 591. № 7851. P. 620–626.
66. van den Brink S.C., van Oudenaarden A. // Trends Cell Biol. 2021. V. 31. № 9. P. 747–759.
67. Amadei G., Handford C.E., Qiu C., De Jonghe J., Greenfeld H., Tran M., Martin B.K., Chen D.Y., Aguilera-Castrejon A., Hanna J.H., et al. // Nature. 2022. V. 610. № 7930. P. 143–153.
68. Tarazi S., Aguilera-Castrejon A., Joubran C., Ghanem N., Ashouokhi S., Roncato F., Wildschutz E., Haddad M., Oldak B., Gomez-Cesar E., et al. // Cell. 2022. V. 185. № 18. P. 3290–3306 e25.
69. Niwa H., Miyazaki J.-I., Smith A.G. // Nat. Genet. 2000. V. 24. № 4. P. 372–376.
70. Masui S., Nakatake Y., Toyooka Y., Shimosato D., Yagi R., Takahashi K., Okochi H., Okuda A., Matoba R., Sharov A.A., et al. // Nat. Cell Biol. 2007. V. 9. № 6. P. 625–635.
71. Ivanova N., Dobrin R., Lu R., Kotenko I., Levorse J., DeCoste C., Schafer X., Lun Y., Lemischka I.R. // Nature. 2006. V. 442. № 7102. P. 533–538.
72. Wang Z., Oron E., Nelson B., Razis S., Ivanova N. // Cell Stem Cell. 2012. V. 10. № 4. P. 440–454.
73. Surmacz B., Fox H., Gutteridge A., Fish P., Lubitz S., Whiting P. // Stem Cells. 2012. V. 30. № 9. P. 1875–1884.
74. Tristan C.A., Ormanoglu P., Slamecka J., Malley C., Chu P.-H., Jovanovic V.M., Gedik Y., Jethmalani Y., Bonney C., Barnaeva E., et al. // Stem Cell Repts. 2021. V. 16. № 12. P. 3076–3092.
75. Brons I.G., Smithers L.E., Trotter M.W., Rugg-Gunn P., Sun B., Chuva de Sousa Lopes S.M., Howlett S.K., Clarkson A., Ahrlund-Richter L., Pedersen R.A., et al. // Nature. 2007. V. 448. № 7150. P. 191–195.
76. Tesar P.J., Chenoweth J.G., Brook F.A., Davies T.J., Evans E.P., Mack D.L., Gardner R.L., McKay R.D. // Nature. 2007. V. 448. № 7150. P. 196–199.
77. Nakaki F., Hayashi K., Ohta H., Kurimoto K., Yabuta Y., Saitou M. // Nature. 2013. V. 501. № 7466. P. 222–226.
78. Kojima Y., Kaufman-Francis K., Studdert J.B., Steiner K.A., Power M.D., Loebel D.A., Jones V., Hor A., de Alencastro G., Logan G.J., et al. // Cell Stem Cell. 2014. V. 14. № 1. P. 107–120.
79. Morgani S.M., Hadjantonakis A.K. // Curr. Top. Dev. Biol. 2020. V. 137. P. 391–431.
80. Nakamura T., Mine N., Nakaguchi E., Mochizuki A., Yamamoto M., Yashiro K., Meno C., Hamada H. // Dev. Cell. 2006. V. 11. № 4. P. 495–504.
81. Shen M.M. // Development. 2007. V. 134. № 6. P. 1023–1034.
82. Kondo S., Miura T. // Science. 2010. V. 329. № 5999. P. 1616–1620.

Intraventricular Administration of Exosomes from Patients with Amyotrophic Lateral Sclerosis Provokes Motor Neuron Disease in Mice

A. V. Stavrovskaya[1*], D. N. Voronkov[1], A. K. Pavlova[1], A. S. Olshanskiy[1], B. V. Belugin[2], M. V. Ivanova[1], M. N. Zakharova[1], S. N. Illarioshkin[1*]

[1]Research Center of neurology, Ministry of Science and Higher Education of the Russian Federation, Moscow, 125367 Russian Federation

[2]National Research Center for Epidemiology and Microbiology named after the honorary academician N. F. Gamaleya, Moscow, 123098 Russian Federation

[*]E-mail: snillario@gmail.com

Received September 21, 2024; in final form, October 02, 2024

DOI: 10.32607/actanaturae.27499

ABSTRACT **Amyotrophic lateral sclerosis (ALS) is a severe disease of the central nervous system (CNS) characterized by motor neuron damage leading to death from respiratory failure. The neurodegenerative process in ALS is characterized by an accumulation of aberrant proteins (TDP-43, SOD1, etc.) in CNS cells. The trans-synaptic transmission of these proteins via exosomes may be one of the mechanisms through which the pathology progresses. The aim of this work was to study the effect of an intraventricular injection of exosomes obtained from the cerebrospinal fluid (CSF) of ALS patients on the motor activity and CNS pathomorphology of mice. The exosomes were obtained from two ALS patients and a healthy donor. Exosome suspensions at high and low concentrations were injected into the lateral brain ventricles of male BALB/c mice (n = 45). Motor activity and physiological parameters were evaluated twice a month; morphological examination of the spinal cord was performed 14 months after the start of the experiment. Nine months after administration of exosomes from the ALS patients, the animals started exhibiting a pathological motor phenotype; i.e., altered locomotion with paresis of hind limbs, coordination impairment, and increasing episodes of immobility. The motor symptoms accelerated after administration of a higher concentration of exosomes. The experimental group showed a significant decrease in motor neuron density in the ventral horns of the spinal cord, a significant increase in the number of microglial cells, and microglia activation. The TDP43 protein in the control animals was localized in the nuclei of motor neurons. TDP43 mislocation with its accumulation in the cytoplasm was observed in the experimental group. Thus, the triggering effect of the exosomal proteins derived from the CSF of ALS patients in the development of a motor neuron pathology in the experimental animals was established. This confirms the pathogenetic role of exosomes in neurodegenerative progression and makes it possible to identify a new target for ALS therapy.**

KEYWORDS **amyotrophic lateral sclerosis, neurodegeneration, motor neurons, exosomes, TDP43.**

ABBREVIATIONS **ALS – amyotrophic lateral sclerosis; FTD – frontotemporal dementia; OF – open field test; NB – narrowing beam test; SDH – succinate dehydrogenase; CNS – central nervous system; CSF – cerebrospinal fluid; IBA1 – allograft inflammatory factor 1, or ionized calcium binding adaptor molecule 1; IL – interleukin; PGP9.5/UCHL1 – protein gene product 9.5/ubiquitin carboxyl-terminal hydrolase L1.**

INTRODUCTION

Amyotrophic lateral sclerosis (ALS) is a severe neurodegenerative disease, which remains incurable today. ALS is characterized by selective degeneration of the upper and lower motor neurons localized in the brain motor cortex and peripheral nuclei, respectively (brainstem and anterior horns of the spinal cord) [1]. Such a localization of the pathological process in ALS leads to progressive neurogenic muscle weakness, which eventually results in the deterioration of such

vital functions as breathing and swallowing. This, in turn, inevitably leads to respiratory failure, requiring invasive ventilation and gastrostomy. The disease is characterized by a pronounced clinical heterogeneity, depending on the primary localization of neurodegenerative changes (bulbar and spinal levels), the degree of involvement of the upper and/or lower motor neurons, the progression rate, and the presence of pathogenic mutations.

ALS is an orphan disease; its prevalence is about 5 cases per 100,000 population per year, and the incidence ranges from 2 to 3 cases per 100,000 population per year [2]. The average age of development of the disease's first symptoms lies in the range of 55 to 65 years; however, in recent decades, there has been a clear trend towards a decrease in the age of the disease onset and an increase in ALS incidence [3]. In most patients, the cause of ALS remains unknown; these cases are classified as sporadic, about 90% of them. Genetically determined (familial) ALS forms associated with causal mutations in various genes account for approximately 10% of all cases [1]. The key molecular drivers in ALS pathogenesis include dysproteostasis, aberrant RNA metabolism, impaired endosomal and vesicular transport, mitochondrial dysfunction, neuroinflammation, etc.; the significance of these elements remains to be clarified [2]. The existence of different genetic forms of ALS makes it possible to design representative cellular and animal models of the disease based on the expression of mutations in the genes *SOD1*, *TARDBP*, *FUS*, etc. in model organisms; transgenic B6SJL-Tg (SOD1–G93A) mice are the most commonly used animals in these experiments [3].

Recent studies hold that extracellular vesicles, mainly exosomes, play a major role in the neurodegenerative progression in the central nervous system (CNS) [4]. Exosomes are encapsulated particles enriched with various molecules, including membrane and cytoplasmic proteins, lipids, and nucleic acids [5]. Exosomes act as effective transport systems and deliver molecular cargo to recipient cells, which makes them one of the most important tools of intercellular communication in both physiological and pathological processes [6]. Exosomes originate from intracellular multivesicular bodies and are 30–150 nm in diameter [7]. During maturation, exosomes are exported to the extracellular space; they can further enter the bloodstream and even cross the blood-brain barrier (BBB) [8]: hence, exosomes can be found in various biological fluids [9, 10]. Many of the protein products of ALS-associated genes are found in exosomes, which enables their transfer between neuronal and glial cells in various brain regions, contributing to the progression of neurodegeneration [11]. These proteins include SOD1, TDP-43, FUS, and proteins with dipeptide repeats characteristic of intracellular inclusions in mutant *C9orf72* [6]. Braak et al. proposed several hypotheses on neurodegenerative progression in the CNS in ALS [12]. One of the most convincing hypotheses implies the transfer of pathological proteins between adjacent CNS regions via exosome transport. The spread of symptoms to adjacent anatomical regions typical of ALS apparently is clinically a manifestation of the transfer of pathologically aggregated proteins between neighboring cells and within interconnected CNS regions.

The aim of this work was to study the effect of intraventricular administration of an exosome fraction taken from the cerebrospinal fluid (CSF) of patients with sporadic ALS and a healthy donor on the motor activity of model animals and their CNS pathomorphology.

EXPERIMENTAL

Obtaining the exosome suspension

The exosomes used in the study were obtained from two ALS patients. Patient ALS110 is a 48-year-old male with stage 4a cervicothoracic ALS and overall disease duration of 8 months; patient ALS111 is a 67-year-old male with stage 4a cervicothoracic ALS and disease duration of 26 months. The sample material, hereinafter referred to as the control, was obtained from a clinically healthy 57-year-old woman.

The exosomes were isolated from CSF according to the Total Exosome Isolation (from other body fluids) kit instructions (Invitrogen, ref. 4484456). All procedures were performed under aseptic conditions. Prior to isolation, a 0.5 ml CSF aliquot was successively centrifuged at 2,000 *g* and 4°C for 30 min. The cleared supernatant was then centrifuged at 10,000 *g* and 4°C for 30 min. The resulting supernatant was thoroughly mixed with the Total Exosome Isolation reagent, incubated at 2–8°C for 1 h, and the exosomes were pelleted by centrifugation at 10,000 *g* and 2–8°C for 1 h. The resulting pellet was re-suspended in 40 μl of phosphate buffer.

Exosome concentration in the suspension was assessed by evaluating one of its main markers; namely, CD9. The exosome concentration in the purified suspension was 7×10^8; it was designated as high (H). In turn, a suspension with a low (L) concentration of exosomes was obtained by diluting the H suspension 10-fold with phosphate buffer. These two dilutions (H, L) were used for administration to the experimental animals.

The animals

The study was performed in male BALB/c mice (n = 45) aged 2.5 months (at the beginning of the experiment) and weighing 22–25 g. The animals were obtained from the nursery of the Stolbovaya branch of the Federal State Budgetary Scientific Institution Scientific Center for Biomedical Technologies of the Federal Medical and Biological Agency, Russia. Procedures on the animals were performed in accordance with the requirements of the European Convention for the Protection of Vertebral Animals Used for Experimental and Other Scientific Purposes (CETS No. 170), Order of the Ministry of Health of the Russian Federation No. 119N dated April 1, 2016, On approval of the Principles of good laboratory practice and also guided by the Requirements for working with laboratory rodents and rabbits (National State Standard No. 33216-2014). The animals were kept in standard vivarium conditions with free access to food and water in a 12-hour day/night cycle. Prior to the experiment, the animals had undergone a 14-day quarantine. The study was approved by the Ethics Committee of the Scientific Center of Neurology.

To administer the exosome suspension to mice, the animals were placed in a Lab Standard Stereotaxic Instrument frame (Stoelting, USA) and 2 μl of the suspension were injected bilaterally into the lateral ventricles of the brain through holes drilled in the skull. The administration was performed using the following coordinates from the Mouse Brain Atlas: AP – -0.22; L – 1.0; V – 2.3 [13]. Zoletil-100 (Virbac Sante Animale, France) and Xyla (Interchemie Werken "de Adelaar BV", Netherlands) were used for anesthesia. A standard Zoletil-100 solution (500 mg in 5 ml) was diluted in saline at a 1 : 4 ratio and injected intramuscularly in an amount of 1.5 mg of the active substance per 25 g of mouse weight. Xylu was diluted in saline at a 1 : 2 ratio and administered intramuscularly in an amount of 0.6 mg per 25 g of mouse weight.

All the animals were divided into five groups of nine mice each: the control and experimental groups, which received drugs at either a high or low dose.

Physiological study

The health of the experimental mice was checked twice a week, and changes in motor activity were assessed twice a month. Animal health was examined based on changes in weight, the presence of a porphyrin secretion from the nose and eyes, coat condition, etc. To evaluate the extent of the resulting motor and neurological disorders, the Open Field (OF) and Narrowing Beam (NB) tests were employed.

The OF represented a 40 × 40 × 20 cm box made of polyvinyl chloride (workshops of the Brain Institute of the Scientific Center of Neurology). The mouse was placed in the center, and its motor activity was recorded for 3 min using the ANY-maze Video Tracking software (Stoelting Inc., USA).

The NB setup was composed of two 100-cm long bars superimposed on each other (Open Science, Russia). The width of the upper bar ranged from 0.5 to 2 cm, and the height was 1 cm. The width of the lower bar was 2.5 to 4 cm. The narrow end of the beam had a cage (shelter) with a removable lid and an opening in the frontal panel, through which the animal could get inside. The entire setup was elevated 70 cm above ground. The experimental animal had to traverse the upper bar from the beginning of the path to the shelter. The traversal time and percentage of limb slips onto the lower bar of the total number of steps on the NB were recorded.

Behavioral tests were conducted 11 months after exosome administration. The results are presented in the article.

Morphological study

For the morphological study, spinal cord samples were obtained from the ALS111(H) experimental group. The control group consisted of four mice from the same batch as those participating in the experiment. In addition, we used samples from the transgenic ALS model mice (B6SJL-Tg (B6SJL-Tg (SOD1–G93A) line) obtained in our previous study, for comparison [3]. Mice were decapitated, the spine was removed, and the spinal cord was isolated under a binocular microscope. Lumbar regions of the spinal cord were fixed in 4% formalin. After fixation, the samples were immersed in 30% sucrose, placed in an OCT medium, and 12-μm-thick sections were prepared on a Sakura Tissue-Tek cryostat. For immunohistochemical examination, antibodies to the neuronal protein PGP9.5/UCHL1 (ubiquitin carboxyl-terminal hydrolase L1), microglia marker IBA1 (allograft inflammatory factor 1, or ionized calcium binding adaptor molecule 1), and the proteins involved in the pathogenesis of ALS–SOD1 and TDP-43 were used. For antigen retrieval, sections in Tris-EDTA buffer (antigen retrieval solution, pH 9.0, Nordic Biosite) were heated in a steamer for 15 min. The sections were then incubated with primary antibodies. Antibody binding was confirmed using the immunofluorescence method. For this, corresponding secondary goat and donkey antibodies labeled with fluorochromes CF488 and CF555 (Sigma, USA) were used. The reaction was conducted according to the antibody manufacturer's instructions. In addition, succinate dehydrogenase (SDH) activity in

formazan formation [14] was detected in freshly frozen sections of the anterior tibial muscle of two experimental animals after exosome injection and two transgenic SOD1–G93A ALS model mice using the conventional histochemical technique.

The samples were examined on a Nikon Eclipse Ni-U microscope. Neurons were counted using the previously described protocol [15]. The immunofluorescence intensity of IBA1 staining was evaluated using the NIS-Elements software. The assessment was performed in at least 12 L1–L5 sections of the right side of the spinal cord from each animal, and the obtained data were averaged.

Statistical analysis

The obtained data were processed using the Statistica 12.0 software and one-way analysis of variance (ANOVA) with subsequent post-hoc intragroup comparisons using the Fisher's criterion for unequal groups, as well as the Mann–Whitney test. The results are presented as the mean and standard error (M ± SEM), indicating the statistical significance of differences between the compared groups for the studied parameters. Differences were considered statistically significant at $p < 0.05$.

RESULTS

The first signs of motor disorders in individual animals were noted 9 months after exosome administration. By month 10–11, the number of mice with signs of disease had increased (*Fig. 1*), primarily among animals in the ALS111(H) and ALS110(H) groups; i.e., mice receiving a higher drug dose. Examination revealed fur thinning, minor porphyrin discharges from the eyes and nose, and a decrease in body weight (*Fig. 2B*).

Behavioral testing of the animals demonstrated a significant decrease in motor activity, an increase in the period and episodes of immobility in the OF test (*Fig. 2D,E*), impaired coordination, an increase in the time required to complete the NB test (*Fig. 2F*), and partial paresis of hind limbs. The OF test showed a decrease in the distance traveled ($p = 0.0276$) and an increase in the time of immobility in the ALS111(H) group ($p = 0.0466$) compared to the control group. A decrease in the distance traveled ($p = 0.0035$) and an increase in the immobility time ($p = 0.0045$) were also observed in the ALS111(H) group compared to the ALS110(H) group. The NB test (*Fig. 2F*) showed significant changes in hind limb performance in mice. The number of hind limb slips statistically significantly increased in the ALS111(L) ($p = 0.0101$) and ALS111(H) ($p = 0.0119$) groups compared to the control. A decrease in the number of forelimb slips was also noted in the ALS111(H) group compared to the ALS110(H) group ($p = 0.04$). ALS110(L) and ALS110(H) mice did not show any impairments in the performance of both forelimbs and hind limbs.

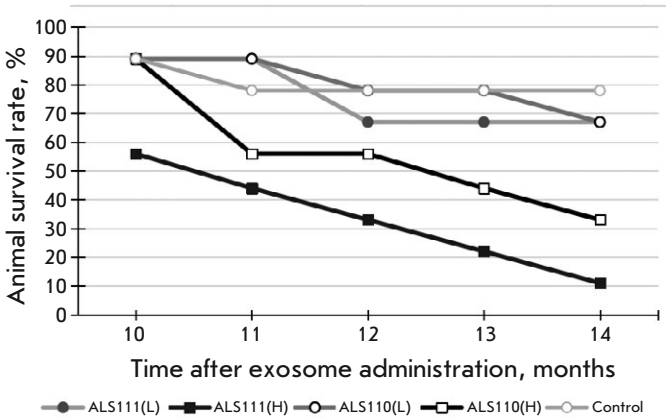

Fig. 1. Dynamics of survival of experimental mice in groups

Changes observed in mouse appearance, gait, and locomotion after exosome injection differ from the normal age range and are similar to ALS signs in the transgenic B6SJL-Tg (SOD1–G93A) mouse disease model (see *Fig. 2A–C*).

The animals with the most pronounced motor disorders (dragging up of the hind limbs, impaired gait, and decreased motor activity) were used for histological examination 14 months after the start of the experiment. Performing behavioral tests at this time point proved impossible due to the development of severe neurological disorders by the animals.

Evaluation of the number of motor neurons revealed a significant decrease in their density in the ventral horns of the spinal cord after administration of the high dose of ALS111 compared to the control. In addition, a significant increase in the number of microglial cells and microglia activation in the experimental group, as well as a statistically significant increase in the intensity of staining for the microglial marker IBA1, were noted (*Fig. 3A,E*).

An analysis of the TDP-43 protein in the neuronal cytoplasm showed a predominant nuclear localization of TDP-43 in the control mice. Protein mislocation, with its accumulation in the cytoplasm, was observed in individual neurons in the experimental group (*Fig. 3B*).

No aggregated SOD1 form was detected in spinal motor neurons in the controls. Individual inclusions of aggregated SOD1 were found in the experimental mice (*Fig. 3C*); however, no pronounced neuronal death was observed. Transgenic SOD1–G93A mice

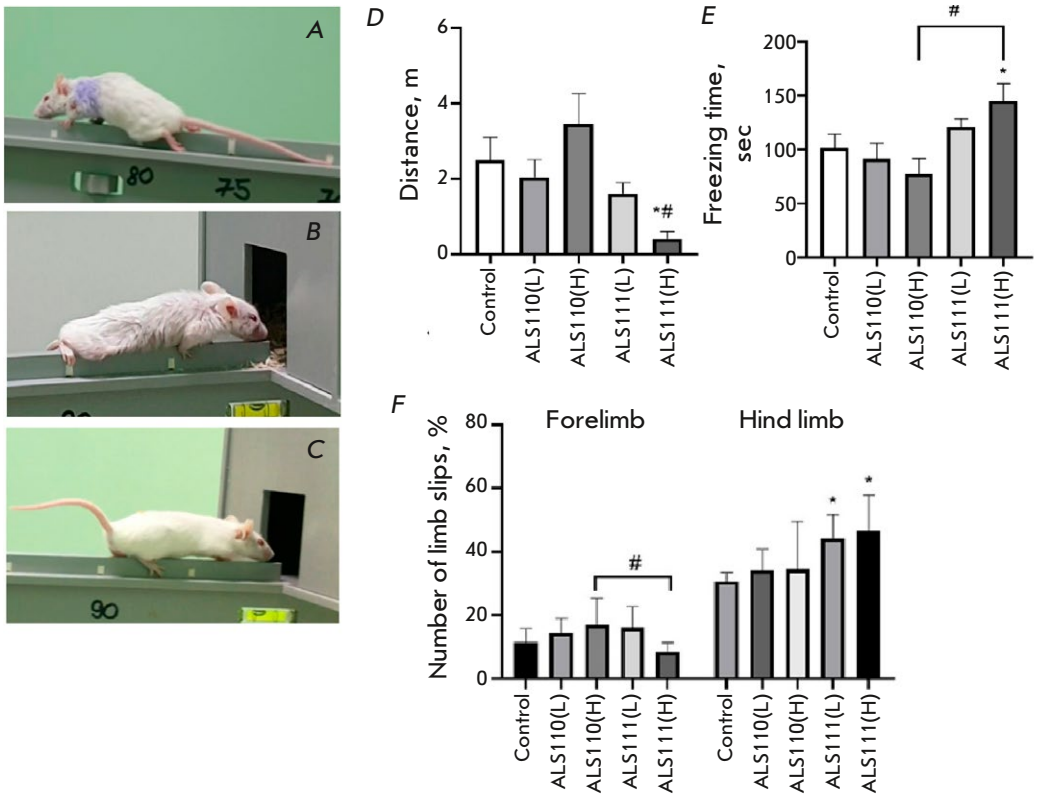

Fig. 2. Appearance of G93A (*A*) and ALS111 mice (*B*) after the onset of ALS symptoms. Control animal (*C*); distance traveled (*D*) and immobility time (*E*) during OF testing; number of limb slips from the upper bar (in %) per NB (*E*). * $p < 0.05$ compared to the control group. # $p < 0.05$ compared to the ALS110 (H) group. Data are presented as mean ± SEM

exhibiting multiple SOD1 aggregates and a decreased number of motor neurons in the spinal cord were used as a positive control.

The histochemical response to the SDH activity in the skeletal muscles of the animals revealed a trend towards an increase in the enzyme activity in the experimental group. This process is characteristic of muscle metabolic reprogramming in ALS (*Fig. 3D*); it has been also previously observed in B6SJL-Tg (SOD1–G93A) mice [3].

DISCUSSION

A common feature of neurodegenerative diseases is the progressive death of neurons (with selective vulnerability of individual disease subtypes in specific pathologies) and aggregation of the misfolded proteins that play a key role in the disease [16]. In ALS, the pathological process develops locally with the death of motor neurons and progresses predictably throughout the CNS along certain neuroanatomical pathways [17]. In our out study, we showed that, as early as 9 months after intraventricular administration of exosomes from the CSF of ALS patients, animals began to exhibit a typical motor phenotype: a change in locomotion with paresis of hind limbs, impaired coordination, and an increase in the time and number of episodes of immobility, as demonstrated by physiological studies. This phenotype was similar to that of transgenic animals expressing the G93A mutation in *SOD1* [3]. It is important to note that the rate of development of motor symptoms depended on the concentration of the injected exosome suspension. This is consistent with the concept of an incubation period required, during which a protein with a prion-like domain (e.g., TDP-43 and SOD1) converts normal protein forms to pathological ones [16, 18]. In the case of a higher concentration of exosomes initiating the neurodegenerative process, this period is reduced.

One of the mechanisms observed in various neurodegenerative diseases is secretion of the native and membrane-associated pathological protein in extracellular vesicles (exosomes) into the extracellular space, followed by its uptake by neighboring cells via receptor-mediated endocytosis or pinocytosis [18–20]. An alternative mechanism is trans-synaptic transmission through anterograde and/or retrograde transport [21, 22].

One of the main pathomorphological characteristics of ALS is the presence of ubiquitin-positive cytoplasmic inclusions (stress granules) in neurons containing TDP-43 protein aggregates, as observed in autopsy samples from ALS patients [23, 24]. Identification

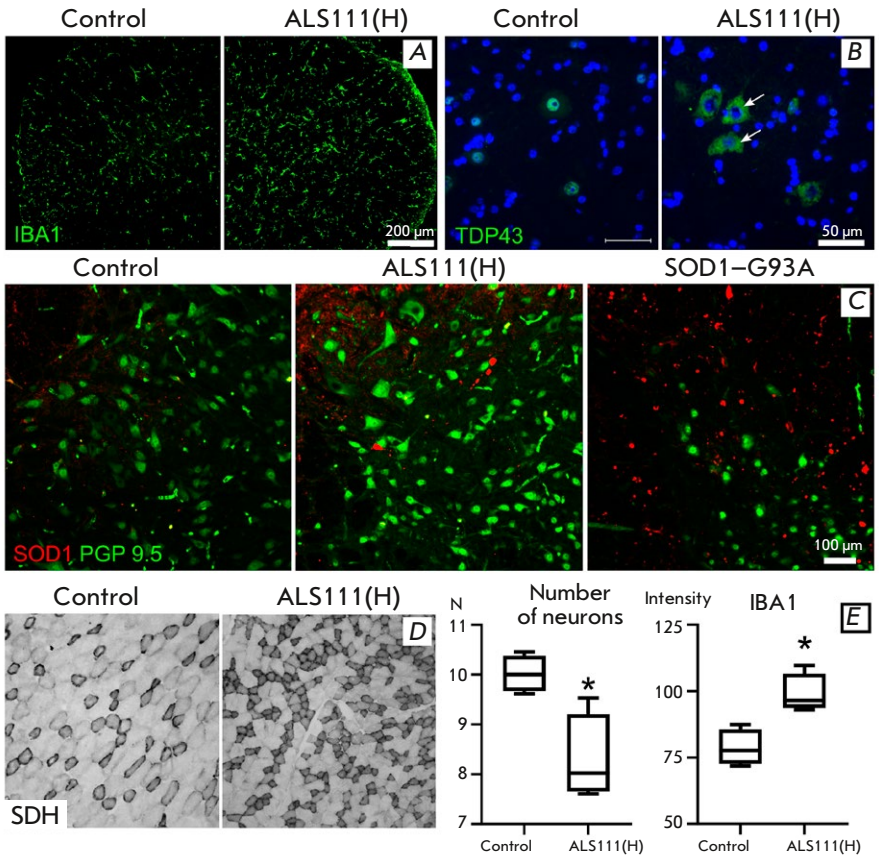

Fig. 3. Morphological examination. (*A*) – microglia activation. Microglia marker protein IBA1 staining. Ventral horn of the spinal cord, lumbar region. (*B*) TDP43 localization (green color) in motor neurons. Arrows indicate TDP43 localization in the cytoplasm. Ventral horn of the spinal cord, lumbar section. (*C*) SOD1 accumulation in the spinal cord of experimental animals. SOD1 (red) and PGP9.5 (green) localization. Ventral horn of the spinal cord, lumbar region. (*D*) – increase in the number of SDH-positive fibers. Anterior tibial muscle. (*E*) Changes in motor neurons and neuroglia. Decrease in the number of motor neurons of the ventral horns of the spinal cord (cells in the field of view), increase in the intensity of the staining for the microglia marker protein IBA1. * $p < 0.05$, Mann-Whitney criterion. Data are presented as a median and the interquartile range

of causal mutations in the *TARDBP* gene encoding TDP-43 confirmed the importance of this protein in the pathogenesis of ALS [25] and frontotemporal dementia (FTD) [26]. The TDP-43 aggregation is observed in neurons in approximately 97% of all ALS cases and almost half of FTD cases [27]. TDP-43 is a highly conserved DNA/RNA-binding protein that executes various functions in the cell, including the regulation of transcription and alternative RNA splicing [28]. TDP-43 consists of four domains: an amino-terminal domain, two RNA recognition motifs, and a carboxyl-terminal domain with prion-like properties [29]. In normal conditions, TDP-43 is located predominantly in the nucleus [30]. In ALS patients, the protein adopts a pathological conformation. Once this protein is captured trans-synaptically by the recipient cell, it interacts with endogenous TDP-43, thus triggering (in the prion-like fashion) aggregation of intrinsic TDP-43 and thereby spreading the pathology to other CNS structures [31, 32]. The CSF and CNS tissue from ALS and FTD patients has been shown to cause TDP-43 aggregation and induce TDP-43 proteinopathy in both cell cultures and *in vivo* [32–34]. In such diseases as ALS or FTD, TDP-43 mislocation and an increase in its cytoplasmic level are noted in the cell, which results in the formation of protein inclusions in the cytoplasm and impairment of its functions in the cell nucleus [35]. In our study, we used spinal cord samples from mice with the most pronounced motor disorders (14 months after the start of the experiment) for immunohistochemical analysis, which demonstrated TDP-43 mislocation, with predominant accumulation in the neuron cytoplasm. These results are consistent with the data obtained by other researchers.

There is data on the intercellular transport of TDP-43 aggregates via exosomes [36]. Exosomal secretion of such pathological proteins as β-amyloid, Tau, the prion protein, and α-synuclein was also reported in other neurodegenerative diseases [16, 20]. Exosomal transport of TDP-43 plays an important role in ALS pathogenesis, since significantly higher levels of exosomal TDP-43 are detected in the brain and CSF biopsy samples from ALS patients compared to controls [33, 37].

In addition to transmission between neurons, the spread of pathological proteins between neurons and glia (astrocytes, microglia, and/or oligodendrocytes) has also been reported [20]. For instance, the Tau protein can enter astrocytes [38] and microglia, which

play a key role in the spread of pathological Tau protein via exosome transport [38, 39]. In our study, staining of spinal cord samples from the experimental animals for the microglial marker IBA1 revealed an increase in the number of microglial cells and their activation, which indicates a direct involvement of innate immunity in the molecular mechanisms of motor neuron death. The inflammatory response occurring in the pathology has some beneficial effects, restoring tissue integrity and homeostasis; however, chronic neuroinflammation depletes the regenerative potential of microglia [40]. Microglia is activated via inflammasomes, which are high-molecular complexes in the cytosol of immune cells that mediate the activation of pro-inflammatory caspases [41]. A crucial intracellular factor inflammasomes respond to in ALS is the accumulation of toxic aggregates of the TDP-43, SOD1, and other proteins that cause neuroinflammation in neurons [42]. The inflammasome activation cascade initiates the release of interleukins (IL)-1β and IL-18 and causes pyroptosis. Pyroptosis is programmed cell death mediated by gasdermin D and the influx of sodium ions and water, which lead to cell swelling with membrane rupture and the release of the cytosol content into the extracellular space, resulting in the spread of pathological proteins in CNS cells [43].

In contrast to sporadic ALS forms, which are characterized by the presence of TDP-43 as the main component of intracellular inclusions [24], familial disease forms with a verified mutation in *SOD1* are characterized by predominant deposition of the mutant SOD1 protein [44]. It is important to note that cellular aggregates of wild-type SOD1 are also detected in some other familial ALS cases and individual cases of sporadic forms lacking *SOD1* mutations [45]. This might explain the aggregated SOD1 deposits we found in the experimental animals lacking the *SOD1* mutation. In addition, the low amount of deposits explains the relative preservation of motor neurons. At the same time, analysis of the positive control (SOD1–G93A transgenic mice) revealed multiple SOD1 aggregates and a decreased number of motor neurons, which die as a result of the toxic effect of SOD1 on the cell through the gain-of-function mechanism.

In recent years, several innovative approaches to ALS treatment using exosomes and extracellular vesicles have been proposed [46]. Most of these methods involve the use of exosomes for a targeted delivery of various neurotrophic factors and microRNAs through the BBB in order to inhibit the motor neuron death. Considering the fact that, in the ALS pathogenesis, exosomes presumably mediate one of the main mechanisms of pathology progression in the CNS, which is also shown in the present work, we can contemplate the possibility of modulating the neurodegenerative process by inhibiting exosome transport at its various stages. One such promising method aimed at inhibiting the spread of the neurodegenerative process by exosomes is immune blocking of exosome fusion with the motor neuron membrane using anti-CD63 antibodies and, presumably, other key exosome markers [47]. In addition to such an effect on exosomes, an important issue in inhibiting the exosomic pathway in ALS remains the development of drugs that selectively block the transfer of proteins with an altered conformation and prion-like properties.

Thus, in this study, we demonstrated the triggering effect of exosomal proteins from the CSF of ALS patients in the development of motor neuron death in experimental animals. The presented data confirm the pathogenetic role of exosomes in the spread of the neurodegenerative process in the disease and open up a possibility for identifying new targets for ALS therapy. ●

This work was supported by the Ministry of Science and Higher Education of the Russian Federation for major scientific projects in priority areas of scientific and technological development (project No. 075-15-2024-638).

REFERENCES

1. Feldman E.L., Goutman S.A., Petri S., Mazzini L., Savelieff M.G., Shaw P.J., Sobue G. // Lancet. 2022. V. 400. № 10360. P. 1363–1380.
2. Hardiman O., Al-Chalabi A., Chio A., Corr E.M., Logroscino G., Robberecht W., Shaw P.J., Simmons Z., van den Berg L.H. // Nat. Rev. Dis. Primers. 2017. V. 5. P. 17071.
3. Stavrovskaya A.V., Voronkov D.N., Artemova EH.A., Belugin B.V., Shmarov M.M., Yamshchikova N.G., Gushchina A.S., Ol'shanskij A.S., Narodickij B.S., Illarioshkin S.N. // Nervno-myshechnye bolezni. 2020. No. 3. P. 63–73.
4. Ivanova M.V., Chekanova E.O., Belugin B.V., Tutykhina I.L., Dolzhikova I.V., Zakrojshchikova I.V., Vasil'ev A.V., Zakharova M.N. // Nejrokhimiya. 2019.V. 36. No. 3. P. 195–207.
5. Ivanova M.V., Chekanova E.O., Belugin B.V., Dolzhikova I.V., Tutykhina I.L., Zakharova M.N. // Nejrokhimiya. 2020. V. 37. No. 3. P. 271–279.
6. Gagliardi D., Bresolin N., Comi G.P., Corti S. // Cell Mol. Life Sci. 2021. V. 78. № 2. P. 561–572.
7. Cocucci E., Meldolesi J. // Trends Cell Biol. 2015. V. 25. P-64–372.

8. Matsumoto J., Stewart T., Banks W.A., Zhang J. // Curr. Pharm. Des. 2017. V. 23. P. 6206–6214.
9. Kourembanas S. // Annu. Rev. Physiol. 2015. V. 77. P. 13–27.
10. Théry C., Amigorena S., Raposo G., Clayton A. // Curr. Protocol Cell Biol. 2006. V. 30. P. 3.22.1–3.22.29.
11. Silverman J.M., Fernando S.M., Grad L.I., Hill A.F., Turner B.J., Yerbury J.J., Cashman N.R. // Cell Mol. Neurobiol. 2016. V. 36. P. 377–381.
12. Braak H., Brettschneider J., Ludolph A.C., Lee V.M., Trojanowski J.Q., Del Tredici K. // Nat. Rev. Neurol. 2013. V. 9. № 12. P. 708–714.
13. Paxinos G., Franklin K.B.J. The mouse brain in stereotaxic coordinates. San Diego etc.: Acad. Press, 2001.
14. Berston M. Gistokhimiya fermentov. M.: Mir, 1965. p. 464.
15. Austin A., Beresford L., Price G., Cunningham T., Kalmar B., Yon M. // Curr. Protocols. 2022. V. 2. e428.
16. Peng C., Trojanowski J.Q., Lee V.M.-Y. // Nat. Rev. Neurol. 2020. V. 16. P. 199–212.
17. Ravits J.M., La Spada A.R. // Neurology. 2009. V. 73. P. 805–811.
18. Goedert M., Clavaguera F., Tolnay M. // Trends Neurosci. 2020. V. 33. P. 317–325.
19. Saman S., Kim W., Raya M., Visnick Y., Miro S., Saman S., Jackson B., McKee A.C., Alvarez V.E., Lee N.C.Y., Hall G.F. // J. Biol. Chem. 2012. V. 287. P. 3842–3849.
20. Uemura N., Uemura M.T., Luk K.C., Lee V.M.-Y., Trojanowski J.Q. // Trends Mol. Med. 2020. V. 26. № 10. P. 936–952.
21. Mezias C., Rey N., Brundin P., Raj A. // Neurobiol. Dis. 2020. V. 134. P. 104623.
22. Schaser A.J., Stackhouse T.L., Weston L.J., Kerstein P.C., Osterberg V.R., López C.S., Dickson D.W., Luk K.C., Meshul C.K., Woltjer R.L., et al. // Acta Neuropathol. Commun. 2020. V. 8. P. 150.
23. Arai T., Hasegawa M., Akiyama H., Ikeda K., Nonaka T., Mori H., Mann D., Tsuchiya K., Yoshida M., Hashizume Y., Oda T. // Biochem. Biophys. Res. Commun. 2006. V. 351. P. 602–611.
24. Neumann M., Sampathu D.M., Kwong L.K., Truax A.C., Micsenyi M.C., Chou T.T., Bruce J., Schuck T., Grossman M., Clark C.M., et al. // Science. 2006. V. 314. № 5796. P. 130–133.
25. Sreedharan J., Blair I.P., Tripathi V.B., Hu X., Vance C., Rogelj B., Ackerley S., Durnall J.C., Williams K.L., Buratti E., et al. // Science. 2008. V. 319. № 5870. P. 1668–1672.
26. Borroni B., Bonvicini C., Alberici A., Buratti E., Agosti C., Archetti S., Papetti A., Stuani C., Di Luca M., Gennarelli M., Padovani A. // Hum. Mutat. 2009. V. 30. № 11. P. 974–983.
27. Tan R.H., Yang Y., Kim W.S., Dobson-Stone C., Kwok J.B., Kiernan M.C., Halliday G.M. // Acta Neuropathol. Commun. 2017. V. 5. № 1. P. 76.
28. Buratti E., Baralle F.E. // J. Biol. Chem. 2001. V. 276. P. 36337–36343.
29. Cohen T.J., Lee V.M.Y., Trojanowski J.Q. // Trends Mol. Med. 2011. V. 17. № 11. P. 659–667.
30. Ayala Y.M., Zago P., D'Ambrogio A., Xu Y.-F., Petrucelli L., Buratti E., Baralle F.E. // J. Cell Sci. 2008. V. 121. P. 3778–3785.
31. Smethurst P., Newcombe J., Troakes C., Simone R., Chen Y.-R., Patani R., Sidle K. // Neurobiol. Dis. 2016. V. 96. P. 236–247.
32. Tamaki Y., Ross J.P., Alipour P., Castonguay C.-É., Li B., Catoire H., Rochefort D., Urushitani M., Takahashi R., Sonnen J.A., et al. // PLoS Genet. 2023. V. 19. № 2. e1010606.
33. Ding X., Ma M., Teng J., Teng R.K.F., Zhou S., Yin J., Fonkem E., Huang J.H., Wu E., Wang X. // Oncotarget. 2015. V. 6. № 27. P. 24178–24191.
34. Nonaka T., Masuda-Suzukake M., Arai T., Hasegawa Y., Akatsu H., Obi T., Yoshida M., Murayama S., Mann D.M.A., Akiyama H., Hasegawa M. // Cell Rep. 2013. V. 4. № 1. P. 124–134.
35. Gambino C.M., Ciaccio A.M., Lo Sasso B., Giglio R.V., Vidali M., Agnello L., Ciaccio M. // Diagnostics. 2023. V. 13. P. 416.
36. Doyle L.M., Wang M.Z. // Cells. 2019. V. 8. № 7. P. 727.
37. Iguchi Y., Eid L., Parent M., Soucy G., Bareil C., Riku Y., Kawai K., Takagi S., Yoshida M., Katsunoet M., et al. // Brain. 2016. V. 139. P. 3187–3201.
38. Perea J.R., López E., Carlos Díez-Ballesteros J., Ávila J., Hernández F., Bolós M. // Front. Neurosci. 2019. V. 13. P. 442.
39. Asai H., Ikezu S., Tsunoda S., Medalla M., Luebke J., Haydar T., Wolozin B., Butovsky O., Kügler S., Ikezu T. // Nat. Neurosci. 2015. P. 18. № 11. P. 1584–1593.
40. Kempuraj D., Thangavel R., Natteru P.A., Selvakumar G.P., Saeed D., Zahoor H., Zaheer S., Iyer S.S., Zaheer A. // J. Neurol. Neurosurg. Spine. 2016. V. 1. № 1. P. 1003.
41. Martinon F., Burns K., Tschopp J. // Mol. Cell. 2002. V. 10. № 2. P. 417–426.
42. Komine O., Yamanaka K. // Nagoya J. Med. Sci. 2015. V. 77. № 4. P. 537–549.
43. Lieberman J., Wu H., Kagan J.P. // Sci. Immunol. 2019. V. 4. № 39. eaav144.
44. Valentine J.S., Doucette P.A., Zittin Potter S. // Annu. Rev. Biochem. 2005. V. 74. P. 563–593.
45. Rotunno M.S., Bosco D.A. // Front. Cell. Neurosci. 2013. V. 7. P. 253.
46. Bobis-Wozowicz S., Marbán E. // Front. Cell. Dev Biol. 2022. V. 10. P. 919426.
47. Afonso G.J.M., Cavaleiro C., Valero J., Mota S.I., Ferreiro E. // Cells. 2023. V. 12. P. 1763.

Comparative Analysis of Spacer Targets in CRISPR-Cas Systems of Starter Cultures

A. A. Fatkulin[1], T. A. Chuksina[1], N. P. Sorokina[2], I. T. Smykov[2], E. V. Kuraeva[2], E. S. Masezhnaya[2], K. A. Smagina[2], M. Yu. Shkurnikov[1*]

[1]Higher School of Economics, Faculty of Biology and Biotechnology, Moscow, 101000 Russian Federation

[2]Gorbatov Federal Research Center for Food Systems, Moscow, 109316 Russian Federation

*Email: mshkurnikov@hse.ru

Received October 09, 2024; in final form, November 07, 2024

DOI: 10.32607/actanaturae.27533

ABSTRACT **Dairy production facilities represent a unique ecological niche for bacteriophages of lactic acid bacteria. Throughout evolution, bacteria have developed a wide range of defense mechanisms against viral infections caused by bacteriophages. The CRISPR-Cas system is of particular interest due to its adaptive nature. It allows bacteria to acquire and maintain specific resistance to certain bacteriophages. In this study, we investigated the CRISPR-Cas systems of lactic acid bacteria. Special attention was paid to the specificity of the spacers in CRISPR cassettes. CRISPR-Cas systems were found in the genomes of 43% of the lactic acid bacteria studied. Additionally, only 13.1% of the total number of CRISPR cassette spacers matched bacteriophage genomes, indicating that many predicted spacers either lack known phage targets or are directed against other types of mobile genetic elements, such as plasmids.**

KEYWORDS **bacteriophage, CRISPR-Cas systems, cheesemaking, starter cultures, One Health.**

ABBREVIATIONS **R-M – restriction-modification system; Abi – abortive infection system.**

INTRODUCTION

In the production of fermented dairy products, starter cultures are used to promote milk fermentation and to form a product with distinctive textural, aromatic, and flavor properties [1]. However, the lactic acid bacteria used in this process can be susceptible to bacteriophage infection [2], as dairy production facilities represent a unique ecological niche for bacteriophages of lactic acid bacteria, which are present in raw milk [3].

Throughout evolution, bacteria have developed a wide range of defense mechanisms aimed at protecting themselves against viral infections caused by bacteriophages. These mechanisms include, among others, abortive infection (Abi) systems, restriction-modification (R-M) systems, and CRISPR-Cas systems [4]. The particular interest in CRISPR-Cas systems is due to their adaptive nature, which allows bacteria to acquire and maintain specific resistance to certain bacteriophages [5]. CRISPR-Cas-mediated immunity is found in approximately half of sequenced bacteria and in most archaea [6], making it one of the key elements of antiviral defense in prokaryotes.

Currently, two classes of CRISPR-Cas systems are recognized, consisting of six types (I–VI) which differ in their mechanisms of action and constituent elements [6]. Despite this diversity, all CRISPR-Cas systems share a number of characteristic features. The main element of each CRISPR-Cas system is the CRISPR locus. It contains CRISPR-associated (cas) genes that are responsible for interacting with foreign nucleic acids, as well as a CRISPR cassette: short palindromic repeat sequences of DNA separated by unique insertions — spacers. The spacers are fragments of foreign DNA integrated into the bacterial genome as a result of a previous infection [5]. They determine the sequence that will be recognized by Cas nucleases and, consequently, play a key role in CRISPR-Cas immunity. Most spacers are relatively short: for example, it is known that for the I-E and I-F subtypes, spacer lengths range from 31 to 33 bp, while for I-B, I-C, I-D, and I-U, they range from 34 to 37 bp [7].

The mechanism of action of the CRISPR-Cas system can be divided into several key stages: when foreign nucleic acid enters the bacterial cell, new spacers are integrated into the CRISPR cassette. This is followed by the transcription of the spacers, leading to the formation of precursor CRISPR-RNAs (pre-crRNA), which are then processed into mature

crRNAs. These crRNAs, binding with Cas nucleases, form an active complex capable of recognizing and binding to the complementary sequence of foreign DNA or RNA. Upon target binding, the foreign genetic material is degraded, providing protection to the cell from repeated infections [5]. For successful degradation of the bacteriophage genome, the target region must have a high degree of homology with the spacer. It has been previously shown, for instance, that the presence of three or more mutations can lead to an almost complete inactivation of CRISPR-Cas immunity [8].

In this study, the CRISPR-Cas systems of lactic acid bacteria were investigated. Special attention was paid to the specificity of the CRISPR cassette spacers, which allowed for an assessment of these bacteria's resistance to known bacteriophages.

EXPERIMENTAL

The genome sequences of lactic acid bacteria, as well as bacteriophages from the *Caudoviricetes* class, were obtained from the NCBI database. The genomic data were preprocessed to remove duplicates. The PADLOC tool [9] was used to identify CRISPR-Cas systems in bacterial genomes. MinCED [10] was used to predict spacers in the bacterial genomes, after which they were aligned to the phage genome sequences using Bowtie2 [11], applying the "–end-to-end" option and the "–very-sensitive" preset. To establish the functions of the regions to which the spacers were aligned, the bacteriophage genomes were further annotated using Pharokka [12]. To assess the overrepresentation of functional groups among the spacer targets, the proportion of spacers aligned to genes in each group and the proportion of genes in each group relative to the total were calculated. Then, to determine whether the distribution of spacers across groups was uniform, a Fisher's exact test following the "one-vs-all" principle was applied.

RESULTS

A total of 563 genomes of lactic acid bacteria, belonging to 6 species, were obtained from the NCBI database (*Table 1*). Using PADLOC, CRISPR-Cas systems were identified in 243 of these genomes (*Table 1*), corresponding to approximately 43% of all the genomes studied. The predicted CRISPR-Cas systems belong to 6 different subtypes: I-B, I-C, I-E, I-G, II-A, and II-C (*Fig. 1*). In the genomes of *Lactiplantibacillus plantarum*, *Lacticaseibacillus paracasei*, and *Lacticaseibacillus rhamnosus*, subtype II-A systems dominate, which may be an indirect indication of their important role in the defense mechanisms of these species. Among the strains of *Lacticaseibacillus casei*, the subtypes I-C and II-A are prevalent, while for *Lactobacillus helveticus*, the subtypes I-B and I-C are characteristic. In the genomes of *Propionibacterium freudenreichii*, subtype I-G predominates.

The total number of spacers predicted using MinCED in the bacterial genomes amounted to 6,971 (*Table 2*); however, many sequences are overrepresented within species. For this reason, the number of unique spacers among the studied species was only 3,477. The distribution of the lengths of the predicted spacers (*Fig. 2*) is consistent with previously published data [7]. Subsequent alignment to the genomes of 21,261 phages of the *Caudoviricetes* class, obtained from the NCBI database, yielded 916 matches (*Table 2*), of which only 485 are unique in terms of sequence and species origin.

All the obtained alignments correspond to the genomes of 69 phages, which were previously described as bacteriophages of lactic acid bacteria (*Fig. 3*). Functional annotation of the phage genomes revealed that the predicted spacers more frequently aligned to the genes encoding tail proteins, the genes involved in packaging, and the genes participating in DNA metabolism (adjusted p-value < 0.05) (*Table 3*).

DISCUSSION

The study revealed the presence of CRISPR-Cas systems in 43% of the investigated lactic acid bacterial genomes, confirming their significant role in the defense mechanisms of these microorganisms against foreign nucleic acids, including bacteriophage genetic material. The results also demonstrate the diversity of CRISPR-Cas systems across different species of lactic acid bacteria.

The relatively low percentage of spacers matching bacteriophage genomes (only 13.1% of the total) may indicate that many of the predicted spacers either do not have known phage targets or are directed against other types of mobile genetic elements, such as plasmids. This observation also highlights the need for further research to deepen our understanding of the interactions between CRISPR-Cas systems and various mobile genetic elements. Additionally, the discovery and description of new, previously unknown bacteriophages remains a relevant area of study.

Notably, among the spacer targets, genes responsible for viral particle packaging, tail protein genes, and genes involved in DNA metabolism are overrepresented, as these regions are likely to be more conserved due to their functions related to key stages of the viral life cycle, such as virion assembly and entry into the host cell.

It is also noteworthy that the phage spectra to which *Lacticaseibacillus paracasei*, *Lacticaseibacillus*

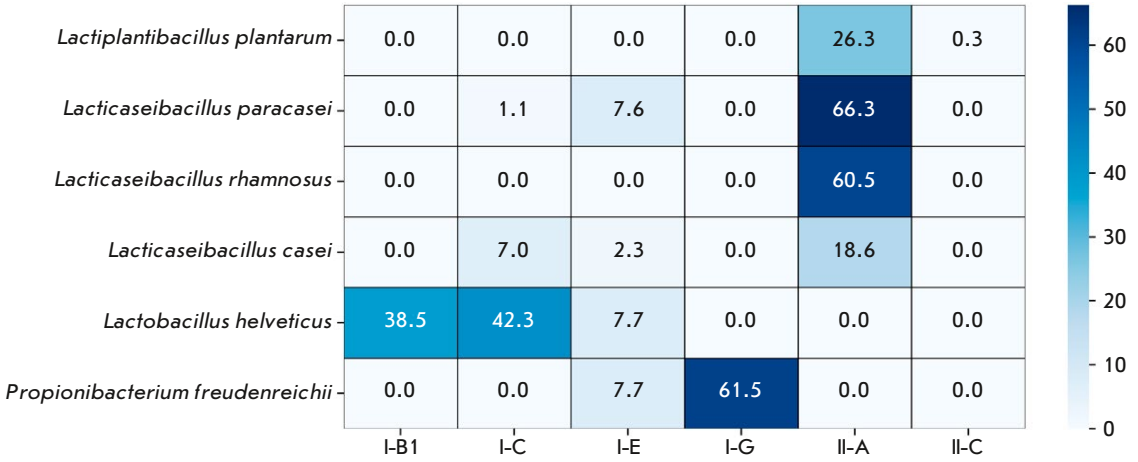

Fig. 1. Proportion (%) of CRISPR-Cas Systems in the Genomes of LAB

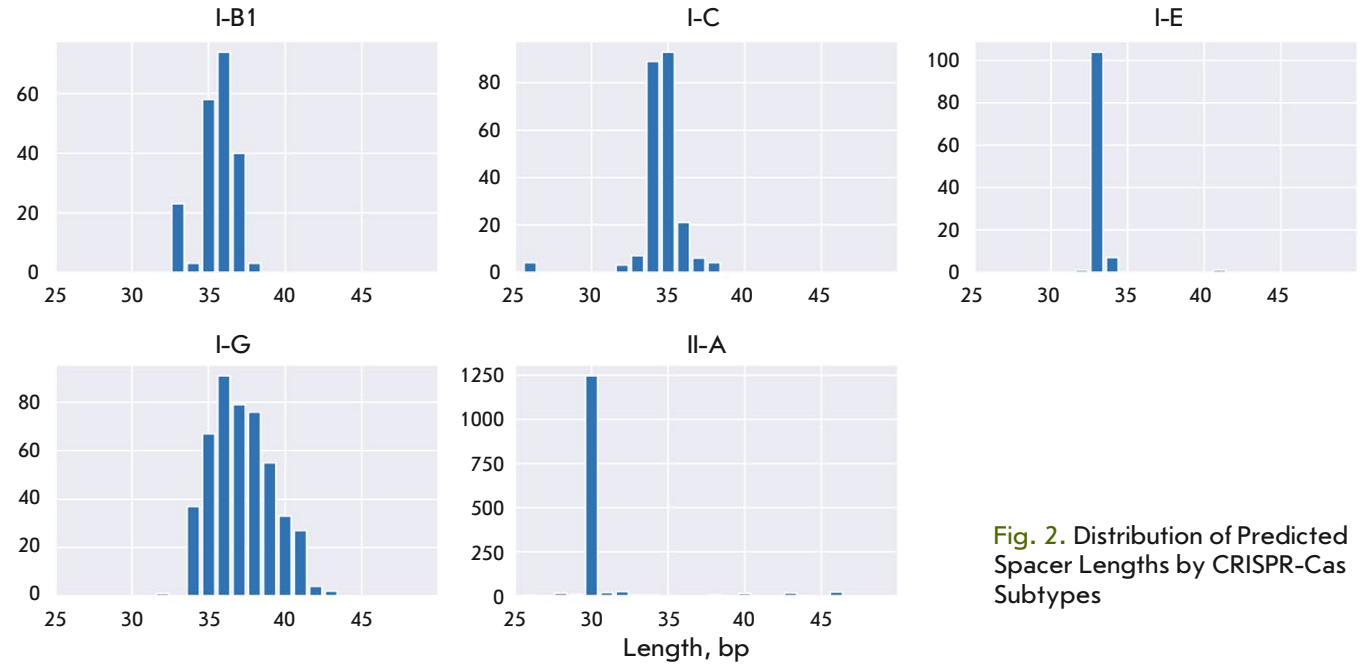

Fig. 2. Distribution of Predicted Spacer Lengths by CRISPR-Cas Subtypes

Table 1. Distribution of CRISPR-Cas Systems in the Genomes of Lactic Acid Bacteria

Species Name	Number of Genomes	Contains CRISPR-Cas, %
Lactiplantibacillus plantarum	300	80 (26.7)
Lacticaseibacillus paracasei	92	68 (73.9)
Lacticaseibacillus rhamnosus	76	46 (60.5)
Lacticaseibacillus casei	43	10 (23.3)
Lactobacillus helveticus	26	22 (84.6)
Propionibacterium freudenreichii	26	17 (65.4)
	563	243

Table 2. Distribution of Spacers in the Genomes of LAB

Species Name	Total Predicted	Identified in Phages, %
Lactiplantibacillus plantarum	1519	67 (4.4)
Lacticaseibacillus paracasei	2128	296 (13.9)
Lacticaseibacillus rhamnosus	1239	289 (23.3)
Lacticaseibacillus casei	379	53 (14.0)
Lactobacillus helveticus	778	48 (6.2)
Propionibacterium freudenreichii	928	163 (17.6)

Table 3. Genes Overrepresented Among Spacer Targets

Gene (according to Pharokka annotation)	Adjusted *p*-value
Terminase small subunit	3.8×10^{-6}
Head-tail adaptor Ad1	2.5×10^{-3}
Head scaffolding protein	3.6×10^{-3}
Major tail protein	3.8×10^{-3}
DNA repair exonuclease	3.9×10^{-2}

rhamnosus, and *Lacticaseibacillus casei* strains are resistant display a clear similarity. This fact, combined with the similarity of the CRISPR-Cas system subtypes found in the genomes of these strains, may suggest common defense mechanisms or indicate that these bacteria have followed similar evolutionary paths in developing resistance to bacteriophages.

In this study, we conducted a comprehensive analysis of CRISPR-Cas systems found in the genomes of lactic acid bacteria. The results largely align with previously published data; however, in our work, we used the most up-to-date information sources and focused on studying CRISPR-Cas-mediated immunity in several strains. Additionally, we examined the specificity of the identified spacers in more detail, including investigating the functions of the regions they target. Thus, the results described in this article not only broaden the current understanding of the role of CRISPR-Cas in the adaptive immunity of lactic acid bacteria, but also underscore the importance of further research in this area.

CONCLUSION

Further research is needed to better understand the role of the CRISPR-Cas system in protecting starter cultures from bacteriophages and to evaluate its impact on the fermentation process. The abundance of bacteriophages infecting starter cultures in dairy facilities highlights the importance of analyzing the resistance spectrum of starter cultures for their rational combination, depending on the phage spectrum in raw milk. ●

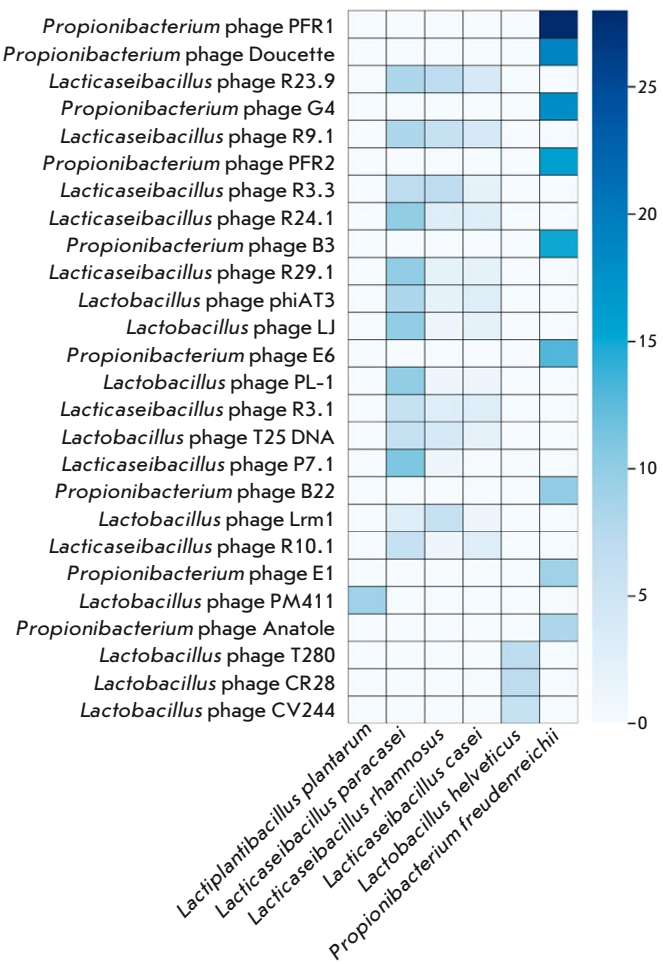

Fig. 3. Alignments of Unique Spacers to Bacteriophage Genomes. Phages with fewer than 5 spacers aligned from each species were excluded for better visual clarity

This work was supported by the Ministry of Science and Higher Education of the Russian Federation for large scientific projects in priority areas of scientific and technological development (Grant No. 075-15-2024-483).

REFERENCES

1. Frantzen C.A., Kleppen H.P., Holo H. // Appl. Environ. Microbiol. 2018. V. 84. № 3. P. e02199-17.
2. Lahbib-Mansais Y., Mata M., Ritzenthaler P. // Biochimie. 1988. V. 70. № 3. P. 429–435.
3. Romero D.A., Magill D., Millen A., Horvath P., Fremaux C. // FEMS Microbiol. Rev. 2020. V. 44. № 6. P. 909–932.
4. van Houte S., Buckling A., Westra E.R. // Microbiol. Mol. Biol. Rev. 2016. V. 80. № 3. P. 745–763.
5. Nussenzweig P.M., Marraffini L.A. // Annu. Rev. Genet. 2020. V. 54. № 1. P. 93–120.
6. Makarova K.S., Wolf Y.I., Iranzo J., Shmakov S.A., Alkhnbashi O.S., Brouns S.J.J., Charpentier E., Cheng D., Haft D.H., Horvath P., et al. // Nat. Rev. Microbiol. 2020. V. 18. № 2. P. 67–83.
7. Kuznedelov K., Mekler V., Lemak S., Tokmina-Lukaszewska M., Datsenko K.A., Jain I., Savitskaya E., Mallon J., Shmakov S., Bothner B., et al. // Nucl. Acids Res. 2016. V. 44. № 22. P. 10849–10861.
8. Xue C., Seetharam A.S., Musharova O., Severinov K., Brouns S.J., Severin A.J., Sashital D.G. // Nucl. Acids Res. 2015. V. 43. № 22. P. 10831–10847.
9. Payne L.J., Todeschini T.C., Wu Y., Perry B.J., Ronson C.W., Fineran P.C., Nobrega F.L., Jackson S.A. // Nucl. Acids Res. 2021. V. 49. № 19. P. 10868–10878.
10. Bland C., Ramsey T.L., Sabree F., Lowe M., Brown K., Kyrpides N.C., Hugenholtz P. // BMC Bioinformatics. 2007. V. 8. № 1. P. 209.
11. Langmead B., Salzberg S.L. // Nat. Meth. 2012. V. 9. № 4. P. 357–359.
12. Bouras G., Nepal R., Houtak G., Psaltis A.J., Wormald P.-J., Vreugde S. // Bioinformatics. 2023. V. 39. № 1. P. btac776.
13. Crawley A.B., Henriksen E.D., Stout E., Brandt K., Barrangou R. // Sci. Rep. 2018. V. 8. № 1. P. 11544.
14. Horvath P., Coûté-Monvoisin A.-C., Romero D.A., Boyaval P., Fremaux C., Barrangou R. // Internat. J. Food Microbiol. 2009. V. 131. № 1. P. 62–70.

Peptide Mimicking Loop II of the Human Epithelial Protein SLURP-2 Enhances the Viability and Migration of Skin Keratinocytes

O. V. Shlepova[1†], T. Ya. Gornostaeva[1,2†], I. D. Kukushkin[1,2], V. N. Azev[3], M. L. Bychkov[1], Z. O. Shenkarev[1,2], M. P. Kirpichnikov[1,5], E. N. Lyukmanova[1,2,4,5*]

[1]Shemyakin–Ovchinnikov Institute of Bioorganic Chemistry, Moscow, 117997 Russian Federation
[2]Moscow Center for Advanced Studies, Moscow, 123592 Russian Federation
[3]Branch of the Shemyakin–Ovchinnikov Institute of Bioorganic Chemistry, Pushchino, 142290 Russian Federation
[4]Shenzhen MSU–BIT University, Longgang District, Shenzhen, Guangdong Province, 518172 China
[5]Interdisciplinary Scientific and Educational School of Moscow University "Molecular Technologies of the Living Systems and Synthetic Biology", Department of Biology, Lomonosov Moscow State University, Moscow, 119234 Russian Federation
*E-mail: lyukmanova_ekaterina@smbu.edu.cn
† – these authors contributed equally to this work
Received August 16, 2024; in final form, November 07, 2024
DOI: 10.32607/actanaturae.27494

ABSTRACT **The secreted human protein SLURP-2 is a regulator of epithelial homeostasis, which enhances the viability and migration of keratinocytes. The targets of SLURP-2 in keratinocytes are nicotinic and muscarinic acetylcholine receptors. This work is devoted to the search for the SLURP-2 functional regions responsible for enhancing keratinocyte viability and migration. We produced synthetic peptides corresponding to the SLURP-2 loop regions and studied their effect on the viability and migration of HaCaT skin keratinocytes using the WST-8 test and scratch-test, respectively. The highest activity was exhibited by a loop II-mimicking peptide that enhanced the viability of keratinocytes and stimulated their migration. The peptide activity was mediated by interactions with α7- and α3β2-nAChRs and suppression of the p38 MAPK intracellular signaling pathway. Thus, we obtained new data that explain the mechanisms underlying SLURP-2 regulatory activity and indicate the promise of further research into loop II-mimicking peptides as prototypes of wound healing drugs.**

KEYWORDS **SLURP-1, SLURP-2, Ly6/uPAR, nicotinic acetylcholine receptor, keratinocytes, migration, wound healing.**

ABBREVIATIONS **α-Bgtx – α-bungarotoxin; ACh – acetylcholine; Atr – atropine; Dhβe – dihydro-β-erythroidine hydrobromide; mAChR – muscarinic acetylcholine receptor; Mec – mecamylamine; MII – α-conotoxin MII; MLA – methyllycaconitine; mTOR – mammalian target of rapamycin; nAChR – nicotinic acetylcholine receptor; Nf-kB – nuclear factor kB; p38 MAPK – mitogen-activated protein kinase p38; Src – non-receptor tyrosine kinase Src; STAT3 – signal transducer and activator of transcription 3.**

INTRODUCTION

Ly6/uPAR family proteins are expressed in many human tissues and cells [1]. Ly6/uPAR proteins exhibit a wide range of functions and are involved in regulation of cell proliferation, migration, intercellular interactions, immune cell maturation, macrophage activation, and cytokine production. They are also involved in cognitive processes [1–3]. Some of these proteins are ligands of nicotinic and muscarinic acetylcholine receptors (nAChRs and mAChRs, respectively). Acetylcholine receptors regulate various processes, in particular epithelial cell growth, migration, and differentiation [4, 5]. Acetylcholine receptor ligands may be used as prototypes of drugs effective in diseas-

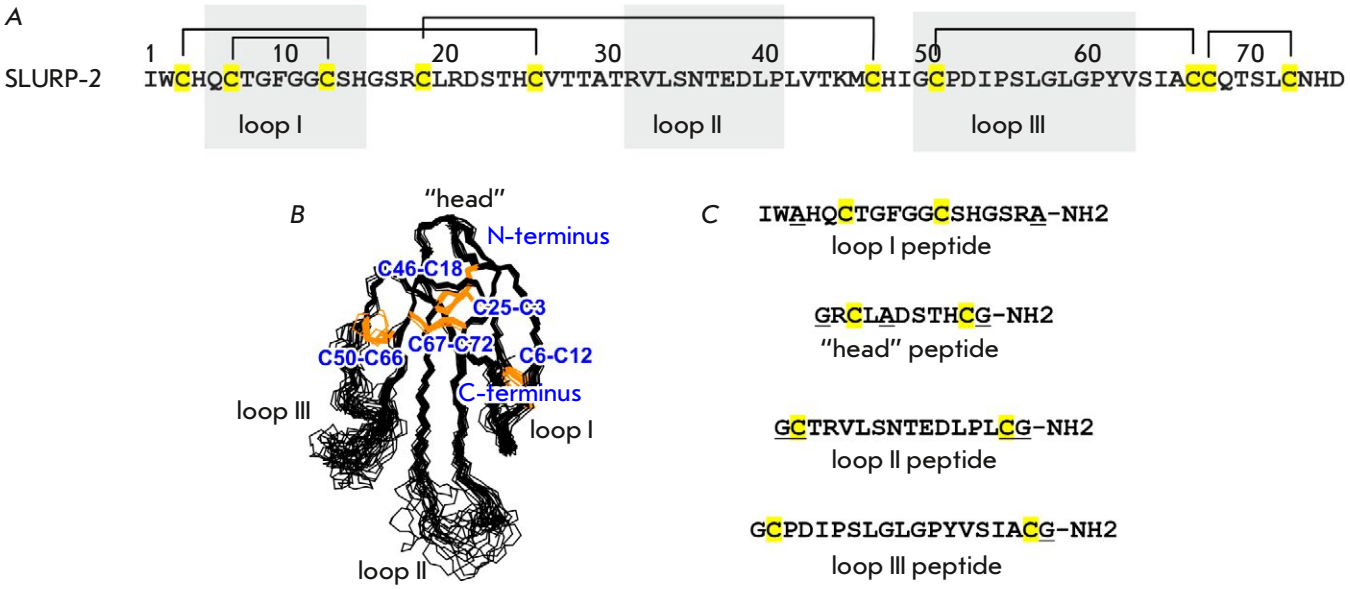

Fig. 1. The structures of SLURP-2 and peptides corresponding to the protein loops and "head." (*A*) Amino acid sequence of SLURP-2. (*B*) Spatial structure of SLURP-2 [17]. (*C*) Amino acid sequence of peptides corresponding to the SLURP-2 loops and "head." Cysteine residues are shown in yellow or orange, and disulfide bonds are shown as lines connecting two cysteine residues

es arising from dysfunction of these receptors [6, 7]. Human secreted Ly6/uPAR proteins, SLURP-1 and SLURP-2, are auto/paracrine regulators of epithelial homeostasis and ligands of acetylcholine receptors [8–11]. SLURP-1 inhibits the growth and migration of normal and tumor cells [12–15]. This protein used to be considered as a prototype of anticancer drugs that target α7-nAChR [12, 16]. The SLURP-2 protein stimulates the proliferation and migration of oral keratinocytes Het-1A and may serve as a prototype of wound-healing drugs [17, 18]. SLURP-2 can interact with the α3, α4, α5, α7, β2, and β4 subunits of nAChR, as well as with M1 and M3 mAChRs. SLURP-2 inhibits current through the ion channel of α4β2- and α3β2-nAChRs, whereas at low concentrations it potentiates α7-nAChR [17]. In this case, SLURP-2 accelerates the migration of Het-1A keratinocytes via interaction with α7-nAChR [18] and stimulates keratinocyte proliferation through interactions with α3β2-nAChR and mAChRs [17]. The replacement of the amino acid residue R20 by alanine at the "head" of the SLURP-2 molecule enhances the inhibition of the current through α7-nAChR and accelerates the migration of keratinocytes [18].

The functional epitopes of Ly6/uPAR proteins (also called three-finger proteins due to their characteristic three-finger fold, *Fig. 1A,B*) are loop regions [19]. In this study, we generated synthetic fragments corresponding to the SLURP-2 loop regions and studied how they affect the migration and viability of HaCaT skin keratinocytes. A loop II-mimicking peptide was found to increase keratinocyte viability via interaction with α7-nAChR and stimulate migration via interaction with α3β2-nAChR and inhibition of p38 MAPK activation. The findings of this study suggest that the loop II-mimicking peptide may be a promising wound-healing agent.

EXPERIMENTAL

Cell culture

Human HaCaT cells (immortalized human skin keratinocyte line) were received from the American Type Culture Collection (ATCC, USA). The cells were cultured at 37°C and 5% CO_2 in a DMEM medium (PanEco, Russia) containing 2 mM L-glutamine and 25 mM glucose and supplemented with 10% fetal bovine serum (Biosera, France), which is designated below as a complete medium. The cells were cultured at 37°C and 5% CO_2 and were passaged at least twice a week.

Production of SLURP-2 and its peptide mimetics

The recombinant SLURP-2 protein was produced in *E. coli* cells as described previously [20]. Peptides mimicking the SLURP-2 first, second, and third loops and head (*Fig. 1B*) were prepared by chemical synthesis according to [15]. The purity and correct spatial structure of (poly)peptides were confirmed by mass spectrometry, high-performance liquid chromatography, and ^{1}H-NMR spectroscopy.

Table 1. The oligonucleotide primers used in the study

Gene	Oligonucleotide sequence	
	Forward primer	Reverse primer
RPL13A	TCAAAGCCTTCGCTAGTCTCC	GGCTCTTTTTGCCCGTATGC
ITGA1	ATAAGTGGCCCAGCCAGAGA	CAGCAGCGTAGAACAACAGTG
ITGA2	CGGTTATTCAGGCTCACCGA	GCTGACCCAAAATGCCCTCT
ITGA3	CCTGCACCCCAAAAACATCA	AGGTCCTGCCACCCATCATT
ITGA5	GGGCTTCAACTTAGACGCGGA	CCCCAAGGACAGAGGTAGACA
ITGA6	GGTGGAGAGACTGAGCATGA	GTCAAAAACAGCAGGCCTAAGTA
ITGA9	GACCGCGATGATGAGTGGAT	GATGAGCACAGGCCAACACA
ITGAV	GACTCCTGCTACCTCTGTGC	GAAGAAACATCCGGGAAGACG
ITGB1	CCGCGCGGAAAAGATGAAT	CCACAATTTGGCCCTGCTTG
ITGB3	ATTGGAGACACGGTGAGCTT	ACTCAAAGGTCCCATTGCCA
SNAI1	GGTTCTTCTGCGCTACTGCT	TGCTGGAAGGTAAACTCTGGAT
SNAI2	ACTGGACACACATACAGTGATT	ACTCACTCGCCCCAAAGATG

Effects of SLURP-2, its peptide mimetics, and acetylcholine receptor inhibitors on the viability of HaCaT cells

The cells were seeded in 96-well plates (5×10^3 cells per well). After 24 h, SLURP-2 or its peptide mimetics at a concentration of 100 nM prepared from a 1 mM stock solution in 100% DMSO by dilution with the complete medium were added to the cells. Then, the cells were incubated at 37°C and 5% CO_2 for 24 h. The lack of any effect of 0.01% DMSO on cell viability and migration was confirmed in a separate experiment.

To investigate the influence of acetylcholine receptor inhibitors on the effects of SLURP-2 and loop II, HaCaT cells were pre-incubated with atropine (Atr (Sigma-Aldrich, USA), a non-selective mAChR inhibitor), α-conotoxin MII (α-CTxMII (Tocris, UK), a selective α3β2-nAChR inhibitor), dihydro-β-erythroidine (Dhβe (Sigma-Aldrich), a selective α4β2-nAChR inhibitor), and methyllycaconitine (MLA (Sigma-Aldrich), a selective α7-nAChR inhibitor), which were diluted in the complete medium, for 30 min. For all inhibitors, a concentration of 1 μM was used, as determined previously [17]. Next, SLURP-2 or loop II at a concentration of 100 nM and the corresponding inhibitors at a concentration of 1 μM were added to the cells. The cells were then additionally incubated for 24 h.

To assess viability, 5 μL of the CCK-8 reagent (Servicebio, China) were added to the cells, and they were incubated at 37°C and 5% CO_2 for 1 h. Further, the optical density at 450 nm was measured on a Bio-Rad 680 plate reader (Bio-Rad, USA) and the background value, measured at 655 nm, was subtracted. The resulting data were analyzed using the Graphpad Prism 9.5.0 software (GraphPad Software, USA).

Effects of SLURP-2, its peptide mimetics, and acetylcholine receptor inhibitors on HaCaT cell migration

The effects of SLURP-2, its peptide mimetics, and acetylcholine receptor inhibitors (Atr, α-CTxMII, Dhβe, and MLA) on HaCaT cell migration in an *in vitro* wound-healing model (scratch assay) were analyzed using the previously described procedure [15]. HaCaT cells were seeded in 96-well plates (3×10^4 cells/well) and grown at 37°C and 5% CO_2 for 24 h. Then, a vertical scratch was made with a sterile 10 μL pipette tip (GenFollower tip, E-FTB10S, China). The cells were washed with PBS, and SLURP-2 or its peptide mimetics at a concentration of 100 nM, or receptor inhibitors at a concentration of 1 μM (Atr, α-CTxMII, Dhβe, MLA), alone or mixed with SLURP-2 or the loop II-mimicking peptide, diluted from a 1 mM stock solution in 100% DMSO using a serum-free medium, were added to the cells. Images of the wells with scratched cell monolayers were analyzed after 0 and 24 h at 20× magnification using a CloneSelect Imager cell analysis system (Molecular Devices, USA). The images were digitized, and the scratch area was estimated by calculating the percentage of scratch area covered by migrating cells using the ImageJ (NIH, USA) and MS Excel (Microsoft, USA) software. The results were analyzed using the Graphpad Prism 9.5.0 software (GraphPad Software).

Real-time PCR

Total mRNA was extracted from the cultured cells using a HiPure Total RNA Plus kit (Magen, China) according to the manufacturer's instructions. Total cDNA was synthesized using a MINT Reverse Transcriptase kit (Evrogen, Russia) according to the

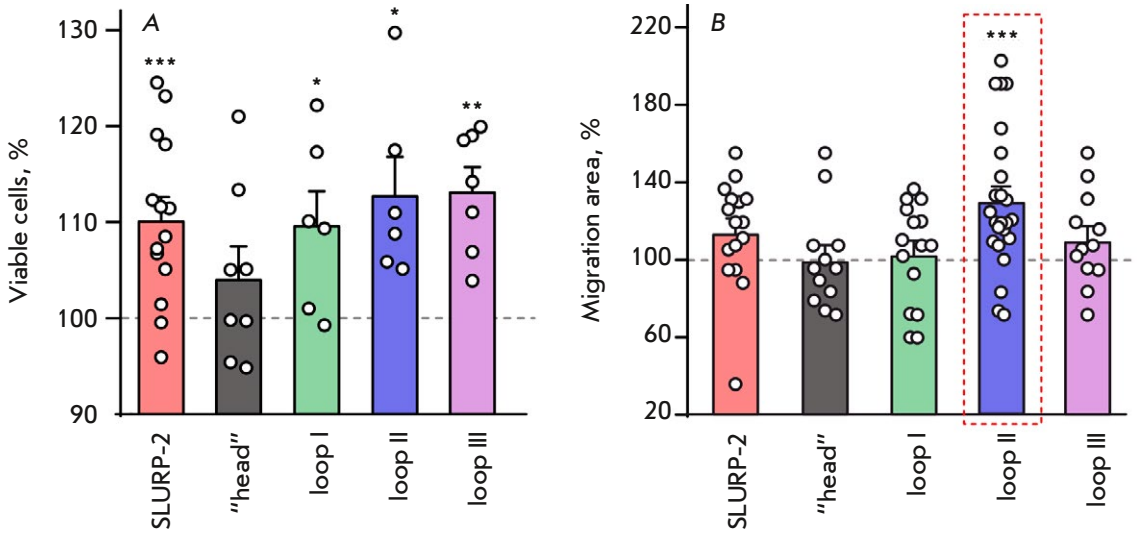

Fig. 2. The effects of SLURP-2 and peptides on the viability and migration of HaCaT keratinocytes. (*A*) Effects of 100 nM SLURP-2 and peptides on the viability of HaCaT keratinocytes. Data are shown as percentage of control ± standard error of the mean ($n = 6–14$); 100% of viable cells corresponds to untreated cells. * $p < 0.05$, ** $p < 0.01$, and *** $p < 0.001$ indicate a significant difference from the control (100%) according to the one-sample Student's *t*-test. (*B*) Effects of 100 nM SLURP-2 and peptides on the migration of HaCaT keratinocytes. Data are shown as a percentage of the control ± standard error of the mean ($n = 12–24$); 100% corresponds to untreated cells. *** $p < 0.001$ indicates a significant difference from the control (100%) according to the one-sample Student's *t*-test

manufacturer's protocol. Next, real-time PCR was performed using the primers listed in *Table 1* and a ready-to-use mixture for quantitative PCR that contained a fluorescent dye SYBR Green I from a 5X qPCRmix-HS SYBR kit (Evrogen).

The negative controls contained all PCR mixture components, except cDNA, and did not produce a signal. All PCR reactions were performed using a Roche Light cycler 96 with real-time detection. Data were analyzed using the Light-Cycler 96 SW1.01 software. Gene expression levels were normalized to the expression levels of the housekeeping gene *RPL13A*.

Protein phosphorylation analysis

Phosphorylation of cellular signaling proteins was analyzed using Bio-Plex magnetic particles (Bio-Rad, USA). Cells were incubated with 100 nM SLURP-2 or loop II prepared from a 1 mM stock solution in 100% DMSO by dilution with the complete medium, for 24 h. Then, the cells were lysed using buffer provided by the manufacturer. Analysis was performed on a Bio-Rad 200 flow cytometer (Bio-Rad) according to the manufacturer's instructions and using the Bio-Plex Manager 6.2 software (Bio-Rad).

Statistical data processing

Data are presented as a mean ± standard error of the mean (SEM). The number of samples (n) is shown in the figure legends. Statistical analysis was performed using the GraphPad Prism 9.5.0 software. Normality of the distribution was assessed using the Shapiro–Wilk test. The analysis was performed using the one-sample Student's *t*-test (in the case of comparison with the normalized control, *Figs. 2–5*) and the one-way ANOVA test, followed by the Dunnett's test (in the case of multiple comparisons, *Fig. 3*). Differences between groups were considered statistically significant at $p < 0.05$.

RESULTS AND DISCUSSION

SLURP-2 loops I, II, and III are important for enhancing skin keratinocyte viability

The loops of Ly6/uPAR proteins are considered functional epitopes responsible for the activity of three-finger proteins [19]. Previously, we showed that a SLURP-1 loop I-mimicking peptide exhibited similar antitumor activity as the full-length protein [15, 16]. In the present study, we decided to identify the SLURP-2 regions responsible for its activity, namely, for enhancing the viability and stimulating the migration of keratinocytes, which had been shown previously [17, 18, 21]. For this purpose, peptides containing SLURP-2 loop I-, II-, and III-mimicking regions as well as the "head" of the molecule (*Fig. 1*) were prepared using chemical synthesis.

Investigation of the effects of SLURP-2 and the peptides on the viability of HaCaT skin keratinocytes revealed that SLURP-2 increased keratinocyte viability (*Fig. 2A*). In this case, the "head" peptide did not affect keratinocyte viability, whereas loops I-, II-, and III-mimicking peptides stimulated the viability of keratinocytes, similarly to the effect of the full-length SLURP-2 (*Fig. 2A*).

Thus, loops I, II, and III are important SLURP-2 regions required for enhancing the viability and, possibly, proliferation of keratinocytes. The lack of any activity of the SLURP-2 "head" peptide indicates that this region of the full-length protein is not involved in the interaction with the target responsible for stimulating keratinocyte viability. Perhaps, the inactive "head" compensates for the increased activity of loop II whereas the activity of loops I and III is similar to that of the full-length protein. This suggestion is supported by the fact that the replacement of amino acid residue R20 by alanine in the SLURP-2 "head" leads to the stimulation of keratinocyte migration [18].

The SLURP-1 protein had been anticipated to interact simultaneously with different targets: α7-nAChR and the epidermal growth factor receptor [15]. In this case, the interaction with the second target was mediated by the SLURP-1 "head." Probably, the situation is similar in the case of SLURP-2, where loop II and the "head" interact with different targets, compensating for their influence on the viability of keratinocytes. It is noteworthy that, unlike SLURP-2, the epithelial protein SLURP-1 does not increase but decreases the viability of oral keratinocytes Het-1A, and that its functional region is loop I [22].

Loop II activates the migration of skin keratinocytes via interaction with α3β2-nAChR

Previously, SLURP-2 was shown to enhance the migration of Het-1A keratinocytes via interaction with α7-nAChR [18]. In the present work, we studied the effects of SLURP-2 and its peptide mimetics on the migration of HaCaT skin keratinocytes. SLURP-2, loops I and III, and the "head" were found not to exert a significant effect on the migration of HaCaT keratinocytes (*Fig. 2B*) in a scratch closure model. In this case, loop II accelerated keratinocyte migration by ~30% (*Fig. 2B*). Probably, SLURP-2, interacting with different acetylcholine receptor subtypes, is able to both increase and decrease cell migration, with the overall effect dependent on the expression of certain receptors in specific cells.

SLURP-2 is known to interact with the nAChR α3, α4, α5, α7, β2, and β4 subunits and M1 and M3 mAChRs [17]. To elucidate the interaction with which receptor is responsible for the stimulating effect of SLURP-2 loop II on the keratinocyte migration, the effect of loop II was studied in the presence of inhibitors of different acetylcholine receptor subtypes: atropine (Atr), a non-selective mAChR inhibitor; α-conotoxin MII (α-CTxMII), a selective α3β2-nAChR inhibitor; dihydro-β-erythroidine hydrobromide (Dhβe), a selective α2β4-nAChR inhibitor; and methyllycaconitine (MLA), a selective α7-nAChR inhibitor. We demonstrated that inhibition of α3β2-nAChR by α-CTxMII canceled the effect of loop II on HaCaT keratinocyte migration. Concomitant use of atropine and Dhβe with loop II did not significantly affect migration, with the obtained values being not significantly different from the effect of loop II. The obtained data do not indicate whether mAChR and α2β4-nAChR are involved in the effect of loop II on migration (*Fig. 3A*). Thus, loop II stimulates skin keratinocyte migration via the interaction with α3β2-nAChR and, possibly, mAChR and α2β4-nAChR. It is worth noting that in a previously constructed model of the SLURP-2–α3β2-nAChR interaction, loop II was the main SLURP-2 region interacting with this receptor and forming the largest number of contacts in the complex [17]. In this case, inhibitors of other acetylcholine receptors did not significantly affect the effect of loop II.

The effects of SLURP-2 and loop II on skin keratinocyte viability are mediated by the interaction with α7-nAChR

In this work, we also studied the influence of inhibitors of different acetylcholine receptor subtypes (atropine, α-conotoxin MII, Dhβe, and MLA) on the effect of SLURP-2 and loop II on keratinocyte viability. Pre-incubation of the cells with MLA was shown to completely abolish the stimulating effect of SLURP-2 and loop II on the viability of HaCaT cells (*Fig. 3B*). However, none of the inhibitors, except MLA, had a significant effect on the activity of SLURP-2 and loop II. In this case, atropine, α-conotoxin MII, and Dhβe, together with SLURP-2 and loop II, did not significantly increase the viability compared to that in the control. Therefore, the contribution of mAChR, α3β2-nAChR, and α2β4-nAChR to the effects of SLURP-2 and loop II on viability requires further research. Thus, the ability of the SLURP-2 protein and loop II peptide to enhance keratinocyte viability is mediated by the interaction with α7-nAChR and, probably, mAChR, α3β2-nAChR, and α2β4-nAChR.

However, SLURP-2 has been previously shown to enhance the viability of Het-1A oral keratinocytes through interaction with α3β2-nAChR, but not with α7-nAChR [17]. Involvement of different receptors in the regulation of SLURP-2 activity in oral and

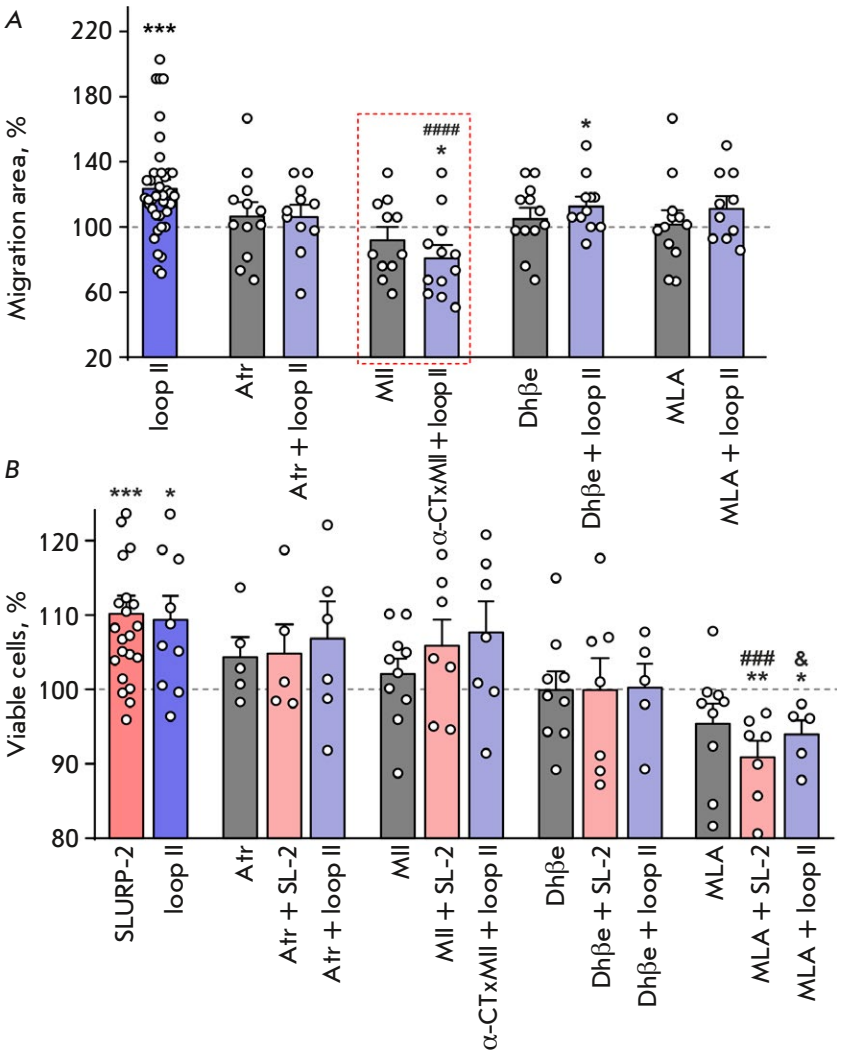

Fig. 3. The effects of SLURP-2, peptides, and inhibitors of different acetylcholine receptors on the viability and migration of HaCaT keratinocytes. (*A*) Effects of the loop II peptide (100 nm) and inhibitors of different acetylcholine receptors (1 μM) on the migration of HaCaT keratinocytes. Data are shown as a percentage of the control ± standard error of the mean ($n = 11–40$); 100% corresponds to the migration area of untreated cells. * $p < 0.05$ and *** $p < 0.001$ indicate a significant difference from the control (100%) according to the one-sample Student's *t*-test. #### $p < 0.001$ indicates a difference from the loop II group according to the one-way ANOVA test, followed by the Dunnett's/hoc test. (*B*) Effects of inhibitors of different acetylcholine receptors on the activity of SLURP-2 and the loop II peptide. Data are shown as a percentage of the control ± standard error of the mean ($n = 4–14$); 100% of viable cells corresponds to untreated cells. * $p < 0.05$, ** $p < 0.01$, and *** $p < 0.001$ indicate a significant difference from the control (100%) according to the one-sample Student's *t*-test. ### $p < 0.001$ indicates a difference from the SLURP-2 group according to the one-way ANOVA test, followed by the Dunnett's/hoc test; & $p < 0.05$ indicates a difference from the loop II group according to the one-way ANOVA test followed by the Dunnett's/hoc test

skin keratinocytes may be associated with the different expression profiles of certain receptors in different cells and tissues of the body and lies within the framework of the "polygamous" activity of the epithelial protein that is able to interact with various acetylcholine receptors [17].

The effects of SLURP-2 and loop II on the viability and migration of skin keratinocytes are not associated with altered expression of integrins and SNAI transcription factors

Integrins are known to regulate adhesion, migration, and proliferation of epithelial cells, in particular skin keratinocytes [23, 24]. Also, the factors that regulate the migration and differentiation of keratinocytes include the SNAI1 and SNAI2 transcription factors [25]. We ventured that the effects of SLURP-2 and loop II on viability and migration may be related to the influence on expression of integrins or SNAI transcription factors. However, we did not find any significant changes in the expression of the *ITGA1*, *ITGA2*, *ITGA3*, *ITGA5*, *ITGA6*, *ITGA9*, *ITGB1*, *ITGB3*, *SNAI1*, and *SNAI2* genes in HaCaT keratinocytes after incubation with SLURP-2 or loop II for 24 h compared to that in the control (untreated cells, *Fig. 4*). Thus, the effects of SLURP-2 and loop II on the viability and migration of HaCaT keratinocytes are not related to changes in the expression of the genes encoding integrins and SNAI1, or SNAI2 transcription factors.

The effects of SLURP-2 and loop II on skin keratinocytes are related to the suppression of the p38 MAPK and mTOR signaling pathways

Previously, the SLURP-1 protein was shown to inhibit the activity of intracellular signaling cascades associated with AKT, PTEN phosphatase, and mTOR protein kinase in tumor cells [15]. We venture that the effects of SLURP-2 and loop II could also be related to

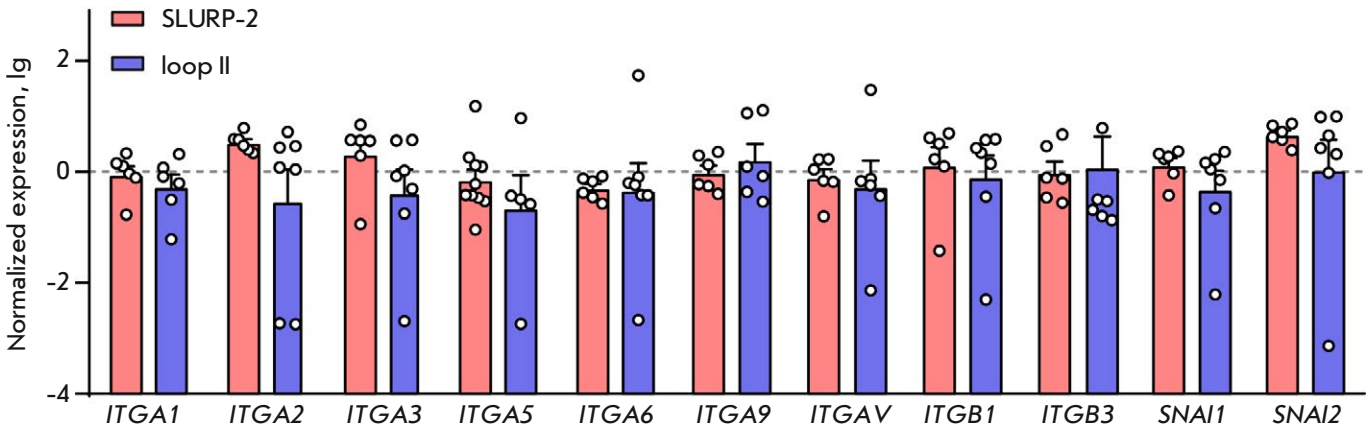

Fig. 4. The effects of 100 nM SLURP-2 and loop II peptide on the expression of mRNAs encoding α1, α2, α3, α5, α6, α9, β1, and β3 integrins and the SNAI1 and SNAI2 transcription factors. Data are normalized to the mean expression value in untreated cells and shown as lg ± standard error of the mean ($n = 5–10$). Gene expression is normalized to that of the housekeeping gene *RPL13A*

the regulation of the intracellular signaling cascades associated with proliferation and migration. In addition, we investigated the effects of SLURP-2 and loop II on the activity of the STAT3 and NF-kB transcription factors involved in the regulation of gene expression in epithelial cells and associated with α7-nAChR activation [26–29]. Using the Bioplex magnetic bead array analysis, we showed that both SLURP-2 and the loop II peptide inhibited phosphorylation and, therefore, the activation of p38 MAPK kinase in HaCaT keratinocytes after 24-h incubation (*Fig. 5*). Furthermore, SLURP-2 – but not loop II – reduced mTOR kinase phosphorylation in HaCaT keratinocytes (*Fig. 5*).

It is known that p38 MAPK activation can cause keratinocyte apoptosis and, therefore, decrease the number of viable cells [30, 31]. At the same time, α7-nAChR activation inhibits p38 MAPK phosphorylation and activation [32]. Previously, SLURP-2, at a concentration of 100 nM, was shown to potentiate α7-nAChR in the presence of acetylcholine [17]. Thus, we may suggest potentiation of α7-nAChR in HaCaT keratinocytes in the presence of 100 nM SLURP-2, which in turn leads to the suppression of the p38 MAPK signaling pathway and an increase in the number of viable cells. This suggestion is consistent with a previously proposed model of the SLURP-2–α7-nAChR interaction where SLURP-2 loop II interacts with the open (active) state of α7-nAChR [17]. This also indicates that activation of this receptor is associated with suppression of the p38 MAPK signaling pathway, with prevention of the apoptosis of HaCaT keratinocytes and an increase in the number of viable cells in the presence of loop II.

It is worth noting that inhibition of mTOR phosphorylation can lead to suppression of keratinocyte migration [33]. Yet we failed to uncover any significant effects of SLURP-2 on migration (*Fig. 2B*). In this case, loop II stimulates migration via the interaction with α3β2-nAChR (*Fig. 3*) and does not inhibit the intracellular signaling cascade associated with mTOR (*Fig. 5*). Probably, other SLURP-2 regions (not loop II) are involved in the inhibition of mTOR phosphorylation, which contributes negatively to migration stimulation by the full-length protein.

Incubation of oral keratinocytes Het-1A with SLURP-1 was previously shown to activate the transcription factor NF-kB [34]. SLURP-1 is known to be a negative modulator of α7-nAChR [35]. Thus, the lack of a potentiating effect on NF-kB phosphorylation in the presence of both SLURP-2 and loop II supports our suggestion that both of these molecules potentiate α7-nAChR at the tested concentration in HaCaT keratinocytes. This is consistent with suppression of the p38 MAPK signaling pathway (*Fig. 5*).

CONCLUSION

In this study, we produced synthetic peptides corresponding to the SLURP-2 loop fragments (“head”, loop I, loop II, and loop III peptides) and investigated how they affect the viability and migration of skin keratinocytes. The “head” peptide did not affect either the viability or the migration of keratinocytes. Loop I- and loop III-mimicking peptides were shown to increase the viability and to not affect the migration of keratinocytes. The loop II-mimicking peptide was found to exhibit the highest activity. It stimulated both the viability and migration of keratino-

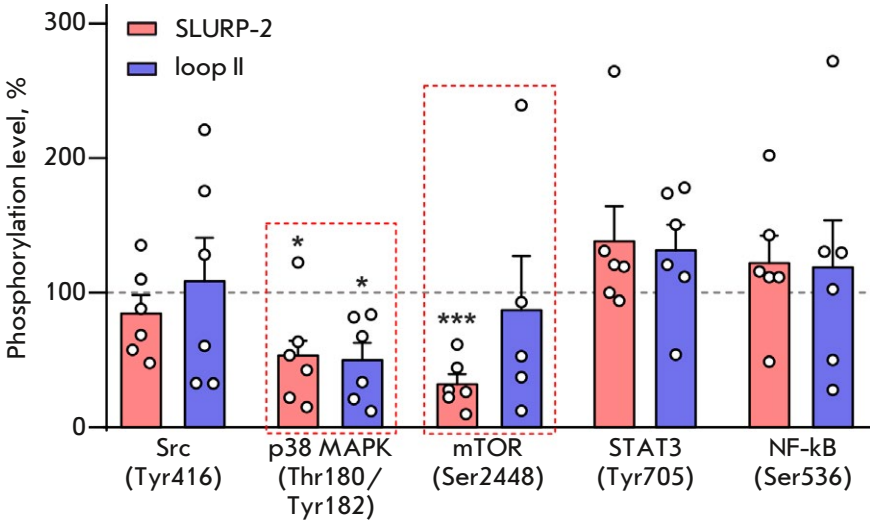

Fig. 5. The effects of 100 nM SLURP-2 and loop II peptide on phosphorylation of signaling proteins: Src (Tyr416), p38 MAPK (Thr180/Tyr182), mTOR (Ser2448), STAT3 (Tyr705), and NF-kB (Ser536). Data are shown as a percentage of the control ± standard error of the mean ($n = 5$ to 6); 100% corresponds to the phosphorylation level in untreated cells. * $p < 0.05$ and *** $p < 0.001$ indicate a significant difference from the control (100%) according to the one-sample Student's *t*-test

cytes through the interaction with α7-nAChR and α3β2-nAChR, respectively. In this case, the SLURP-2 protein itself was shown to increase only the viability of keratinocytes and to not affect their migration. The differences in effects of SLURP-2 and loop II on HaCaT keratinocyte viability and migration are likely linked to the ability of the full-length protein to interact with several targets simultaneously, as well as with inhibition of mTOR phosphorylation, which is not relevant to loop II. Thus, we have gained new knowledge about the regulation of epithelial cell homeostasis by the human epithelial protein SLURP-2. Our findings indicate prospects for further research into the properties of loop II and its potential as a prototype for the development of new wound-healing drugs. ●

This study was supported by the Russian Science Foundation (project No. 23-24-00636).

The authors are thankful to Irina Chulina for assistance with the chemical synthesis of the studied peptides.

M.P. Kirpichnikov and E.N. Lyukmanova are part of an innovative drug development team based on structural biology and bioinformatics at the Shenzhen MSU–BIT University (#2022KCXTD034).

REFERENCES

1. Loughner C.L., Bruford E.A., McAndrews M.S., Delp E.E., Swamynathan S., Swamynathan S.K. // Hum. Genomics. 2016. V. 10. P. 10.
2. Shenkarev Z.O., Shulepko M.A., Bychkov M.L., Kulbatskii D.S., Shlepova O.V., Vasilyeva N.A., Andreev-Andrievskiy A.A., Popova A.S., Lagereva E.A., Loktyushov E.V., et al. // J. Neurochem. 2020. V. 155. № 1. P. 45–61.
3. Kulbatskii D., Shenkarev Z., Bychkov M., Loktyushov E., Shulepko M., Koshelev S., Povarov I., Popov A., Peigneur S., Chugunov A., et al. // Front. Cell. Dev. Biol. 2021. V. 9. P. 662227.
4. Kulbatskii D.S., Bychkov M.L., Lyukmanova E.N. // Rus. J. Bioorg. Chem. 2018. V. 44. № 6. P. 595–607.
5. Shulepko M., Bychkov M., Kulbatskii D., Lyukmanova E. // Rus. J. Bioorg. Chem. 2019. V. 45. № 2. P. 66–74.
6. Papke R.L., Lindstrom J.M. // Neuropharmacology. 2020. V. 168. P. 108021.
7. Hone A.J., McIntosh J.M. // Pharmacol. Res. 2023. V. 190. P. 106715.
8. Arredondo J., Chernyavsky A.I., Grando S.A. // Life Sci. 2007. V. 80. № 24–25. P. 2243–2247.
9. Arredondo J., Chernyavsky A.I., Webber R.J., Grando S.A. // J. Invest. Dermatol. 2005. V. 125. № 6. P. 1236–1241.
10. Arredondo J., Chernyavsky A.I., Jolkovsky D.L., Webber R.J., Grando S.A. // J. Cell. Physiol. 2006. V. 208. № 1. P. 238–245.
11. Arredondo J., Chernyavsky A.I., Grando S.A. // Biochem. Pharmacol. 2007. V. 74. № 8. P. 1315–1319.
12. Lyukmanova E., Bychkov M., Sharonov G., Efremenko A., Shulepko M., Kulbatskii D., Shenkarev Z., Feofanov A., Dolgikh D., Kirpichnikov M. // Br. J. Pharmacol. 2018. V. 175. № 11. P. 1973–1986.
13. Shulepko M.A., Bychkov M.L., Shlepova O.V., Shenkarev Z.O., Kirpichnikov M.P., Lyukmanova E.N. // Internat. Immunopharmacol. 2020. V. 82. P. 106303.
14. Shulepko M.A., Bychkov M.L., Lyukmanova E.N., Kirpichnikov M.P. // Dokl. Biochem. Biophys. 2020. V. 493. № 1. P. 211–214.
15. Bychkov M.L., Shulepko M.A., Shlepova O.V., Kulbatskii D.S., Chulina I.A., Paramonov A.S., Baidakova L.K., Azev V.N., Koshelev S.G., Kirpichnikov M.P., et al. // Front. Cell. Dev. Biol. 2021. V. 9. P. 739391.
16. Shlepova O.V., Shulepko M.A., Shipunova V.O., By-

chkov M.L., Kukushkin I.D., Chulina I.A., Azev V.N., Shramova E.I., Kazakov V.A., Ismailova A.M., et al. // Front. Cell. Dev. Biol. 2023. V. 11. P. 1256716. doi: 10.3389/fcell.2023.1256716.
17. Lyukmanova E., Shulepko M.A., Shenkarev Z., Bychkov M., Paramonov A.S., Chugunov A., Kulbatskii D., Arvaniti M., Dolejsi E., Schaer T., et al. // Sci. Rep. 2016. V. 6. P. 30698. doi: 10.1038/srep3069.
18. Bychkov M.L., Shlepova O.V., Shulepko M.A., Kulbatskii D.S., Bertrand D., Kirichenko A.V., Shenkarev Z.O., Kirpichnikov M.P., Lyukmanova E.N. // Rus. J. Bioorg. Chem. 2024. V. 50. № 3. P. 696–705.
19. Vasilyeva N.A., Loktyushov E.V., Bychkov M.L., Shenkarev Z.O., Lyukmanova E.N. // Biochemistry (Moscow). 2017. V. 82. № 13. P. 1702–1715.
20. Lyukmanova E.N., Shulepko M.A., Bychkov M.L., Shenkarev Z.O., Paramonov A.S., Chugunov A.O., Arseniev A.S., Dolgikh D.A., Kirpichnikov M.P. // Acta Naturae. 2014. V. 6. № 4. P. 60–66.
21. Chernyavsky A.I., Kalantari-Dehaghi M., Phillips C., Marchenko S., Grando S.A. // Wound Repair Regen. 2012. V. 20. № 1. P. 103–113.
22. Shulepko M.A., Bychkov M.L., Shenkarev Z.O., Kulbatskii D.S., Makhonin A.M., Paramonov A.S., Chugunov A.O., Kirpichnikov M.P., Lyukmanova E.N. // J. Invest. Dermatol. 2021. V. 141. № 9. P. 2229–2237.
23. Watt F.M. // EMBO J. 2002. V. 21. № 15. P. 3919–3926.
24. Longmate W.M., DiPersio C.M. // Adv. Wound Care (New Rochelle). 2014. V. 3. № 3. P. 229–246.
25. Sou P.W., Delic N.C., Halliday G.M., Lyons J.G. // Internat. J. Biochem. Cell Biol. 2010. V. 42. № 12. P. 1940–1944.
26. Chen Y., Lian P., Peng Z., Wazir J., Ma C., Wei L., Li L., Liu J., Zhao C., Pu W., et al. // Cell Death Discov. 2022. V. 8. № 1. P. 141.
27. Kwok H.-H., Gao B., Chan K.-H., Ip M.S.-M., Minna J.D., Lam D.C.-L. // Cancers (Basel). 2021. V. 13. № 21. P. 5345.
28. Arredondo J., Chernyavsky A.I., Jolkovsky D.L., Pinkerton K.E., Grando S.A. // Life Sci. 2007. V. 80. № 24–25. P. 2191–2194.
29. Stegemann A., Böhm M. // Exp. Dermatol. 2019. V. 28. № 3. P. 276–282.
30. Fukada S., Ohta K., Sakuma M., Akagi M., Kato H., Naruse T., Nakagawa T., Shigeishi H., Nishi H., Takechi M., et al. // Oral Dis. 2024. V. 30. № 2. P. 639–649.
31. Nys K., van Laethem A., Michiels C., Rubio N., Piette J.G., Garmyn M., Agostinis P. // J. Invest. Dermatol. 2010. V. 130. № 9. P. 2269–2276.
32. Uwada J., Nakazawa H., Mikami D., Islam M.S., Muramatsu I., Taniguchi T., Yazawa T. // Biochem. Pharmacol. 2020. V. 182. P. 114297.
33. Wu X., Sun Q., He S., Wu Y., Du S., Gong L., Yu J., Guo H. // BMC Anesthesiol. 2022. V. 22. № 1. P. 106.
34. Chernyavsky A.I., Arredondo J., Galitovskiy V., Qian J., Grando S.A. // Am. J. Physiol. Cell Physiol. 2010. V. 299. № 5. P. C903–C911.
35. Lyukmanova E.N., Shulepko M.A., Kudryavtsev D., Bychkov M.L., Kulbatskii D.S., Kasheverov I.E., Astapova M.V., Feofanov A.V., Thomsen M.S., Mikkelsen J.D., et al. // PLoS One. 2016. V. 11. № 2. P. e0149733.

The Antibacterial Activity of Yeasts from Unique Biocenoses

O. V. Shulenina[1], E. A. Sukhanova[1], B. F. Yarovoy[1], E. A. Tolstyko[1], A. L. Konevega[1,2,3*], A. Paleskava[1,2**]

[1]Petersburg Nuclear Physics Institute named by B.P. Konstantinov of National Research Centre "Kurchatov Institute", Gatchina, 188300 Russian Federation

[2]Peter the Great St. Petersburg Polytechnic University, St. Petersburg, 195251 Russian Federation

[3]National Research Centre "Kurchatov Institute", Moscow, 123182 Russian Federation

*E-mail: Konevega_AL@pnpi.nrcki.ru

**E-mail: Polesskova_EV@pnpi.nrcki.ru

Received September 30, 2024; in final form, October 24, 2024

DOI: 10.32607/actanaturae.27527

ABSTRACT **The replenishment of our stock of substances that possess a therapeutic potential is an important objective in modern biomedicine. Despite the important advances achieved in chemical synthesis, the natural diversity of organisms and microorganisms remains an important source of biologically active compounds. Here, we report the results of our study of a unique collection containing more than 3,000 samples of yeasts found on the Kamchatka Peninsula, the Kuril Islands, and Sakhalin Island, Russia. Since yeast and bacteria coexist in a variety of habitats and can interact with each other, we analyzed the antibacterial activity of the collection of yeast strains towards *E. coli* cells using a fluorescent bacterial reporter. It was uncovered that the Sakhalin strains for the most part stimulate bacterial growth, while most of the strains found on the Kamchatka Peninsula possess inhibitory properties. Moreover, the samples with the most pronounced antibacterial activity, identified as members of the genus *Cryptococcus (Naganishia)*, were found in a gorge in the vicinity of Pauzhetka village on the Kamchatka Peninsula on wormwood (*Artemisia vulgaris*) and thistle (*Onopordum acanthium*). Our data indicate that the combination of a plant and its growth site is important for the emergence of yeast strains capable of secreting antibacterial compounds.**

KEYWORDS **antibiotics, biodiversity, yeast, collection, fluorescent reporter system.**

INTRODUCTION

The lack of strict oversight of the use of antimicrobial agents in medicine and livestock results in the emergence and spread of antibiotic-resistant pathogenic bacteria [1], making it necessary to look for new pharmaceuticals. The flora and fauna are an important source of biologically active compounds that have stood the test of time [2, 3]. Particular yeast strains have been studied well as they are heavily used in the food industry or as model organisms in research [4]. Some yeast metabolites can reduce the blood cholesterol level and act as immunomodulators or antifungal drugs [5]. The genera *Candida*, *Pichia*, and *Saccharomyces* exhibit antibacterial activity [5–8]. However, yeasts are, biologically and chemically, incredibly diverse and yeast populations from isolated regions remain underinvestigated: they may possess unique properties [3].

In this paper, we study a unique collection of yeast gathered in the Russian Far East. The uniqueness of the collection has to do with the geography of these regions. Kamchatka and the Kuril Islands are parts of the Pacific Ring of Fire, which is characterized by heightened volcanic and seismic activity. The population of these regions is not numerous, and tourism is poorly developed; so, its nature is faintly exposed to the direct influence of civilization. The Kamchatka Peninsula, which is almost cut off from the mainland, has the highest concentration of volcanoes on Earth: 30 active ones out of more than 300 volcanoes. On the Kamchatka Peninsula and Kuril Islands, there is a dense network of mountain rivers rich in fresh water, lakes with high mineralization in volcanic areas heated by volcanic gases, and low-salted lagoon lakes. On the sides and in the craters of dormant volcanoes, there are hydrothermal, gas, and mud ejections of various temperatures and varying acidity, containing various natural inorganic compounds at high concentrations. Yeasts from Sakhalin exist at the same latitudes as species from the Kamchatka Peninsula and the Kuril Islands, but they are not affected by extreme environmental factors. Furthermore, un-

like other species in the collection, the strains from Sakhalin were found closer to areas of human activity.

The objective of this study was to reveal and investigate isolates of the yeast collection that contain antimicrobial compounds in their culture liquids. We applied a reporter system that, apart from antimicrobial activity detection, allows one to sort potential antibacterials based on their mechanism of action. This double-reporter approach in identifying substances that cause ribosome stalling or induce the SOS response due to DNA damage was successfully used to screen a library of synthetized organic compounds [9] and actinomycetes extracts [10–13]. The approach was designed for application on agar plates thereby minimizing the need for pipetting, reagents, and consumables. At the same time, fluorescent protein reporter assay on petri plates does not allow for a quantitative assessment of antibacterial action by exploiting mechanisms other than ribosome stalling or DNA damage. Additionally, the reporter sensitivity determined using a few antibiotics in a liquid medium was up to two orders of magnitude higher than that on agar [9].

Hence, in order to increase the chance of detecting even minor biologically active compounds in yeast culture liquids that could affect bacterial viability, we adapted a fluorescent double-reporter system to a liquid medium. To increase the sensitivity even further, we utilized an *E. coli* JW5503 bacterial strain lacking the *tolC* gene and coding for an essential component of several efflux systems [14]. The applied version of the reporter system was validated using 15 antibiotics with a known mechanism of action.

The assay was employed on 810 samples from the yeast collection, wherein 251 samples were from the Sakhalin collection and 559 samples were from the Kamchatka collection. The Sakhalin strains for the most part stimulated bacterial growth, while most of the strains from Kamchatka exhibited inhibitory properties. Our data point to the importance of the combination of the plant and its place of origin for the emergence of yeast strains secreting antibacterial compounds.

EXPERIMENTAL

The yeast and yeast-like fungi collection

The collection of yeast, containing over 3,000 samples, was gathered during several expeditions led by V.P. Stepanova and B.F. Yarovoy to extreme regions of Russia: the Kuril Islands, the Kamchatka Peninsula in August–September 1988, 1989, and 1994, and the Sakhalin Island in August–September 2004 [15]. The microorganisms in the collection were obtained from substrates, such as living plants, fallen parts of plants, soil, and insects. Substrates were collected on the sides of volcanoes, near the active zones, and in river and creek valleys.

The yeast isolates were obtained under laboratory conditions. Long-term storage was done at –80°C in the Yeast Peptone Dextrose (YPD) Broth (Sigma-Aldrich, USA) supplemented with 25% glycerol [16].

At the initial stage of collection description, 98 randomly selected strains were identified using the morphological and biochemical approaches [17, 18]. Among the selected strains were representatives of 20 known species: *Candida haemulorni, Candida sake, Candida sorbosivorans, Cryptococcus albidus, Cryptococcus hungaricus, Cryptococcus laurentii, Debaryomyces hansenei, Metschnikowia reukaufii, Pichia farinosa, Rhodotorulla aurantiaca, Rhodotorula glutinis, Rhodotorula minuta, Rhodotorula mucilaginosa, Saccharomyces cerevisiae, Sporobolomyces roseus, Sporidiobolus salmonicolor, Torulaspora delbrueckii,* and *Tremella foliacea*, as well as one member of each of the genera *Bullera* and *Trichosporon*. These species belong to all three known classes of fungi: (1) ascomycetes – 6 species; (2) basidiomycetes – 2 species; and (3) deuteromycetes – 12 species. The species diversity of the collection closely tracks the data on the characteristic yeast species composition of the northern latitudes of Western Siberia and Alaska [19].

Several samples of the collection have already been shown to be able to absorb various types of pollutants, such as radionuclides and heavy metal ions [15, 20].

Preparation of yeast culture liquids

The yeast strains were grown on the surface of a YPD agar plate for 3 days at room temperature. The culture was observed morphology-wise to ensure cellular purity. The cells were transferred into a YPD liquid medium and incubated at room temperature for 3 days on a shaker. Culture liquids were separated from the cells by centrifugation at 4 000 g for 15 min at 4°C using a Union 5KR centrifuge (Hanil Science Industrial) and concentrated 15 to 20-fold using a Concentrator Plus centrifuge concentrator (Eppendorf AG) at room temperature for 8–9 h. The concentrated culture liquids were stored at –20°C.

Double fluorescent protein reporter for identification of the substances causing bacterial ribosome stalling or DNA damage

The double fluorescent protein reporter plasmid pDualrep2 carries the *rfp* gene under the control of the SOS-induced *sulA* gene promoter and the gene of the Katushka2S protein downstream of the mod-

ified tryptophan attenuator (tryptophan codons are replaced with alanine ones) under the control of the constitutive T5 promoter [9, 21]. Modification of the tryptophan attenuator results in a disruption in the movement of the ribosome that is due to specific translation inhibitors rather than to tryptophan starvation.

The *E. coli* JW5503 strain (lacking the *tolC* gene coding for the essential component of the efflux system) transformed by the reporter plasmid pDualrep2 (Amp^R) synthesizes RFP in the presence of DNA-damaging (SOS response-causing) agents; and Katushka2S, in the presence of translation-stalling chemicals [9]. The fluorescent signal of RFP becomes detectable at 574 nm upon excitation at 553 nm; for Katushka2S, at 633 and 588 nm, respectively.

Analysis of antibacterial activity using the reporter system

The reporter bacterial culture was grown until OD_{600} = 0.5–1 at 37°C in a LB medium containing 100 μg/mL ampicillin and stored at 4°C overnight. The next day, the culture was diluted with a fresh LB medium to OD_{600} = 0.1. Wells of a 96-well culture plate were filled with 200 μL of the cell culture. The sample was added to the bacteria suspension in the wells. The culture plate was incubated in a plate shaker-thermostat at 37°C. The various degrees of fluorescence for reporter proteins RFP (553/574 nm), Katushka2S (588/633 nm), and OD_{600} in the culture plate were measured in an EnSpire 2300 plate reader (Perkin Elmer). The results were analyzed using the GraphPad Prism 6.0 software.

To validate our system, 2 μL of known antibiotics at sublethal concentrations were added into the wells with the bacteria suspension. We chose several translation inhibitors with different modes of action, such as gentamicin, chloramphenicol, fusidic acid, neomycin, hygromycin B, kanamycin, puromycin, tetracycline, erythromycin, and streptomycin. The panel of drugs inducing the SOS response consisted of nalidixic acid, levofloxacin, ciprofloxacin, and rifampicin.

The concentrated culture liquids (5 μL) were added into the bacterial suspension in the wells of the culture plate. In this dosing manner, sample concentration in the plate's wells was 2–2.5 times lower than that of the original, non-concentrated sample. The samples with the best inhibitory properties were tested in triplicate.

Data processing

We calculated the S/S_0 ratio, where S is the reporter fluorescent signal or OD_{600} of the reporter bacterial culture in the presence of a test sample and S_0 is the reporter fluorescent signal or OD_{600} of the bacterial culture without additives.

A set of S/S_0 values for control was obtained to calculate the background interval. The distribution normality was confirmed with a confidence level of 99% using the D'Agostino–Pearson omnibus test in the GraphPad Prism 6.0 software. The background interval was defined as [mean-3σ; mean+3σ]. Background intervals: SOS activation signal after 5 h, [0.87; 1.13]; SOS activation signal after 24 h, [0.82; 1.18]; translation inhibition signal after 5 h, [0.93; 1.07]; translation inhibition signal after 24 h, [0.85; 1.15]; and OD_{600} after 5 h, [0.95; 1.05]; OD_{600} after 24 h, [0.97; 1.03].

Table 1. The primers used for taxonomic identification

Regions	Primer sequences [22]
ITS1-5.8S-ITS2	ITS1 (forward) 5'- TCCGTAGGTGAACCTGCGG-3' ITS4 (reverse) 5'-TCCTCCGCTTATTGATATGC-3'
26S rDNA (part 1)*	LROR (forward) 5'- ACCCGCTGAACTTAAGC-3' LR3 (reverse) 5'-CCGTGTTTCAAGACGGG-3'
26S rDNA (part 2)*	LR3R (forward) 5'-GTCTTGAAACACGGACC-3' LR7 (reverse) 5'-TACTACCACCAAGATCT-3'

*The PCR product of 26S rDNA obtained with the primers LROR and LR7 contains more than 1,000 bp and was obtained with four primers.

Taxonomic identification

For the taxonomic identification of the yeast isolates, cell walls were destroyed by zymolyase (Zymo Research) in 1 M sorbitol and 0.1 M EDTA (pH 8.0). Total genomic DNA was extracted using a DNeasy Blood & Tissue Kit (Qiagen) and visualized by 1% agarose gel electrophoresis. The ITS1-5.8S-ITS2 and D1/D2 domains of the 26S rDNA (nrLSU) [22] were amplified using the primers listed in *Table 1*. The PCR products were purified using the NucleoSpin Gel and a PCR cleanup kit (Macherey-Nagel). The same primers were used for sequencing. The sequencing results were processed using The Basic Local Alignment Search Tool (BLAST) (http://www.ncbi.nlm.nih.gov/BLAST).

RESULTS

Validation of the reporter system using a set of known antibiotics

We chose a number of inhibitors with different mechanisms of action as we tested the specificity of the

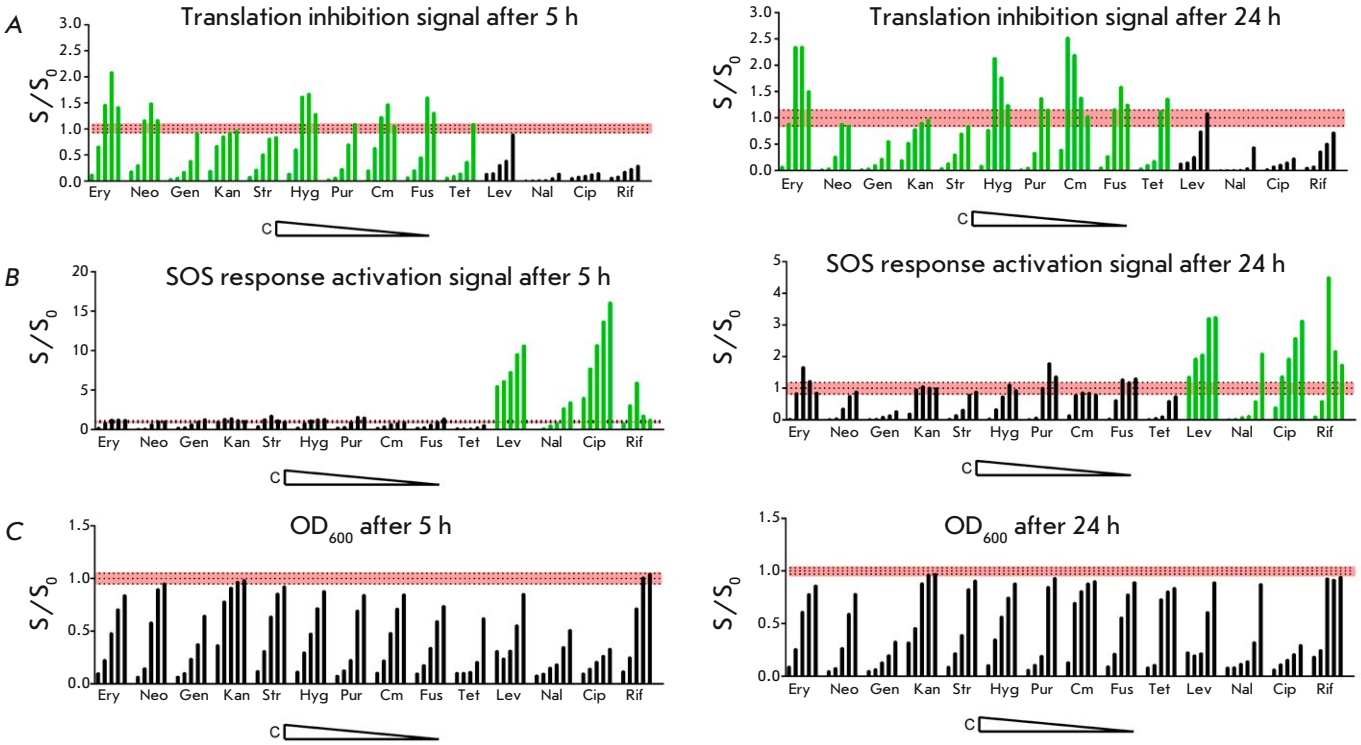

Fig. 1. Testing the double fluorescent protein reporter assay on known antibiotics. The vertical axis shows the S/S_0 ratio, where S is the reporter fluorescent signal or OD_{600} detected in the presence of a sample; S_0, without the sample. The horizontal axis shows the applied antibiotics; for each antibiotic, the concentrations (C) are arranged in descending order. Erythromycin (Ery) 10, 5, 2.5, 1.25, and 0.6 μg/mL; neomycin (Neo) 20, 10, 5, 2.5, and 1.25 μg/mL; gentamicin (Gen) 20, 10, 5, 2.5, and 1.25 μg/mL; kanamycin (Kan) 30, 15, 7.5, 3.8, and 1.9 μg/mL; streptomycin (Str) 12.5, 6.3, 3.1, 1.6, and 0.8 μg/mL; hygromycin B (Hyg) 100, 50, 25, 12.5, and 6.3 μg/L; puromycin (Pur) 15, 7.5, 3.8, 1.9, and 0.9 μg/mL; chloramphenicol (Cm) 0.7, 0.35, 0.18, 0.09, and 0.04 μg/mL; fusidic acid (Fus) 10, 5, 2.5, 1.25, and 0.6 μg/mL; tetracycline (Tet) 1.2, 0.6, 0.3, 0.15, and 0.075 μg/mL; levofloxacin (Lev) 0.1, 0.05, 0.025, 0.013, and 0.006 μg/mL; nalidixic acid (Nal) 100, 50, 25, 12.5, 6.3, and 3.1 μg/mL; ciprofloxacin (Cip) 1, 0.5, 0.25, 0.13, and 0.06 μg/mL; rifampicin (Rif) 25, 12.5, 6.3, 3.1, and 1.6 μg/mL. The red area indicates the range of background values. (*A*) Ribosome stalling reporter signal after incubation for 5 h (left) and 24 h (right). Green bars mark the ribosome-targeting antibiotics; black ones denote the antibiotics activating the SOS response. (*B*) The SOS response activation reporter signal after 5 h (left) and 24 h (right) of incubation. Green bars mark the antibiotics that activate the SOS response; black ones denote ribosome-targeting antibiotics. (*C*) Cell growth values after 5 h (left) and 24 h (right) of incubation

analysis of antibacterial activity using the reporter system in a liquid medium. This choice ensured that all the antibiotics could suppress bacterial growth, whereas the synthesis of reporter proteins happened selectively as a result of ribosome stalling (expression of the fluorescent reporter protein Katushka2S) or events that damaged the DNA (expression of RFP). We used five to six sublethal concentrations of the antibiotics to visualize the profile of the reporters' expression.

The vast majority of ribosome-targeting inhibitors can block the particular translation reactions responsible for ribosome arrest. Thus, chloramphenicol (fenicols) and erythromycin (macrolides) bind at the entrance of the nascent peptide exit channel and interfere with peptide bond formation, depending on the length and sequence of a growing amino acid chain [23, 24]. Both antibiotics vigorously activate the expression of Katushka2S (*Fig. 1*). A comparable level of induction of Katushka2S was observed upon the addition of translocation inhibitors: hygromycin B (aminoglycosides) blocks the movement of tRNA during the elongation cycle [25], whereas fusidic acid (fusidines) inhibits the dissociation of EF-G from the ribosome [26]. Tetracycline (polyketides), which binds the small ribosomal subunit and affects tRNA delivery to the ribosome [27], and puromycin, which integrates the growing polypeptide chain causing its

premature termination [28], increased the reporter fluorescence level above its baseline after incubation for 24 h.

Aminoglycosides interfere with translation mainly by reducing ribosome selectivity, which results in the insertion of incorrect amino acids into the nascent peptide chain, rather than ribosome pausing [29]. Neomycin induced some degree of reporter fluorescence after 5 h of incubation, followed by the disappearance of the signal at time point 24 h, whereas other members of the group (gentamicin, kanamycin, and streptomycin) did not stimulate Katushka2S synthesis at all.

Addition of quinolones (nalidixic acid, levofloxacin, ciprofloxacin), which block DNA replication [30], and ansamycin (rifampicin), which stops RNA synthesis in the cell [31], reduces the Katushka2S fluorescence level below the background at almost all the tested concentrations. Meanwhile, RFP expression remained substantially upregulated within the entire period of detection; the signal was amplified up to 15-fold compared to that of the untreated cells after 5-h incubation. Interestingly enough, some translation inhibitors also stimulated the emergence of the RFP signal; however, none of them exceeded the S/S_0 ratio = 2 during 24 h of incubation.

Hence, 5 h of incubation is enough to draw a conclusion as to whether the tested substance activates the SOS response, whereas detection of the compounds causing ribosome arrest may require an extension of incubation to 24 h.

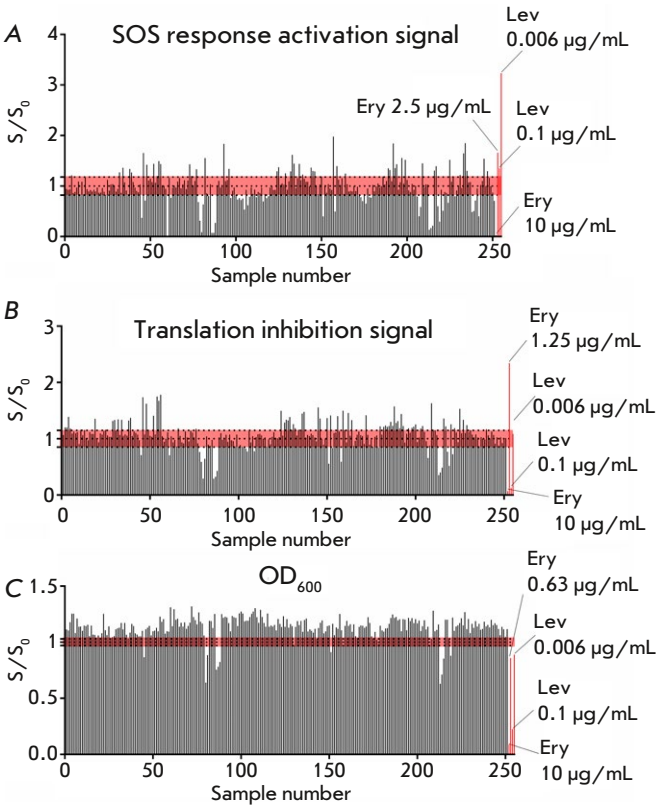

Fig. 2. Application of the double fluorescent protein reporter assay on the Sakhalin yeast collection. The vertical axis shows the S/S_0 ratio, where S is the reporter fluorescent signal or OD_{600} induced in the presence of a sample; S_0 is the reporter fluorescent signal or OD_{600} induced without a sample after 24 h. The horizontal axis shows sample number. Data for erythromycin (Ery) (10, 2.5, 1.25, 0.6 μg/mL) and levofloxacin (Lev) (0.1, 0.006 μg/mL) are used as positive controls. The red area indicates the range of background values. (*A*) The SOS response activation reporter signal. (*B*) Translation inhibition reporter signal. (*C*) The OD_{600} values

Analysis of the antibacterial activity of yeast culture liquids

We analyzed the antibacterial activity of the entire Sakhalin collection, which contained 251 strains (*Fig. 2*). Eleven samples of culture liquids were deemed to reduce the bacterial growth rate; however, none of them appeared to activate expression of the reporter proteins. Meanwhile, 233 samples were shown to stimulate cell growth, likely due to the presence of some nutritious components. Interestingly enough, among the stimulators we identified 74 samples that appeared to induce ribosome stalling and 50 samples that activate the SOS response. This observation implies a level of complexity of the content of the extracts: relatively low amounts of inhibiting components unable to overcome the probiotic action but still detectable by the reporter system. Hence, moderate antibacterial activity with an unidentified mechanism of action was established for 4% of the Sakhalin collection, while probiotic activity was detected in 93% of the extracts. However, it is possible that fractionation of crude extracts could lead to the detection of additional substances exhibiting antibacterial activity.

The yeast collection from Kamchatka contains more than 2,500 samples. We tested 559 of them, and 482 appeared to suppress cell growth, while 41 stimulated it, and 36 had no impact (*Fig. 3*).

We uncovered two samples that induce expression of Katushka2S, 46 samples that stimulate RFP expression, and one sample that activates both reporter signals simultaneously with cell growth suppression. Both Katushka2S inducers demonstrated a decreased RFP signal, and all 46 samples that increase the SOS response signal appeared to lower the translation inhibition reporter signal. It is reasonable to assume

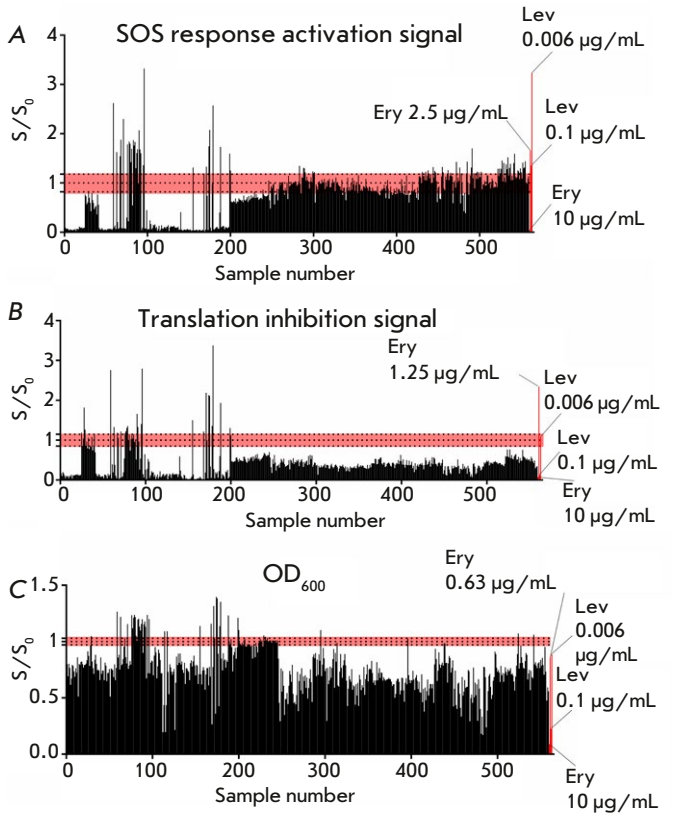

Fig. 3. Application of the double fluorescent protein reporter assay on the yeast collection from the Kamchatka Peninsula. The vertical axis shows the S/S_0 ratio, where S is the reporter fluorescent signal or OD_{600} induced in the presence of a sample; S_0 is the reporter fluorescent signal or OD_{600} induced without a sample after 24 h. The horizontal axis shows the sample number. The data for erythromycin (Ery) (10, 2.5, 1.25, 0.6 μg/mL) and levofloxacin (Lev) (0.1, 0.006 μg/mL) are used as positive controls. The red area indicates the range of background values. (*A*) The SOS response activation reporter signal. (*B*) Translation inhibition reporter signal. (*C*) The OD_{600} values

that these extracts may contain ribosome stalling and DNA damaging substances, respectively. The sample that stimulates the expression of both reporter proteins has a profile that resembles that of ribosome stalling antibiotics rather than of SOS response inducers.

In the group of cell growth inhibitors, 471 samples appear to push the Katushka2S signal below its baseline. For about half of them (213 extracts), the expression of RFP stood at the baseline level. Similar effects were produced by translation inhibitors that do not lead to ribosome stalling (*Fig. 1*). Eight samples were shown to inhibit cell growth without affecting the Katushka2S signal, reducing the RFP signal to a level comparable to that of given concentrations of neomycin and tetracycline. This case may be indicative of the presence of an inhibitor that does not induce a SOS response but whose mechanism of action could be associated with translational impairment.

Among the extracts that enhance cell growth, we found 21 samples that induce ribosome stalling and 30 that activate the SOS response. We also identified one sample that activates the SOS response but did not impair cell growth. Potentially, these extracts contain low concentrations of antibacterial components.

Hence, contrary to the Sakhalin collection, only 7% of the tested collection from Kamchatka was shown to exhibit probiotic activity. Antibacterial action of varying intensity was observed for 86% of the evaluated samples; a number of extracts caused the activation of the SOS response and ribosome stalling.

Most of the inhibiting extracts had comparable fluorescence signal profiles, with significantly decreased Katushka2S expression and a near-baseline RFP level. Similar behavior was demonstrated by the translation inhibitors that did not cause ribosome stalling, suggesting that the behavior may be a potential inhibition mechanism exploited by yeast extracts.

Among all the studied samples, 44 from Kamchatka exhibited pronounced antibacterial properties (OD_{600} of the bacterial culture was more than twofold lower compared to the reference). The substrate collection spots in Kamchatka were chosen in close proximity to mud, water, or gas emissions: the Pauzhetka, Ozernovsky, Mutnovsky, Esso settlements and their environs, the vicinity of Skalistaya Hill and Kuril Lake. Twenty-eight of the 44 isolates were found in the gorge located about 200 m away from the Pauzhetka geothermal power plant; 11 isolates, on thistle (*Onopordum acanthium*); and 17 isolates, on wormwood (*Artemisia vulgaris*).

Knotweed, bluegrass, columbine, speedwell, etc. were also collected in this gorge; however, their yeast isolates did not exhibit any pronounced antibacterial properties. Wormwood and thistle were also collected in other areas: wormwood, in Tikhaya Bay of Kuril Lake (one isolate with pronounced antibacterial properties), on the coast of the Sea of Okhotsk in the vicinity of the Ozernovsky settlement, on flatland near the Pauzhetka settlement, on the slopes of Skalistaya Hill (no isolates with pronounced antibacterial properties); thistle, in Tikhaya Bay of Kuril Lake, on the slopes of Skalistaya Hill (no isolates with pronounced antibacterial properties), on the flatland near the Mutnovsky settlement (one isolate with pronounced antibacterial properties).

The culture liquids of 43 out of the 44 isolates exhibiting pronounced antibacterial properties reduced

reporter signals below their control level; i.e., they did not induce activation of the SOS response or ribosome arrest.

Taxonomic identification

We selected 19 samples of cultural liquids that suppressed cell growth with the S/S_0 ratio lying in the range of 0.17–0.97. Three samples (with the collection numbers KI-55-1-9-1, KI-55-1-9-3*, and KI-53-1-13a*) appeared to possess the strongest inhibitory properties; their S/S_0 values lay in the range of 0.17–0.29. Four samples (with collection numbers KI-1-1, KI-3-6a, KI-19-1a, and KI-31-3) provoked an increase in the SOS response activation reporter signal.

This group was shown to contain predominantly members of the *Cryptococcus (Naganishia)* genus (*Table 2*). Species diversity was as follows: five strains, *Cryptococcus adeliensis*; four strains, *Naganishia (Cryptococcus) albidosimilis*; two strains, *Naganishia (Cryptococcus) diffluens*; one strain, *Naganishia (Cryptococcus) liquefaciens*; four strains, *Naganishia (Cryptococcus) vishniacii*; two strains, *Candida parapsilosis*; and one strain, *Rhodotorula mucilaginosa*.

The yeast isolates KI-55-1-9-1, KI-55-1-9-3*, and KI-53-1-13a*, which exhibit the most vigorous antibacterial activity, belong to the *Naganishia (Cryptococcus) albidosimilis* and *Naganishia (Cryptococcus) adeliensis* species. The strains KI-1-1, KI-3-6a, KI-19-1a, and KI-31-3, whose culture liquids stimulated the SOS response, belong to the *Naganishia (Cryptococcus) albidosimilis, Naganishia (Cryptococcus) adeliensis*, and *Candida parapsilosis* species.

Table 2. The results of the taxonomic identification of yeast strains whose culture liquids exhibited antibacterial properties

Collection number of a strain	Species affiliation of a strain / the corresponding BLAST sequence number
KI-1-1	*Cryptococcus adeliensis / JX188117.1*
KI-3-6a	*Cryptococcus adeliensis / JX188117.1*
KI-19-1a	*Candida parapsilosis / KT282393.1*
KI-174-4a	*Candida parapsilosis / KT282393.1*
KI-17-5-1a	*Rhodotorula mucilaginosa / MN006694.1*
KI-18-1a	*Naganishia diffluens / MK793259.1, MT303133.1*
KI-53-1-6d	*Cryptococcus adeliensis / JX188117.1*
KI-80-1	*Naganishia liquefaciens / MG722803.1*
KI-81-2-1	*Naganishia vishniacii / OM337523.1*
KI-55-1-1**	*Naganishia diffluens / MK793259.1, MT303133.1*
KI-46-5c-2	*Naganishia albidosimilis / MW248429.1, MT127371.1*
KI-31-3	*Naganishia albidosimilis / MW248429.1, MT127371.1*
KI-39-5	*Naganishia vishniaci / OM337523.1*
KI-151-0	*Naganishia vishniacii / OM337523.1*
KI-223-1b	*Naganishia vishniacii / OM337523.1*
KI-193-3	*Cryptococcus adeliensis / JX188117.1, JX188114.1*
KI-55-1-9-1	*Naganishia albidosimilis / LC203701.1, LC203699.1, MW248429.1*
KI-55-1-9-3*	*Naganishia albidosimilis / LC203701.1, LC203699.1, MW248429.1*
KI-53-1-13a*	*Naganishia adeliensis / JX188117.1, JX188114.1, LC202041.1*

DISCUSSION

The current extinction rates of our biodiversity are estimated to be approximately 100 to 1,000 times higher than those over the past centuries [32]. The ongoing loss of biodiversity results in the disappearance of at least one important bioactive molecule every two years [33]. The discovery and storage of biomaterial, with subsequent organization of species collections, followed by investigations of these collections, contribute to efforts at biodiversity preservation [2, 3].

In this study, we have analyzed the antibacterial activity of yeast strains found in the Kamchatka Peninsula and Sakhalin Island against reporter *E. coli* Δ*tolC* cells. The absence of the *tolC* gene improved assay sensitivity [9, 34] by increasing compound dissemination into the cell, which is highly preferable for multicomponent biological crude extracts with potentially low concentrations of bioactive compounds.

High-throughput screening of bioactive substances is usually performed on bacterial lawn using agar plates [35]. However, bacterial cultures on solid media and in liquid differ metabolically. The proteomes of a single *E. coli* colony have only 68% protein overlap in the case of two culturing conditions [36]. Hence, despite the widespread use of the dual-fluorescent reporter system on solid media [9], it was important to validate its application in a liquid medium using a set of known antibiotics. Notably, SOS response activators dramatically increased the RFP fluorescence after 5 h of incubation with bacterial cells, whereas differentiation of translation inhibitors into ribosome stalling and miscoding agents was possible only after 24 h into the experiment. In general, our results are in line with the previously obtained findings in [9], proving the applicability of this system in liquids.

The modification to the assay introduced offers several advantages. First, it allows one to monitor the

density of the cell culture by measuring OD_{600}, enabling the evaluation of the probiotic and antibacterial properties of a sample. It also makes it possible to add a test substance at different bacterial growth phases. This might be relevant as bacterial sensitivity to antibiotics depends on the metabolic state of the cell [37]. Second, it is possible to record both an increase and a decrease in the reporter signal with respect to the reference level. Reduction of the fluorescence level, accompanied by lowering of $OD_{600,}$ may indicate cell death, whereas a decrease in the fluorescence followed by an increase in OD_{600} over the starting values may indicate profound changes in the cellular metabolism [24]. Third, the "drug–bug" race begins on an agar plate when a testing sample meets the medium [35]. Sample molecules diffuse into agar, creating a dynamically changing concentration gradient, while bacterial growth progresses along the gradient. The result is a competition of cell growth rates and diffusion rates of the test drug. In the case of samples with low bioactive concentrations, this effect may impair the analysis. Meanwhile, the assay for the analysis of antibacterial activity in a liquid medium has several drawbacks such as a longer processing time, greater amount of consumables, and the impossibility of analyzing poorly soluble substances.

We analyzed the antibacterial properties of the yeast collection and compared the data obtained for samples from Sakhalin and Kamchatka. Interestingly, no significant antimicrobial properties were found in the Sakhalin samples; on the contrary, the samples were predominantly probiotics. Strains from the Kamchatka Peninsula exhibited strong antibacterial properties, and several strains led to the activation of reporter signals in the test system. However, 43 of the 44 isolates with the strongest antibacterial properties did not lead to the activation of the SOS response and ribosome stalling, suggesting that the bioactive substances released may disrupt the bacterial membrane integrity or suppress the ability of bacteria to form biofilms [38]. In the present study, yeast culture liquids were obtained without the destruction of yeast cells; therefore, it is most likely that wild yeasts would excrete biologically active metabolites into the extracellular space.

Taxonomic identification of yeast strains revealed that isolates exhibiting the strongest antimicrobial properties belong to the *Naganishia (Cryptococcus)* genus. This agrees with previous reports on the toxicity of yeast isolates of the *Naganishia (Cryptococcus)* genus discovered in various geographical areas. The *Naganishia albida* and *Naganishia diffluens* species found in the alkaline water lake region Wadi El-Natrun, Egypt, were found to possess antibacterial activity against *E. coli* and *Staphylococcus capitis* [39]; a probable pathogenicity of the *Naganishia adeliensis* strains for living organisms and their production of secondary metabolites, including mycotoxins, was reported for yeast discovered in the vicinity of Lodz, Poland [40].

We established that more than half of the strains with pronounced antibacterial properties were collected in the gorge near the Pauzhetka geothermal power plant on thistle and wormwood. Moreover, it was the combination of the plants and their growth sites that led to the emergence of this bioactivity in yeast culture liquids. The gorge near Pauzhetka village is a biotope combining high humidity, low light, and soil heating from hydrothermal vents. Such conditions foster a significant biodiversity of microorganisms. Yeasts are known to be able to protect the host plant against mycopathogens by attaching to the surface of fungi and secreting enzymes that destroy the mycopathogens' cell walls [38]. In the case of high competition, the concentration of these yeast enzymes can be increased and have a destructive impact on bacterial membranes as well. Meanwhile, wormwood and thistle contain bioactive sesquiterpene lactones [41, 42], which possesses antimycotic properties [43]. Comfortable environmental conditions could induce yeast cells to develop resistance to these compounds, for example, by synthesizing enzymes capable of modifying sesquiterpene lactones to a safe form, or by synthesizing low-molecular-weight components that disrupt the biosynthesis of sesquiterpene lactones. These bioactive molecules could also have a negative effect on bacterial cells. It is known that plants with antimicrobial properties "cultivate" mutualistic microflora with similar bioactivity. Thus, the antibacterial potential of pomegranate peel can be determined not only by the nature of its own components, but also by microorganisms, and local yeast, in particular [44].

The true mechanisms by which yeast culture liquids apply antibacterial action can be determined only after the isolation and identification of bioactive components. But the uniqueness of the discovered biocenosis in this study is beyond doubt and can be used as a template for similar expeditions. The researchers note the need to analyze interactions not only within individual groups of microorganisms (bacteria with bacteria or yeasts with yeasts), but also the interactions between groups for a deeper understanding of how they function and the environmental impact they have [45]. Our work contributes to the research into the interactions that exist in microbial communities within certain biocenoses, emphasizing the importance of using an integrated approach when searching for biologically active substances.

CONCLUSIONS

We were able to identify the strains of a yeast collection that exhibit antibacterial and probiotic properties. That discovery affirms the value of the uniqueness of the Far East collection and demonstrates the need to preserve and research biodiversity. ●

This work was supported by the Russian Science Foundation (grant No. 22-14-00278).

The authors would like to thank the research team of P.V. Sergiev (Moscow State University) for kindly providing the double fluorescence reporter strain, to S.A. Bulat for advice about taxonomic identification of yeasts, and to Y.A. Pushchina for assistance in analyzing the antibacterial activity of the yeast collection.

REFERENCES

1. Seal B.S., Lillehoj H.S., Donovan D.M., Gay C.G. // Animal Hlth Res. Rev. 2013. V. 14. № 1. P. 78–87.
2. Beutler J.A. // Curr. Protocols Pharmacol. 2009. V.46. P. 9.11.1–9.11.21.
3. Neergheen-Bhujun V., Awan A.T., Baran Y., Bunnefeld N., Chan K., Dela Cruz T.E., Egamberdieva D., Elsässer S., Johnson M.V., Komai S., et al. // J. Global Hlth. 2017. V. 7. № 2. P. 020304.
4. Tao Z., Yuan H., Liu M., Liu Q., Zhang S., Liu H., Jiang Y., Huang D., Wang T. // J. Microbiol. Biotechnol. 2023. V. 33. № 2. P. 151–166.
5. Aly A.H., Debbab A., Proksch P. // Fungal Diversity. 2011. V. 50. P. 3–19.
6. Younis G., Awad A., Dawod R.E., Yousef N.E. // Veterinary World. 2017. V. 10. № 8. P. 979–983.
7. Deveau A., Bonito G., Uehling J., Paoletti M., Becker M., Bindschedler S., Hacquard S., Hervé V., Labbé J., Lastovetsky O.A., et al. // FEMS Microbiol. Rev. 2018. V. 42. № 3. P. 335–352.
8. Gut A.M., Vasiljevic T., Yeager T., Donkor O.N. // Microbiology. 2018. V. 164. № 11. P. 1327–1344.
9. Osterman I.A., Komarova E.S., Shiryaev D.I., Korniltsev I.A., Khven I.M., Lukyanov D.A., Tashlitsky V.N., Serebryakova M.V., Efremenkova O.V., Ivanenkov Y.A., et al. // Antimicrob. Agents Chemother. 2016. V. 60. № 12. P. 7481–7489.
10. Liu S., Wang T., Lu Q., Li F., Wu G., Jiang Z., Habden X., Liu L., Zhang X., Lukianov D.A., et al. // Front. Microbiol. 2021. V. 12. P. 604999.
11. Liu S.W., Jadambaa N., Nikandrova A.A., Osterman I.A., Sun C.H. // Microorganisms. 2022. V. 10. № 5. P. 989.
12. Wang T., Li F., Lu Q., Wu G., Jiang Z., Liu S., Habden X., Razumova E.A., Osterman I.A., Sergiev P.V., et al. // J. Pharmaceut. Anal. 2021. V. 11. № 2. P. 241–250.
13. Volynkina I.A., Zakalyukina Y.V., Alferova V.A., Belik A.R., Yagoda D.K., Nikandrova A.A., Buyuklyan Y.A., Udalov A.V., Golovin E.V., Kryakvin M.A., et al. // Antibiotics. 2022. V. 11. № 9. P. 1198.
14. Koronakis V., Eswaran J., Hughes C. // Annu. Rev. Biochem. 2004. V. 73. P. 467–489.
15. Suslov A.V., Suslova I.N., Bagiian G.A., Davydenko S.G., Stepanova V.P., Sukhanova E.A., Iarovoĭ B.F. // Radiation Biology. Radioecology. 2004. V. 44. № 5. P.574–578.
16. MacDonald P.N. (Ed) Two-Hybrid Systems: Methods and Protocols Methods in Molecular Biology. Springer Science & Business Media, 2008. V. 177. 336 p.
17. Barnett J.A., Payne R.W., Yarrow D. (Eds) Yeasts: Characteristics and identification. Cambridge Univ. Press, 1983. 811 p.
18. Kreger-van Rij N.J.W. (Ed) The Yeasts: a taxonomic study. Amsterdam: Elsevier, 1984. 1082 p.
19. Poliakova A.V., Chernov I.Iu., Panikov N.S. // Mikrobiol. 2001. V. 70. № 5. P.714–720.
20. Stepanova V.P., Suslov A.V., Suslova I.N., Sukhanova E.A., Yarovoy B.F., Verbenko V.N. // Marine Biol. J. 2020. V. 5. № 3. P. 64–73.
21. Sergiev P.V., Osterman I.A., Golovina A.Ya., Laptev I.G., Pletnev P.I., Evfratov S.A., Marusich E.I., Leonov S.V., Ivanenkov Ya.A., Bogdanov A.A., et al. // Chem. 2016. V. 62. № 2. P.117–123.
22. Raja H.A., Miller A.N., Pearce C.J., Oberlies N.H. // J. Nat. Prod. 2017. V. 80. № 3. P. 756–770.
23. Tenson T., Lovmar M., & Ehrenberg M. // J. Mol. Biol. 2003. V. 330. № 5. P. 1005–1014.
24. Stokes J.M., Lopatkin A.J., Lobritz M.A., & Collins J.J. // Cell Metabolism. 2019. V. 30. № 2. P. 251–259.
25. Borovinskaya M.A., Shoji S., Fredrick K., & Cate J.H. // RNA. 2008. V. 14. № 8. P. 1590–1599.
26. Fernandes P. // Cold Spring Harb. Perspectives Med. 2016. V. 6. № 1. P. a025437.
27. Chopra I., & Roberts M. // Microbiol. Mol. Biol. Rev. MMBR. 2001. V. 65. № 2. P. 232–260.
28. Aviner R. // Comput. Struct. Biotechnol. J. 2020. V. 18. P. 1074–1083.
29. Kotra L.P., Haddad J., & Mobashery S. // Antimicrobial Agents and Chemotherapy. 2000. V. 44. № 12. P. 3249–3256.
30. Fàbrega A., Madurga S., Giralt E., & Vila J. // Microb. Biotechnol. 2009. V. 2. № 1. P. 40–61.
31. Campbell E.A., Korzheva N., Mustaev A., Murakami K., Nair S., Goldfarb A., Darst S.A. // Cell. 2001. V. 104. № 6. P. 901–912.
32. Pimm S.L., Jenkins C.N., Abell R., Brooks T.M., Gittleman J.L., Joppa L.N., Raven P.H., Roberts C.M., Sexton J.O. // Science. 2014. V. 344. № 6187. P. 1246752.
33. Pimm S.L., Russell G.J., Gittleman J.L., Brooks T.M. // Science. 1995. V. 269. № 5222. P. 347–350.
34. Fan J., de Jonge B.L., MacCormack K., Sriram S., McLaughlin R.E., Plant H., Preston M., Fleming P.R., Albert R., Foulk M., et al. // Antimicrobial Agents and Chemotherapy. 2014. V. 58. № 12. P. 7264–7272.
35. Audrey W. // Antimicrobial susceptibility testing protocols / Eds Schwalbe R., Steele-Moore L., Goodwin A.C. Boca Raton: CRC Press Taylor and Francis Group, 2007. P. 53–72.
36. Fortuin S., Nel A.J.M., Blackburn J.M., Soares N.C. // J. Proteomics. 2020. V. 228. P. 103929.
37. Lobritz M.A., Belenky P., Porter C.B., Gutierrez A., Yang J.H., Schwarz E.G., Dwyer D.J., Khalil A.S., Collins J.J. // Proc. Natl. Acad. Sci. USA. 2015. V. 112. № 27.

P. 8173–8180.
38. Georgescu A.M., Corbu V.M., & Csutak O. // Curr. Issue. Mol. Boil. 2024. V. 46. № 5. P. 4721–4750.
39. Sipiczki M., & Selim S.A. // Antonie van Leeuwenhoek. 2019. V. 112. № 4. P. 523–541.
40. Wójcik A., Kurnatowski P., & Błaszkowska J. // Internat. J. Occup. Med. Environ. Hlth. 2013. V. 26. № 3. P. 477–487.
41. Csupor-Löffler B., Zupkó I., Molnár J., Forgo P., & Hohmann J. // Nat. Prod. Commun. 2014. V. 9. № 3. P. 337–340.
42. Chen X.Y., Liu T., Hu Y.Z., Qiao T.T., Wu X.J., Sun P.H., Qian C.W., Ren Z., Zheng J.X., & Wang Y.F. // Front. Chem. 2022. V. 10. P. 948714.
43. Nawrot J., Adamski Z., Kamińska-Kolat B., Kubisiak-Rzepczyk H., Kroma A., Nowak G., & Gornowicz-Porowska J. // Plants. 2021. V. 10. № 6. P. 1180.
44. Utama G.L., Rahmah S.A., Kayaputri I.L., & Balia R.L. // J. Adv. Pharm. Technol. Res. 2022. V. 13. № 1. P. 56–60.
45. Senne de Oliveira Lino F., Bajic D., Vila J.C.C., Sánchez A., & Sommer M.O.A. /// Nat. Commun. 2021. V. 12. № 1. P. 1498.

Bacteriocin from the Raccoon Dog Oral Microbiota Inhibits the Growth of Pathogenic Methicillin-Resistant *Staphylococcus aureus*

M. N. Baranova[1], E. A. Soboleva[1], M. A. Kornienko[2], M. V. Malakhova[2], Yu. A. Mokrushina[1,3], A. G. Gabibov[1,3], S. S. Terekhov[1], I. V. Smirnov[1,3*]

[1]Shemyakin–Ovchinnikov Institute of Bioorganic Chemistry, Russian Academy of Sciences, Moscow, 117997 Russian Federation

[2]Federal Research and Clinical Center of Physical-Chemical Medicine, Federal Medical Biological Agency, Moscow, 119435 Russian Federation

[3]Faculty of Chemistry, Lomonosov Moscow State University, Moscow, 119991 Russian Federation

*E-mail: ivansmr@inbox.ru

Received December 11, 2023; in final form, November 18, 2024

DOI: 10.32607/actanaturae.27349

ABSTRACT **The growing incidence of infections caused by antibiotic-resistant strains of pathogens is one of the key challenges of the 21st century. The development of novel technological platforms based on single-cell analysis of antibacterial activity at the whole-microbiome level enables the transition to massive screening of antimicrobial agents with various mechanisms of action. The microbiome of wild animals remains largely underinvestigated. It can be considered a natural reservoir of biodiversity for antibiotic discovery. Here, the *Staphylococcus pseudintermedius* E18 strain was isolated from the oral microbiome of a raccoon dog (*Nyctereutes procyonoides*) using a microfluidic ultrahigh-throughput screening platform. *S. pseudintermedius* E18 efficiently inhibited the growth of pathogenic methicillin-resistant *Staphylococcus aureus* (MRSA). It was established that the main active substance of the *S. pseudintermedius* E18 strain was a bacteriocin with a molecular weight of 27 kDa. The identified bacteriocin had a high positive charge and an extremely narrow spectrum of activity. Bacteriocin *S. pseudintermedius* E18 was inactivated by elevated temperature, proteinase K, and EDTA. Further investigation on the structure of the bacteriocin produced by *S. pseudintermedius* E18 will provide a comprehensive understanding of its mechanism of action, which will open up prospects for developing novel DNA-encoded antimicrobials.**

KEYWORDS **ultra-high-throughput screening, antimicrobial resistance, antimicrobial peptides, lytic enzymes.**

Searching for novel antimicrobials is essential, since bacteria are constantly evolving and develop resistance to new antibiotics [1]. The application of novel platforms based on the metabolomics, genomic, and transcriptomic sequencing techniques, followed by bioinformatics analysis, as well as the drive toward alternative microbial culture methods offers new opportunities for antibiotic activity screening of naturally occurring substances.

Animal microbiomes are a unique reservoir that can be tapped in the search for novel antimicrobials [2–4]. Probiotic microorganisms are of special interest as potential producers of antibiotics [5, 6]. Although probiotic strains and commensal bacteria can have indirect implications on the microbiome by influencing the host immune system [7] or producing functionally important enzymes [8], the direct pathogen-killing mechanism is typical of most bacteriocins.

Here, we conducted ultra-high-throughput screening of the salivary microbiome of the raccoon dog (*Nyctereutes procyonoides*) to isolate strains producing substances exhibiting an antimicrobial activity against *S. aureus* and identify the metabolites responsible for their antagonistic properties.

Previously, we described a platform for ultra-high-throughput screening of microbial communities (*Fig. 1*) [2, 9] that was based on cocultivation of individual microbial cells with a reporter pathogen strain in isolated droplets of double emulsion, followed by the isolation of active phenotypes by flu-

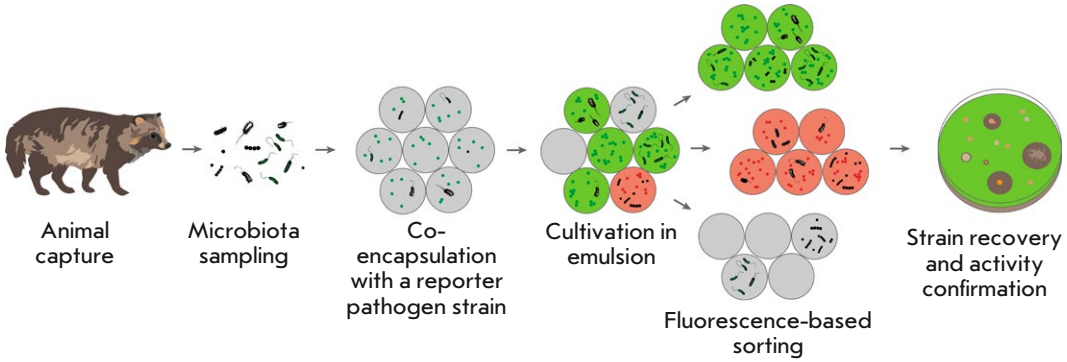

Fig. 1. Schematic diagram of an ultra-high-throughput screening platform for selecting microorganisms that inhibit the growth of a target bacterium

Table 1. Mass spectrometric identification and antagonistic activity of the isolated strains against *S. aureus*

Strain	Microorganism	Growth inhibition zones of *S. aureus*, diameter, mm	Maximum activity in liquid culture	
			Inhibitory dilution factor	Cultivation duration, days
E14	*Bacillus pumilus*	11 ± 2	61 ± 9	2
E18	*Staphylococcus pseudintermedius*	5 ± 1	256 ± 47	4
E32	*Bacillus amyloliquefaciens*	4* ± 1	5 ± 1	2
EB10	*Pasteurella dagmatis*	0.9 ± 0.1	8 ± 1	8
EB16	*Ralstonia insidiosa*	3.1 ± 0.4	–	–
EB27	*Curtobacterium luteum*	–	4 ± 1	1
EB30	*Brachybacterium sp.*	–	2.1 ± 0.5	1

*Diffuse zone of inhibition.

orescence-activated cell sorting. This platform was used to profile the oral microbiome of the raccoon dog and to identify the strains exhibiting an activity against *S. aureus*.

Screening revealed six phenotypically different strains reproducibly inhibiting the growth of *S. aureus* on a BHI agar medium and in liquid culture (activity was evaluated using the twofold serial dilution method). The strains were identified by matrix-assisted laser desorption ionization time-of-flight mass spectrometry (MALDI-TOF MC) (*Table 1*).

The *S. pseudintermedius* E18 strain exhibited the highest activity against *S. aureus* in the liquid medium (*Fig. 2A*). A more detailed analysis of the dynamics of the antagonistic effect of the producer strain was conducted to accumulate and identify the active substance (*Fig. 2B*).

The active substance was purified by solid-phase extraction using a LPS-500 sorbent (*Table 2*). Most of the substance could not be eluted by increasing the acetonitrile concentration in the buffer solution at pH 5.0; 0.1% trifluoroacetic acid (TFA) in an aqueous acetonitrile solution was used for elution.

As a result of 1.5 h of incubation at 60°C, the substance produced by the E18 strain lost its antibiotic activity. Because of thermal lability and the elution pattern during solid-phase extraction, we assumed it to be a high-molecular-weight substance. Active samples of the culture medium supplemented with 50 mM sodium phosphate, pH 7.5, were exposed to proteinase K (0.1 mg/mL). After 3 h of incubation at 37°C, the inhibitory activity against *S. aureus* was completely lost. Since the compound tentatively had a protein nature, the respective methods were used for its further purification.

The first purification stage involved ion exchange chromatography using the SP Sepharose sorbent (*Table 3*).

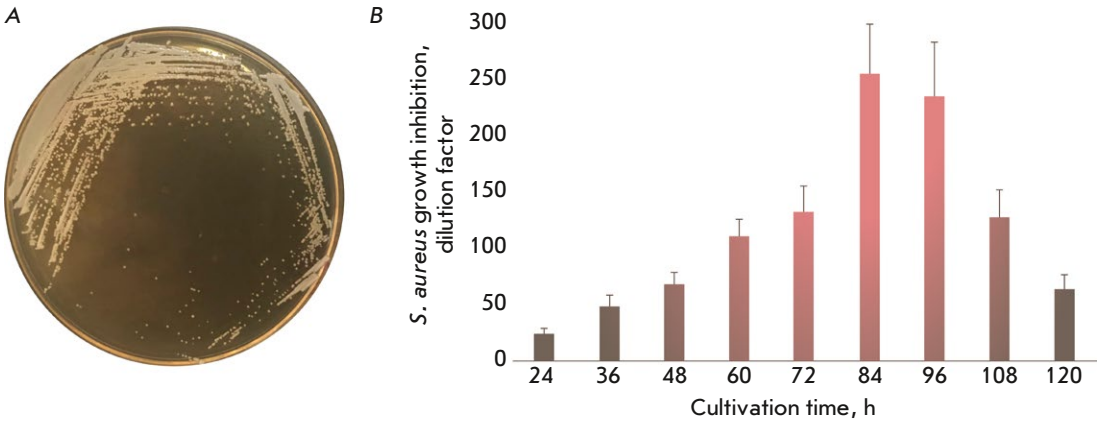

Fig. 2. (*A*) The phenotype of the E18 producer strain on a BHI agar medium; (*B*) the dynamics of E18 strain active metabolite production

Table 2. Purification of the substance produced by the E18 strain by pulsed solid-phase extraction using the LPS-500 sorbent

Buffer solution	A	B	A + C, %C		
			40	70	100
Activity according to inhibitory dilution, % of applied sample	2 ± 1	9 ± 1	12 ± 3	68 ± 7	11 ± 2

Note. Buffer A: 10 mM NH_4OAc, 5% acetonitrile, pH 5.0; buffer B: 10 mM NH_4OAc, 80% acetonitrile, pH 5.0; buffer C: 0.1% TFA, 80% acetonitrile.

A Heparin Sepharose chromatography column (GE Healthcare, USA) and buffer solutions A (20 мМ HEPES, pH 7.0) and B (20 мМ HEPES, 1 M NaCl, pH 7.0), with a flow rate of 1 mL/min, were used at the second purification stage. Linear gradient elution with buffer B was performed for 20 min (*Fig. 3A,B*). The retention time indirectly indicated that the protein carried a high positive charge.

Size exclusion chromatography using a Superdex 75 column in buffer solution containing 20 mM HEPES and 250 mM NaCl (pH 7.0, flow rate, 0.4 mL/min) was employed at the third purification stage. Activity corresponded to the protein ~ 27 kDa in size (*Fig. 3C*); retention time was ~ 23 min.

A purified protein was used for the functional studies. The minimum inhibitory concentration of this protein against *S. aureus* was 0.05 ± 0.02 μg/mL. The resulting bacteriocin was highly specific: its MIC values against *Escherichia coli*, *Pseudomonas aeruginosa*, *Klebsiella pneumoniae*, *Enterococcus faecium*, *Acinetobacter baumannii*, *Enterobacter cloacae*, *Streptococcus pneumoniae*, and *Bacillus cereus* were above 10 μg/mL, indication that it exhibited no antimicrobial activity against these bacteria.

Hence, the *S. pseudintermedius* strain produces class III bacteriocin, the thermolabile 27 kDa polypeptide inhibiting the growth of bacteria belonging to the genus *Staphylococcus* [10–12]. Class III bacteriocins include bacteriolysins, tailocins, and nonlytic proteins. Bacteriolysins are the best studied subclass of such organisms. The known members of bacteriolysins are metal-dependent proteases catalyzing the hydrolysis of peptide bridges or stem peptides in peptidoglycan in a target bacterium [12]. A hypothesis was put forward that the protein isolated from *S. pseudintermedius* is also a peptidoglycan hydrolase. Incubation of the protein in the presence of 10 mM EDTA at 25°C for 15 min rendered it completely inactive. Therefore, the substance mediating the antistaphylococcal activity of the *S. pseudintermedius* strain is a metal-dependent enzyme, which is typical of bacteriolysins.

CONCLUSIONS

The development of antimicrobial resistance by pathogenic bacteria has revived interest in antimicrobial agents that can target bacterial membranes and cell walls [13]. Ultra-high-throughput screening of the microbiota of a racoon dog uncovered the *S. pseudintermedius* E18 strain. It was demonstrated by chromatographic fractionation that this strain produces an antimicrobial agent acting as a lytic enzyme. ●

This work was supported by the Russian Science Foundation (grant No. 19-14-00331).

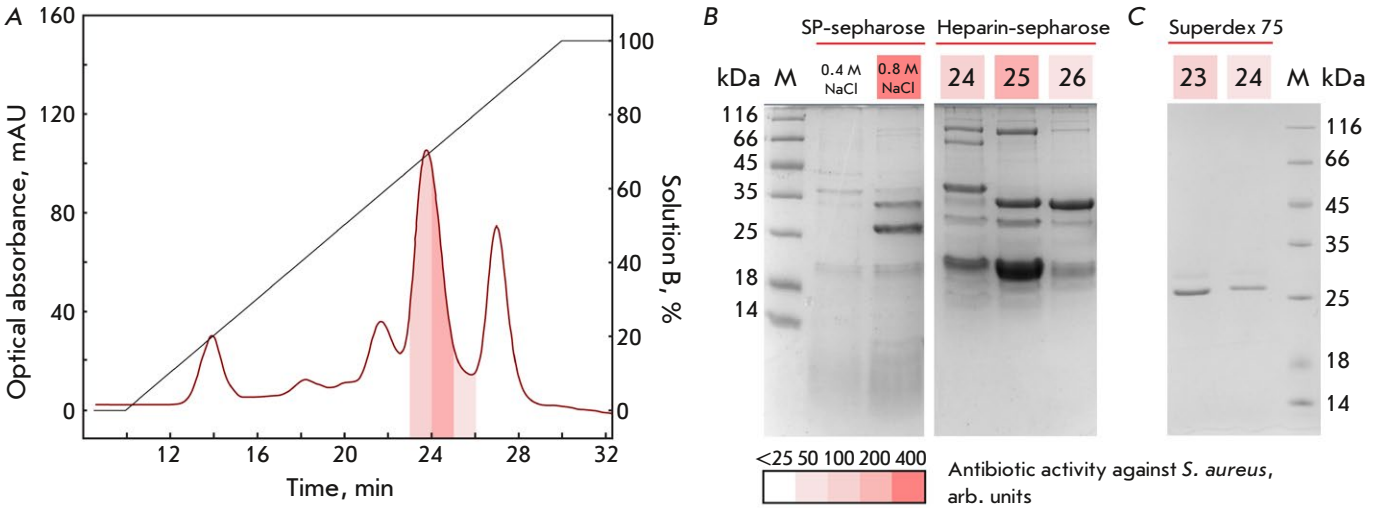

Fig. 3. Chromatographic purification of the protein responsible for the activity of the *S. pseudintermedius* E18 strain. Fractions with the highest antistaphylococcal activity are shown in red. (*A*) Representative chromatogram obtained by fractionation of active metabolites of *S. pseudintermedius* E18 using a Heparin Sepharose column. (*B*) Representative 15% SDS-PAGE patterns. Protein purification by chromatography using the SP Sepharose sorbent and subsequent purification using a Heparin Sepharose column. (*C*) Representative 15% SDS-PAGE pattern. Fractions obtained as a result of protein purification by gel filtration using a Superdex 75 column

Table 3. Purification of the substance produced by the E18 strain by cation exchange chromatography using the SP Sepharose sorbent

Content of buffer B, %	0	20	40	60	80	100
Activity according to inhibitory dilution, % of applied sample	6 ± 5	2 ± 1	15 ± 3	26 ± 7	21 ± 5	11 ± 2

Note. Buffer A: 10 mM NH_4OAc, pH 6.0; buffer B: 10 mM NH_4OAc, 1 M NaCl, pH 6.0. Fractions corresponding to the 60 and 80% of buffer B content (600 and 800 mM NaCl, respectively) were used further in the work.

REFERENCES

1. https://www.who.int/news/item/27-02-2017-who-publishes-list-of-bacteria-for-which-new-antibiotics-are-urgently-needed.
2. Terekhov S.S., Smirnov I.V., Malakhova M.V., Samoilov A.E., Manolov A.I., Nazarov A.S., Danilov D.V., Dubiley S.A., Osterman I.A., Rubtsova M.P., et al. // Proc. Natl. Acad. Sci. USA. 2018. V. 115. № 38. P. 9551–9556.
3. Adnani N., Rajski S.R., Bugni T.S. // Nat. Prod. Rep. 2017. V. 34. № 7. P. 784–814.
4. Akbar N., Siddiqui R., Sagathevan K.A., Khan N.A. // Appl. Microbiol. Biotechnol. 2019. V. 103. № 10. P. 3955–3964.
5. Pereira W.A., Mendonça C.M.N., Urquiza A.V., Marteinsson V.Þ., LeBlanc J.G., Cotter P.D., Villalobos E.F., Romero J., Oliveira R.P.S. // Microorganisms. 2022. V. 10. № 9. P. 1705.
6. Liao S.F., Nyachoti M. // Anim. Nutr. 2017. V. 3. № 4. P. 331–343.
7. Liang L., Yang C., Liu L., Mai G., Li H., Wu L., Jin M., Chen Y. // Microb. Cell Fact. 2022. V. 21. № 1. P. 88.
8. El-Saadony M.T., Alagawany M., Patra A.K., Kar I., Tiwari R., Dawood M.A.O., Dhama K., Abdel-Latif H.M.R. // Fish Shellfish Immunol. 2021. V. 117. P. 36–52.
9. Terekhov S.S., Smirnov I.V., Stepanova A.V., Bobik T.V., Mokrushina Y.A., Ponomarenko N.A., Belogurov A.A., Rubtsova M.P., Kartseva O.V., Gomzikova M.O., et al. // Proc. Natl. Acad. Sci. USA. 2017. V. 114. № 10. P. 2550–2555.
10. Meade E., Slattery M.A., Garvey M. // Antibiotics. 2020. V. 9. № 1. P. 32.
11. Heng N.C.K., Tagg J.R. // Nat. Rev. Microbiol. 2006. V. 4. № 2. P. 160.
12. Zimina M., Babich O., Prosekov A., Sukhikh S., Ivanova S., Shevchenko M., Noskova S. // Antibiotics. 2020. V. 9. № 9. P. 553.
13. Bush K. // Rev. Sci. Tech. 2012. V. 31. № 1. P. 43–56.

GENERAL RULES

Acta Naturae publishes experimental articles and reviews, as well as articles on topical issues, short reviews, and reports on the subjects of basic and applied life sciences and biotechnology.

The journal *Acta Naturae* is on the list of the leading periodicals of the Higher Attestation Commission of the Russian Ministry of Education and Science. The journal Acta Naturae is indexed in PubMed, Web of Science, Scopus and RCSI databases.

The editors of *Acta Naturae* ask of the authors that they follow certain guidelines listed below. Articles which fail to conform to these guidelines will be rejected without review. The editors will not consider articles whose results have already been published or are being considered by other publications.

The maximum length of a review, together with tables and references, cannot exceed 50,000 characters with spaces (approximately 30 pages, A4 format, 1.5 spacing, Times New Roman font, size 12) and cannot contain more than 16 figures.

Experimental articles should not exceed 30,000 symbols (approximately 15 pages in A4 format, including tables and references). They should contain no more than ten figures.

A short report must include the study's rationale, experimental material, and conclusions. A short report should not exceed 12,000 symbols (5–6 pages in A4 format including no more than 12 references). It should contain no more than three figures.

The manuscript and all necessary files should be uploaded to www.actanaturae.ru:

1) text in Word 2003 for Windows format;
2) the figures in TIFF format;
3) the text of the article and figures in one pdf file;
4) the article's title, the names and initials of the authors, the full name of the organizations, the abstract, keywords, abbreviations, figure captions, and Russian references should be translated to English;
5) the cover letter stating that the submitted manuscript has not been published elsewhere and is not under consideration for publication;
6) the license agreement (the agreement form can be downloaded from the website www.actanaturae.ru).

MANUSCRIPT FORMATTING

The manuscript should be formatted in the following manner:

- Article title. Bold font. The title should not be too long or too short and must be informative. The title should not exceed 100 characters. It should reflect the major result, the essence, and uniqueness of the work, names and initials of the authors.
- The corresponding author, who will also be working with the proofs, should be marked with a footnote *.
- Full name of the scientific organization and its departmental affiliation. If there are two or more scientific organizations involved, they should be linked by digital superscripts with the authors' names. Abstract. The structure of the abstract should be very clear and must reflect the following: it should introduce the reader to the main issue and describe the experimental approach, the possibility of practical use, and the possibility of further research in the field. The average length of an abstract is 20 lines (1,500 characters).
- Keywords (3 – 6). These should include the field of research, methods, experimental subject, and the specifics of the work. List of abbreviations.
- INTRODUCTION
- EXPERIMENTAL PROCEDURES
- RESULTS AND DISCUSSION
- CONCLUSION

  The organizations that funded the work should be listed at the end of this section with grant numbers in parenthesis.
- REFERENCES

  The in-text references should be in brackets, such as [1].

RECOMMENDATIONS ON THE TYPING AND FORMATTING OF THE TEXT

- We recommend the use of Microsoft Word 2003 for Windows text editing software.
- The Times New Roman font should be used. Standard font size is 12.
- The space between the lines is 1.5.
- Using more than one whole space between words is not recommended.
- We do not accept articles with automatic referencing; automatic word hyphenation; or automatic prohibition of hyphenation, listing, automatic indentation, etc.
- We recommend that tables be created using Word software options (Table → Insert Table) or MS Excel. Tables that were created manually (using lots of spaces without boxes) cannot be accepted.
- Initials and last names should always be separated by a whole space; for example, A. A. Ivanov.
- Throughout the text, all dates should appear in the "day.month.year" format, for example 02.05.1991, 26.12.1874, etc.
- There should be no periods after the title of the article, the authors' names, headings and subheadings, figure captions, units (s – second, g – gram, min – minute, h – hour, d – day, deg – degree).
- Periods should be used after footnotes (including those in tables), table comments, abstracts, and abbreviations (mon. – months, y. – years, m. temp. – melting temperature); however, they should not be used in subscripted indexes (T_m – melting temperature; $T_{p.t}$ – temperature of phase transition). One exception is mln – million, which should be used without a period.
- Decimal numbers should always contain a period and not a comma (0.25 and not 0,25).
- The hyphen ("-") is surrounded by two whole spaces, while the "minus," "interval," or "chemical bond" symbols do not require a space.
- The only symbol used for multiplication is "×"; the "×" symbol can only be used if it has a number to its

right. The "·" symbol is used for denoting complex compounds in chemical formulas and also noncovalent complexes (such as DNA·RNA, etc.).
- Formulas must use the letter of the Latin and Greek alphabets.
- Latin genera and species' names should be in italics, while the taxa of higher orders should be in regular font.
- Gene names (except for yeast genes) should be italicized, while names of proteins should be in regular font.
- Names of nucleotides (A, T, G, C, U), amino acids (Arg, Ile, Val, etc.), and phosphonucleotides (ATP, AMP, etc.) should be written with Latin letters in regular font.
- Numeration of bases in nucleic acids and amino acid residues should not be hyphenated (T34, Ala89).
- When choosing units of measurement, SI units are to be used.
- Molecular mass should be in Daltons (Da, KDa, MDa).
- The number of nucleotide pairs should be abbreviated (bp, kbp).
- The number of amino acids should be abbreviated to aa.
- Biochemical terms, such as the names of enzymes, should conform to IUPAC standards.
- The number of term and name abbreviations in the text should be kept to a minimum.
- Repeating the same data in the text, tables, and graphs is not allowed.

GUIDENESS FOR ILLUSTRATIONS

- Figures should be supplied in separate files. Only TIFF is accepted.
- Figures should have a resolution of no less than 300 dpi for color and half-tone images and no less than 600 dpi.
- Files should not have any additional layers.

REVIEW AND PREPARATION OF THE MANUSCRIPT FOR PRINT AND PUBLICATION

Articles are published on a first-come, first-served basis. The members of the editorial board have the right to recommend the expedited publishing of articles which are deemed to be a priority and have received good reviews.

Articles which have been received by the editorial board are assessed by the board members and then sent for external review, if needed. The choice of reviewers is up to the editorial board. The manuscript is sent on to reviewers who are experts in this field of research, and the editorial board makes its decisions based on the reviews of these experts. The article may be accepted as is, sent back for improvements, or rejected.

The editorial board can decide to reject an article if it does not conform to the guidelines set above.

The return of an article to the authors for improvement does not mean that the article has been accepted for publication. After the revised text has been received, a decision is made by the editorial board. The author must return the improved text, together with the responses to all comments. The date of acceptance is the day on which the final version of the article was received by the publisher.

A revised manuscript must be sent back to the publisher a week after the authors have received the comments; if not, the article is considered a resubmission.

E-mail is used at all the stages of communication between the author, editors, publishers, and reviewers, so it is of vital importance that the authors monitor the address that they list in the article and inform the publisher of any changes in due time.

After the layout for the relevant issue of the journal is ready, the publisher sends out PDF files to the authors for a final review.

Changes other than simple corrections in the text, figures, or tables are not allowed at the final review stage. If this is necessary, the issue is resolved by the editorial board.

FORMAT OF REFERENCES

The journal uses a numeric reference system, which means that references are denoted as numbers in the text (in brackets) which refer to the number in the reference list.

For books: the last name and initials of the author, full title of the book, location of publisher, publisher, year in which the work was published, and the volume or issue and the number of pages in the book.

For periodicals: the last name and initials of the author, title of the journal, year in which the work was published, volume, issue, first and last page of the article, doi. Must specify the name of the first 10 authors. Ross M.T., Grafham D.V., Coffey A.J., Scherer S., McLay K., Muzny D., Platzer M., Howell G.R., Burrows C., Bird C.P., et al. // Nature. 2005. V. 434. № 7031. P. 325–337. doi: 10.1038/nature03440.

References to books which have Russian translations should be accompanied with references to the original material listing the required data.

References to doctoral thesis abstracts must include the last name and initials of the author, the title of the thesis, the location in which the work was performed, and the year of completion.

References to patents must include the last names and initials of the authors, the type of the patent document (the author's rights or patent), the patent number, the name of the country that issued the document, the international invention classification index, and the year of patent issue.

The list of references should be on a separate page. The tables should be on a separate page, and figure captions should also be on a separate page.

The following e-mail addresses can be used to contact the editorial staff: actanaturae@gmail.com, tel.: (495) 727-38-60.